UNIVERSITY OF Southampton

University of Southampton Research Repository

Copyright © and Moral Rights for this thesis and, where applicable, any accompanying data are retained by the author and/or other copyright owners. A copy can be downloaded for personal non-commercial research or study, without prior permission or charge. This thesis and the accompanying data cannot be reproduced or quoted extensively from without first obtaining permission in writing from the copyright holder/s. The content of the thesis and accompanying research data (where applicable) must not be changed in any way or sold commercially in any format or medium without the formal permission of the copyright holder/s.

When referring to this thesis and any accompanying data, full bibliographic details must be given, e.g.

Thesis: Author (Year of Submission) "Full thesis title", University of Southampton, name of the University Faculty or School or Department, PhD Thesis, pagination.

Data: Author (Year) Title. URI [dataset]

UNIVERSITY OF SOUTHAMPTON

FACULTY OF NATURAL AND ENVIRONMENTAL SCIENCES

Ocean and Earth Science

Volume 1 of 1

Biogeochemistry of trace metals in European shelf seas

by

Dagmara Rusiecka

Thesis for the degree of Doctor of Philosophy

March 2018

UNIVERSITY OF SOUTHAMPTON

ABSTRACT

FACULTY OF NATURAL AND ENVIRONMENTAL SCIENCES

Ocean and Earth Sciences

Thesis for the degree of Doctor of Philosophy

BIOGEOCHEMISTRY OF TRACE METALS IN EUROPEAN SHELF SEAS

by Dagmara Rusiecka

Shelf seas are considered an important source of trace metals (TMs) to the open ocean. However, the processes controlling distributions of dissolved TMs (DTMs) in shelf seas, their seasonal variability and the mechanisms facilitating off-shelf transport to the open ocean are not well constrained. Reported here is the first seasonal study of the DTMs, cadmium (DCd), zinc (DZn), nickel (DNi) copper (DCu) manganese (DMn), cobalt (DCo), aluminium (DAl) and lead (DPb) and their contrasting biogeochemical behaviours in the Celtic Sea continental system.

Strong correlations (r^2 = 0.91 – 0.97, n = 454) between nutrient-like metals (DCd, DZn, DCu, DNi, DCo (surface waters only)) and macronutrients (phosphate (PO_4^{3-}) and silicic acid (SiO_4^{4-}) were observed over all seasons (autumn, spring and summer) indicating that biological uptake in the euphotic zone and remineralization of sinking phytoplankton debris in deeper waters form key controls on their distributions. The correlation between DAl and PO_4^{3-} (r^2 = 0.80) and SiO_4^{4-} (r^2 = 0.85) in the upper waters (< 1500 m depth) mimicked the DZn distributions, which was a surprising observation and requires further investigation. Variable DTM ratios relative to PO_4^{3-} were observed across different seasons in off-shelf surface waters and for DCd and DZn (full depth profiles) across the continental shelf. Observations from the Celtic Sea region suggest the influence of distinct water masses, phytoplankton community structure and potentially metal specific biogeochemical processes, on DTMs distributions on a seasonal time-scale.

Dissolved Co and Mn were more strongly influenced by scavenging and sedimentary inputs. Vertical distributions of DMn showed a typical scavenged type behaviour with enhanced surface waters concentrations from atmospheric inputs combined with photochemical stabilisation. Enhanced DMn and DCo concentrations were observed close to slope sediments and extended

away from the shelf at intermediate depths. These observations were related to suspended sediments as indicated by increased signals in turbidity and short-lived ^{223}Ra and ^{224}Ra isotopes (tracers of sediment inputs). This implies that resuspended shelf or slope sediments can act as a source of DMn and DCo that can be transported to the adjacent open ocean. The full depth relationship of DCo with PO_4^{3-} revealed a shift in dominant biogeochemical processes controlling DCo vertical distributions in the study region. While biological uptake and remineralization were dominant processes in surface waters, as indicated by a strong correlation with PO_4^{3-} ($r = 0.89$), a gradual decoupling of DCo from PO_4^{3-} at intermediate depths was suggestive of progressive scavenging and less pronounced remineralization and a significant negative correlation ($r = -0.72$) in deeper waters (> 1500 m depth) was suggestive of scavenging as the dominant process at these depths.

Beside the natural sources of DTMs, anthropogenic activities have resulted in enhanced DTMs emissions to the environment over the past centuries. Lead has a strong anthropogenic signal as a result of the combustion of leaded fuel and coal. Presented here is the first combined DPb, labile Pb (LpPb) and particulate Pb (PPb) distributions from the Celtic Sea since the phasing out of leaded fuel in Europe. Concentrations of DPb in surface waters have decreased by 4-fold over the last four decades. Nevertheless, a distinct anthropogenic Pb signal was observed from the Mediterranean Sea at intermediate depths, showing that Pb can transported over long distances (>2500 km). Benthic DPb fluxes exceeded the atmospheric Pb fluxes in the region, indicating the importance of sediments as a contemporary Pb source. A strong positive correlation between DPb, PPb and LpPb indicates a dynamic equilibrium between the phases and the potential for particles to 'buffer' the DPb pool.

This study highlights the requirements of continuing efforts in regulating Pb emissions but also of detailed seasonal TMs studies in coastal systems in future. Results reported here provide insights into distinct biogeochemical processes in oceanographically dynamic shelf seas and demonstrates the potential of Pb in constraining ocean circulation patterns.

Table of Contents

Table of Contents i
Table of Tables v
Table of Figures vii
Academic Thesis: Declaration Of Authorship xv
Acknowledgements xvii
Definitions and Abbreviations xix
Publications, Presentations, Awards and Fieldwork xxi
Chapter 1 Introduction 1
1.1 History 2
1.2 The role of trace metals in marine organisms 2
1.3 Biogeochemistry of trace metals in the global ocean 4
1.3.1 Nutrient-like trace metals 4
1.3.2 Scavenged type trace metals 5
1.3.3 Hybrid type metals 6
1.4 Sources and sinks of trace metals 7
1.4.1 Deep oceanic waters and internal recycling 7
1.4.2 Rivers 7
1.4.3 Atmosphere 9
1.4.4 Sediments 10
1.4.5 Hydrothermal vents 11
1.4.6 Biological uptake and scavenging 12
1.4.7 Organic matter complexation 13
1.5 Shelf seas and the marine cycle of trace metals 13
1.5.1 Shelf sediments as a source of trace metals 14
1.5.2 Trace metals transport within nepheloid layers 15
1.5.3 Anthropogenic impact on trace metals distributions in marine environment 16
1.6 Aims and hypotheses 19
Chapter 2 Methods 21
2.1 Introduction 22
2.2 Study region and sampling plan 22
2.3 Clean procedures 23
2.3.1 Acid washing 23

2.3.2 Seawater Sampling and sample acidification....24
2.3.3 Handling....25
2.4 Dissolved trace metals analysis....25
2.4.1 Sample pre-concentration: SeaFast automated system....25
2.4.1.1 Reagents....25
2.4.1.2 Spike solutions....26
2.4.1.3 Seawater sample preparation....27
2.4.1.4 Preconcentration resin....27
2.4.1.5 Sample pre-concentration....28
2.4.1.6 Blanks 30
2.4.2 Sample analysis: Inductively Coupled Plasma Mass Spectrometry (ICP-MS)....31
2.4.2.1 Reagents....31
2.4.2.2 Spike solutions: ICP-MS....32
2.4.2.3 Tuning 32
2.4.2.4 Analysis....32
2.4.2.5 Corrections....32
2.4.2.6 Calculation of elemental concentrations....34
2.4.2.7 Data exclusion....36
2.4.2.8 Unit conversion....36
2.4.2.9 Mean concentrations of dissolved trace metals....37
2.4.3 Linear correlations (Pearson), one way ANOVA and least significant difference tests37
2.4.4 Seasonal mixed layer depth....38
2.5 Other analytical methods....38
2.5.1 Dissolved Aluminium analysis....38
Chapter 3 A seasonal study of dissolved Cd, Zn, Co, Ni and Cu in North East Atlantic shelf seas.39
3.1 Introduction....40
3.2 Materials and methods....41
3.3 Results....42
3.3.1 Hydrography....42
3.3.2 Principal component analysis....48
3.3.3 Macronutrient distributions....48
3.3.4 Trace metals distributions....54
3.4 Discussion....59

3.4.1 Continental shelf break 60

3.4.1.1 Seasonal variability in surface waters 61

3.4.1.2 DCd, DZn DAl and DCo relationship with PO_4^{3-} in full depth profiles 63

3.4.1.3 Ni and Cu relationship with macronutrients 67

3.4.2 Continental shelf system 67

3.5 Summary and conclusions 73

Chapter 4 Biogeochemical process controlling manganese and cobalt distributions in European Shelf Seas 75

4.1 Introduction 76

4.2 Materials and methods 78

4.3 Results and discussion 79

4.3.1 Hydrography 79

4.4 Distributions of DCo and DMn 82

4.4.1 Relationship between dissolved cobalt and manganese with phosphate 84

4.4.2 DMn spatial variability in surface waters 86

4.4.3 DMn minima within MOW 87

4.4.4 Benthic source of DMn and DCo 88

4.4.4.1 Continental shelf sediments 88

4.4.4.2 Continental shelf break nepheloid layers 91

4.4.4.3 Subsurface dissolved Mn plumes 94

4.5 Summary and conclusions 95

Chapter 5 Anthropogenic Signatures of Lead in The Northeast Atlantic 97

5.1 Introduction 98

5.2 Study region, materials and methods 99

5.3 Results and discussion 100

5.3.1 Long range Pb transport in MOW 102

5.3.2 Sediment release of particle reactive element 105

5.3.3 Recent Pb sources in the NE Atlantic shelf region 109

5.4 Conclusions 110

Chapter 6 Conclusions 115

6.1 Hypothesis 1 revisited: 115

6.2 Hypothesis 2 revisited: 116

6.3 Hypothesis 3 revisited: 117
6.4 Future work 119
Appendix A Other methods 121
A.1 Other analytical methods 122
A.1.1 Dissolved iron 122
A.1.2 Particulate and leachable trace metals analysis 122
A.1.3 Trace metal aerosol sample collection, digestion and analysis 123
A.1.4 Radium isotopes sampling and analysis 125
A.1.5 Extended Optimum Multiparameter (extOMP) analysis 125
A.1.6 The propagation time of Mediterranean Outflow Water 126
A.1.7 Macronutrients 127
Appendix B Anthropogenic Signature of Lead in the Northeast Atlantic: original manuscript ... 129
References 139

Table of Tables

Table 1. Biochemical functions of metalloproteins within marine phytoplankton (Morel et al. 2003; Twining & Baines 2013). 3

Table 2 Fluxes of trace metals to the Ocean or coastal waters. River fluxes do not take into account estuarine removal processes and atmosphere fluxes represent total (dry + wet) depositional fluxes. 8

Table 3 DMn sedimentary flux estimates in various ocean margin regions. 15

Table 4 Examples of trace metals commercial applications and environmental release 18

Table 5 GEOTRACES reference material results for various trace metals. Dissolved Cd, DCo and DPb are given in pmol kg^{-1} and DNi, DCu, DZn, DMn and DAl are given in nmol kg^{-1}. 37

Table 6 Average concentrations ($\pm \sigma$) of nutrients and metals in the various water masses of the Celtic Sea shelf break region in late autumn (November, DY018), spring (April, DY029) and summer (July, DY033). Nitrate and nitrite (NO_x^-), phosphate (PO_4^{3-}) and silicic acid (SiO_4^{4-}) are in μmol kg^{-1}, dissolved manganese (DMn), nickel (DNi), copper (DCu), zinc (DZn) and aluminium (DAl) are in nmol kg^{-1}, dissolved cobalt (DCo), cadmium (DCd) and lead (DPb) are in pmol kg^{-1}. 51

Table 7 DPb data compilation to date from various European coastal environments. [a] Indicates values extracted from the published figures therefore not representing the exact values reported, [b] indicates measurements by ASV and [c] indicates measurements by GFAAS for the same study. 101

Table 8 Configuration of the input for the extOMP analysis. Source water definitions for the respective parameters were taken from (García-Ibáñez et al. 2015) except were noted - ENACW: Eastern North Atlantic Central Water; MOW: Mediterranean Outflow Water (GLODAPv2); SAIW: Subarctic Intermediate Water; LSW: Labrador Sea Water; NEADW: Northeast Atlantic Deep Water (GLODAPv2). Last rows give the parameter weighting and the stoichiometrical ratio. 126

Table of Figures

Figure 1.1 Profiles of dissolved cadmium (left) and phosphate (right) in the Pacific (red triangles) and Atlantic Oceans (blue squares). Data taken from (Bruland et al. 1978) station 64 (Pacific Ocean) and (Danielsson et al. 1985) station 87 (Atlantic Ocean, 48.3^{o} N, 20.0 ^{o} W).....5

Figure 1.2 Left: profiles of dissolved aluminium in the Pacific (red triangles), Atlantic Oceans (blue squares) and Mediterranean Sea (green circles). Data taken from: station ER-11 (Indian Ocean, 30.0^{o} S, 65.0^{o} E, GI04 section (Thi Dieu Vu & Sohrin 2013)) station 39 (Atlantic Ocean, 2.5^{o} N, 41.7^{o} W, GA02 section, (Middag et al. 2015)) and from (Rolison et al. 2015): station 11 (Mediterranean Sea, 37.4^{o} N, 16.0^{o} E, GA04 section).....6

Figure 1.3 Dissolved cobalt vertical depth profile in the North Atlantic. Data taken from IDP 2017, station 1 (39.7^{o} N, 14.2^{o} W) section GA04, (Rolison 2016).....7

Figure 1.4 Global flux of dissolved manganese from shelf sediments, based on extrapolations of observations from different locations. The method of extrapolation is the same as that used in by Elrod et al. 2004 with dissolved manganese flux in various regions to the global shelf area of 3 x 10^{13} m^2 (Menard & Smith 1966). The data comes from the following sources: Iberian margin (van der Zee et al. 2001), Monterey Bay (Berelson et al. 2003) and (Landing & Bruland 1987), New England margin (Charette et al. 2016), Oregon/Californian coast (McManus et al. 2012) and Peruvian continental margin (Sanial et al. 2017) and (Scholz et al. 2011).....16

Figure 2.1 Station locations across canyon T1_C (white and red circles), spur T2_S (green circles) transects, and on-shelf transect (black circle) during three research expeditions in November (DY018), April (DY029), and July (DY033). Blue diamond represents Penlee Point Atmospheric Observatory (PPAO) station. Map is generated using GeoMapApp, http://www.geomapapp.org (Ryan et al., 2009).....23

Figure 2.2 Structure of the Wako preconcentration resin (Kagaya et al. 2009).....28

Figure 2.3 Schematic set-up of SeaFast system and valve positions. Entire set-up including autosampler unit, syringe system and valve module, blue lines contours indicate sample flow path (A). Sample loading on resin and matrix rinsing, line contours indicate sample and reagent flow (blue: sample, green: de-ionized water, purple: buffer, dark blue: sample-buffer mix) (B). Sample elution step, line contours indicate the flow path of reagents (red: elution acid (EA), orange: 1M

HNO_3 (C). Column conditioning , line contours indicate the flow path of the reagents (green: de-ionized MQ water, purple: buffer, brown: de-ionized water-buffer mix) (D). Figure taken from Rapp et al. 2017.....29

Figure 2.4 Schematic diagram of a sector-field inductively couple plasma mass spectrometer (ICP-MS) (Ring et al. 2016).....33

Figure 3.1. Upper panel (a): salinity distributions along the canyon transects (T1_C, left) and along the spur transects (T2_S, right) in November (DY018) (top), April (DY029) (middle) and July (DY033) (bottom). Bottom panel (b): the percentage distribution of MOW along the canyon (T1_C) and spur (T2_S) transects in November (DY018) (left), April (DY029) (middle) and July (DY033) (left). For the full OMP results see Figure 3.2.....44

Figure 3.2 The percentage distribution of Source Water Types in the Celtic Sea region plotted against depth (a) and potential density anomaly (b) along the canyon (T1_C) and spur (T2_S) transects in November (DY018) (i), April (DY029) (ii) and July (DY033) (iii). ENACW (East North Atlantic Central Water), SAIW (Subarctic Intermediate Water), LSW (Labrador Sea Water), MOW (Mediterranean Outflow Water), NEADW (North East Atlantic Deep Water).....45

Figure 3.3 Plot of principal component loadings of 13 variables (n = 454): salinity, dissolved manganese (DMn), cobalt (DCo), lead (DPb), aluminium (DAl), cadmium (DCd), nickel (DNi), zinc (DZn), copper (DCu), nitrate and nitrite (N+N), phosphate (P), silicic acid (Si), salinity and turbidity on the continental slope of the Celtic Sea over all seasons. Red circles indicate positively correlated groups of variables.....47

Figure 3.4 Salinity distribution along the on-shelf transect (a) in November (top), April (middle) and July (bottom) and (b) vertical depth profile of temperature at station CCS in November (blue diamonds and red squares), April (green triangles and purple horizontal lines) and July (orange crosses and yellow circles).....48

Figure 3.5 Upper panel: phosphate distributions along the canyon transects (T1_C, left), and along the spur transects (T2_S, right), in November (DY018) (top), April (DY029) (middle) and July (DY033) (bottom). Bottom panel: phosphate distributions across the shelf in November (top), April (middle) and July (bottom)..... 49

Figure 3.6 Upper panel: nitrate and nitrite distributions along the canyon transects (T1_C, left), and along the spur transects (T2_S, right), in November (DY018) (top), April (DY029) (middle) and

July (DY033) (bottom). Bottom panel: nitrate and nitrite distributions across the shelf in November (top), April (middle) and July (bottom)..... …….....50

Figure 3.7 Upper panel: silicic acid distributions along the canyon transects (T1_C, left), and along the spur transects (T2_S, right), in November (DY018) (top), April (DY029) (middle) and July (DY033) (bottom). Bottom panel: silicic acid distributions across the shelf in November (top), April (middle) and July (bottom).....53

Figure 3.8 Upper panel: dissolved cadmium distributions along the canyon transects (T1_C, left), and along the spur transects (T2_S, right), in November (DY018) (top), April (DY029) (middle) and July (DY033) (bottom). Bottom panel: dissolved cadmium distributions across the shelf in November (top), April (middle) and July (bottom).....54

Figure 3.9 Upper panel: dissolved nickel distributions along the canyon transects (T1_C, left), and along the spur transects (T2_S, right), in November (DY018) (top), April (DY029) (middle) and July (DY033) (bottom). Bottom panel: dissolved nickel distributions across the shelf in November (top), April (middle) and July (bottom).....55

Figure 3.10 Upper panel: dissolved zinc distributions along the canyon transects (T1_C, left), and along the spur transects (T2_S, right), in November (DY018) (top), April (DY029) (middle) and July (DY033) (bottom). Bottom panel: dissolved zinc distributions across the shelf in November (top), April (middle) and July (bottom).....56

Figure 3.11 Upper panel: dissolved copper distributions along the canyon transects (T1_C, left), and along the spur transects (T2_S, right), in November (DY018) (top), April (DY029) (middle) and July (DY033) (bottom). Bottom panel: dissolved copper distributions across the shelf in November (top), April (middle) and July (bottom).....58

Figure 3.12 Box plots of concentrations of phosphate (a), nitrate and nitrite (b), silicic acid (c), dissolved cadmium (d), nickel (e), copper (f), zinc (g), aluminium (h) and cobalt (i) in November left column of each plot, April middle column and July right column.....60

Figure 3.13 Relationships between phosphate and dissolved cadmium (a), zinc (b), nickel (c) and silicate and dissolved copper (d) for full depth profiles during all seasons. Red squares in plot (b) indicate phosphate concentrations < 0.4 μmol kg^{-1} where the linear correlation was not significant, green squares indicate outliers omitted in the linear analysis. Examination of

relationships between phosphate and dissolved aluminium (e) and silicic acid and aluminium (f) (waters above Mediterranean Outflow Waters). Dissolved aluminium (g) and dissolved cobalt (h) relationship with phosphate in surface waters during all seasons.....62

Figure 3.14 Station locations across GEOTRACES sections: GA03 in 2010 (red circles) (Noble et al. 2015), GA04 in 2013 (green triangles), GA01 in 2014 (black squares) and our study region in 2014 (yellow stars). Map generated using GeoMapApp, http://www.geomppapp.org (Ryan et al. 2009). Station 5 in the Alboran Sea (Western Mediterranean Sea) formed part of the GA04 expedition in 2013.Figure 3.15 Examination of full depth profiles of dissolved cadmium (left) and dissolved zinc (right) along the GA03 GEOTRACES section GA03 section, stations UGT-10-01 – UGT-10-05 (cadmium) and stations UGT-10-03 and UGT-10-05, IDP 2017.....65

Figure 3.15 Examination of full depth profiles of dissolved cadmium (left) and dissolved zinc (right) along the GA03 GEOTRACES section GA03 section, stations UGT-10-01 – UGT-10-05 (cadmium) and stations UGT-10-03 and UGT-10-05, IDP 2017.....66

Figure 3.16 Dissolved copper (left) and dissolved cobalt (right) versus salinity for full depth datasets across the shelf during all seasons. Open symbols indicate data points excluded from the linear analysis.....68

Figure 3.17 Relationship of dissolved Zn (a, c, e) and dissolved Cd (b, d, f) with phosphate in November (DY018) (top), April (DY029) (middle) and July (DY033) (all stations) (bottom) on the continental shelf. Open symbols indicate data points excluded from the linear analysis.....69

Figure 3.18 Dissolved zinc:phosphate (blue) and dissolved cadmium:phosphate (green) ratios at on-shelf stations (J04 - CCS), shelf edge station (CS2) in April and on the continental slope.....70

Figure 3.19 Near surface (< 25 m) concentrations of phosphate (left), dissolved cadmium (middle) and dissolved zinc (right) in November (top) and April (bottom) plotted against the section distance from Site A (0 km), across the shelf (J stations and CCS), shelf break (CS2) and off-shelf transects. In the upper panel J05 and J06 stations are indicated in blue, CCS and CS2 stations in green and off-shelf transects stations in red. Bottom panel J02-J06 stations are indicated in orange, CCS in green, CS2 in blue and off-shelf transects stations in red. Black arrow indicates the shelf break at 200 m isobaths.....71

Figure 4.1. Dissolved manganese distribution plots along (a) the canyon transects (T1_C, left), and along (b) the spur transects (T2_S, right), in November (DY018) (top), April (DY029) (middle) and July (DY033) (bottom). Black lines represent the density range of DMn concentration enhancement within identified nepheloid layers.....80

Figure 4.2 Dissolved cobalt distribution plots along (a) the canyon transects (T1_C, left), and along (b) the spur transects (T2_S, right), in November (DY018) (top), April (DY029) (middle) and July (DY033) (bottom). Black lines represent the density range of DMn concentration enhancement within identified nepheloid layers.....81

Figure 4.3 Dissolved manganese distribution plots along the on-shelf transect in November (DY018) (top), April (DY029) (middle) and July (DY033) (bottom).....82

Figure 4.4 Dissolved cobalt distribution plots along the on-shelf transect in November (DY018) (top), April (DY029) (middle) and July (DY033) (bottom).....83

Figure 4.5. Full depth relationship of dissolved cobalt and phosphate in all seasons. Red squares represent seasonal mixed layer (SML), green diamonds represent East North Atlantic Central Waters (ENACW), blue triangles represent Mediterranean Outflow Waters (MOW) and orange circles represent North East Atlantic Deep Waters (NEADW).....85

Figure 4.6. Sections of turbidity along the on-shelf transect in November (DY018) (top), April (DY029) (middle) and July (DY033) (bottom).....88

Figure 4.7. Sections of turbidity along the canyon transects (T1_C, left), and along the spur transects (T2_S, right), in November (DY018) (top), April (DY029) (middle) and July (DY033) (bottom). Black lines represent the density range of DMn concentration enhancement.....89

Figure 4.8 Upper panel: dissolved manganese (red circles), iron (blue triangles), cobalt (green crosses), turbidity (grey diamonds) and $^{224}Ra_{xs}$ measurements at Site A in November (left), April (middle) and July (left). Bottom panel: particulate manganese (red circles) and cobalt (green crosses) at Site A in November (left) and July (middle) and relationship of particulate manganese and cobalt below thermocline at Site A in April and July (right).....90

Figure 4.9. Upper panel: depth profiles of DMn (left) and $^{224}Ra_{xs}$ (right) at stations S08 (blue diamonds), S09 (red squares) and S10 (green triangles). Bottom panel: turbidity measurements at

stations S08 (left), S09 (middle) and S10 (left) during DY018 (November). Black horizontal lines indicate the density range of elevated concentrations of dissolved manganese and cobalt during DY018 (November).....91

Figure 4.10 Upper panel: vertical depth profiles of dissolved manganese (red triangles) and cobalt (blue diamonds) plotted against potential density anomaly at stations C01 – C04 in November (a-d). Bottom panel: turbidity measurements against potential density anomaly at stations C01 – C04 in November (e-h) and vertical depth profiles $^{224}Ra_{xs}$ measurements at station C03 (green square) and C04 (orange circle) in November. Red horizontal rectangle in both panels indicates the density range of elevated concentrations of dissolved manganese and cobalt. Brown horizontal rectangle indicates elevated concentrations of these metals in bottom waters.....92

Figure 4.11 Particulate manganese (top left and bottom left) and cobalt (right) distribution plots along the canyon transects (T1_C, left), and along the canyon transect in November (DY018) (top) and July (DY033) (bottom). Black lines represent the density range of DMn concentration enhancement within identified nepheloid layers.....93

Figure 5.1 Upper panel: dissolved lead distribution plots (a) along the canyon transects (T1_C, left), (b) along the spur transects (T2_S, middle), and (c) and along the on-shelf transect (left) in November (DY018) (top), April (DY029) (middle), and July (DY033) (bottom). Bottom panel: (d) example of dissolved aluminum distribution plots from November (DY018) along the canyon (T1_C) transect (left) and spur (T2_S) transect (right). For the full dissolved aluminum results please see Figure 5.3. Black lines represent Mediterranean Outflow Water density range contour plots. (e) Reduction of DPb concentrations in the Celtic Sea slope region over the last 30 years. Data are from Brügmann et al. (1985, green circles), Lambert et al. (1991, blue triangles), and Cotté-Krief et al. (2002, yellow squares), and this study is represented by the S08 station in April (DY029) by red diamonds. 100

Figure 5.2 Boxplot of DPb concentrations in four distinctive water masses; seasonal mixed layer, upper waters, MOW and deep waters in all three seasons.....102

Figure 5.3 Dissolved aluminium distribution plots (a) along the canyon transects (T1_C, left), (b) along the spur transects (T2_S, right) in November (DY018) (top), April (DY029) (middle) and July (DY033) (bottom). Black lines represent MOW density range contour plots.....103

Figure 5.4 Propagation time of MOW from Mediterranean Sea to Gulf of Cadiz (black line) and from Gulf of Cadiz to the Celtic Sea continental shelf break (red line) with y-axis representing probability density function.....104

Figure 5.5 DPb (top) and DAl (bottom) concentrations along the salinity gradient across the Strait of Gibraltar, GA04 stations 1 - 4 (red) and this study (yellow). Mediterranean deep water end member concentrations (green) represent GA04 station 5 from the Alboran Sea in close proximity to the Strait of Gibraltar. End member data points were taken below the upper layer inflow of ENACW and above the bottom waters with potential sediment resuspension. Black lines indicate correlations of dissolved metal concentrations and salinity across GA04 stations 1-4 and the Celtic Sea.....106

Figure 5.6. Upper panel: depth profiles of DPb (circles), PPb (triangles), LpPb (squares), turbidity (diamonds), and ^{224}Raxs (crosses) at Site A in November (DY018) (left), April (DY029) (middle), and July (DY033) (left). Bottom panel: depth profiles of DPb (circles), PPb (triangles), ^{224}Raxs (squares), and turbidity (black line) at station C03 (left) and C04 (right) in November (DY018).....107

Figure 5.7 Turbidity measurement plots (a) along the canyon transects (T1_C, left), (b) along the spur transects (T2_S, right) in November (DY018) (top), April (DY029) (middle) and July (DY033) (bottom). Black lines represent MOW density range contour plots.....108

Figure 5.8 Linear correlations between DPb and PPb (top), DPb and LpPb (bottom) at C03:C04 stations in November (> 700 m depth) and Site A in all seasons (below the seasonal thermocline).....110

Figure 5.9 Depth profiles of DPb (red circles), DFe (black squares), DMn (blue triangles) at Site A in November (DY018) (top), April (DY029) (middle) and July (DY033) (bottom).....111

Figure 5.10 (a) The distribution of salinity along the on-shelf transect in November (DY018, top), April (DY029, middle) and July (DY033, bottom). (b) Relationship between DPb and salinity across on-shelf stations at 20 m depth in April (red squares) and July (blue circles).....112

Figure 5.11 DMn concentrations (top) and temperature measurements (bottom) along (a) the canyon transects (T1_C) and (b) along the spur transects (T2_S, right) in November (DY018).....113

Table of Figures

Academic Thesis: Declaration Of Authorship

I, Dagmara Rusiecka declare that this thesis and the work presented in it are my own and has been generated by me as the result of my own original research.

Biogeochemistry of trace metals in European shelf seas

I confirm that:

1. This work was done wholly or mainly while in candidature for a research degree at this University;
2. Where any part of this thesis has previously been submitted for a degree or any other qualification at this University or any other institution, this has been clearly stated;
3. Where I have consulted the published work of others, this is always clearly attributed;
4. Where I have quoted from the work of others, the source is always given. With the exception of such quotations, this thesis is entirely my own work;
5. I have acknowledged all main sources of help;
6. Where the thesis is based on work done by myself jointly with others, I have made clear exactly what was done by others and what I have contributed myself;
7. Parts of this work have been published as:

Rusiecka, D. et al., 2018. Anthropogenic Signatures of Lead in the Northeast Atlantic. *Geophysical Research Letters*. DOI:10.1002/2017GL076825

Signed: .....

Date: .....

Acknowledgements

There are no words to thank people that joined and supported me through this amazing journey...

I will be forever grateful to my supervisors, Eric Achterberg for giving me the opportunity, supervision and continuous guidance, Martha Gledhill for not letting me drown in the sea of the PhD challenges and never-ending enthusiasm for science, Doug Connelly for his supervision and guidance, in particular at the beginning of my PhD in Southampton. Thank you for all your advice and the support.

I would like to acknowledge all the crew and scientists on-board the *RRS Discovery*'. Thank you to the 'Team Fe', Maeve Lohan, Angie Milne, Simon Ussher and Matthew Fishwick for the help with sampling, great company and keeping me sane. In particular to Antony, my partner in crime. The question 'filter or fill' will always bring great memories of hours/days/weeks/months of sampling to Ed Sheeran and Coldplay and exploding pressurised Niskin bottles. Thank you to dirrrrrty Kyle and Amber and your 'I am Titanium remix' during the trace metal clean Titanium CTD casts and all other incredible people that made my time at sea an amazing experience.

Thank you to all my friends in Germany, UK and Poland for the continuous encouragement. In particular to my girls for the amazing support throughout my PhD, Judyta, Ula, Ola, Insa and Anna for always being there for me and being the greatest friend I could ever ask for. To Anna 'Rose' for all the fun times and absolutely amazing memories from my time in Kiel. Kieler Woche 2016 and 2017 will always have a special place in my heart. Thank you to GEOMAR for 'adopting' me for over 3 years and all the people that made me feel welcome.

Finally, thank you to my family for all the encouragement an support but in particular to my mum that always believed in me and stood right my side./ Chciałabym również podziękować z całego serca mojej rodzinie za wsparcie, a przede wszystkim mamie która zawsze we mnie wierzy i jest przy mnie.

I would like to dedicate this PhD thesis to the greatest mum for all her efforts put into my education./ Tą pracę doktorską chciałabym dedykować najwspanialszej mamie na swiecie, mojej mamie, za wszystkie lata ciężkiej pracy nad moją edukacją.

'The capacity to learn is a gift; the ability to learn is a skill; the willingness to learn is a choice'

Brian Herbert

This research was funded by NERC research grant NE/K001973/1.

Definitions and Abbreviations

TMs: Trace metals

DTMs: Dissolved trace metals

Cd: Cadmium

Ni: Nickel

Cu: Copper

Zn: Zinc

Co: Cobalt

Fe: Iron

Mn: Manganese

Cd: Cadmium

Al: Aluminium

Ra: Radium

Th: Thorium

Ac: Actinium

Ti: Titanium

U: Uranium

In: Indium

HNLC: High Nutrient Low Chlorophyll

CA: Carbonic Anhydrase

GFAAS: Graphite Furnace Atomic Absorption Spectrometer

ICP-MS: Inductively Coupled Plasma Mass Spectrometer

ICP-OES: Inductively Coupled Plasma Optical Emission Spectrometer

MC-ICP-MS: Multicollector Inductively Coupled Plasma Mass Spectrometer

FIA: Flow Injection Analysis

DTMs: Dissolved trace metals

TSS: Total Suspended Solids

NOM: Natural Organic Matter

BATS: Bermuda Atlantic Time Series

AMT: Atlantic Meridional Transect

NLs: Nepheloid layers

INLs: Intermediate nepheloid layers

BNLs: Bottom nepheloid layers

ENLs: Enhanced nepheloid layers

SPM: Suspended Particulate Matter

Definitions and Abbreviations

CFC: Chlorofluorocarbon

TTD: Transit Time Distribution

SML: Seasonal mixed layer

ENACW: East North Atlantic Central Water

MOW: Mediterranean Outflow Water

NEADW: Northeast Atlantic Deep Water

LSW: Labrador Sea Water

SAIW: Subarctic Intermediate Water

ExtOMP: Extended Optimal Multiparameter analysis

SSB: Shelf Sea Biogeochemistry

LDPE: Low-density Polyethylene

FEP: Fluorinated propylene ethylene

HCl: Hydrochloric acid

HNO_3: nitric acid

HF: Hydrofluoric acid

UV: Ultra Violet

PP: Polypropylene

PTFE: Polytetrafluoroethylene

UpA: Ultra pure acid

PFA: perfluoroalkoxy polymer

NH_4Ac: Ammonium acetate buffer

EA: Elution acid

ID: Isotope Dilution

HEPA: High efficiency particulate air

MoO: Molybdenum oxide

ME: Multielement

LSD: Least Significant Difference

AB: Acid blank

Publications, Presentations, Awards and Fieldwork

Peer-reviewed publications

Rusiecka, D., Gledhill, M., Milne A., Achterberg, E.P., Annett A.L., Atkinson, S.,… Connelly, D. (2018). Anthropogenic Signatures of Lead in the Northeast Atlantic. *Geophysical Research Letters*. https://doi.org/10.1002/2017GL076825

Rapp, I., Schlosser, C., **Rusiecka, D.**, Gledhill, M., Achterberg, E.P. (2017). Automated preconcentration of Fe, Zn, Cu, Ni, Cd, Pb, Co and Mn in seawater with analysis using high resolution sector field inductively-coupled plasma mass spectrometry. *Analytica Chimica Acta, 976,* 1-13. https://doi.org/10.1016/j.aca.2017.05.008

Birchill, A., Milne A., Woodward, E. M. S., Harris, C., Annett A., **Rusiecka, D.**,… Lohan, M. C. (2017). Seasonal iron depletion in temperate shelf seas. *Geophysical Research Letters, 44*(17), 8987-8996. https://doi.org/10.1002/2017GL073881

Annett, A. L., Birchill, A., Hopkins, J., Homoky, W. B., Thomas, A. L., Milne, A., **Rusiecka, D.**, Achterberg, E. P., Sharples, J., Woodward, E. M. S., Statham, P. J., Lohan, M. C., Geibert, W. (In revision for Nature Geoscience). Large, rapid and persistent input of oxic ocean margin iron by nepheloid layers

Presentations

-08/2017: Goldschmidt 2017 conference oral presentation: 'Anthropogenic Lead as a Signature of Mediterranean Waters in the Deep North Atlantic'

-06/2017: SSB Annual Meeting 2017 poster presentation: '(Un)leaded European shelf seas?'

-12/2016: Invited talk/lecture: 'Human and the environment: chemical oceanography', University of Wroclaw, Poland

-09/2016: Challenger Society 2016 conference oral presentation: ' Contrasting biogeochemical behaviours of trace metals in shelf seas'

-09/2016: Scientific Advisory Board evaluation poster presentation: 'Direct visual observations of nanoparticles in the Celtic Sea'

-04/2016: Ocean Sciences 2016 international conference poster presentation: 'Direct visual observations of nanoparticles in the Celtic Sea'

Awards

-04/2017: ISOS Travel grant Goldschmidt 2017 international conference, Paris, France

-09/2017: 1st place for multidisciplinary workshop, NextGen@Helmholtz 2016 conference, Braunschweig, Germany

-05/2016: ISOS Travel grant Challenger Society 2016 conference, Liverpool, UK

-01/2016: 12 month PhD stipend extension with additional £7000 research expenses awarded by NERC

-09/2015: ISOS Travel grant Ocean Sciences 2016 conference, New Orleans, USA

Oceanographic cruises

10/2014 – 11/2014, *RRS Discovery* (DY017): Southampton – Outer Hebrides – Falmouth

11/2014 – 12/2014, *RRS Discovery* (DY018): Falmouth – Celtic Sea – Southampton

04/2015 – 04/2015, *RRS Discovery* (DY029): Southampton – Celtic Sea – Southampton

07/2015 – 08/2015, *RRS Discovery* (DY033): Southampton – Celtic Sea – Southampton

Chapter 1 Introduction

Preface

Our understanding of the biogeochemical cycles of iron (Fe) has improved substantially over the last decades, yet other trace metals have not received as much scientific attention despite their fundamental biological roles for marine organisms. To address the current gaps in our knowledge, this PhD thesis examines specific biogeochemical processes determining the distributions of the dissolved trace metals, aluminium (Al), cadmium (Cd), nickel (Ni), copper (Cu), zinc (Zn), manganese (Mn), cobalt (Co), lead (Pb) in the Celtic Sea shelf environment over three seasons, thus providing insights into trace metals cycling in an oceanographically dynamic shelf system. This project forms part of a work package that studies the benthic and pelagic physico-chemical speciation of Fe in the Celtic Sea and potential of the off-shelf transport within large Shelf Sea Biogeochemistry (SSB) Programme. The overall aim of the SSB Programme is to gain insights to carbon and nutrient cycles and their controls on primary production in the shelf sea environment. The SSB Programme contributes to the GEOTRACES Programme as a process study.

The aim of chapter 1 is to provide the reader with a broad overview of biogeochemical cycling of several trace metals in the marine environment. Each metal has unique chemical properties and different sources and sinks. They are subject to specific processes related to chemical complexation, biological uptake and consequently feature unique relationships with one another, macronutrients and phytoplankton species. Further, in-depth discussion of distinct processes influencing the biogeochemistry of trace metals in the Celtic Sea region are described in chapters 3 – 5. Certain metals are chosen as examples to describe specific biogeochemical processes, in Chapter 1. Although this PhD thesis does not focus on the Fe biogeochemistry, in some instances Fe, due to its complex marine cycling, is also included to compare and contrast the observations made in this PhD project. For in depth description of physico-chemical speciation of Fe in the Celtic Sea region reader is referred to the PhD thesis by A.Birchill (2017).

1.1 History

Our understanding of marine concentrations and distributions of trace metals has expanded tremendously since the early 1970s. This major advance in knowledge was associated with improvement in analytical chemistry and ultra sensitive instrumentation along with implementation of trace metal clean techniques. The progress in analytical techniques started with the introduction of the graphite furnace atomic absorption spectrometer (GFAAS) in 1969, as the first instrument which provided a sensitivity high enough to measure sub-nanomolar trace metal concentrations (L'vov 1969), which are typical for the open ocean. The more recent development of inductively coupled plasma mass spectrometry (ICP-MS) in 1983 offered even lower sensitivities, greater precision and analysis speed along with simultaneous multielemental analysis (Longerich 2012). Additionally to these 'shore-based' instruments, portable methods such as stripping voltammetry and flow injection analysis (FIA) provided an opportunity for shipboard analysis (Obata et al. 1993). Due to the ultra-low oceanic levels of TMs (Bruland & Lohan 2004), contamination risk during sampling, sample handling and analysis is exceptionally high. These issues led to development of TM clean working practices, specialised equipment (TM clean sampling rosettes, laminar flow hoods) and laboratories with highly sensitive analytical instrumentation.

1.2 The role of trace metals in marine organisms

Over the past four decades extensive experimental and field studies have revealed the bioessential character of some TMs and thus their potential to control primary production and the community structure of marine phytoplankton (Martin & Fitzwater 1988; Martin et al. 1990; Tsuda et al. 2003; Landry et al. 2000; Browning et al. 2017; Moore et al. 2013). Iron has received the most attention out of all TMs, because in some oceanic regions the Fe concentrations in surface waters are sufficiently low to be limiting to phytoplankton growth (Moore et al. 2013). These regions are characterised by high nitrate and low chlorophyll (HNLC) conditions, where Fe concentrations are depleted relative to other nutrients leading to limitations of phytoplankton community growth. Natural fertilization in the form of atmospherically deposited Fe enriched volcanic ash has been observed in Fe depleted surface waters of the N. Atlantic and N. Pacific Ocean (Achterberg et al. 2013; Olgun et al. 2011). In these oceanic systems, a substantial decline in nitrate concentrations coincided with an increase in chlorophyll concentrations indicative of Fe stress. Recent evidence from the South Atlantic gyre suggested that some regions can be Fe and nitrate co-limited and that only simultaneous addition of both nutrients can stimulate the phytoplankton growth (Browning et al. 2017). Interestingly, subsequent addition of Co or

Table 1. Biochemical functions of metalloproteins within marine phytoplankton (Morel et al. 2003; Twining & Baines 2013).

Metal	Protein	Role
Fe	Cytochromes	Electron transport in photosynthesis and respiration
	Ferrodoxin	Electron transport in photosynthesis and nitrogen fixation
	Nitrate and nitrite reductase	Nitrate to ammonia conversion
	Nitrogenase	Nitrogen fixation
	Catalase	Hydrogen peroxide to water conversion
	Peroxidase	Reactive oxygen species reduction
	Superoxide dismutase	Superoxide disproportionation to hydrogen peroxide and oxygen
Zn	Carbonic anhydrase	Carbon dioxide hydration and dehydration
	Alkaline phosphatase	Phosphate esters hydrolysis
	Superoxide dismutase	Superoxide disproportionation to hydrogen peroxide and oxygen
Mn	O_2 – evolving enzyme	Water oxidation during photosynthesis
	Superoxide dismutase	Superoxide disproportionation to hydrogen peroxide and oxygen
Ni	Urease	Urea hydrolysis
	Superoxide dismutase	Superoxide disproportionation to hydrogen peroxide and oxygen
Cu	Plastocyanin	Photosynthesis electron transport
	Cytochrome oxidase	Mitochondrial electron transport
	Superoxide dismutase	Superoxide disproportionation to hydrogen peroxide and oxygen
Co	Vitamin B_{12}	Carbon and hydrogen transfer reactions
	Carbonic anhydrase	Carbon dioxide hydration and dehydration
Cd	Carbonic anhydrase	Carbon dioxide hydration and dehydration (observed only in diatoms)

Co-containing vitamin B_{12} further enhanced the chlorophyll concentrations, suggestive of an important role of other TMs. Several other elements, in particular first row transition metals, manganese (Mn), cobalt (Co), nickel (Ni), copper (Cu), zinc (Zn) are also bioessential and form active centres in metabolically vital metalloenzymes (Table 1) (Morel et al. 2003). Cobalt, Cd, Zn, Ni and Cu form active sites of vitamins (e.g. cobalamin, Co) or enzymes such as carbonic anhydrase (Zn, Co, Cd), urease (Ni) and plastocyanin (Cu) required in vital metabolic functions such as uptake and assimilation of inorganic carbon and urea (Morel et al. 2003). Additionally, biogeochemical cycles of Zn, Co, and Cd are linked through the biochemical replacement of one another within carbonic anhydrase (CA) (Sunda & Huntsman 1995). On the other hand, low Zn concentrations can accelerate the uptake rate of other trace metals, such as Co (Sunda &

Huntsman 1995) and Cd (Sunda & Huntsman 1998a). However, some TMs at high concentrations can also have a toxic and thus inhibitory effect on phytoplankton growth. Free Cu^{2+} ions are extremely toxic to marine organisms (Gledhill et al. 1997) at relatively low concentrations (10^{-10} M; (Sunda et al. 1987)) and (section 1.4.7), whilst eg. Pb has no biological function but is one of the most toxic elements (WHO 1995) (section 1.5.3). Therefore, there is growing evidence for the important biological roles of TMs other than Fe and because their marine cycles are closely interlinked, they should not be considered as individual entities. Furthermore, trace metals potentially influence the primary productivity and global carbon cycle through their bioessential role in phytoplankton biological functions. These aspects are further discussed in section 1.4.6 and Chapter 3.

1.3 Biogeochemistry of trace metals in the global ocean

Seawater concentration profiles of most TMs have been measured in all oceanic basins providing insights into their biogeochemical cycles. Seawater samples are usually filtered through 0.4 or 0.2 μm membranes in order to separate smaller and thus potentially more bioavailable species referred to as 'dissolved' from the 'particulate' fraction which is more inert with respect to uptake by phytoplankton. Dissolved trace metals (DTMs) have been classified according to their oceanic vertical depth profiles into: 'nutrient-like' (eg. DCd, DZn, DNi, DCu), 'scavenged-type' (eg. DAl, DMn, DPb) and 'hybrid-type' (DFe, DCo, DMn, DCu) (Bruland & Lohan 2004).

1.3.1 Nutrient-like trace metals

The distributions of dissolved nutrient-like DTMs eg. DCd, DZn, DCu, DNi resemble vertical depth profiles of the major macronutrients (nitrate, phosphate and silicic acid), with depleted concentrations in surface waters due to biological uptake and enhanced concentrations with depth as a result of remineralization and dissolution of sinking organic matter (Chapter 3). Nutrient-like TMs, similarly to macronutrients, are not susceptible to scavenging processes in deep waters resulting in relatively long residence time of 40 000 – 50 000 years (Bruland 1980). Consequently, their concentrations increase along the global ocean conveyor belt, as the deep ocean waters age, and are distinctively higher in the older deep Pacific Ocean relative to the younger deep Atlantic Ocean. As evident from Figure 1.1, strong interbasin fractionation is observed in the vertical distributions of dissolved DCd, perhaps the most striking example of a nutrient-like metal in the oceans. Boyle et al. (1976) reported the first cadmium distribution in seawater and demonstrated a strong correlation of DCd with phosphate. Since then, remarkably strong correlations with macronutrients of other nutrient-like TMs have been observed

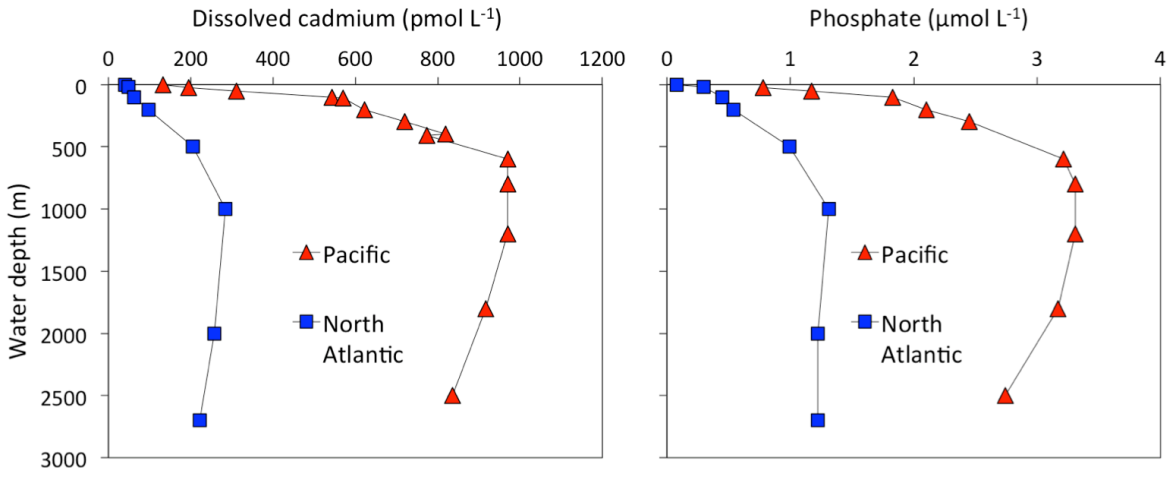


Figure 1.1 Profiles of dissolved cadmium (left) and phosphate (right) in the Pacific (red triangles) and Atlantic Oceans (blue squares). Data taken from (Bruland et al. 1978) station 64 (Pacific Ocean) and (Danielsson et al. 1985) station 87 (Atlantic Ocean, 48.3° N, 20.0° W).

throughout the global ocean, in the North Atlantic (Cd: Roshan & Wu 2015; Wu & Roshan 2015; Yeats 1998), South Atlantic (Cd: Xie et al. 2015; Zn: Wyatt et al. 2014), Pacific (Cd: Boyle et al. 1976; Boyle 1988; Bruland 1980; Bruland et al. 1978; Roshan et al. 2017), Indian (Cd: Saager et al. 1992), and Southern Oceans (Cd, Zn: Saito et al. 2010). Consequently, nutrient-like TMs have been used as paleoproxies for nutrient content of deep waters in the past (Boyle 1988). The fossil record of e.g. Cd that strongly correlates with macronutrients in the present ocean may serve as an indirect proxy of past nutrient conditions. Cadmium/calcium ratio in benthic foraminifera can trace back past Cd concentrations, and through correlation with phosphate, can allow estimations of macronutrient concentrations in the in the water column.

1.3.2 Scavenged type trace metals

The scavenged-type metals such as Al, Mn and Pb, have strong interactions with particles resulting in a short residence time of < 100 – 1000 years in deeper waters (Bruland & Lohan 2004) and 3 – 5 years in surface waters (Orians & Bruland 1986; Bacon et al. 1976; Nozaki et al. 1976)) (Chapter 4 and Chapter 5). In many ocean regions, scavenged-type metals exhibit surface water maxima due to atmospheric inputs and photoreduction dissolution processes in case of redox sensitive metals (e.g. Mn, (Sunda et al. 1983; Sunda & Huntsman 1988)). Dissolved Al is probably a prime example of scavenging-type metals in the global ocean. It is the third most abundant element in the Earth's crust (Taylor 1964) yet it is present at nanomolar concentrations in seawater (Bruland & Lohan 2004) (Figure 1.2) as a consequence of particle scavenging which acts as a strong removal mechanism for the Al dissolved pool. The distributions of scavenged-type dissolved metals are driven by proximity to their major sources such as inputs of atmospheric dust, rivers, sediment resuspension and hydrothermal vents (Bruland & Lohan 2004). Because

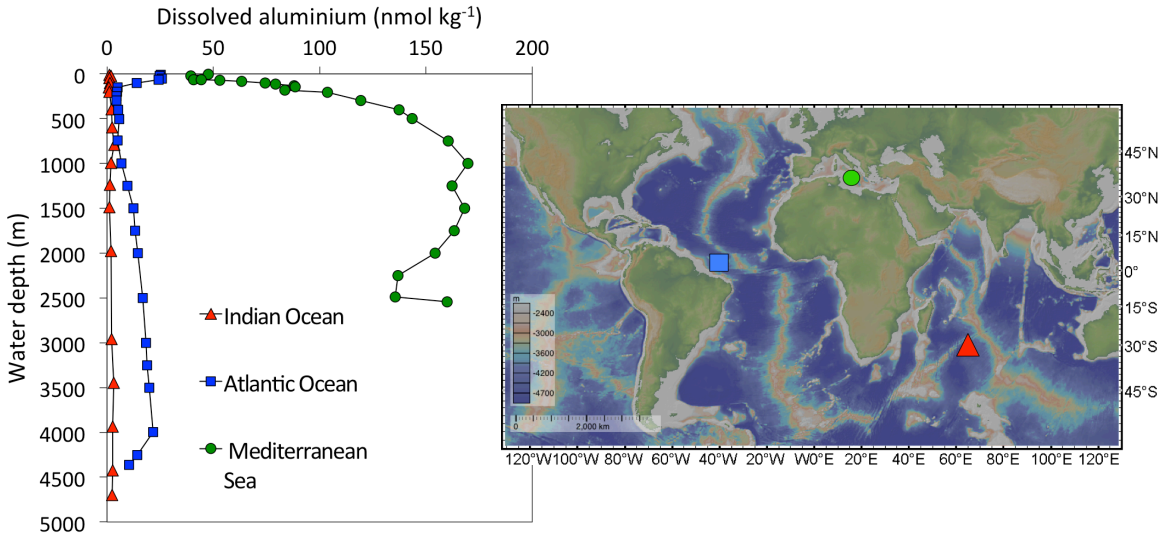


Figure 1.2 Left: profiles of dissolved aluminium in the Pacific (red triangles), Atlantic Oceans (blue squares) and Mediterranean Sea (green circles). Data taken from: station ER-11 (Indian Ocean, 30.0° S, 65.0° E, GI04 section (Thi Dieu Vu & Sohrin 2013)) station 39 (Atlantic Ocean, 2.5° N, 41.7° W, GA02 section, (Middag et al. 2015)) and from (Rolison et al. 2015): station 11 (Mediterranean Sea, 37.4° N, 16.0° E, GA04 section). Right: map showing station locations in the Indian (red triangle), Atlantic Oceans (blue square) and in the Mediterranean Sea (green circles).

these metals have a high particle affinity, their concentrations tend to decrease with distance from the source, thus can be used as source tracers. The main input of DAl to surface ocean is particle dissolution from atmospheric dust, and thus Al has been used to estimate the dust inputs to oceanic surface waters (Measures & Vink 2000). The highest DAl concentrations have been observed in the Mediterranean Sea (up to 80 nmol kg^{-1}) due to inputs from the Saharan desert (Rolison et al. 2015) with a build-up in deeper waters (up to 175 nmol kg^{-1}). Due to the enclosed nature of the basin, DAl concentrations in the Mediterranean Sea are significantly higher relative to the open Atlantic and Indian Ocean basins (Figure 1.2). Furthermore, in contrast to the nutrient-like metals, DAl concentrations in the Atlantic Ocean are elevated (Middag et al. 2015) in comparison to the Indian Ocean. Basin fractionation of DAl is likely a consequence of higher dust inputs over the Atlantic, Al particle affinity and progressive scavenging during water mass transport along the global conveyor belt.

1.3.3 Hybrid type metals

Dissolved TMs such as Co, Mn and Fe are subject to biological uptake, remineralization, scavenging processes, with concentrations influenced by the magnitude of their local sources. These elements consequently exhibit hybrid-type vertical distributions (Figure 1.3) (Chapter 4). Similarly to nutrient-like depth distribution (Figure 1.1), DCo vertical profile is observed to have low (picomolar) concentrations in surface waters (due to biological uptake) that increase with depth (through remineralization of sinking organic particles) and decrease in deeper waters, due

to scavenging processes, similarly to scavenged type depth distributions (Figure 1.2). Hybrid-type vertical distributions of DCo have been observed in continental margin regions, Benguela-Angolan margin (Noble et al. 2012), Central California coast (Biller & Bruland 2013), Mauritanian and New England coastal waters (Noble et al. 2017). In contrast, DMn vertical depth profiles exhibit surface maxima as a result of photochemical reduction of particulate MnO_2 to Mn(II), which retains Mn in solution, with scavenging at depth. However, as a result of sedimentary inputs, DMn concentrations may increase towards the seafloor (Laës et al. 2007).

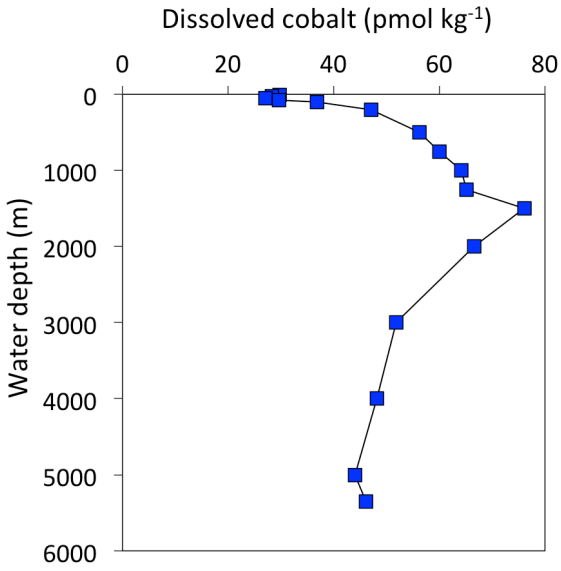


Figure 1.3 Dissolved cobalt vertical depth profile in the North Atlantic. Data taken from IDP 2017, station 1 (39.7° N, 14.2° W) section GA04, (Rolison 2016).

1.4 Sources and sinks of trace metals

1.4.1 Deep oceanic waters and internal recycling

Remineralisation of sinking particles in the oceanic waters is a primary source of nutrient-like DTMs such as Cd, Zn, Ni and Cu to the water column. Metals are assimilated within biogenic particles in surface waters that sink and remineralize in deeper waters subsequently releasing DTMs and macronutrients. Nutrient-rich deeper waters can return to surface waters through vertical mixing, upwelling and winter overturning (Biller & Bruland 2013; Porter et al. 2016; Birchill et al. 2017). Similarly to macronutrients, TMs undergo multiple cycles in the water column until eventual export to sediments in the form of larger particles or particle aggregates (Hutchins & Bruland 1994).

1.4.2 Rivers

The average concentrations of DAl, DMn and DFe in rivers is in the micromolar range, which is three orders of magnitude higher relative to the nanomolar concentrations observed in the global ocean (Gaillardet et al. 2003; Bruland & Lohan 2004). The significant decrease in DTM concentrations across the river-sea interface is a reflection of estuarine removal mechanisms with

complex chemical processes such as flocculation, salting-out and sedimentation (Boyle et al. 1977). In river waters DTMs are mostly present as colloids (0.02 – 0.2 μm) that are organically coated and slightly negatively charged (Howard 2005). Once DTMs enter more saline estuarine environment with higher ionic strength, compression of the colloidal double layer and immediate precipitation occur (Boyle et al. 1977). For example, a significant decline in DMn concentrations from 729 to 36.4 nM (95%) in the Severn estuary has been observed in the freshwater to seawater interface (Morris 1984). However, estuarine flocculation of DTMs does not necessarily mean complete removal of dissolved species as portion of the suspended particulate matter may remain in suspension in the form of colloids (Gustafsson et al. 2000; Mayer 1982). Additionally, in the coastal environment particulate TMs may be released back to the water column through several processes including diffusive benthic inputs of redox sensitive metals (Mn, Co, Fe, Cu) (Froelich et al. 1979; Stockdale et al. 2010; Heggie & Lewis 1984) and sediment resuspension (Laës et al. 2007) and/or stabilized by the organic matter (Rue & Bruland 1995) and thus, may be available for transfer to the open ocean (Noble et al. 2017; Laës et al. 2007). Therefore, the total fluvial flux to coastal environment can still be significant (Table 2). However, the estimation of fluvial fluxes of TMs is difficult due to complexity of estuarine processes and scarce sampling of the major systems that requires specialised equipment and TM clean techniques.

Table 2 Fluxes of trace metals to the Ocean or coastal waters. River fluxes do not take into account estuarine removal processes and atmosphere fluxes represent total (dry + wet) depositional fluxes.

Element	River (kmol yr^{-1}) [a]	Atmosphere (μmol m^{-2} yr^{-1}) [b]		Sediments (μmol m^{-2} yr^{-1})
		Open ocean	Coastal/Seas	
Al	44 444	100 - 2000	590 – 10 000	-
Cd	26.7	0.21- 0.80	0.20 - 38	-
Pb	14.5	0.068 – 7.0	0.01 – 4.5 [c]	9.9 – 15.0 [c]
Mn	23 133	0.73 – 10.4	10 - 170	140 – 4850 [d]
Fe	44 265	132 - 600	220 - 4570	17 – 1570 [e,f,g]
Co	93.4	0.042 – 0.46	0.6 – 6.6	100 [f]
Cu	866	0.63 – 16	5.0 - 205	-
Ni	511	1.4 – 1.5	6.3 - 66	1.6 ± 0.6 [g]
Zn	352	0.37 – 21	50 - 1370	2.4 ± 0.79 [g]

[a] (Gaillardet et al. 2003), [b] Atmosphere: (Mason 2013 and references therein), [c] Rusiecka et al. 2018, [d] (van der Zee et al. 2001; Berelson et al. 2003; Landing & Bruland 1987; Charette et al. 2016; McManus et al. 2012; Sanial et al. 2017; Scholz et al. 2011), [e] (Elrod et al. 2004), [f] (Sanial et al. 2017), [g] (Warnken et al. 2001).

1.4.3 Atmosphere

The atmosphere is one of the main sources to the surface ocean of land derived bioessential metals such as Fe, Mn and Co (Jickells 2005; Rijkenberg et al. 2014; Noble et al. 2017) and a major source of Al and Pb (Measures et al. 2008; Middag et al. 2015; Wu & Boyle 1997). It is particularly important in remote oceanic regions where it serves as an important way of metal transport to surface waters. A good example are HNLC regions, where Fe availability can affect the primary production (Boyd & Ellwood 2010a). Natural fertilization of Fe-depleted surface waters through volcanic-derived ash particles stimulated phytoplankton growth and nutrient drawdown in the N. Atlantic and N. Pacific (Achterberg et al. 2013; Olgun et al. 2011). The concentrations of DMn are typically elevated relative to deeper waters due to atmospheric Mn inputs, with concentrations maintained by photoreduction processes that alter the redox state of Mn from insoluble Mn (IV) to soluble Mn (II) species (Sunda et al. 1983; Sunda & Huntsman 1988). Aluminium surface waters concentrations are strongly driven by the proximity and magnitude to dust sources. The DAl maximum in surface waters (> 30 nmol kg^{-1}) observed in the Western North Atlantic was associated with long range Atlantic Saharan dust transport (Middag et al. 2015). Lead is another example of atmospherically supplied metal that strongly impacts the surface water concentrations. In contrast to Al, the vast majority of Pb in the atmosphere comes from anthropogenic high temperature activities such as leaded fuel and coal combustion (J. F. Wu & Boyle 1997; Lee et al. 2014). A DPb maximum (~160 pmol kg^{-1}) in surface waters was observed at the peak of the leaded fuel utilization in 1970s when the clean air act was put in place due to toxic Pb properties. Lead concentrations decreased (< 20 pmol kg^{-1}) since the implementation of the leaded fuel phase out process and strict environmental regulations (Boyle et al. 2014; Bridgestock et al. 2016) as a result of lower Pb inputs to the atmosphere.

Various processes influence the surface water concentrations of atmospherically derived metals, including the deposition mechanism, particle source, particle size and distance from the source. The solubility of atmospheric particles varies between the wet and dry deposition mechanisms, with the first delivering more DPb to surface waters (Bridgestock et al. 2016) and the importance of these mechanisms varies temporally and spatially (Powell et al. 2015; Patey et al. 2015; Baker et al. 2013). The solubility of atmospheric particles is strongly related to their source and character, while Al in lithogenic particles is less soluble (0.45%) due to incorporation into refractory aluminosilicate matrices, anthropogenically derived metals (eg. Pb, Zn, Cu) usually adsorbed onto particle surfaces are more soluble (up to 90%) (Jickells et al. 2016; Luo et al. 2008; Thuróczy et al. 2010). Additionally, anthropogenic aerosols are usually dominated by the smaller size particles that therefore can be transported long distances prior to deposition (Jickells et al. 2016).

The estimation of atmospheric fluxes of TMs to surface waters is difficult due to expensive ship deployments and a lack of sufficient number of remote sites across the oceanic basins that would provide routine sampling opportunities. The North Atlantic Ocean has seen routine and long term sampling at eg. Bermuda Atlantic Time Series (BATS) station (Tian et al. 2008), Cape Verde (Patey et al. 2015) and intensive ship sampling (Baker et al. 2013; Powell et al. 2015) delivered by the international SOLAS and GEOTRACES Programmes and the Atlantic Meridional Transect (AMT) time series. Yet, the majority of remote oceanic regions is still heavily under sampled.

The distinct influence of atmospheric inputs of certain DTMs can also be observed at oceanic intermediate depths. Lead and aluminium are excellent examples of atmospherically derived metals that were subducted into the ocean interior and transported long distances (Noble et al. 2015; Measures et al. 2015; Zurbrick et al. 2018; Bridgestock et al. 2018; Rusiecka et al. 2018) Thus, these elements can be used to trace water mass transport and oceanic circulation patterns. These aspects are further discussed in Chapter 5.

1.4.4 Sediments

Sediments of continental shelves and shelf breaks are important source of DTMs to overlying waters with potential subsequent transfer to the open ocean (Elrod et al. 2004; Sanial et al. 2017). As mentioned in previous sections, particles enter coastal waters through the atmosphere and rivers and can ultimately be deposited in sediments. Particulate metals that settle in sediments can return to the dissolved phase of pore waters through reductive dissolution and with potential of subsequent diffusion to water column (Froelich et al. 1979; Klar et al. 2017) or in form of nanoparticle/colloids (Homoky et al. 2013) or via physical resuspension (bottom current, storms, internal tides, tides) (Kalnejais et al. 2007). In sediments oxygen is depleted due to microbial decomposition of organic carbon, which may lead to anoxic conditions (Froelich et al. 1979). As oxygen is depleted, redox reaction utilize alternative electron acceptors (oxidants) in the following energetically favourable order: $O_2 > NO_3^- > Mn^{4+} > Fe^{3+} > SO_4^{2-} > CO_2$ (Froelich et al. 1979). Consequently, this leads to reductive dissolution of insoluble species (Fe^{3+}, Mn^{4+}) and distinctive depth zones in sediments where the maximum concentration of soluble species (Fe^{2+}, Mn^{3+}/Mn^{2+}) is observed (Froelich et al. 1979). Microbial reduction processes can produce large inventories of the soluble metal species in porewaters that can partially (13 – 29% (Sundby & Silverberg 1985)) be released to the water column through diffusion, tidal pumping or sediment resuspension (Elrod et al. 2004; Johnson et al. 1992; Warnken et al. 2001; Klar et al. 2017). From a thermodynamic point of view, it is assumed that the vast majority of the soluble species Fe^{2+} and Mn^{2+} released to oxic conditions in seawater are rapidly oxidised and return to sediments as oxi-hydroxide precipitates (Liu & Millero 2002; Sundby & Silverberg 1985). The magnitude of the benthic TMs inputs to the overlying waters depends on several factors, including sediment and

bottom water oxygen concentrations (Lohan & Bruland 2008), the amount of organic matter (Slomp et al. 1997), pH of sediments (Hong et al. 2011; Atkinson et al. 2007), sediment type (Komárek & Zeman 2004) and the amount of suspended solids.

Manganese and Fe are redox sensitive metals that undergo abovementioned reductive dissolution related to organic matter oxidation in sediments. It has been observed that the redox conditions of sediments and the quantity of organic matter deposited in sediments may determine if the sediments become sufficiently depleted in O_2 and NO_3^- to cause Fe and Mn reduction with subsequent release to overlying water column (Lohan & Bruland 2008; Slomp et al. 1997). Some other TMs, such as Pb are pH sensitive and the Pb solubility increases with decline in pH, and below pH 5, Pb is mostly present as soluble Pb^{2+} species (Marani et al. 1995). However, in particle-rich benthic boundary layers, dissolved species may be adsorbed on particle surfaces and consequently be scavenged (Homoky et al. 2016). Furthermore, two other mechanisms have been shown to maintain dissolved species in oxic seawater. Association of metals with colloids (0.02 – 0.2) that have longer residence time in seawater in comparison to bulk sediment particles due to large surface area to volume ratio and/or organic complexation of metals with dissolved organic compounds, preventing metals precipitation (Boyd & Ellwood 2010; Klar et al. 2017; Homoky et al. 2011; Homoky et al. 2013). Some other bioessential metals (eg. Co) and contaminants (eg. Pb) are associated with Fe/Mn precipitates and thus can also be released along with Fe and Mn following reduction of these elements (Stockdale et al. 2010; Heggie & Lewis 1984; Lee et al. 2015; Noble et al. 2015; Rusiecka et al. 2018). Our knowledge about the mechanisms of benthic release of elements other than Fe and Mn is underdeveloped. Further discussion of sedimentary TMs sources and challenges of flux calculations can be found in section 1.5.1 and sedimentary inputs of Mn and Co are reported in Chapter 4 and of Pb in Chapter 5.

1.4.5 Hydrothermal vents

Submarine hydrothermal activity has been observed in all oceanic basins (Beaulieu et al. 2015) and vents release high concentrations of TMs into the deep ocean (Edmond et al. 1979; Von Damm et al. 1985). When seawater penetrates downward into the fractured Earth's oceanic crust, it is heated up to 400 – 500^o C and chemically modified through reactions with the rocks. At high temperatures fluid rises rapidly back to the deep ocean and is expelled into the overlying waters, often in the form of black smoke. The hydrothermally supplied fluids act as a source of a range of dissolved TM species eg. DMn and DFe but also act as a sink of a range of eg. DPb, DCu. In the Pacific Ocean, elevated DFe, DMn (Hatta et al. 2015) and DAl concentrations (Measures et al. 2015) propagated thousands of kilometres into the ocean interior, whilst concentrations DCu (Jacquot & Moffett 2015) and DPb (Noble et al. 2015) were reduced relative to seawater above and below the plume. The dissolved species released from the hydrothermal vents precipitate

upon contact with significantly colder seawater in form of sulphide and oxide metal rich particles or are scavenged onto particles (Jacquot & Moffett 2015; Noble et al. 2015; Metz & Trefry 1993; Zierenberg et al. 2000; German et al. 1991). Similarly to riverine and sedimentary inputs, metals may remain in solution through organic complexation or in form of colloids and nanoparticles (Sander & Koschinsky 2011).

1.4.6 Biological uptake and scavenging

The main two mechanisms of TM removal from the seawater are active biological uptake or passive scavenging onto particle surfaces. Nitrogen and phosphorus are assimilated and removed from the surface oceanic waters at a so called 'Redfield ratio' (Falkowski 2000) and with more recent acknowledgments of the bioessential roles of TMs, this ratio has been extended to TMs ('extended Redfield Ratio' (Ho et al. 2003)). However, the relationship of TM:C can vary over a few orders of magnitude depending on metals availability in surface waters (section 1.2) (Sunda & Huntsman 1995; Sunda & Huntsman 1998a), phytoplankton species and their biochemical demands (Finkel et al. 2007; Twining & Baines 2013), and/or oceanic regime (Twining & Baines 2013). Finkel et al (2007) showed highly variable Cd:P ratios in various phytoplankton species ranging from almost 50 fold higher in coccolithophore relative to cyanobacteria. Additionally, the biochemical demand of coastal species in comparison to their open ocean relatives can also span over a large range. Furthermore, as discussed in section 1.2, it has been shown that DTMs such as Cd, Co and Zn can replace each other in enzymes (Price & Morel 1990; Morel et al. 1994; Sunda & Huntsman 1995) confirming the complexity of biogeochemical interactions of TMs in the marine environment. Further discussion of TMs and biological interactions can be found in Chapter 3.

Distributions of DTMs such as DPb, DAl, DMn, DCo and DFe are strongly influenced by the passive adsorption onto wide variety of particle surfaces (Bruland & Lohan 2004; Noble et al. 2012) ranging from dead or living biogenic particles, Fe and Mn oxyhydroxides, $CaCO_3$, opal, lithogenic matter (Lam et al. 2015), but also by oxidation by Mn-oxidizing bacteria (DMn and DCo) (Moffett & Ho 1996). The high particle affinity of these metals results in scavenging and hybrid-type vertical depth distributions as described in section 1.3. However, the rates of scavenging and affinity for different type of particle differs between DTMs. Basin scale plumes of DFe, DMn and DCo have been observed in Benguela – Angola oxygen minimum zone (Noble et al. 2012). Interestingly, concentrations of these metals extended to a different degree into the Atlantic, which was associated to specific scavenging rates of each metal. Whilst, DFe was scavenged the fastest (0.0025 km^{-1}), DMn was 2.5 times slower (0.001 km^{-1}) and DCo concentrations gradient did not change significantly away from the coast. The distinctively lower DCo concentration gradient relative to DMn was attributed to either lower DCo concentrations present in seawater, preferential oxidation of DMn relative to DCo or a different degree of complexation of Co.

Although scavenging has been established as one of the key processes controlling DTMs distributions in the marine environment, our understanding of the exact mechanisms is still poorly constrained with consequences for the success of ocean biogeochemical models.

1.4.7 Organic matter complexation

Some bioessential TMs are present in seawater as chelates with metal binding organic ligands, e.g. Fe (Gledhill & van den Berg 1994), Zn (Bruland 1989; Ellwood & Van den Berg 2000) Cu (Coale & Bruland 1988; Buck & Bruland 2005), Co (Saito & Moffett 2001; Saito et al. 2005) Ni (Nimmo & Chester 1993; Nimmo et al. 1989) and Cd (Bruland 1992). Although the exact structure of these complexes is still largely unknown, their crucial roles in marine ecosystems has been shown to control metals concentrations and bioavailability and to reduce metals toxicity. Free Zn^{2+} ions are assumed to be easily assimilated by the phytoplankton species (Sunda & Huntsman 1995), yet up to 98% of the total DZn pool is present as organic complexes, thus potentially influencing Zn bioavailability (Bruland 1989; Ellwood & Van den Berg 2000). In contrast, free Cu^{2+} cupric ions are soluble in seawater but highly toxic to marine organisms (Brand et al. 1986). However, more than 99% of DCu pool is organically complexes, thereby reducing Cu toxicity (Coale & Bruland 1988; Buck & Bruland 2005). On the other hand, organic complexation stabilizes DCo (90%) and DFe (99%), which reduces their susceptibility to particle scavenging and precipitation in seawater and thus, maintains their bioavailable dissolved pools (Saito & Moffett 2001; Rue & Bruland 1995). Therefore, organic complexation plays an important role in distributions and bioavailability of TMs in seawater.

1.5 Shelf seas and the marine cycle of trace metals

Shelf seas cover ~9% of the global ocean area and comprise < 0.5% of its volume, yet feature a 2.5 times greater carbon fixation rate relative to the open ocean (Simpson & Sharples 2012). Coastal systems contribute to 16% of global oceanic primary production and > 40% of the total annual particulate organic carbon export and therefore have a disproportionate impact on the marine carbon cycle (Simpson & Sharples 2012; Muller-Karger et al. 2005). Shelf seas may be an important source of TMs to the open ocean due to their proximity to the major TMs sources (section 1.4). Although the crucial role of various TMs in carbon uptake processes and thus their potential influence in the biological carbon pump have been reported, detailed studies of TMs biogeochemistry in productive shelf sea systems are scarce. Moreover, considering that coastal waters are subject to increasing anthropogenic impacts, with their potential for the off-shelf

transport of bioessential metals and contaminants to the open ocean, detailed shelf sea studies are required.

1.5.1 Shelf sediments as a source of trace metals

Only recently sediments have been recognised as an important, if not major source of bioessential DMn, DCo, DCu, DFe metals but also of contaminants (DPb) to overlying waters (Elrod et al. 2004; Sanial et al. 2017; Laës et al. 2007; Noble et al. 2012; Biller & Bruland 2013b; Rusiecka et al. 2018) (section 1.4.4). Shelf seas, due to their large sediment – water interface have the potential to facilitate high sedimentary fluxes. In case of DFe, shelf sediment may be a greater source than the global atmospheric flux to the ocean (Elrod et al. 2004). Local sedimentary fluxes of DMn, DCo and DPb are reported to exceed the atmospheric inputs to the water column in the Peruvian and Celtic Sea continental margin (Sanial et al. 2017; Rusiecka et al. 2018). Distinct benthic inputs of TMs have also been observed in other marginal regions eg. Angolan (Noble et al. 2012), Bay of Biscay (Laës et al. 2007; van der Zee et al. 2001) Kerguelen Plateau (Bown et al. 2012), Monterey Bay (Berelson et al. 2003; Landing & Bruland 1987) and along the Californian coast (Biller & Bruland 2013; Elrod et al. 2004; McManus et al. 2012).

The benthic fluxes of TMs are difficult to estimate. Beside the complexity of natural processes influencing the benthic TMs release as described in section 1.4.4, a choice of accurate method for the flux measurement may be an important factor (Homoky et al. 2016). Various approaches have been implemented to calculate the sedimentary fluxes of TMs (Table 3). The diffusive benthic flux can be estimated using vertical TM distributions in porewaters, in situ benthic chambers and core chambers incubators, or Radium (Ra) sedimentary input tracer measurements (Homoky et al. 2016). Porewater estimations rely on metal concentration gradient between metal enriched porewaters in sediments and overlying seawater and with the assumption of the Fick's first law of diffusion, a benthic flux can be quantified (Homoky et al. 2016). These estimates assume that diffusion is the only mechanism of metal transport, which may lead to flux underestimation due to influence of other processes such as advection and physical mixing (eg. bottom currents) and biological activity (bioturbation and bioirrigation) (Homoky et al. 2016). Benthic chambers, enclosed containers deployed and maintained over the sediments that directly measure the flux at in situ conditions, tend to take into account the biological aspect but similarly to porewaters measurements, not the physical component (McManus et al. 2012). Radium-224 and ^{223}Ra among several other radioisotopes, have been successfully implemented for the estimations of benthic TM release fluxes. Short-lived ^{223}Ra (11.43 days) and ^{224}Ra (3.66 days) are continuously produced through the decay of thorium (^{227}Th and ^{228}Th) isotopes in sediments as their primary source (Moore 2000). In contrast to particle reactive Th, Ra is soluble in seawater and thus diffusive fluxes can be estimated (Sanial et al. 2017). Considering their short half lives, these radioisotopes

are perhaps the most suitable to calculate recent benthic inputs to seawater. However, short-lived Ra isotopes require high seawater volumes and on-board isotope measurements (Moore 2000).

The magnitude of DMn fluxes estimated in various marginal regions (Table 3) and extrapolated to the global shelf area (3 x 10^{13} m^2, (Menard & Smith 1966)) differ by more than an order of magnitude (Figure 1.4). The uncertainty in the estimate is related to difficulties in accurate flux measurement, the complexity of processes that influence sedimentary inputs, and the variations between geographical areas that span from upwelling regions (Californian coast), Oxygen Minimum Zones (Peruvian margin), slopes with high turbidity (Iberian margin). When a similar approach was applied to DFe flux estimates, the range spanned 2 – 4 orders of magnitude (Birchill 2017).

Table 3 DMn sedimentary flux estimates in various ocean margin regions.

Region	DMn sedimentary flux μmol m^{-2} yr^{-1}	Method	References
Iberian margin	370 - 4850	Pore water	(van der Zee et al. 2001)
Monterey Bay	3560	In situ incubation chamber	(Berelson et al. 2003)
Monterey Bay	140	Sediment traps	(Landing & Bruland 1987)
New England	220	^{228}Ra	(Charette et al. 2016)
Oregon/California	2900 ± 1800	Benthic chamber	(McManus et al. 2012)
Peruvian margin	3300	^{228}Ra	(Sanial et al. 2017)
Peru upwelling	400	Pore water	(Scholz et al. 2011)

1.5.2 Trace metals transport within nepheloid layers

Nepheloid layers (NLs) may enable off-shelf transport of DTMs to the open ocean (Noble et al. 2017; Laës et al. 2007). They can be described as plumes or clouds of suspended particulate matter that occur near the seafloor in bottom waters (benthic NLs (BNLs)) and at intermediate depths (intermediate NLs (INLs)). These phenomenon are typically observed on continental shelves, continental slopes and within submarine canyons due to enhanced physical oceanographic mechanisms generating sediment resuspension, internal tides, internal waves and slope currents in these regions (McCave et al. 2001). Nepheloid layers can propagate off-shelf over long distances along isopycnal surfaces (Gardner et al. 2017), thus serving as a potential

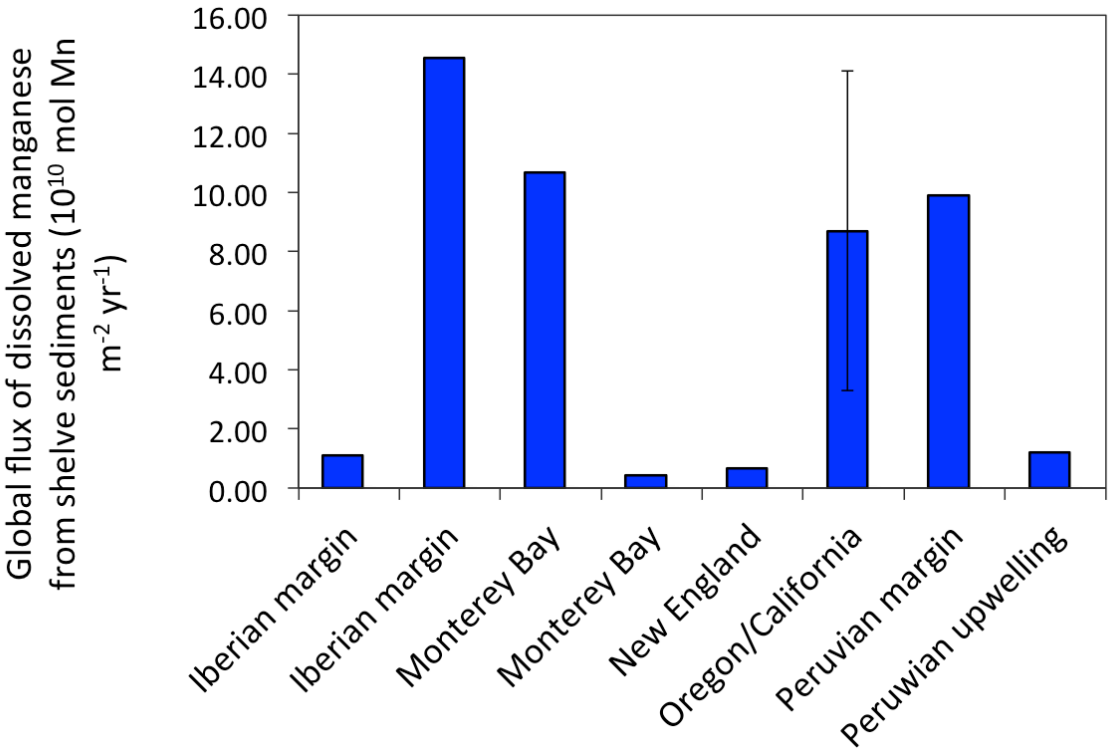


Figure 1.4 Global flux of dissolved manganese from shelf sediments, based on extrapolations of observations from different locations. The method of extrapolation is the same as that used in by Elrod et al. 2004 with dissolved manganese flux in various regions to the global shelf area of 3 x 10^{13} m^2 (Menard & Smith 1966). The data comes from the following sources: Iberian margin (van der Zee et al. 2001), Monterey Bay (Berelson et al. 2003) and (Landing & Bruland 1987), New England margin (Charette et al. 2016), Oregon/Californian coast (McManus et al. 2012) and Peruvian continental margin (Sanial et al. 2017) and (Scholz et al. 2011).

mechanism for the long range transport of TMs to the open ocean. Yet, very little is known about the role of NLs in the off-shore transport of TMs due to their transient and unpredictable nature and scarce sampling opportunities. Recently, commercial bottom trawling activities have been recognised as one of the biggest anthropogenic impacts on the seafloor and consequently a major driver of sediment transport at depths below the reach of storm waves, feeding enhanced NLs (ENLs) to the water column (Martín et al. 2014). Enhanced NLs have an order of magnitude higher concentrations of suspended particulate matter (SPM) in comparison to naturally occurring INLs (Wilson 2016). Therefore, ENLs have the potential to enhance DTMs off-shelf transport. However, this aspect and its environmental consequences is lacking direct observations.

1.5.3 Anthropogenic impact on trace metals distributions in marine environment

Coastal marine ecosystems are subject to enhanced anthropogenic disturbances due to the proximity of persistent and pronounced chronic land based pollution (Halpern et al. 2008) (Table 4), with prediction of the British and Norwegian shelf seas to be the most impacted by humans activities in Europe (Halpern et al. 2008). More than 40% of the global population lives in areas within 200 km of the ocean and 12 out 15 major cities are coastal and host to much of industrial

activity, and with expanding global population and rapidly growing technological requirement of the society this results in increasing chemical pollution (Visbeck 2018). Many of the metals that form the focus of this thesis (Cu, Zn, Cd, Pb, Co) are economically important to society (Table 4), and therefore have been extracted from the Earth's crust and consequently remobilised from their natural phases and released to the environment as a result of industrial processes. These metals enter the marine environment through high temperature processes, fossil fuel combustion, waste water run-off, mining and smelting activities (Wu & Boyle 1997; Garcia-Ordiales et al. 2017; De Vleeschouwer et al. 2007). Lead is one of few elements for which the impact of human activity on the marine environment is clearly evident. It is a toxic element to all living organisms and may cause health impacts upon exposure to high levels (World Health Organization 1995). Yet, humans have introduced large amounts of Pb into environment and anthropogenic perturbation of the natural biogeochemical cycle of Pb in the ocean that dates back to at least ~1850 (Kelly et al. 2009). High temperature activities, coal and leaded fuel combustion serve as major sources of anthropogenic Pb to the atmosphere (Kelly et al. 2009; Wu & Boyle 1997) in the form of fine aerosol particles that can travel long distances, and are deposited in remote ocean areas (Kumar et al. 2014; Véron & Church 1997). Consequently, surface ocean concentrations of DPb reaching >190 pmol kg^{-1} were observed during the peak of the Pb emissions in 1970-80 (Laumond et al. 1984). Anthropogenic Pb has entirely masked signals of naturally sourced Pb (understood to be ca. 2.2 pmol kg^{-1} in surface waters (Henderson & Maier-Reimer 2002)). To date, leaded fuel has been virtually phased out (except in 3 countries, as of March 2017, UNEP), and overall Pb emissions in Europe have decreased by 63% between 2000 – 2015 (European Environment Agency 2017). Consequently, Pb concentrations in surface waters have decreased significantly from ~170 to <15 pmol kg^{-1} (Boyle et al. 2014), leading to natural Pb signatures re-emerging in the North Atlantic (Bridgestock et al. 2016; Zurbrick et al. 2018). Recent findings from the European coastal waters indicated sediments rather than the atmosphere, as a contemporary source of Pb to overlying waters as a result of historical Pb deposition in sediments (Rusiecka et al. 2018). In contrast, surface waters Pb concentrations have increased to > 100 pmol kg^{-1} in the Pacific Ocean (Gallon et al. 2011) and > 80 pmol kg^{-1} in the Indian Ocean (Echegoyen et al. 2014), suggesting an increase of anthropogenic lead inputs to these oceanic basins. Elevated Pb concentrations in these regions are a result of industrialization, late phase-out and limited environmental regulations. The total Pb emissions from Asia in 1989 exceeded those in the U.S. by at least 3 – 4 fold (Bollhöfer & Rosman 2001), and in 2005 Pb emissions from coal combustion in China exceeded those from historical leaded fuel combustion (Lee et al. 2014). The anthropogenic pollution of the natural environment is usually associated with the start of the 'Industrial Revolution' in the mid-nineteenth century. However, recent evidence revealed that Pb pollution can be dated back to the Roman Empire (~2000 years) (De Vleeschouwer et al. 2007; More et al. 2017) with significant decline in Pb inputs that coincided with the time of the Black Death

pandemic in Europe (~1349 – 1353 C.E.) (More et al. 2017). Therefore, the only time when humans reduced atmospheric lead pollution was when the population and thus anthropogenic activities were drastically reduced.

Major anthropogenic sources of other trace metals from mining, smelting and fossil fuel combustion have left a large legacy in the worldwide environment (Garcia-Ordiales et al. 2017) (Table 4). Metals such as Cu, Zn and Pb have been dissipated for centuries into the environment through ore mining and smelting, yet the maximum inputs occurred during the Industrial Revolution in mid-nineteenth century (De Vleeschouwer et al. 2007; Eckel et al. 2002). Although the mining activities have decreased over the last few decades, their continuous inputs to the environment are still significant through uncontrolled release of metals from mining wastes (Delgado et al. 2011; Jabłońska-Czapla et al. 2016; Abraham & Susan 2017).

The economic market for Co has expanded tremendously in recent years through the application of Co in for example lithium oxide cathode based batteries (Scrosati & Garche 2010). Inappropriate disposal of Co based batteries and Co alloys along with burning of fossil fuels and smelting (Kim et al. 2006; Banza et al. 2009) will likely increase in future and potentially serve as an anthropogenic Co source to the marine environment. In case of Pb, the estimation of its natural concentrations is difficult due to severe environmental pollution before any reliable measurements had been taken. In order to avoid the same mistake with Co and other TMs, understanding the natural cycle is critical to allow the assessment of the potential anthropogenic impacts on the marine environment in future.

Table 4 Examples of trace metals commercial applications and environmental release

Metal	Application	Anthropogenic environmental release
Al	Cans, foils, aeroplane parts, alloys with Cu, Mn, Mg, Si	Mining, ore extraction, coal combustion, waste incinerators
Cu	Electrical equipment, coins, motors, roofing, plumbing	Mining, smelting, agriculture, sewage due to the corrosion of copper plumbing.
Zn	Galvanised steel, transportation, bridges, electricity alloys with Ni and Al	Mining, smelting, steel production, coal and waste combustion
Cd	Ni-Cd batteries, electroplating, alloys with Cu	Non-ferrous metal production, stationary fossil-fuel combustion, waste incineration, iron and steel production, cement production
Pb	Leaded fuel, plumbing, paint, batteries ammunition	Leaded fuel and fossil-fuel combustion, waste incineration, production of non-ferrous metals, iron, steel and cement
Ni	Electroplating, alloys with Fe, Al, Si, Cd-Ni batteries, coins	Fuel and coal combustion, mining, waste incineration, sewage sludge, steel manufacture
Co	Co based magnets, turbines, electroplating, paint, batteries Inappropriate battery disposal	Inappropriate battery disposal, coal combustion, mining, ore extraction

1.6 Aims and hypotheses

The overall aim of this study was to provide insights into seasonal biogeochemical seasonal cycling of trace metals (TMs) in the North-West European continental margin. Seawater sampling consisted of three research cruises in the Celtic Sea in autumn (DY018), spring (DY029) and summer (DY033) and land based multielement analysis. This study examines the seasonal and temporal variability of DCd, DZn, DNi, DCu, DCo, DMn, DAl and DPb along full depth sections in the Celtic Sea region. The thesis is based around contrasting biogeochemical behaviours of these metals, and thus split into 3 hypotheses with supporting objectives:

- Hypothesis 1: Off-shelf vertical distributions of DCd, DZn, DNi and DCu in the Celtic Sea strongly correlate with macronutrients over all seasons due to biological uptake and remineralization processes. In shelf waters, DTM distributions de-couple from macronutrients due to multiple TM sources, and modifications in the coastal zone of oceanic and fresh waters.
- Hypothesis 2: Shelf sediments supply DMn and DCo to overlying waters. Off-shelf transport of DMn and DCo within nepheloid layers is a persistent feature at the continental margin.
- Hypothesis 3: DPb concentrations in surface waters have decreased since the last reports (1995) due to the phasing out of leaded fuel in Europe (between 1980 and 2011) and implementation of strict environmental regulations

Chapter 2 Methods

The aim of this chapter is to describe the methods used to determine concentrations of cadmium (Cd), zinc (Zn), nickel (Ni), copper (Cu), manganese (Mn), cobalt (Co), lead (Pb) and aluminium (Al) that form the primary focus of this thesis. Described are also methods used by other researchers and can be found in Appendix A. The results from other researchers were used to support the interpretation of dissolved trace metals results.

2.1 Introduction

Accurate and precise measurements of trace metals (TMs) in seawater are critical to gain insights into their marine biogeochemical cycles. The major challenges associated with this task are related to the extremely low TM concentrations in seawater (10^{-6} – 10^{-12} M), the seawater sample matrix and ubiquitous contamination risks from reagents and plastic labware and during sample collection and handling. As mentioned in Chapter 1, technological advances and implementation of TM ultra-clean techniques (Cutter et al. 2010; Achterberg et al. 2001) have resulted in the collection of reliable, high quality TM data from all oceanic basins. Additionally, extensive efforts have been put into the production of consensus seawater material (SAFe GEOTRACES, http://es.ucsc.edu/~kbruland/) as a robust method to check the accuracy of the results produced by various analytical methods. A thorough description of all critical steps in ultra-clean TM sample collection and handling can be found in the 'Sampling and Sample-handling Protocols for GEOTRACES cruises' (Cutter et al. 2010), here a brief overview of aspects relevant to the work undertaken in this research is provided.

2.2 Study region and sampling plan

Samples for TM analysis were collected on three separate cruises in the European continental shelf and slope region of the Celtic Sea (Figure 2.1), on board the *RRS Discovery.* The study was part of the UK Shelf Sea Biogeochemistry (SSB) Programme. Two off-shelf transects were sampled at a high spatial resolution (7 stations over < 1^{o}). Transect 1 was located along a canyon (T1_C) and transect 2 (T2_S) along a neighbouring spur, ca. 22 km north of T1_C (Figure 2.1). A spur is a lateral ridge or tongue of land descending from a continental shelf, whilst a submarine canyon is a steep valley in the seabed of the continental slope. In comparison to spurs, submarine canyons are known hotspots of sedimentation, particle and water fluxes to the open ocean due to their specific topography (Stoker et al. 1998). Station C15 was included in the sampling plan in April and in July in order to reduce the distance between stations C02 and C03. Subsequently, station C07 was removed from the sampling plan in April in July. Seawater samples collected at station CS2 in July were not analysed. Station A is located on the continental shelf, in close proximity to the Bristol Channel (Figure 2.1) and is a distinctive station due to specific currents and sediment type. Due to bad weather conditions or time constraints, station J05 was sampled only in November, J04 only in April and July, J02 only in April. Repeat sampling was undertaken during three different seasons, November – December 2014 (DY018), April 2015 (DY029), and July – August 2015 (DY033) to investigate processes influencing the distribution of trace metals in this region.

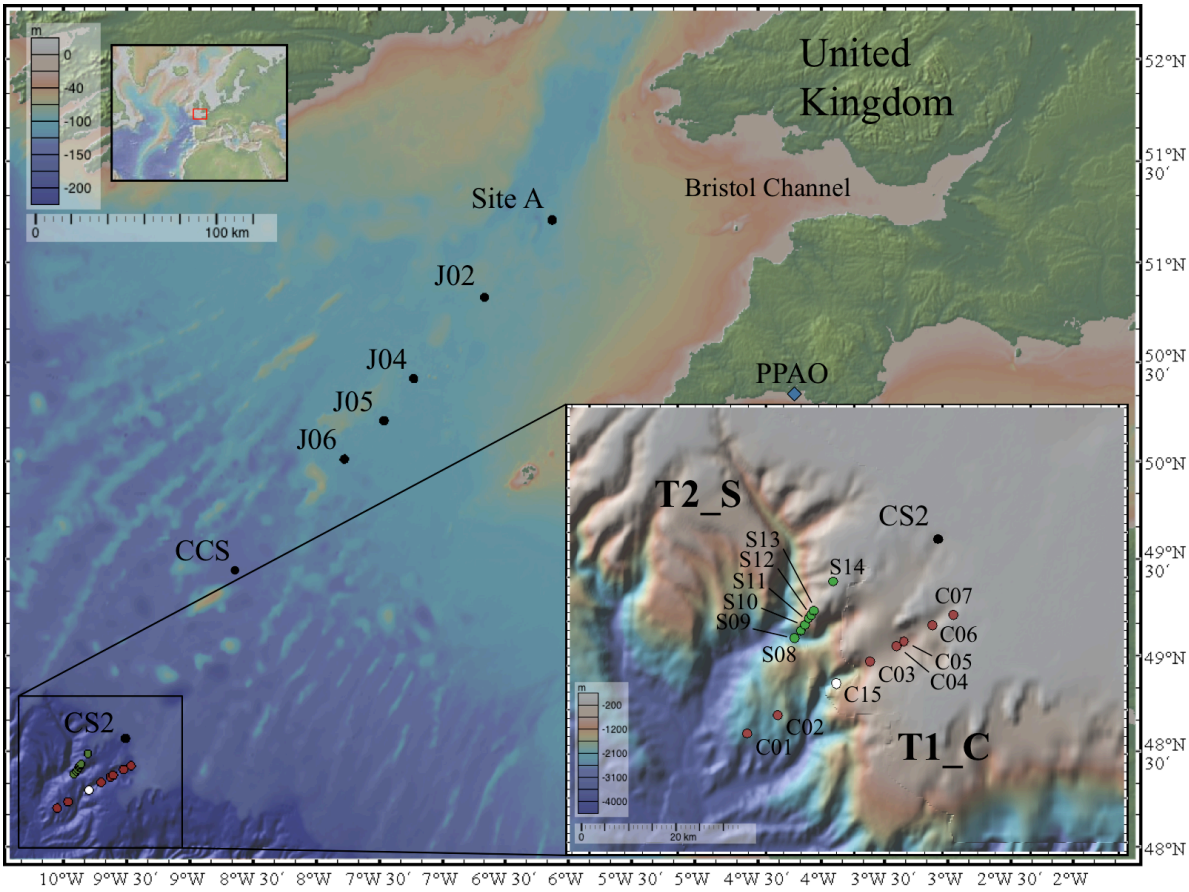


Figure 2.1 Station locations across canyon T1_C (white and red circles), spur T2_S (green circles) transects, and on-shelf transect (black circle) during three research expeditions in November (DY018), April (DY029), and July (DY033). Blue diamond represents Penlee Point Atmospheric Observatory (PPAO) station. Map is generated using GeoMapApp, http://www.geomapapp.org (Ryan et al., 2009).

2.3 Clean procedures

2.3.1 Acid washing

Any material that comes into direct contact with the seawater sample at any stage between sampling and sample analysis, serves as a potential source of TM contamination. Therefore, all materials such as bottles, tubing and filters used in sample processing were acid washed. In this study, all low density polyethylene (LDPE) (Nalgene) sample bottles and any general labware (eg. measuring cylinders) were cleaned via four sequential steps:

(1) Soaked in Mucasol detergent (Sigma Aldrich) for 1-3 days and rinsed 3 times with deionized water (18.2 MΩ cm^{-1}, Milli-Q, Millipore), in order to remove any fat residual on bottle surfaces.

(2) Soaked in 5 M hydrochloric acid (HCl) (reagent grade, Fisher Scientific) for one week and rinsed 3 times with deionized water.

(3) Soaked in 8 M nitric acid (HNO_3) (reagent grade, Fisher Scientific) for one week and rinsed 3 times with deionized water.

(4a) Filled with acidified to 0.02 M HCl (Ultra pure Acid grade, Romil) deionized water.

Acidified sample bottles were stored double-bagged in ziplock bags until sampling at sea. All new fluorinated ethylene propylene (FEP) (Nalgene) bottles used for sample analysis described later in this chapter were cleaned in a similar way (steps 1 – 3) and step 4a was replaced by:

(4b) Soaked overnight (16 hrs) in 1 M HCl (analytical grade, Fisher Scientific) at 45°C followed by UV-irradiated for 4 hours in order to condition the material prior to usage. Bottles were rinsed 5 times with deionized water prior to usage.

This step was added due to significant TM contamination noted when new FEP bottles were not soaked in acid at high temperature and UV-irradiated. No obvious contamination was noted when reusing FEP bottles and therefore, on reuse, FEP bottles were rinsed 3 times with deionized water, filled with acidified to 0.2 M HCl (Ultra pure Acid grade, Romil), UV-irradiated for 2 hours and left to soak for a week.

Polypropylene (PP) 4 ml vials used in preconcentration step described later in this chapter were cleaned prior to use in three sequential steps:

(1) Soaked in Mucasol detergent (Sigma Aldrich) for 1-3 days and rinse 3 times with deionized water, in order to remove any fat residual on vial surfaces.

(2) Heated in 10% v/v HCl (analytical grade, Fisher Scientific) at 45^{o}C overnight (16 hrs) and rinse 3 times with deionized water.

(3) Heated in 10% v/v HNO_3 (analytical grade, Fisher Scientific) at 45^{o}C overnight (16 hrs) and rinse 5 times with deionized water.

(4) Dried upside down inside a class 1000 laminar flow hood bench.

Clean vials were stored double-bagged in ziplock bags until usage.

2.3.2 Seawater Sampling and sample acidification

Trace metal clean Ocean Test Equipment (OTE) sample bottles were always handled wearing vinyl gloves and prepared for sampling by opening the bottles and securing them on the rosette shortly before sampling on the ship's deck. Seawater samples were collected using 24 x 10 L Teflon coated OTE bottles positioned on a titanium (Ti) frame rosette system (housing sensors for conductivity, temperature and depth) and deployed using a Kevlar conducting cable. Samples were collected during the upcast after flushing with seawater during the downcast. On recovery, the OTE bottles taps were protected from the contamination with a dedicated vinyl gloves and transferred immediately into a class 1000 clean sampling laboratory and rinsed thoroughly with deionized water. Then, all OTE bottles were pressurized with filtered (0.2 μm PTFE, Millex-FG 50, Millipore) compressed air. Seawater samples were filtered in-line using a 0.2 μm membrane filter

capsule (Sartorius, Sartobran P) into acid washed 125 ml LDPE bottles. Sample bottles were rinsed three times prior to filling with sample. The Sartobran filters were re-used between samples but always rinsed with at least 0.5 – 1 L of sample before collection. Filters were stored in the fridge between casts and replaced every 3-4 casts. New filters were flushed with at least 10 L of surface seawater prior sampling. All samples were acidified to 0.016 M HCl (pH 1.8 with ultra-pure hydrochloric acid (UpA Romil) under a laminar flow hood and stored double-bagged in ziplock bags until analysis. Diluted acid used for seawater sample acidification was analysed by inductively coupled plasma mass spectrometer (ICP-MS) and its contribution was negligible (<0.1 %) for all TMs.

2.3.3 Handling

Bottles containing seawater samples and reagents, and all acid washed plastic labware were handled with vinyl gloves and stored double-bagged in ziplock bags and opened only in the laminar flow hood bench (ISO 3) in a clean laboratory (ISO 5). When any of the reagents were pipetted, the pipette tip was washed three times with ~3 M HCl (Trace Metal Grade, Fisher Scientific) solution followed by triple rinse with MQ deionized water and one rinse with the required solution.

2.4 Dissolved trace metals analysis

The seawater sample analysis described in this section follows the method described in Rapp et al (2017). However, there were two deviations from the published method and are discussed later in this chapter: lead (Pb) seawater measurements were calibrated using standard addition technique and cadmium (Cd) counts were not corrected for MoO^+ interference. For the purpose of this thesis, all the relevant methods are briefly described in this chapter. For specific methodological details, the reader is referred to the published methods.

The TM analysis consisted of two steps: offline preconcentration using a SeaFast (Sc-4 DX SeaFast pico; Elemental Scientific Inc. (ESI)) automated unit and multielemental analysis using an ICP-MS.

2.4.1 Sample pre-concentration: SeaFast automated system

2.4.1.1 Reagents

All reagents were prepared in deionized water. Nitric acid (SpA, Romil) was purified by single distillation in a sub-boiling perfluoroalkoxy-polymer (PFA) distillation unit (DST-1000, Savillex). The

purity of 1 M the nitric acid was routinely checked before each run on the ICP-MS. Acetic acid and ammonium hydroxide (20 – 22%) were of the highest commercially available purity (Optima, Fisher Scientific). Ammonium acetate (NH_4Ac) buffer (1.5 M) (Milne et al. 2010a; Lagerström et al. 2013; Kagaya et al. 2009) was utilized in the sample preconcentration and was prepared by mixing 140 ml ammonium hydroxide solution with 90 ml of acetic acid solution for 1 L buffer with deionized water. The pH of the buffer was adjusted to pH 8.5 ± 0.05 using either ammonium hydroxide or acetic acid. This solution was always prepared fresh prior to each SeaFast pre-concentration run, used at room temperature and was kept in the fridge when not in use. 1 M HNO_3 was prepared using sub-boiled acid and MQ deionized water. Three solutions of 1 M HNO_3 were prepared for each run: elution HNO_3 (EA) spiked with 250 ng L^{-1} indium (In) for instrumental drift corrections during ICP-MS analysis and TMs elution from the pre-concentration column, HNO_3 used for cleaning the pre-concentration resins, and rinsing HNO_3 used to rinse the autosampler needle between samples. All the reagents were stored in acid washed FEP bottles or PP containers.

2.4.1.2 Spike solutions

Isotope dilution was utilized for quantification of sample and reference seawater concentrations of Cd, Ni, Cu, Zn because these elements have two or more naturally occurring stable isotopes. For Co and Mn, monoisotopic elements, standard addition calibration was employed. In case of Pb, although two stable isotopes ^{207}Pb and ^{208}Pb occur naturally, standard addition calibration was also implemented due to insufficient amount of artificially enriched ^{207}Pb isotope.

Isotope spike

The isotope dilution spike (ID spike) was prepared by Dr. Christian Schlosser by dissolution of solid artificially enriched isotopes (ISOFLEX USA) in concentrated sub-boiled HNO_3 and dilution to 2% HNO_3. Concentrations of each metal were externally calibrated by ICP-optical emission spectroscopy (ICP-OES; 7500 Agilent) and by reverse isotope dilution using a multicollector ICP-MS (MC-ICP-MS; Thermo Fisher Neptune). Spike ratios for $^{60}Ni/^{62}Ni$, $^{63}Cu/^{65}Cu$, $^{66}Zn/^{68}Zn$ and $^{110}Cd/^{111}Cd$ were determined by MC-ICP-MS.

Standard addition solutions

A multielement (Co, Mn, Pb) standard solution was prepared by serial dilution of individual stock standards (CertiPur, Merck) in 0.45 M sub-boiled HNO_3. The final concentrations of standard solution 1 was 0.061 μmol L^{-1} for Mn and 2.828 nmol L^{-1} for Co and Pb and standard solution 2 was 0.61 μmol L^{-1} for Mn and 28.28 nmol L^{-1} for Co and Pb.

2.4.1.3 Seawater sample preparation

Each FEP sample bottle was thoroughly rinsed with few ml of the sample that was discarded prior to pipetting of the sample. Seawater samples were sub-sampled by pipetting (15 ml) into FEP bottles. SAFe GEOTRACES S and D1 consensus materials were prepared with each pre-concentration run to check the accuracy of the method and were treated in exactly the same way as the remaining seawater samples. Every 15th seawater sample, duplicate aliquots were pipetted in order to routinely check the precision of the method. All sample bottles were spiked with 100 µl of diluted ID spike. Every 10th sample, aliquots were pipetted in triplicates and labelled as A – C. Bottles A was treated as a sample and thus were spiked with 100 µl of ID spike, bottle B and C were spiked with 250 µl of standard solution 1 and 2 respectively, and were used as standard calibration points.

Southern Ocean seawater from hereafter referred to as test seawater, was filtered through 0.2 µm pore sized membrane filter (Acropack 500, Pall) into 1 L acid washed LDPE bottles and acidified to 0.016 M HCl (pH 1.8 with ultra-pure hydrochloric acid (UpA Romil) to obtain a pH consistent with the seawater samples. Test seawater was sub-sampled into 7 FEP bottles in the same way as the seawater samples described above and labelled 0 – 6. Bottle 0 was not spiked, the 3 consecutive bottles were spiked with 50 µl, 125 µl and 250 µl of standard solution 1 respectively. Bottles 4 – 6 were spiked with 50 µl, 125 µl and 250 µl of standard solution 2 respectively. This resulted in the 7 point standard addition covering the final concentration range of: 0.009 – 0.464 nmol L^{-1} for Co and Pb and 0.202 – 9.460 nmol L^{-1} for Mn. The test seawater calibration samples were run at the beginning of each pre-concentration run.

Prior to pre-concentration, samples were UV- irradiated by placing tightly closed FEP sample bottles in a home-made UV light box equipped with four low pressure mercury vapour lamps (25 Watt, Philips) for 4 hours. Previous studies have shown that DTMs recovery, in particular for Co and Cu can be reduced due to strong organic complexation of these metals and UV-digestion of the samples effectively break down the organic complexes (Milne et al. 2010). UV-irridiated samples were left to cool down prior to preconcentration.

2.4.1.4 Preconcentration resin

Trace metals were preconcentrated using the Wako chelate resin (Wako Pure Chemical Industries, Japan) with immobilized carboxymethylated pentaethylenehexamine (CM-PEHA) functional groups (Figure 2.2) (Kagaya et al. 2009). The functional groups of the resin were deprotonated/negatively charged over a optimum pH range (6.4 ± 0.2) (Rapp et al. 2017). As the seawater sample was put through the resin column simultaneously with the buffer, TMs were complexed with the negatively charged carboxylic functional groups and tertiary nitrogen atoms

of the resin at the optimum pH. Subsequent elution of TMs was performed with 1 M HNO_3 acid such that the H^+ ions compete for binding sites with TMs and consequently replacing (eluting) all the metals. The recovery of metals from the column exhibited high efficiency for all metals of interest (83 – 100%) except for Mn (60%) and Ni (48%) (Rapp et al. 2017). However, in case of the ID calibration approach for Ni, the isotopic ratio of two $^{60}Ni/^{62}Ni$ remained constant in any of the analytical runs performed in this project. In case of Mn standard addition, a good linear regression (r^2 = > 0.98) was typically observed. Additionally, results of SAFE GEOTRACES reference materials agreed with the published consensus values (Table 5). Thus confirming Wako resin as a suitable preconcentration resin for all metals of interest.

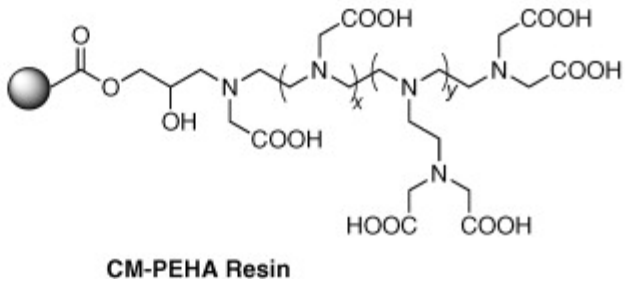


Figure 2.2 Structure of the Wako preconcentration resin (Kagaya et al. 2009).

2.4.1.5 Sample pre-concentration

Seawater samples were pre-concentrated by an automated system (SC-4 DX SeaFast pico; ESI) with online pH buffering and seawater sample matrix removal. Detailed description of the instrumental set-up is provided by Rapp et al. (2017). Briefly the SeaFast automated system consists of 6 reservoirs; elution acid (EA, 1M HNO_3) spiked with In solution, 1 M HNO_3 used to clean the pre-concentration and buffer clean-up resins, de-ionized water, 1.5 M NH_4Ac buffer used to adjust the pH of the sample and two additional 4 L reservoirs containing 1 M HNO_3 used to rinse the sample introduction tubing and valves. Two different resins were used for the sample pre-concentration steps, WAKO (pre-concentration step) and Nobias (buffer clean-up column; ESI). The Wako resin was chosen as the main preconcentration resin due to higher recoveries for Mn and Ni relative to the Nobias resin (Rapp et al. 2017).

Prior to each run, and in particular when fresh buffer was prepared, the exact amount of buffer required to adjust the pH of the sample to 6.4 ± 0.2 was checked. This was done by pre-concentrating 15 ml of test seawater adjusted to the same pH as the sample of interest, and measuring the pH of the waste solution after the sample-buffer mixing step (as described later in

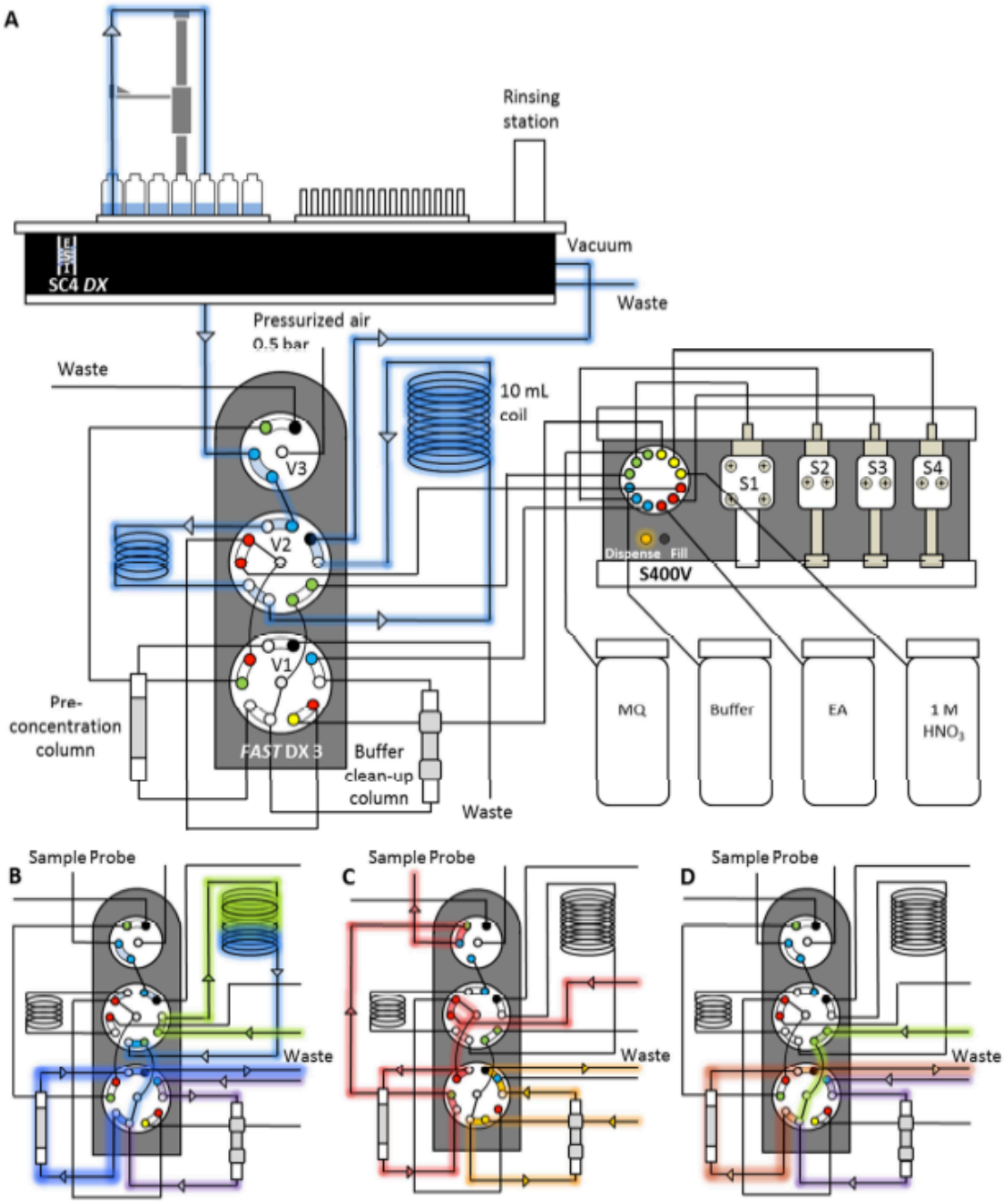


Figure 2.3 Schematic set-up of SeaFast system and valve positions. Entire set-up including autosampler unit, syringe system and valve module, blue lines contours indicate sample flow path (A). Sample loading on resin and matrix rinsing, line contours indicate sample and reagent flow (blue: sample, green: de-ionized water, purple: buffer, dark blue: sample-buffer mix) (B). Sample elution step, line contours indicate the flow path of reagents (red: elution acid (EA), orange: 1M HNO_3 (C). Column conditioning , line contours indicate the flow path of the reagents (green: de-ionized MQ water, purple: buffer, brown: de-ionized water-buffer mix) (D). Figure taken from Rapp et al. 2017.

this section). The amount of buffer added was readjusted using the automated system until the desired pH of the waste solution was achieved.

The seawater samples were placed in an autosampler (4DX FASTready) equipped with a sample probe and a high efficiency particulate air (HEPA) filter. The sample was first introduced

through the sample probe and loaded into a 10 ml coil (Figure 2.3 A). The sample was then loaded onto the pre-concentration resin simultaneously with the set amount of buffer (the pH of the waste solution was checked) and the sample matrix was rinsed off with 10 ml of de-ionized water (Figure 2.3 B). Sample probe and tubing were subsequently rinsed with 1 M HNO_3 for 60 s and the sample was eluted from the pre-concentration resin using 1 ml EA, through the sample probe into acid washed PP vials (Figure 2.3 C). This step provides a 10:1 pre-concentration ratio. Then, the buffer clean-up, pre-concentration resins and sample probe are cleaned by rinsing with 1 M HNO_3 and the pre-concentration resin is conditioned using the buffer solution and de-ionized water (Figure 2.3 D). This set up allowed pre-concentration of approximately 4 samples in 1 hour.

2.4.1.6 Blanks

Blank contributions were determined in two separate parts; the manifold blank and the buffer blank. The manifold blank was the overall contribution from the elution acid, any component of the preconcentration procedure (SeaFast, preconcentration vials), manifold (except the buffer) and ICP-MS analysis. The manifold blank was determined as the concentration of TMs in 1 M HNO_3 after processing through the first three steps from the sample preconcentration method. Two (or more) manifold blanks were collected every 10^{th} sample in order to routinely check for potential system contamination. The buffer blank was determined using two batches of filtered (0.2 μm) North Pacific seawater diluted 1:10 with deionized water and acidified to pH 1.9 and 1.6 with HCl (UpA Romil). The seawater was diluted in order to reduce concentrations of TMs in solutions. Both solutions were treated in the same manner as other samples and were always preconcentrated in replicates (n = 5) with the buffer added (in two different amounts) during the preconcentration step adjusted to the same pH as for seawater samples (6.4 ± 0.2). Buffer contributions were calculated as the difference between the mean TM concentrations. However, some important limitations of this method were identified:

1) This approach includes the contribution from the HCl acid used for acidification as more acid was added to the pH 1.6 solution. However, considering that HCl used was of highest purity (UpA), acid contribution should be insignificant relative to the buffer.
2) North Pacific seawater was split into two separate bottles. The calculation of buffer contribution assumes exactly the same TM concentrations in both bottles.
3) A small inaccuracy between two solutions with low TM concentrations extrapolated to higher volumes could have a significant impact on final TM concentrations in seawater samples, in particular in samples with low TM concentrations.

As a consequence, some samples could not be corrected for the buffer contribution. Typical contribution of the buffer was variable and evident only for Ni (49.5 ± 51.9 pmol kg^{-1}, n = 3) and Zn (27.3 ± 9.2 pmol kg^{-1}, n = 4) in 2 ml of added buffer. The lowest DNi and DZn concentrations in this study were 2.304 ± 9.2 nmol kg^{-1} and 0.210 ± 0.117 nmol kg^{-1} for DNi and DZn respectively (see Chapter 3) thus the buffer contribution was insignificant (<3 %) for DNi but for DZn a buffer contribution of 27.3 pmol kg^{-1} amounted to as much as 10 % of the lowest determined zinc concentrations.

2.4.2 Sample analysis: Inductively Coupled Plasma Mass Spectrometry (ICP-MS)

Inductively coupled plasma mass spectrometry provides a multielement capability, good precision, low detection limits (sub-picomolar concentrations) and rapid results. It consists of two major parts, sample introduction (sample aspiration and ICP) and high resolution mass spectrometer (MS). The sample is introduced into the ICP plasma through the nebulizer in the form of a liquid aspirated with argon. When the aerosol passes through the ICP torch at temperatures of 6000 – 10 000^{o}C, elements are converted into positively charged ions and transported under high vacuum (~1×10^{-7} mbar) through interface (sampler and skimmer) cones. The lenses focus the ion beam through a ~1 mm gap into the electrostatic and magnetic sector. These lenses separate ions by their mass-to-charge (m/z) ratio by alternating AC and DC voltages before they reach the detector. After the separation, the ions are detected by a Faraday detector combined with a dual mode Secondary Electron Multiplier (SEM) detector, and converted into an electric signal proportional to the number of ions reaching the detector surface (Prohaska et al. 2015). However, substantial analytical limitations are also associated with the ICP-MS analysis, including overlapping molecular or isobaric interferences, high cost and maintenance. The most significant interference relevant to work described in this thesis was (MoO^{+}) (McLaren et al. 1987; Wu & Boyle 1997) for ^{111}Cd and ^{110}Cd isotopes. The consequences and correction method are described later in this section.

2.4.2.1 Reagents

1 M HNO_3 used to rinse the autosampler needle in between solutions during analysis was prepared using sub-boiled acid and deionized water that was reused between the analytical runs. The purity of the rinse solution was checked before each run and was recorded. When counts of Fe or Zn (the elements known to be the most susceptible to contamination) increased, a fresh solution was prepared.

2.4.2.2 Spike solutions: ICP-MS

Three solutions were prepared for each ICP-MS run: multielement (ME), ID spike (spike) and 1 M HNO_3 (acid blank, AB). These solutions were analysed every 10^{th} sample in order to obtain the natural (ME) and artificial (spike) elemental isotope ratios required for calculation of metal concentrations (see section 2.4.2.4). These three solutions were used to correct for instrumental isotopic mass bias and to monitor contamination from the sub boiled HNO_3 acid. Multielement solution containing the natural ratio of isotopes of elements of interest (Cd, Ni, Cu, Zn) was prepared by dilution of individual stock standards (CertiPur, Merck) in AB. The spike solution containing the artificial isotope ratios of the elements of interest was prepared by diluting concentrated ID spike solution in AB. Spike and ME solutions were diluted in the same acid in order to correct for contributions from the 1 M HNO_3.

2.4.2.3 Tuning

The instrument was tuned with In and Uranium (U) solution before each run to obtain maximum sensitivity (highest possible counts) and stability (< 1.5%) for both elements. The tuning solution was prepared by dilution of individual stock standards (CertiPur, Merck) in sub boiled 1 M HNO_3 to final concentration of 1 parts per billion (ppb).

2.4.2.4 Analysis

Preconcentrated samples were analysed by means of ICP-MS in low resolution (R = 300) for ^{110}Cd, ^{111}Cd, ^{208}Pb, ^{115}In and in medium resolution (R = 4000) for ^{60}Ni, ^{62}Ni, ^{63}Cu, ^{65}Cu, ^{66}Zn, ^{68}Zn, ^{59}Co, and ^{55}Mn. Low resolution was applied to elements that are not significantly affected by the isobaric interferences (^{111}Cd and ^{110}Cd interference correction is explained later in this section), while the medium resolution was applied to elements with more intense isobaric interferences. The standard ICP-MS sequence consisted of EA analysis (elution acid used in the preconcentration step) in order to routinely asses the purity of the reagents and the system, preconcentrated samples, MB, and three 'ICP-MS spike' solutions analysed every 10^{th} sample. The autosampler needle was rinsed with 1 M HNO_3 for 60 s between measurement of each solution..

2.4.2.5 Corrections

ICP-MS drift corrections

An In spike solution added directly to elution acid used to elute the preconcentrated samples, and to manifold blanks was used to correct for instrumental drift. In the case of ID calibrated

metals (Cd, Ni Cu, Zn), drift correction was not required because the addition of isotopes provides internal consistency.

Corrections for MoO^+ isobaric inferences of ^{111}Cd analysis

Isobaric interferences of MoO^+ on ^{110}Cd and ^{111}Cd have previously been reported (McLaren et al. 1987; Wu & Boyle 1997) and can lead to 3 – 9 pmol L^{-1} overestimation (Rapp et al. 2017) in Cd concentration, which is of potential significance given that surface water Cd concentrations can be as low as 10 pmol kg^{-1} (Wu & Roshan 2015). The isobaric MoO^+ interferences can be corrected for by running ^{95}Mo standard addition solutions (concentration range: eg. 2 – 200 nmol L^{-1}) at the beginning and end of each run and ^{95}Mo measurement in each sample. The slopes from the linear regression of $^{95}Mo/^{110}Cd$ and $^{95}Mo/^{111}Cd$ obtained from the Mo^{95} standard addition solutions are used to correct for MoO^+ interference on both of Cd isotopes as described in Rapp et al. (2017). Dissolved Cd (DCd) concentrations reported here were not corrected for MoO^+ interferences because this aspect was not considered during the initial method set-up. Although the DCd results reported here were not corrected for MoO^+, mean summer dissolved Cd (DCd) concentrations in the seasonal mixed layer (SML) (32.4 ± 13.5 pmol kg^{-1}) agreed with those previously reported in the study region (65 ± 43 pmol kg^{-1}) (June 1995;(Cotté-Krief et al. 2002)) analysed by atomic absorption spectrometry (AAS). However, given that the SAFe S GEOTRACES reference material (19.4 ± 4.5 pmol kg^{-1}) was consistently higher than the consensus value (1.1 ± 0.3 pmol kg^{-1}) the

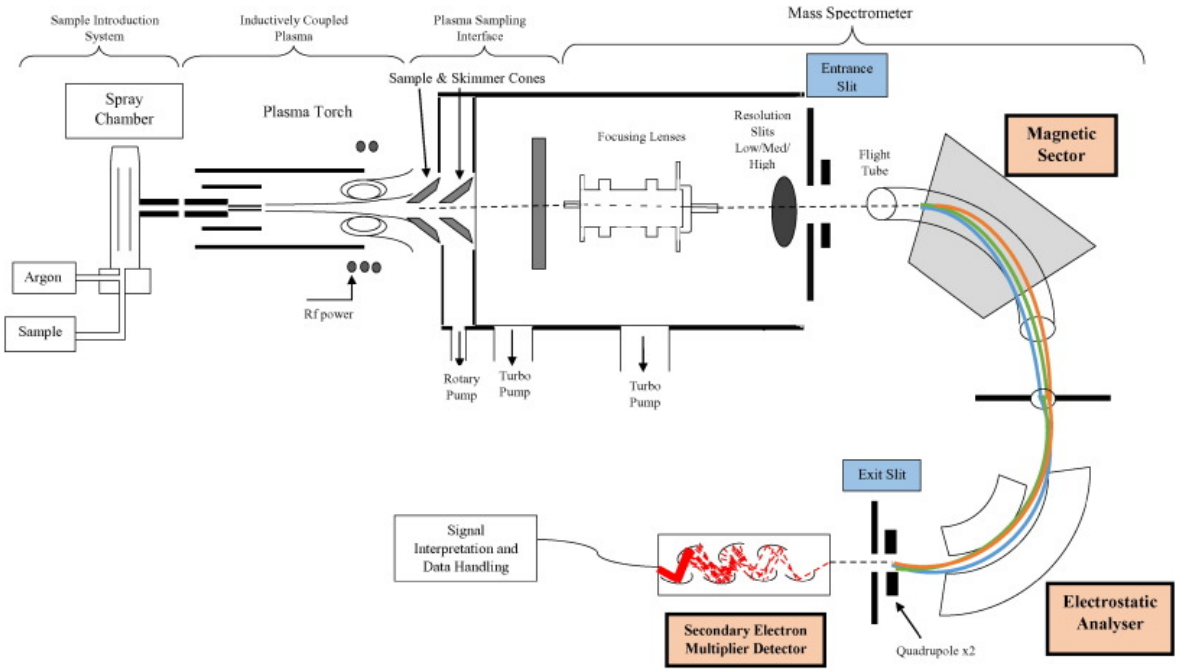


Figure 2.4 Schematic diagram of a sector-field inductively couple plasma mass spectrometer (ICP-MS) (Ring et al. 2016).

lower SML concentrations should be treated with caution. While there was potential for overestimation of DCd concentrations reported here, no deviation from the linear relationship between Cd and P was observed even at low DCd concentrations (< 50 pmol kg^{-1}) (see Chapter 3).

2.4.2.6 Calculation of elemental concentrations

Isotope dilution calculations

The final metal concentrations were calculated as follows:

$$M_{ID} = M_T (R_s - R_a)/(R_n - R_s)/x \qquad \text{eq. 1}$$

M_{ID} = TM concentration in the spike (externally calibrated by ICP-OES and reverse ID-ICP-MS)

R_s = isotopic ratio measured in each sample

R_a = artificial isotopic ratio of the ID spike added to the sample

R_n = natural isotopic ratio of the multielement spike

x = natural abundance of the isotope

$$R_s = si1 - (MBi1)/\ si2 - (MBi2) \qquad \text{eq. 2}$$

si1 = sample counts s^{-1} (cps) for isotope 1

si2 = sample cps for isotope 2

MBi1 = average manifold blank cps for isotope 1

MBi2 = average manifold blank cps for isotope 2

$$R_a = \text{Average } (sp1 - (Ai1)/sp2 - (Ai2)) \qquad \text{eq. 3}$$

sp1 = spike cps for isotope 1 (measured every 10^{th} sample before and after the sample)

sp2 = spike cps for isotope 2 (measured every 10^{th} sample before and after the sample)

Ai1 = acid cps for isotope 1 (diluted acid used to prepare the spike and ME solution)

Ai2 = acid cps for isotope 2 (diluted acid used to prepare the spike and ME solution)

$$R_n = \text{Average } (me1 - (Ai1)/me2 - (Ai2)) \qquad \text{eq. 4}$$

me1 = ME cps for isotope 1 (measured every 10^{th} sample before and after the sample)

me2 = ME cps for isotope 2 (measured every 10^{th} sample before and after the sample)

The final metal concentrations were corrected by the average counts of one manifold blank before and two manifold blanks after the sample was measured. In this way, the contributions from the elution acid, any component of the preconcentration procedure and ICP-MS analysis were corrected for (except for the buffer). Final metal concentrations were corrected for the buffer contribution (as described in section 2.4.1.6) as follows:

$$M_c = M_{ID} - b \qquad \text{eq.5}$$

where

$$b = v1 \times d1/v2 \qquad \text{eq. 6}$$

v1 = volume of buffer added to samples

d1 = difference in concentrations of two diluted seawater solution

v2 = difference in volume of buffer added to two diluted seawater solution

Standard addition approach

The final concentration of metals determined by the standard addition method were calculated as follows:

$$M_{SA} = (c_s/c_{In})/s \qquad \text{eq. 7}$$

c_s = sample cps

c_{In} = Indium cps (added to elution acid)

s = average slope of two the linear regressions (run every 10^{th} sample, before and after the sample)

2.4.2.6.1 Error calculations

Analytical errors were calculated as follows:

Isotope dilution

$$E_{ID} = M_c \sqrt{e} \qquad \text{eq. 8}$$

where

$$e = (ei1/si1)^2 + (ei2/si2)^2 + (\sigma_{me}/R_n)^2 + (\sigma_{sp}/R_a)^2 \qquad \text{eq. 9}$$

ei1 = analytical error cps for isotope 1

ei2 = analytical error cps for isotope 2

σ_{ME} = standard deviation of two ME ratios (measured every 10th sample before and after the sample)

σ_{SP} = standard deviation of two spike ratios (measured every 10th sample before and after the sample)

Standard addition

E_{SA} =

$$E_{SA} = (e_s/e_{In})/s \qquad \text{eq. 10}$$

e_s = sample error cps

e_{In} = Indium error cps (added to elution acid)

2.4.2.7 Data exclusion

Some data points were identified as outliers following the z-score test and were excluded from consideration. The outliers identified in the dataset were potentially a result of analytical issues during sample preconcentration or sample analysis, sample contamination during sampling, sample preparation or sample analysis or extreme natural variability. Once outliers were identified using the z-score as described below, each data point was the plotted in a depth profile to examine the oceanographic consistency. However, the full dataset has been submitted to British Oceanographic Data Centre (BODC), with outliers flagged. The z-scores were calculated for each water mass identified in section 3.3.1 and for each cruise separately as follows:

$$Z = (M_c - M_a)/M\sigma \qquad \text{eq. 11}$$

M_a = average metal concentration in each water mass identified

$M\sigma$ = standard deviation of metal concentration in each water mass identified

All data points that fell outside of the -3 to +3 range were identified as outliers.

2.4.2.8 Unit conversion

All concentration values were converted from pmol L^{-1} and nmol L^{-1} to pmol kg^{-1} and nmol kg^{-1} using a seawater density value of 1.025 kg m^{-3}.

2.4.2.9 Mean concentrations of dissolved trace metals

All the mean concentrations reported in the main text were calculated as average concentrations within the identified density layer and the error is represented by one standard deviation.

Table 5 GEOTRACES reference material results for various trace metals. Dissolved Cd, DCo and DPb are given in pmol kg^{-1} and DNi, DCu, DZn, DMn and DAl are given in nmol kg^{-1}.

	DCd	**DNi**	**DCu**	**DZn**	**DMn**	**DCo**	**DPb**	**DAl**
Reported values	SAFe S: 18.9 ± 4.4 (n = 10)	SAFe S: 2.324 ± 0.216 (n = 10)	SAFe S: 0.705 ± 0.130 (n = 8)	SAFe S: 0.071 ± 0.025 (n = 8)	SAFe S: 0.910 ± 0.063 (n = 8)	SAFe S: 8.2 ± 1.3 (n = 9)	SAFe S: 48.9 ± 1.4 (n = 6)	GS: 27.0 ± 0.6 (n = 6)
	SAFe D1: 979.4 ± 145 (n = 17)	SAFe D1: 8.407 ± 0.144 (n = 15)	SAFe D1: 2.192 ± 0.059 (n = 15)	SAFe D1: 7.134 ± 0.223 (n = 19)	SAFe D1: 0.418 ± 0.020 (n = 29)	SAFe D1: 47.6 ± 1.5 (n = 15)	SAFe D1: 25.3 ± 0.9 (n = 20)	-
Consensus values	SAFe S: 1.1 ± 0.3	SAFe S: 2.28 ± 0.09	SAFe S: 0.52 ± 0.05	SAFe S: 0.069 ± 0.010	SAFe S: 0.790 ± 0.060	SAFe S: 4.8 ± 1.2	SAFe S: 48.0 ± 2.2	GS: 27.5 ± 0.2
	SAFe D1: 991 ± 31	SAFe D1: 8.58 ± 0.26	SAFe D1: 2.27 ± 0.11	SAFe D1: 7.40 ± 0.35	SAFe D2*: 0.350 ± 0.050	SAFe D1: 45.4 ± 4.7	SAFe D1: 27.7 ± 2.6	-

*Currently, there are no consensus values available for SAFe-D1 reference samples but *'SAFe D1 appears similar to SAFe D2, however not enough data has been submitted to report a value'.*

http://www.geotraces.org/science/intercalibration/322-standards-and-reference-materials

2.4.3 Linear correlations (Pearson), one way ANOVA and least significant difference tests

All linear correlations (Pearson) and one way ANOVA analysis were performed using StatPlus:mac statistical tool pack. Least Significant Difference post-hoc test was performed after one-way ANOVA test in order to identify significantly different group of datasets following the formula:

$$LSD_{a,b} = t_{0.05/2,DFW}\sqrt{MSW\ (\frac{1}{na}+\frac{1}{nb})} \qquad \text{eq. 12}$$

where

a and b = are two datasets

t = critical value from the t-distributions

MSW = mean square within groups obtained from the results of one way ANOVA test

n = number of scores used to calculate the means

The groups were significantly different when the absolute difference between the group means was greater than $LSD_{a,b}$.

2.4.4 Seasonal mixed layer depth

The base of the seasonal mixed layer depth for each station was defined as the depth at which temperature changes $|\Delta T|$ = 0.2°C relative to the shallowest temperature value (de Boyer Montégut et al. 2004).

2.5 Other analytical methods

2.5.1 Dissolved Aluminium analysis

Clarisse Mariez, MSc student, GEOMAR and Université de Bretagne Occidentale, France

Seawater was sub-sampled (5 mL) into acid washed 50 ml plastic tubes. An aluminium spectrofluorometric complex was obtained with addition of lumogallion (Hydes & Liss 1976) at pH 5.0 - 5.5 adjusted by addition of ammonium acetate buffer (prepared in the same way as in Rapp et al 2017) and section 2.4.1.1 and heated for 3 hours at 55°C. Samples were analysed by a spectrofluorometer (The Cary Eclipse Fluorometer). Concentrations were determined with 6 point standard addition that ranged between 0 – 30 nmol L^{-1}. Analyses of GEOTRACES reference material agreed with consensus values and are reported in Table 5.

Chapter 3 A seasonal study of dissolved Cd, Zn, Co, Ni and Cu in North East Atlantic shelf seas

The research presented in this chapter is being prepared for publication in *Biogeosciences*

3.1 Introduction

Trace metals (TMs) have the potential to influence the structure and functioning of marine ecosystems through growth limitation of phytoplankton or toxic effects (Moore, et al. 2013; Browning et al. 2017; Sunda & Huntsman 1998). The trace elements cobalt (Co), cadmium (Cd), zinc (Zn), nickel (Ni), and copper (Cu) form active sites in vitamins (cobalamin, Co) or enzymes such as carbonic anhydrase (CA) (Zn, Co, Cd), urease (Ni) and plastocyanin (Cu), required in vital metabolic functions such as uptake and assimilation of inorganic carbon and urea, and electrontransport (Morel et al. 2003). Cobalt is fundamental for cyanobacterial growth (*Prochlorococcus* and *Synechococcus*) (Sunda & Huntsman 1995). Cambialism is known to occur for Zn, Co and Cd, and these elements can partially replace one another in the CA enzyme depending on the phytoplankton species (Price & Morel 1990; Morel et al. 1994; Sunda & Huntsman 1995). In addition, in coccolithophores (*Emiliania huxleyi*) Zn can partly meet Co requirement, and in diatoms (*Thalassiosira pseudonana* and *Thalassiosira oceanica*) Zn can be substituted by Co (Sunda & Huntsman 1995) and Cd (*Thalassiosira weissflogii*) (Morel et al. 1994). In contrast, some metals can be toxic to marine phytoplankton at elevated concentrations, in particular in coastal waters. For example, inorganic Cu is extremely toxic to marine microorganisms (10^{-10} M; (Sunda et al. 1987)) through interference with uptake and/or assimilation of other bioessential micronutrients such as Zn and manganese (Mn), and thus can inhibit phytoplankton growth (Sunda & Huntsman 1998b) and potentially cause shifts in community composition. Therefore, TMs through their fundamental roles in the processes that control inorganic carbon uptake, may influence the biological carbon pump.

Dissolved (< 0.2 μm) trace metals (DTMs) such as DCd, DZn, DNi and DCu have been classified as 'nutrient-like' due to resemblance of their vertical distributions with those of macronutrients. These DTMs thus typically exhibit depleted surface water concentrations with an increase with depth through release upon remineralization of sinking biogenic particles (Bruland & Lohan 2004). Remarkably strong correlations of DCd and DZn with phosphate have been observed throughout the global ocean; in the North Atlantic (DCd: Roshan & Wu 2015; Wu & Roshan 2015; Yeats 1998), South Atlantic (DCd: Xie et al. 2015; DZn: Wyatt et al. 2014), Pacific (DCd: Boyle et al. 1976; Boyle 1988; Bruland 1980; Bruland et al. 1978; Roshan et al. 2017), Indian (DCd: Saager et al. 1992) and Southern Oceans (DCd, DZn: Saito et al. 2010). However, the slopes of TMs correlations with macronutrients vary between ocean regions and are not always strictly linear but often described by more than one distinct slope. Pronounced breaks - termed "kinks" - in the linear relationship of DCd and DZn with phosphate, typically occurs at concentrations between 1.2 – 1.5 μM phosphate (PO_4^{3-}). The cause of these "kinks" has been a matter of debate for over 4 decades (Boyle et al. 1976; Boyle 1988; Cullen 2006; Xie et al. 2015; Elderfield & Rickaby 2000). Some of the 'Cd:P kink' hypotheses point towards a deeper Cd regeneration relative to PO_4^{3-} (Boyle 1988), presence of

water masses with different Cd:P ratios (Xie et al. 2015), iron (Fe) limitation and Zn depletion in surface waters leading to a process called growth rate dilution where phytoplankton growth rate is depressed but not the metal uptake and causing preferential Cd uptake (Cullen 2006), chemical replacements between Co, Zn and Cd in carbonic anhydrase (Sunda & Huntsman 1995; Morel et al. 1994). Considering that Cd:P relationship has been utilized as a proxy for past oceanic processes (Boyle 1988), understanding the exact biogeochemical processes driving TMs:P relationship in modern global ocean is crucial.

A primary goal of the international GEOTRACES program is to gain insights into the fluxes and processes controlling the distributions of trace elements and their isotopes in the global ocean (Anderson et al. 2014). This study contributes to the GEOTRACES programme as a 'Process-Study'. Coastal regions are of interest because the magnitude of supply and removal of TMs in the interface between the continent and ocean, which therefore influences ocean ecosystem structure and productivity. Although, shelf seas comprise 9% of the global ocean area, they contribute 15-20% to global primary productivity (Simpson & Sharples 2012). The Celtic Sea is an ocean margin environment characterised by a wide continental shelf (300 km) and a steep continental slope with a highly complex topography (Bourillet et al. 2003). Quantifying processes that influence the fate of TMs within this environment is crucial for our understanding of the biogeochemistry of the global ocean. Nevertheless, TM studies in shelf seas are scarce due to the complexity of the biogeochemical and physical processes that influence TM distributions in these regions. The aim of the research reported here was to quantify biogeochemical processes influencing the distributions of DCd, DZn, DNi, DCu (full depth investigation) and DCo and DAl (surface waters) on the continental shelf and continental shelf break of the Celtic Sea over three seasons. Work reported here comprises the first comprehensive seasonal study of DCd, DZn, DNi, DCu and DCo and DAl in the Celtic Sea region.

3.2 Materials and methods

Full details of the study region, sampling and methods are provided in Chapter 2. Briefly, samples for trace metal analysis were collected during three different seasons; November – December 2014 (DY018), April 2015 (DY029), and July – August 2015 (DY033) in the Northeast Atlantic continental margin (Celtic Sea) (Figure 2.1), on board *RRS Discovery.* Two off-shelf transects were conducted along a canyon (T1_C, stations C01 – C07, C15), nearby a spur (T2_S, stations S08 – S09) and one on-shelf transect in the Celtic Sea (stations CS2, CCS, J02 – J06, Site A). Trace metal samples were collected following GEOTRACES protocols (Cutter et al. 2010). Dissolved TMs were filtered using a 0.2 µm pore size cartridge filter (Sartobran 300, Sartorius), preconcentrated using an automated system (SC-4 DX SeaFAST pico; ESI) (DCd, DZn, DNi, DCu,

DCo), and analysed by high-resolution inductively coupled plasma-mass spectrometry (HR-ICP-MS; Thermo Fisher Element XR) (Rapp et al. 2017). Dissolved Al was analyzed using spectrofluorometry following (Hydes & Liss 1976). Evaluation of the accuracy and efficiency of these methods was carried out using GEOTRACES reference materials with the results showing good agreement (Table 5). Some data points were identified as outliers following the z-score analysis and were excluded from consideration (Chapter 2). Seawater sampling and handling for macronutrient analysis was carried out according to the International GO-SHIP nutrient manual recommendations (Hydes et al. 2010) and the analysis was carried on board using techniques described in Woodward and Rees (2001). Water mass distribution was quantified using extended Optimum Multiparameter analysis (extOMP) (Hupe & Karstensen 2000; Karstensen & Tomczak 1998; Pollard et al. 2004) (Appendix A). Section plots figures were created with the Ocean Data View (2015) software (Schlitzer 2015) with DIVA gridding settings. Principal component analysis was performed using Matlab software with the script provided by Cathleen Schlundt. Conductivity, temperature and depth (CTD) data was collected and processed on board. Turbidity was measured (Chelsea Technologies Group Aquatrack MKIII fluorometer, wavelength 400 nm, bandwidth 80 nm). Salinity was measured (Sea-Bird SBE 4C sensor) and calibrated on-board using in-situ salinity samples analysed with a Guildline Autosal salinometer. Temperature was measured with Sea-Bird SBE 3plus (SBE 3P) temperature sensor. Dissolved oxygen was measured with Sea-Bird SBE 43 oxygen sensor and calibrated against photometric on-board Winkler titration results. Statistical analysis, one way ANOVA and linear regression were performed using StatPlus:mac statistical tool pack.

3.3 Results

3.3.1 Hydrography

Five different water masses in the study region were identified: a seasonal mixed layer (SML) and East North Atlantic Central Waters (ENACW), Mediterranean Outflow Waters (MOW), Labrador Sea Water (LSW) and North East Atlantic Deep Waters (NEADW). The SML was identified as detailed in Chapter 2 and the remaining water masses were identified by extensive Optimum Multiparameter Analysis (extOMP, Appendix A). ExtOMP results are presented in Figure 3.1 b and Figure 3.2. These observations were consistent with previous reports from the study region (Cotté-Krief et al. 2002).

In general, in all the sampling months the upper water column (< 500 m, < 27.30 kg m^{-3} σ_0) consisted mainly of ENACW. The ENACW was further divided into the SML and upper waters (hereafter ENACW) that overlaid MOW. Below the ENACW, at intermediate depths ~ 500 - 1500

m (27.30 – 27.75 m^{-3} σ_0,), a distinctive salinity maximum, a signature of MOW, was observed (García-Ibáñez et al. 2015; McCartney 1992). The MOW are formed at the Strait of Gibraltar where Mediterranean Sea deep waters mix with ENACW and sink to a depth of ~ 1000 m to form a neutrally buoyant plume that spreads across the North East Atlantic (García-Ibáñez et al. 2015). In our study region, the salinity (35.24 – 35.74) and temperature (4.92 – 10.58^{o}C) within the MOW density range (27.30 – 27.75 kg m^{-3} σ_0) were consistently lower across all seasons in comparison to salinity (35.61 – 36.36) and temperature (7.57 – 12.18^{o}C) of the MOW in the Gulf of Cadiz (GEOTRACES GA04 section, (Rolison 2016)). This indicates the mixing of bottom layers of MOW with colder (3.30^{o}C) and less saline (34.87) LSW (Talley & McCartney 1982) that underlies MOW. Additionally, the salinity within the LSW water mass was higher (34.98) than salinity at formation (34.89), indicating vertical mixing with the more saline MOW. At depths > ~ 2300 m, the temperature (3.30 – 3.03^{o}C) decreased to below the temperature at formation of LSW (Talley & McCartney 1982), indicating the mixing of LSW with colder NEADW (1.98^{o}C). Distinctive seasonal changes were observed in the upper water column. Sea surface temperature decreased from 14.60^{o}C in November to 11.68^{o}C in April and increased to 16.32^{o}C in July. Also, the SML depth varied between 40 – 103 m in November, 30 – 170 m in April and 20 – 30 m in July. These changes were a result of the ocean – atmosphere heat exchange driven by the yearly cycle of solar irradiance (Simpson & Sharples 2012). Seasonal stratification was the strongest in July, as a result of heat gain during the summer season. The lowest sea surface temperature was measured in April as a result of the winter water column overturning and heat loss to the atmosphere during winter. The initiation of water column stratification was observed in April (Birchill et al. 2017). A high variability of the SML depth in November and April was likely influenced by strong internal tides, a distinctive feature in the Celtic Sea (Vlasenko et al. 2015).

Seasonal variations in a density driven along-shelf current has previously been observed in the upper waters of the region and follows SOMA (September/October – March/April) variability (Porter et al. 2016; Pingree & Le Cann 1989). In winter months, this along-slope current flows in a poleward direction due to strong south-westerly winds (Huthnance 1984), whilst in summer months it reverses and flows in an equatorward direction due to relaxation of south-westerly winds and variabilities in sea surface height (Pingree & Le Cann 1989). A slight variability was also observed in the MOW density range where salinity maxima were highest in November (35.74) and slightly lower in April (35.66) and July (35.68). This indicates either slight variations in MOW mixing with ENACW and LSW between seasons during transit, or intra-annual changes in properties of water masses at their origins (Bellanco & Sánchez-Leal 2016; Talley & McCartney 1982). Additionally, a salinity maximum observed in the MOW density range along the canyon transect decreased towards the continental slope from 35.74 to 35.61 in November, 35.66 to 35.52 in April and 35.68 to 35.50 in July (Figure 3.1 a). This feature was not prominent along the spur transect indicating that the canyon topography limited MOW penetration and enhanced

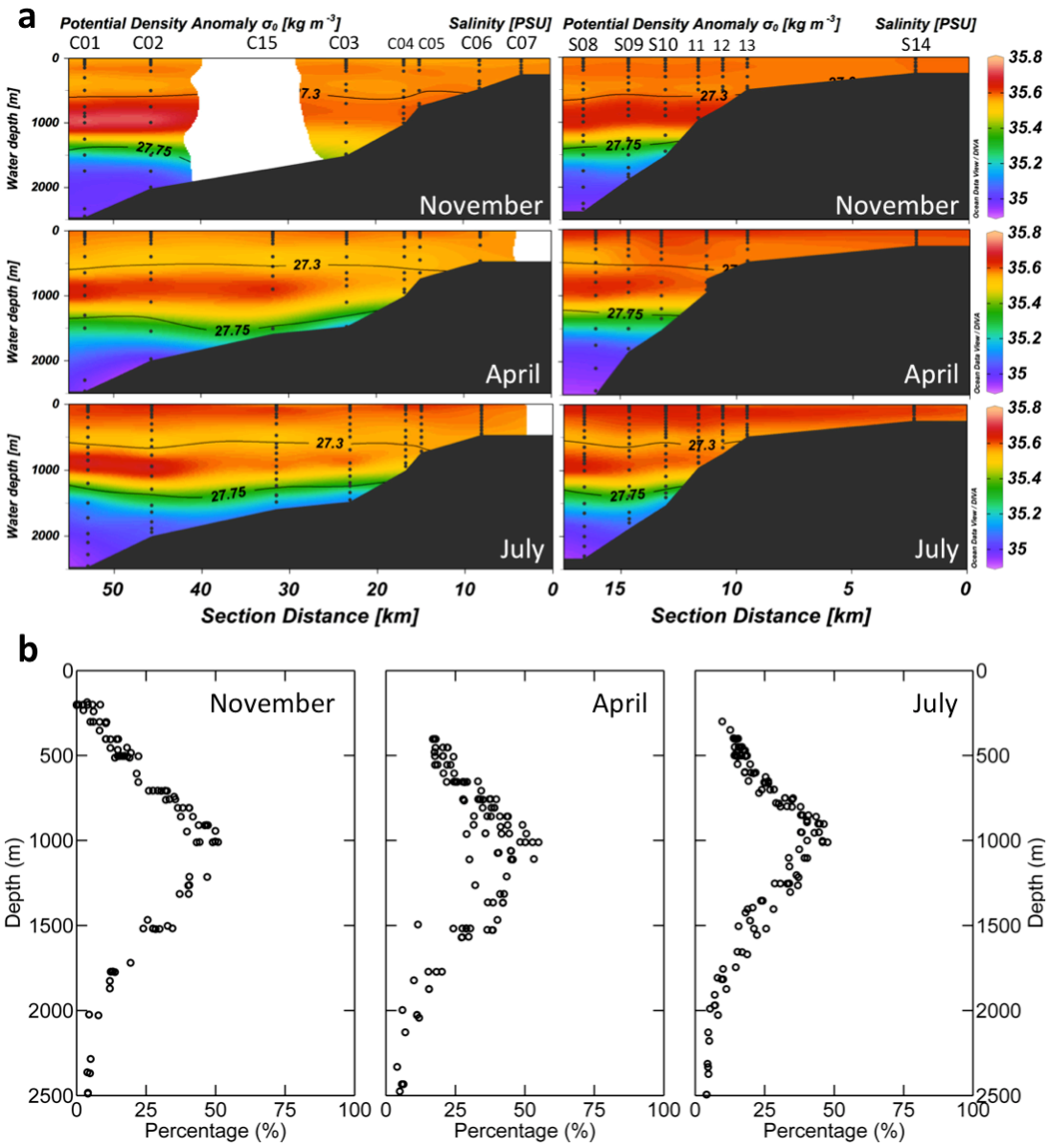


Figure 3.1. Upper panel (a): salinity distributions along the canyon transects (T1_C, left) and along the spur transects (T2_S, right) in November (DY018) (top), April (DY029) (middle) and July (DY033) (bottom). Bottom panel (b): the percentage distribution of MOW along the canyon (T1_C) and spur (T2_S) transects in November (DY018) (left), April (DY029) (middle) and July (DY033) (left). For the full OMP results see Figure 3.2.

vertical mixing over the shelf break. Elevated vertical mixing within submarine canyons has been observed globally due to their complex topography that leads to greater internal wave generation and diapycnal mixing (Gardner 1989; Hotchkiss & Wunsch 1982; Kunze et al. 2002; Carter & Gregg 2002).

Clear seasonal variability on the continental shelf was evident in terms of changes in the SML depth and water column stratification (Figure 3.4b), as a result of the yearly cycle of solar irradiance and subsequently sea surface – atmosphere heat exchange. Here CCS, as the main process station of the SSB Programme, is used as an example for the seasonal temperature and

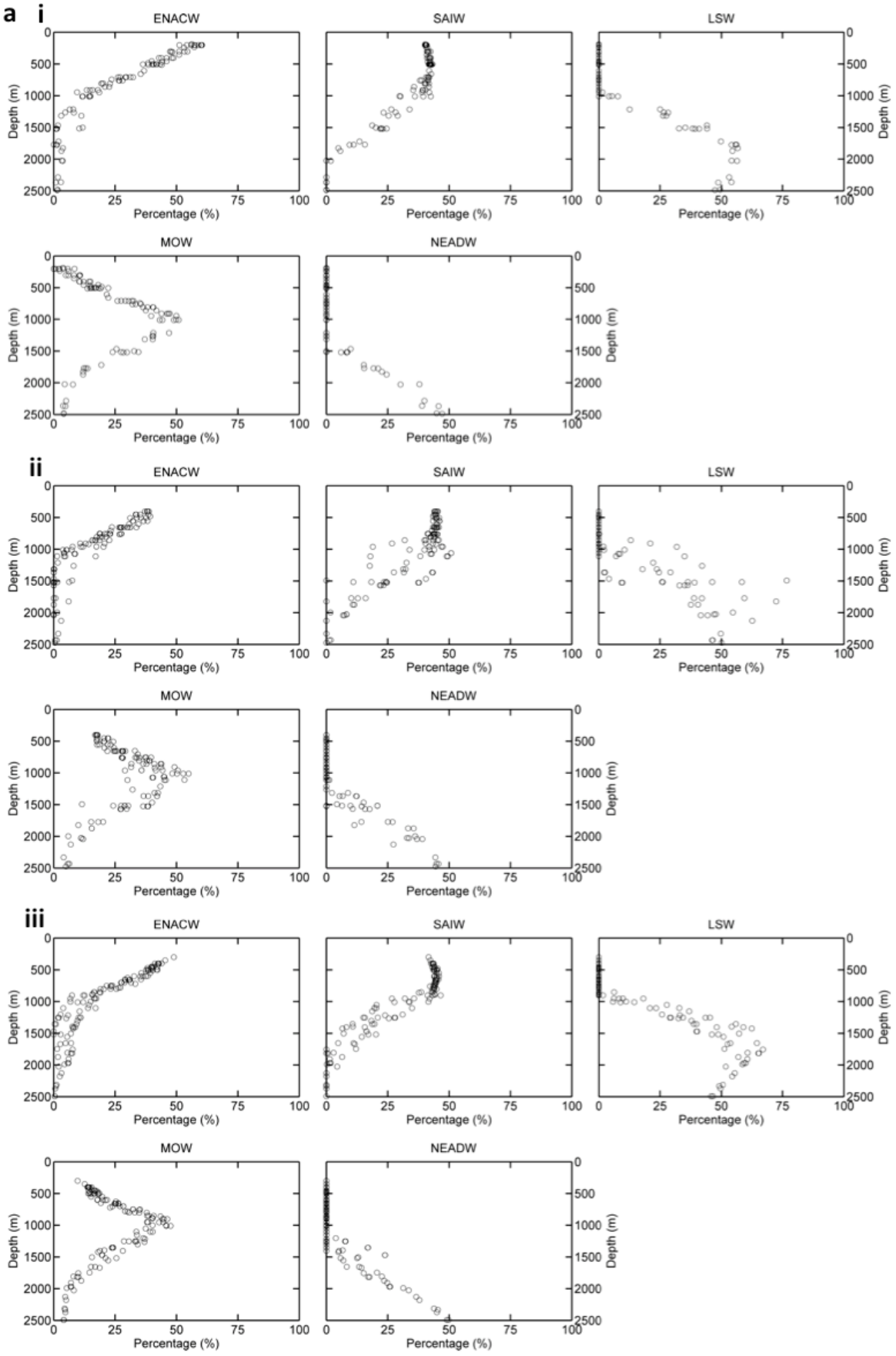


Figure 3.2 The percentage distribution of Source Water Types in the Celtic Sea region plotted against depth (a) and potential density anomaly (b) along the canyon (T1_C) and spur (T2_S) transects in November (DY018) (i), April (DY029) (ii) and July (DY033) (iii). ENACW (East North Atlantic Central Water), SAIW (Subarctic Intermediate Water), LSW (Labrador Sea Water), MOW (Mediterranean Outflow Water), NEADW (North East Atlantic Deep Water).

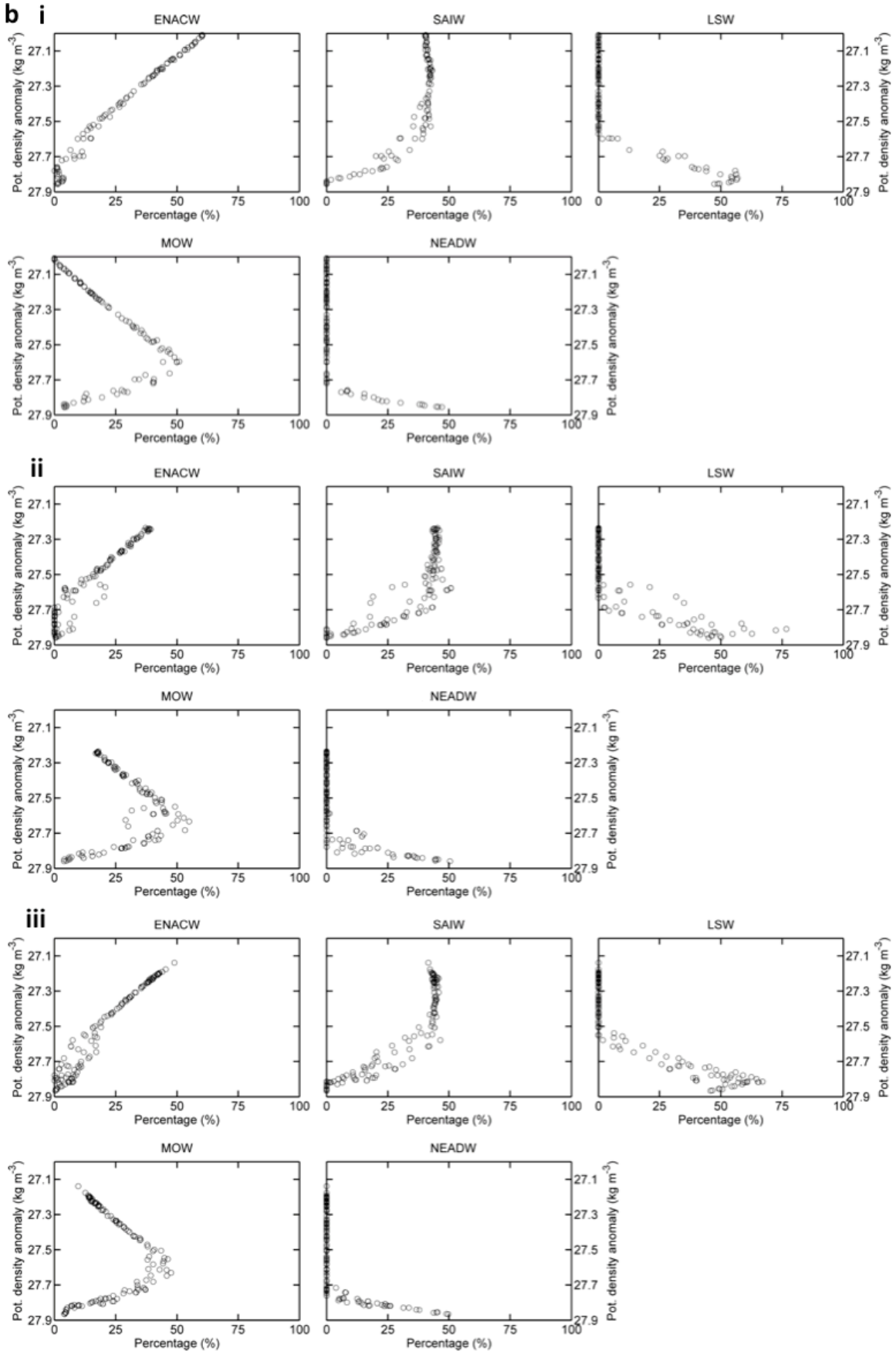


Figure 3.2 Continued

the SML depth changes of the water column in the Celtic Sea. Slight differences were observed at other on-shelf stations relative to CCS, but the patterns of the seasonal cycle were consistent. In November, the water column still exhibited a weak stratification that relaxed throughout the month as evident in declining surface temperatures from 13.7 to 12.8°C (11/11 and 29/11) along with the SML deepening from 32 m to > 50 m. During the winter months, a full water column overturning occurred, and these conditions lasted until the spring as evident in a fully mixed profile on the 3rd of April. The lowest surface water temperatures (10.1°C) where observed in spring when initiation of the water column stratification was observed and the SML shoaled from 51 m to < 30 m. The highest surface water temperatures were recorded in summer (16.3°C, July) along with a fully stratified water column and the shallowest SML < 26 m as a consequence of heat gain from the atmosphere. Seasonal variability in the salinity gradient across the shelf was also evident (Figure 3.5). More saline waters were observed in bottom waters at stations CCS in November in comparison to other months. Fresh water inputs were evident in surface waters at Site A in April and July.

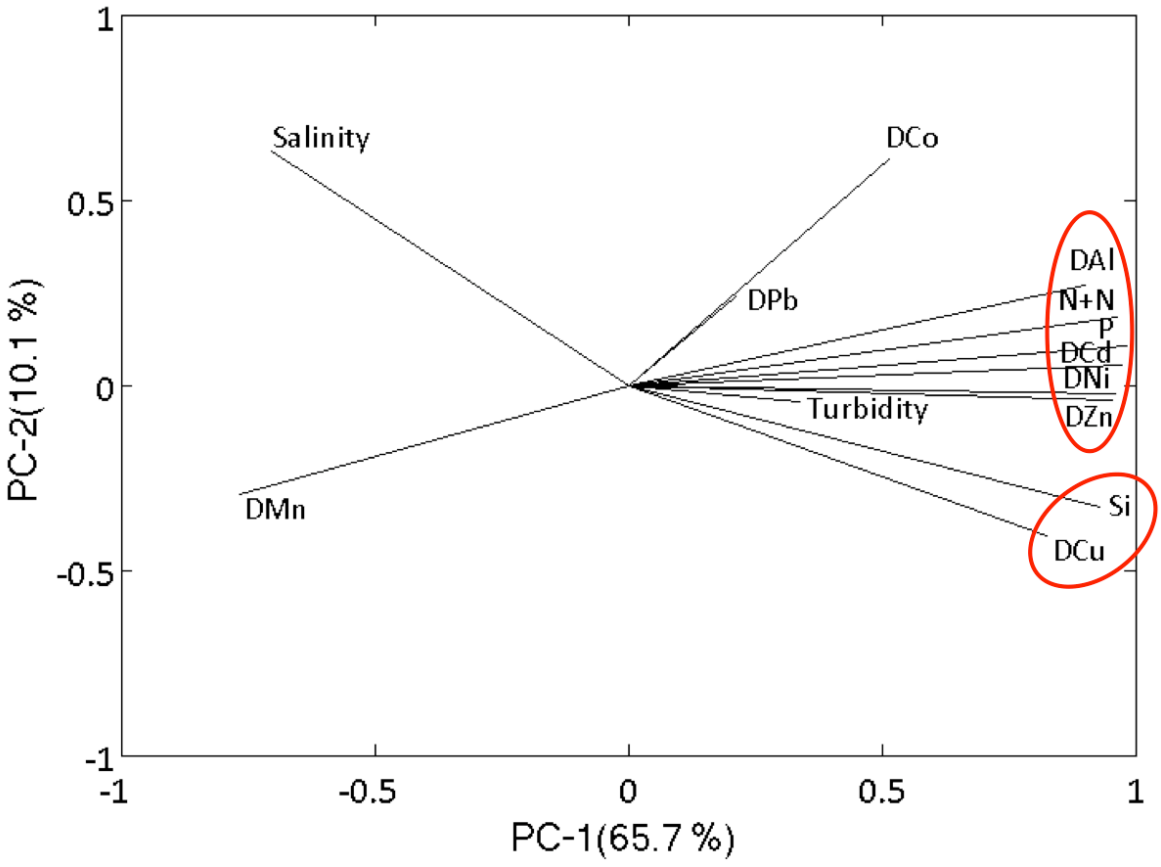


Figure 3.3 Plot of principal component loadings of 13 variables (n = 454): salinity, dissolved manganese (DMn), cobalt (DCo), lead (DPb), aluminium (DAl), cadmium (DCd), nickel (DNi), zinc (DZn), copper (DCu), nitrate and nitrite (N+N), phosphate (P), silicic acid (Si), salinity and turbidity on the continental slope of the Celtic Sea over all seasons. Red circles indicate positively correlated groups of variables.

3.3.2 Principal component analysis

In order to broadly categorize the TMs on the Celtic slope, principal component analysis (PCA) was used to identify the biogeochemical parameters with similar variance. The PCA allowed the number of variables to be compressed without a loss of information and provided a graphical representation of patterns in the dataset. The first two principal components (PC-1 and PC-2) explained 75.7% of variances in the dataset and PC-1 was strongly correlated (principal component loading (PCL) > 0.8) with nine of the original variables, DCd, DZn, DNi, DAl, NO_x^- (N+N), PO_4^{3-} (P), Cu and SiO_4^{4-} (Si) and moderately correlated with DCo (PCL > 0.5), suggestive of similar factors associated with these variables. An anti-correlation was observed for salinity and DMn (PCL > - 0.5) and no correlations was noted for DPb or turbidity (PCL < 0.5). The second principal component (PC-2) explained 10.1% of the variance in the dataset and moderately correlated with salinity and DCo (PCL > 0.5).

3.3.3 Macronutrient distributions

Macronutrient concentrations of phosphate (PO_4^{3-}), nitrate and nitrite (NO^{3-} + NO^{2-}, from here after referred to as NO_x^-) and silicic acid (SiO_4^{4-}) are presented in Table 6 and Figure 3.5, Figure 3.6 and Figure 3.7. In November concentrations ranged between 0.18 – 1.31 μmol kg^{-1} (PO_4^{3-}), 1.62 – 19.51 μmol kg^{-1} (NO_x^-) and 1.02 – 28.48 μmol kg^{-1} (SiO_4^{4-}), whilst in April concentrations ranged

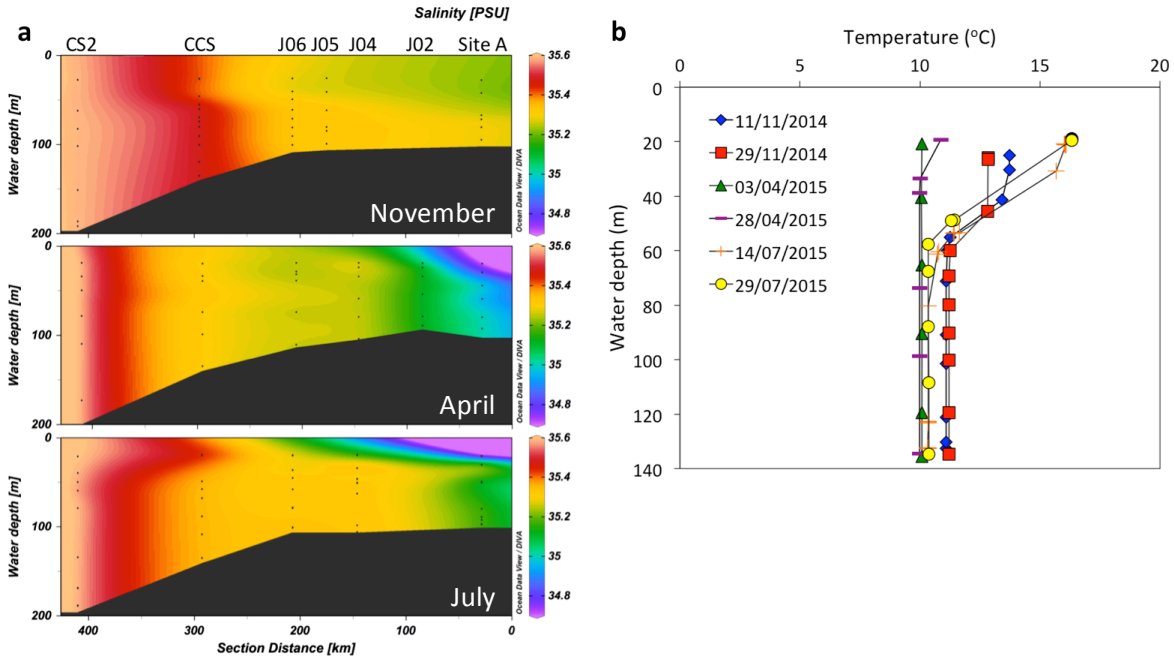


Figure 3.4 Salinity distribution along the on-shelf transect (a) in November (top), April (middle) and July (bottom) and (b) vertical depth profile of temperature at station CCS in November (blue diamonds and red squares), April (green triangles and purple horizontal lines) and July (orange crosses and yellow circles).

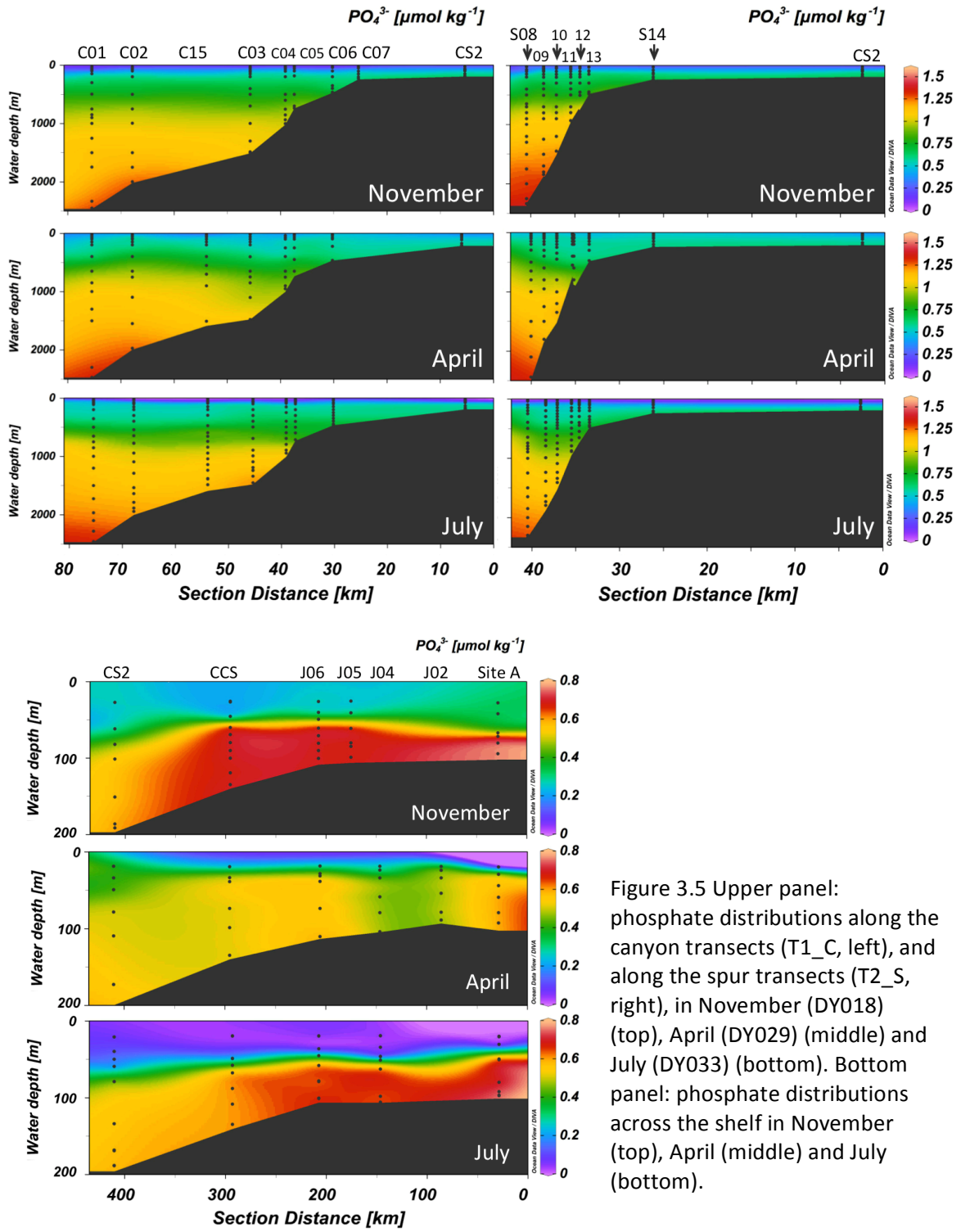
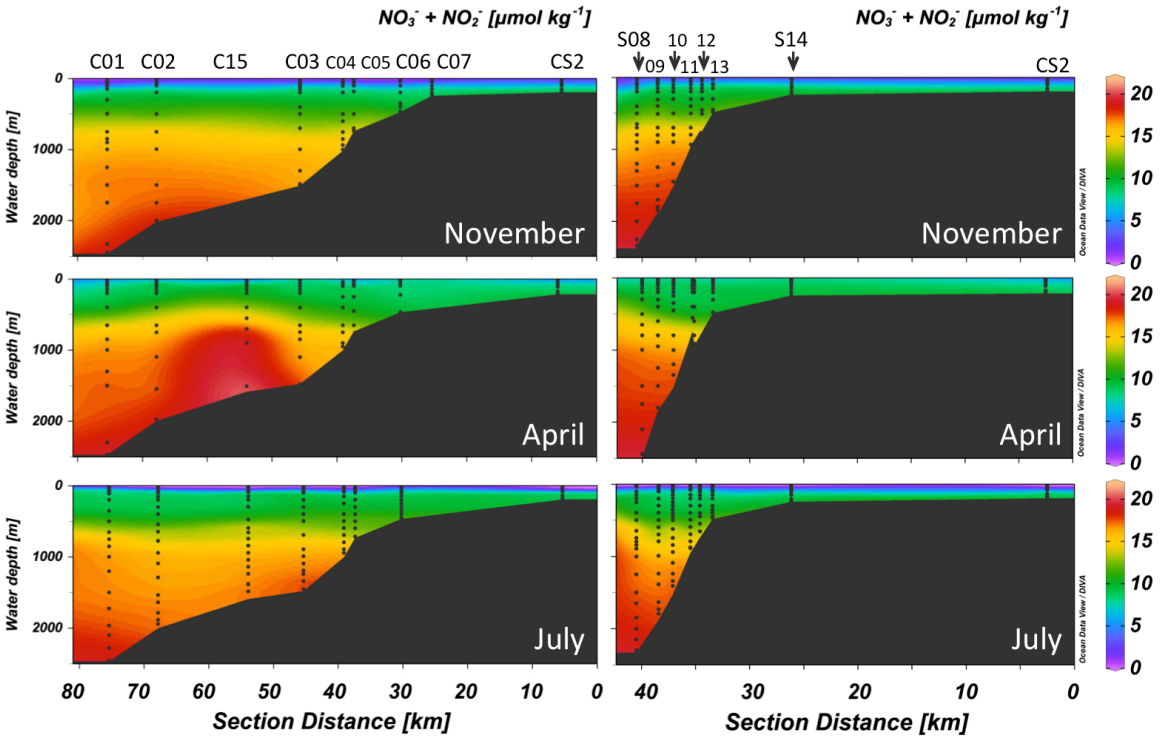


Figure 3.5 Upper panel: phosphate distributions along the canyon transects (T1_C, left), and along the spur transects (T2_S, right), in November (DY018) (top), April (DY029) (middle) and July (DY033) (bottom). Bottom panel: phosphate distributions across the shelf in November (top), April (middle) and July (bottom).

between 0.32 – 1.34 µmol kg^{-1} (PO_4^{3-}), 5.48 – 19.47 µmol kg^{-1} (NO_x^-) and 2.43 – 29.73 µmol kg^{-1} (SiO_4^{4-}) and in July they ranged between 0.05 – 1.34 µmol kg^{-1} (PO_4^{3-}), 0.02 – 19.22 µmol kg^{-1} (NO_x^-) and 0.22 – 29.92 µmol kg^{-1} (SiO_4^{4-}). The lowest macronutrient concentrations were observed in the SML (summarised in Table 6) and differed seasonally: 0.25 ± 0.06 µmol kg^{-1} (PO_4^{3-}, n = 36), 3.09 ± 1.25 µmol kg^{-1} (NO_x^-, n = 36) and 1.38 ± 0.33 µmol kg^{-1} (SiO_4^{4-}, n = 36) in November, 0.49 ± 0.05 µmol kg^{-1} (PO_4^{3-}, n = 51), 8.04 ± 0.82 µmol kg^{-1} (NO_x^-, n = 51) and 3.02 ± 0.21 µmol kg^{-1} (SiO_4^{4-}, n = 51) in April and 0.14 ± 0.09 µmol kg^{-1} (PO_4^{3-}, n = 33), 1.36 ± 1.55 µmol kg^{-1} (NO_x^-, n = 33) and 0.56 ± 0.35 µmol kg^{-1} (SiO_4^{4-}, n = 33)) in July. Seasonal variability in macronutrients concentrations



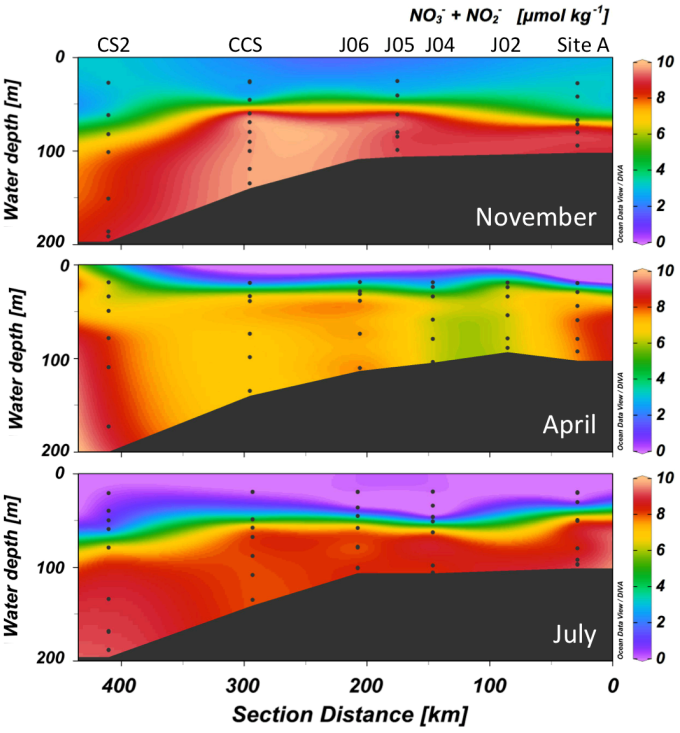


Figure 3.6 Upper panel: nitrate and nitrite distributions along the canyon transects (T1_C, left), and along the spur transects (T2_S, right), in November (DY018) (top), April (DY029) (middle) and July (DY033) (bottom). Bottom panel: nitrate and nitrite distributions across the shelf in November (top), April (middle) and July (bottom).

was significant as confirmed by the one-way ANOVA test: PO_4^{3-} (ANOVA (F(2, 117) = 314.3, p = < 0.05)), NO_x^- (ANOVA (F(2, 117) = 364.9, p = < 0.05)) and SiO_4^{4-} (ANOVA (F(2, 117) = 795.3, p = < 0.05)). Below the SML, macronutrient concentrations generally did not differ seasonally and gradually increased with depth to concentrations of 1.20 ± 0.07 µmol kg^{-1} (PO_4^{3-}, n = 65) 17.90 ± 0.74 µmol kg^{-1} (NO_x^-, n = 64) and 19.34 ± 5.18 µmol kg^{-1} (SiO_4^{4-}, n = 65). These observations were generally in agreement with previous reports for the study region (Cotté-Krief et al. 2002).

Table 6 Average concentrations (± σ) of nutrients and metals in the various water masses of the Celtic Sea shelf break region in late autumn (November, DY018), spring (April, DY029) and summer (July, DY033). Nitrate and nitrite (NO_x^-), phosphate (PO_4^{3-}) and silicic acid (SiO_4^{4-}) are in μmol kg^{-1}, dissolved manganese (DMn), nickel (DNi), copper (DCu), zinc (DZn) and aluminium (DAl) are in nmol kg^{-1}, dissolved cobalt (DCo), cadmium (DCd) and lead (DPb) are in pmol kg^{-1}.

Month	Depth range	Temperature (°C)	Salinity	NO_x^-	PO_4^{3-}	SiO_4^{4-}	DMn	DCo	DCd	DNi	DCu	DZn	DPb	DAl
November	SML	13.5 – 14.6	35.57 – 35.59	3.09 ± 1.25 (n = 36)	0.25 ± 0.06 (n = 36)	1.38 ± 0.33 (n = 36)	0.866 ± 0.174 (n = 36)	55.1 ± 4.5 (n = 36)	69.4 ± 12.8 (n = 36)	2.607 ± 0.147 (n = 36)	1.087 ± 0.035 (n = 36)	0.302 ± 0.102 (n = 36)	47.3 ± 5.9 (n = 35)	5.00 ± 0.89 (n = 34)
	ENACW	10.8 – 14.1	35.6	9.01 ± 2.06 (n = 70)	0.59 ± 0.12 (n = 70)	3.60 ± 1.05 (n = 70)	0.565 ± 0.143 (n = 70)	74.0 ± 6.8 (n = 70)	148.1 ± 30.0 (n = 70)	2.939 ± 0.178 (n = 70)	1.178 ± 0.054 (n = 70)	0.703 ± 0.217 (n = 70)	45.4 ± 6.4 (n = 70)	9.25 ± 2.02 (n = 70)
	MOW	7.4 – 10.6	35.4 – 35.7	15.49 ± 1.07 (n = 35)	0.99 ± 0.07 (n = 35)	9.32 ± 1.69 (n = 35)	0.345 ± 0.062 (n = 35)	76.5 ± 3.3 (n = 35)	249.7 ± 21.9 (n = 35)	3.698 ± 0.210 (n = 35)	1.319 ± 0.079 (n = 33)	1.589 ± 0.247 (n = 35)	49.1 ± 5.8 (n = 35)	18.12 ± 2.18 (n = 35)
	NEADW	3.2 – 6.2	35.0 – 35.3	18.11 ± 0.74 (n = 18)	1.21 ± 0.06 (n = 18)	20.15 ± 5.40 (n = 18)	0.396 ± 0.112 (n = 18)	70.3 ± 5.5 (n = 18)	318.6 ± 20.0 (n = 18)	4.297 ± 0.249 (n = 18)	1.761 ± 0.226 (n = 18)	1.980 ± 0.261 (n = 18)	43.2 ± 4.9 (n = 18)	15.88 ± 1.54 (n = 16)
April	SML	11.2 – 11.8	35.6	8.04 ± 0.82 (n = 51)	0.49 ± 0.05 (n = 51)	3.02 ± 0.21 (n =51)	0.604 ± 0.059 (n = 52)	66.5 ± 4.7 (n = 47)	112.3 ± 24.2 (n = 50)	3.008 ± 0.207 (n = 50)	1.132 ± 0.134 (n = 49)	0.392 ± 0.235 (n = 48)	36.9 ± 6.1 (n = 51)	6.61 ± 1.29 (n = 50)
	ENACW	10.5 – 11.4	35.5 – 35.6	9.81 ± 1.16 (n = 54)	0.59 ± 0.07 (n = 54)	3.79 ± 0.72 (n = 54)	0.645 ± 0.092 (n = 53)	73.3 ± 6.2 (n = 53)	142.4 ± 25.4 (n = 54)	3.059 ± 0.153 (n = 54)	1.142 ± 0.036 (n = 54)	0.516 ± 0.176 (n = 54)	39.2 ± 6.2 (n = 54)	8.72 ± 1.51 (n = 53)
	MOW	7.1 – 10.5	35.41 – 35.66	15.51 ± 1.24 (n = 29)	0.95 ± 0.10 (n = 31)	8.99 ± 1.82 (n = 31)	0.351 ± 0.066 (n = 31)	77.3 ± 5.9 (n = 29)	233.2 ± 29.0 (n = 31)	3.686 ± 0.259 (n = 31)	1.253 ± 0.074 (n = 31)	1.416 ± 0.305 (n = 31)	44.6 ± 5.0 (n = 29)	17.36 ± 2.91 (n =30)
	NEADW	3.1 – 6.7	35.0 – 35.3	18.20 ± 0.70 (n = 13)	1.19 ± 0.08 (n = 14)	19.15 ± 5.82 (n = 14)	0.394 ± 0.180 (n = 14)	71.8 ± 5.1 (n = 11)	302.5 ± 29.5 (n 14=)	4.181 ± 0.247 (n = 14)	1.658 ± 0.271 (n = 13)	1.901 ± 0.296 (n = 14)	43.1 ± 4.6 (n = 14)	16.55 ± 0.67 (n = 14)

Table 6 Continued

Month	Depth range	Temperature (°C)	Salinity	NO_x^-	PO_4^{3-}	SiO_4^{4-}	DMn	DCo	DCd	DNi	DCu	DZn	DPb	DAl
July	SML	13.4 – 17.1	35.6	1.36 ± 1.55 (n = 33)	0.14 ± 0.09 (n = 33)	0.56 ± 0.35 (n = 33)	0.694 ± 0.099 (n = 23)	41.1 ± 8.9 (n = 22)	32.4 ± 13.5 (n = 23)	2.304 ± 0.190 (n = 23)	1.012 ± 0.067 (n = 23)	0.210 ± 0.117 (n = 20)	36.9 ± 4.6 (n = 23)	3.12 ± 0.58 (n = 21)
	ENACW	10.6 – 16.6	35.5 – 35.6	8.38 ± 2.84 (n = 122)	0.52 ± 0.16 (n = 122)	3.10 ± 1.34 (n = 122)	0.674 ± 0.152 (n = 87)	70.9 ± 10.7 (n = 86)	120.7 ± 41.8 (n = 87)	2.832 ± 0.264 (n = 87)	1.110 ± 0.068 (n = 86)	0.502 ± 0.276 (n = 87)	37.9 ± 4.3 (n = 87)	6.90 ± 2.52 (n = 78)
	MOW	6.6 – 10.6	35.3 – 35.7	15.36 ± 1.28 (n =55)	0.98 ± 0.09 (n = 55)	9.26 ± 2.12 (n = 55)	0.356 ± 0.082 (n = 23)	78.5 ± 3.5 (n = 23)	238.3 ± 26.9 (n = 23)	3.661 ± 0.239 (n = 23)	1.283 ± 0.095 (n = 23)	1.488 ± 0.256 (n = 23)	45.0 ± 4.4 (n = 20)	16.04 ± 2.32 (n = 23)
	NEADW	3.0 – 6.5	35.0 – 35.3	17.68 ± 0.71 (n = 33)	1.19 ± 0.06 (n = 33)	18.98 ± 4.88 (n = 33)	0.350 ± 0.053 (n = 16)	71.9 ± 3.5 (n = 17)	299.7 ± 22.0 (n = 17)	4.120 ± 0.234 (n =17)	1.704 ± 0.203 (n = 17)	2.072 ± 0.331 (n =17)	41.8 ± 4.5 (n = 17)	15.87 ± 0.90 (n = 17)

On the continental shelf, macronutrient concentrations ranged between 0.17 – 0.76 μmol kg^{-1} (PO_4^{3-}), 2.03 – 10.20 μmol kg^{-1} (NO_x^-), 0.76 – 5.53 μmol kg^{-1} (SiO_4^{4-}) in November and 0.06 – 0.60 μmol kg^{-1} (PO_4^{3-}), 0.94 – 9.29 μmol kg^{-1} (NO_x^-) and 0.69 – 5.10 μmol kg^{-1} (SiO_4^{4-}) in April and 0.02 – 0.77 μmol kg^{-1} (PO_4^{3-}), 0.02 – 9.23 μmol kg^{-1} (NO_x^-) and 0.20 – 6.11 μmol kg^{-1} (SiO_4^{4-}) in July.

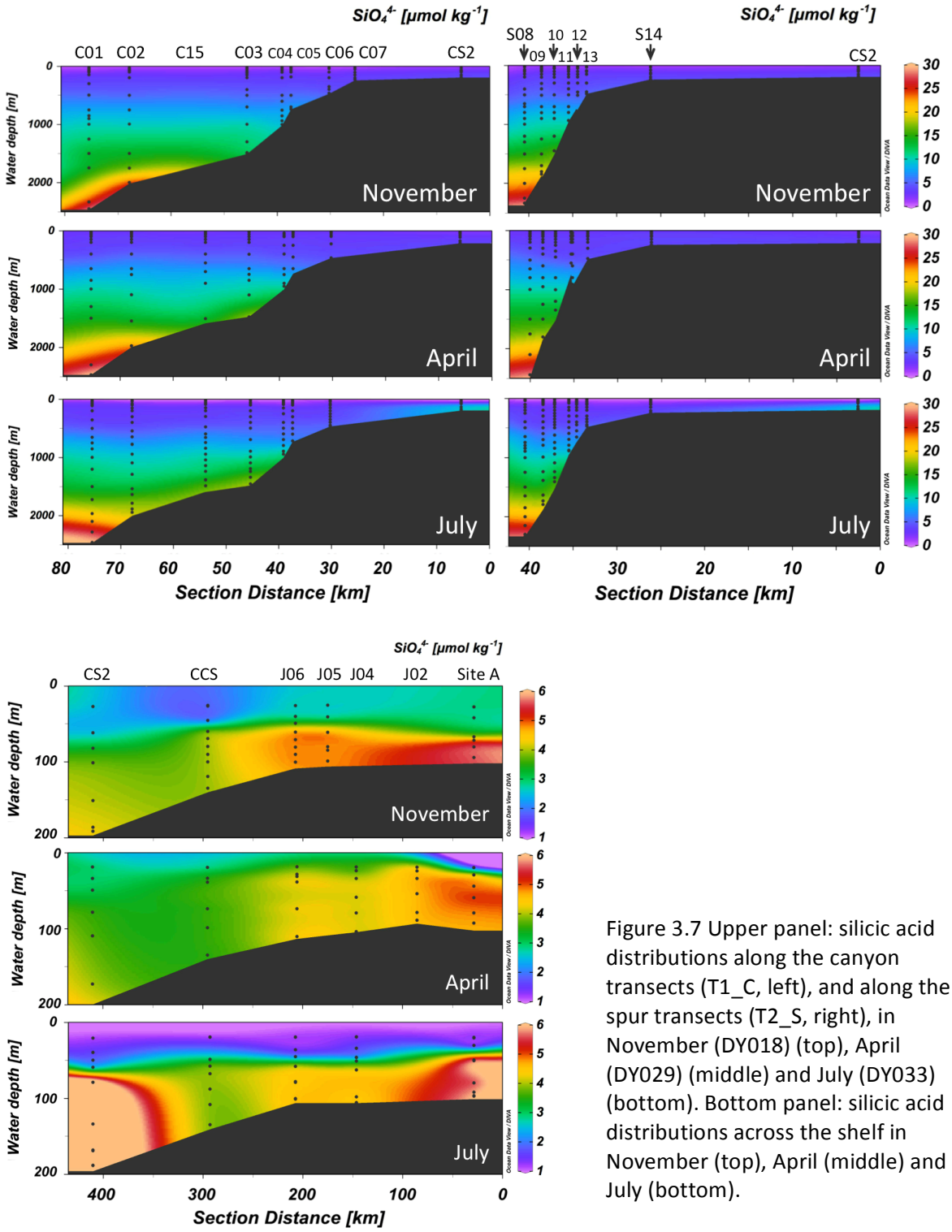


Figure 3.7 Upper panel: silicic acid distributions along the canyon transects (T1_C, left), and along the spur transects (T2_S, right), in November (DY018) (top), April (DY029) (middle) and July (DY033) (bottom). Bottom panel: silicic acid distributions across the shelf in November (top), April (middle) and July (bottom).

3.3.4 Trace metals distributions

Cadmium

Dissolved Cd concentrations are presented in Figure 3.8 and Table 6 and ranged between 56.0 – 355.9 pmol kg^{-1} in November, 39.0 – 357.1 pmol kg^{-1} in April and 15.2 – 347.0 pmol kg^{-1} in July in the continental shelf break region. The lowest DCd concentrations were observed in the SML and differed significantly between seasons (ANOVA (F(2, 106) = 149.2, p = < 0.05)), 69.4 ± 12.8 pmol kg^{-1} (n = 36) in November, 112.3 ± 24.2 pmol kg^{-1} (n = 50) in April and 32.4 ± 13.5 pmol kg^{-1} (n =

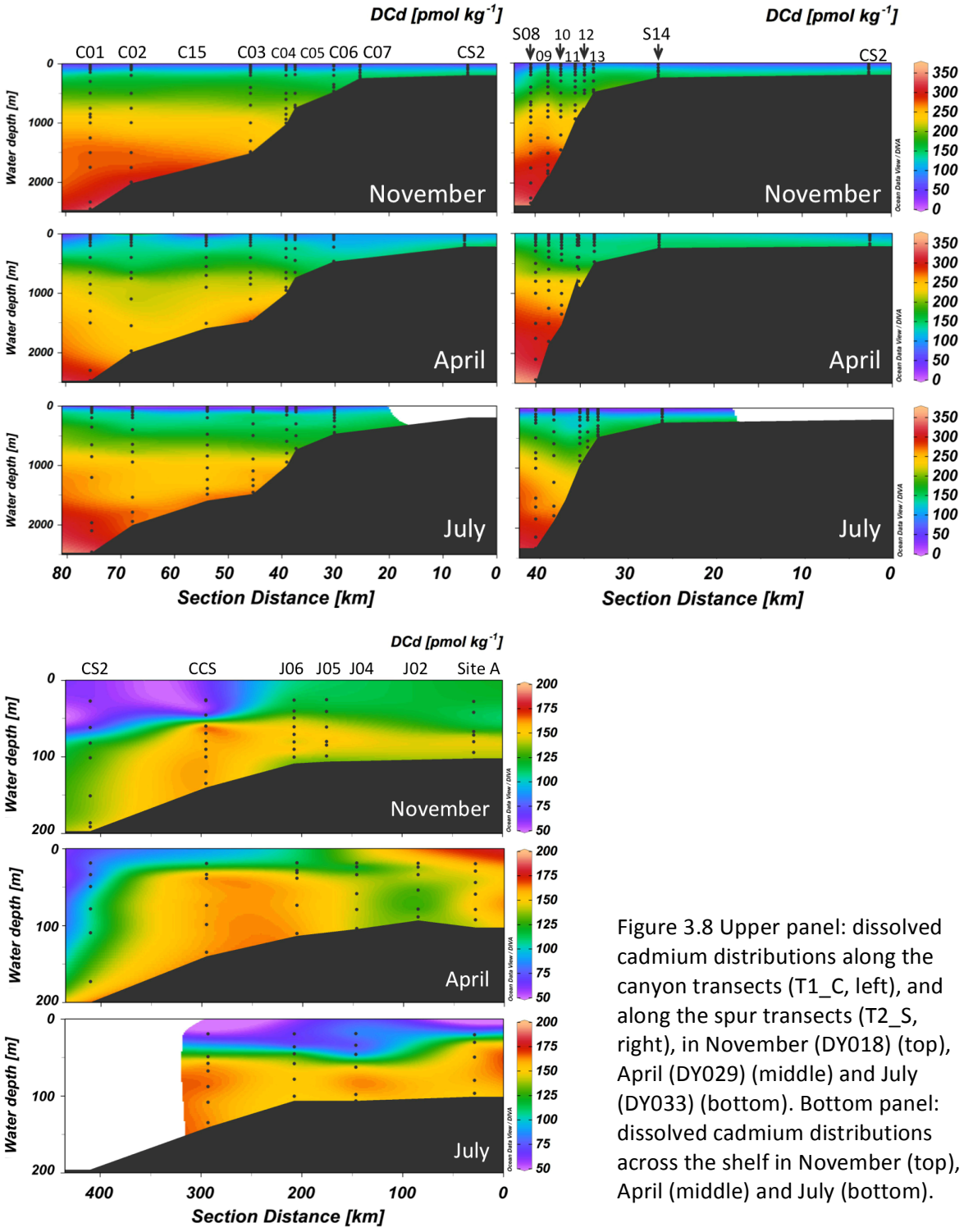


Figure 3.8 Upper panel: dissolved cadmium distributions along the canyon transects (T1_C, left), and along the spur transects (T2_S, right), in November (DY018) (top), April (DY029) (middle) and July (DY033) (bottom). Bottom panel: dissolved cadmium distributions across the shelf in November (top), April (middle) and July (bottom).

23) in July. Below the SML, DCd concentrations generally did not differ seasonally and gradually increased with depth to concentrations of 307.5 ± 24.8 pmol kg^{-1} (n = 49). These observations are in agreement with previous reports from the study region for summer surface (41 ± 20 pmol kg^{-1}, (Cotté-Krief et al. 2002)) (21 ± 6 pmol kg^{-1}, (Le Gall et al. 1999)), winter surface (104 ± 18 pmol kg^{-1} (Cotté-Krief et al. 2002)) and deep waters (310 ± 26 pmol kg^{-1}, (Cotté-Krief et al. 2002)). Dissolved Cd concentrations in surface waters in summer were also in agreement with North East Atlantic open ocean concentrations of 30 pmol kg^{-1} (Saager et al. 1997). Deep water DCd concentrations were in agreement with concentrations (295 ± 28 pmol kg^{-1}, n = 19) at stations USGT-10-1- USGT-

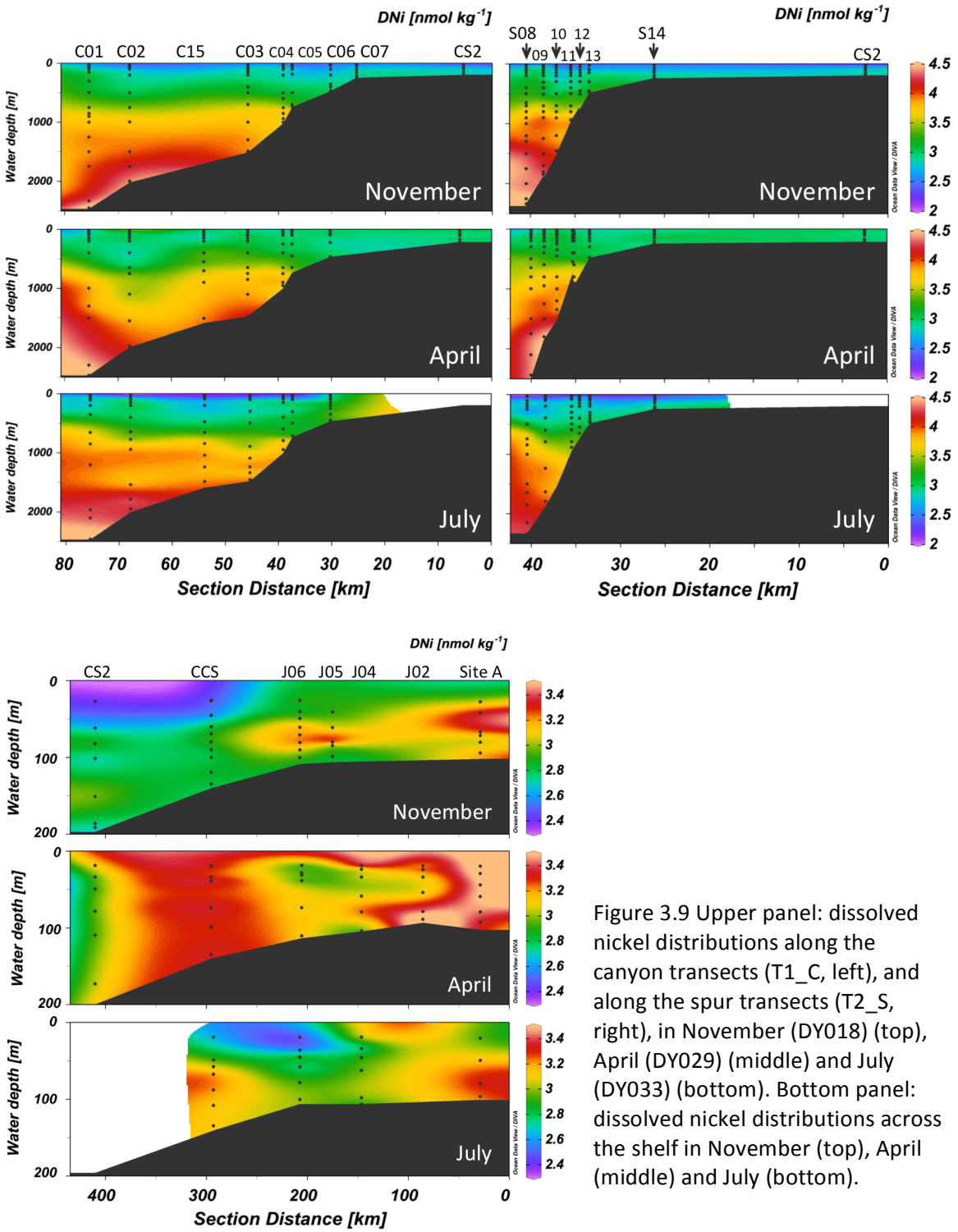


Figure 3.9 Upper panel: dissolved nickel distributions along the canyon transects (T1_C, left), and along the spur transects (T2_S, right), in November (DY018) (top), April (DY029) (middle) and July (DY033) (bottom). Bottom panel: dissolved nickel distributions across the shelf in November (top), April (middle) and July (bottom).

10-5 along GA03 section (Roshan & Wu 2015). On the continental shelf, DCd concentrations ranged between 59.1 – 184.4 pmol kg^{-1} in November, 92.8 – 155.8 pmol kg^{-1} in April and 55.4 – 167.7 pmol kg^{-1} in July with the lowest concentrations observed in surface waters and an increase with depth. DCd concentrations in the Celtic Sea reported here were generally lower than in previous reports (Muller et al. 1994).

Nickel

Dissolved Ni concentrations are presented in Table 6 and Figure 3.9 and ranged between 2.390 – 4.821 nmol kg^{-1} in November, 2.783 – 4.569 nmol kg^{-1} in April and 1.998 – 4.703 nmol kg^{-1} in

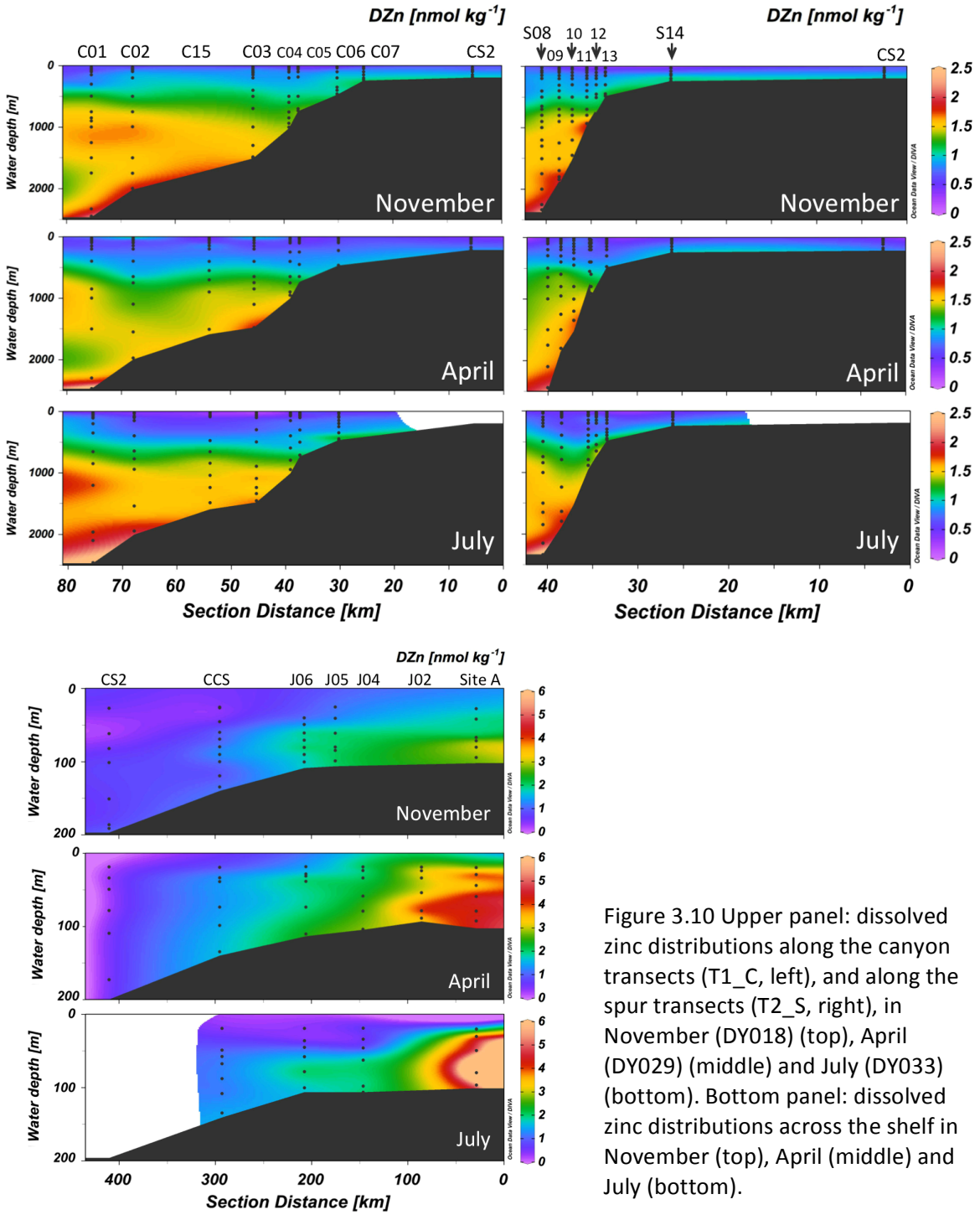


Figure 3.10 Upper panel: dissolved zinc distributions along the canyon transects (T1_C, left), and along the spur transects (T2_S, right), in November (DY018) (top), April (DY029) (middle) and July (DY033) (bottom). Bottom panel: dissolved zinc distributions across the shelf in November (top), April (middle) and July (bottom).

July. The lowest DNi concentrations were observed in the SML and differed significantly between seasons (ANOVA (F(2, 106) = 177.9, p = < 0.05)), 2.607 ± 0.147 nmol kg^{-1} (n = 36) in November, 2.976 ± 0.123 nmol kg^{-1} (n = 50) in April and 2.304 ± 0.190 nmol kg^{-1} (n = 23) in July. Below the SML, DNi concentrations generally did not differ seasonally and gradually increased with depth to concentrations of 4.203 ± 0.250 nmol kg^{-1} (n = 49). These observations were generally in agreement with previous reports from the study region (Cotté-Krief et al. 2002; Le Gall et al. 1999) and open ocean (Saager et al. 1997). However, mean DNi concentrations in the SML reported here were lower than values reported in the study region by Cote-Krief (3.0 ± 0.4 nmol kg^{-1} in summer and 3.5 ± 0.7 nmol kg^{-1} in winter) but in agreement with 2.44 ± 0.21 nmol L^{-1} in winter and 2.33 ± 0.26 nmol L^{-1} in summer reported by Kremling and Pohl (1989) in the study region and with the open ocean values (2.4 ± 0.8 nmol kg^{-1} in summer) (Saager et al. 1997). For deep water DNi concentrations, values reported here were in agreement with DNi concentrations reported for the study region (4.1 ± 0.4 nmol kg^{-1}) (Cotté-Krief et al. 2002) but higher than the open ocean concentrations (3.9 ± 0.9 nmol kg^{-1}) (Saager et al. 1997). On the continental shelf, DNi concentrations ranged between 2.401 – 3.385 nmol kg^{-1} in November, 2.900 – 3.661 nmol kg^{-1} in April and 2.477 – 3.501 nmol kg^{-1} in July. These concentrations were lower than concentrations measured in surface waters around the British coast (4 – 160 nM) (Achterberg et al. 1999).

Zinc

Dissolved Zn concentrations are presented Table 6 and Figure 3.10 and ranged between 0.172 – 2.384 nmol kg^{-1} in November, 0.152 – 2.665 nmol kg^{-1} in April and 0.068 – 2.755 nmol kg^{-1} in July. The lowest DZn concentrations were observed in the SML and differed significantly (ANOVA (F(2, 102) = 18.0, p = < 0.05)) between the autumn and summer and the spring and summer seasons, with no significant difference between autumn and spring seasons concentrations (Fisher's Least Significant Difference post-hoc (LSD) test (Chapter 2)). The DZn concentrations observed in the SML were 0.302 ± 0.102 nmol kg^{-1} (n = 36) in November, 0.338 ± 0.115 nmol kg^{-1} (n = 48) in April and 0.173 ± 0.062 nmol kg^{-1} (n = 20) in July. Below the SML, DZn concentrations generally did not differ seasonally and gradually increased with depth to concentrations of 1.989 ± 0.298 pmol kg^{-1} (n = 49). To my knowledge, there is only one historical DZn full depth profile observation in the Celtic Sea slope region (Danielsson et al. 1985). However, all DZn concentrations reported by Danielsson and co-workers were variable and higher than DZn concentrations reported here. On the continental shelf, DZn concentrations were elevated in comparison to the slope region and ranged between 0.114 – 3.703 nmol kg^{-1} in November, 0.162 – 5.236 nmol kg^{-1} in April and 0.363 – 7.280 nmol kg^{-1} in July with the lowest concentrations observed in surface waters and a general increase with depth. These concentrations were lower than concentrations measured in surface waters around the British coast (8 – 530 nM) (Achterberg et al. 1999).

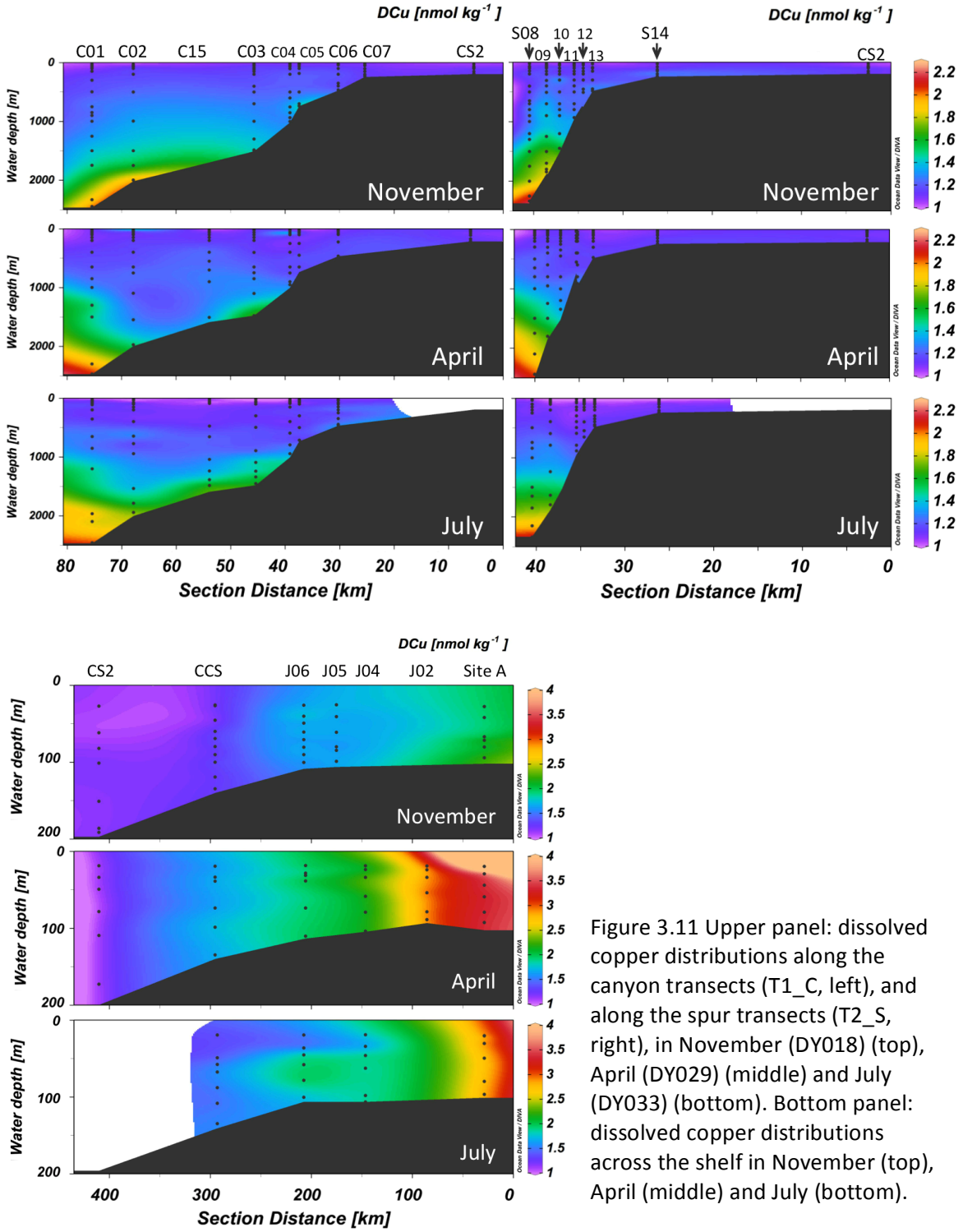


Figure 3.11 Upper panel: dissolved copper distributions along the canyon transects (T1_C, left), and along the spur transects (T2_S, right), in November (DY018) (top), April (DY029) (middle) and July (DY033) (bottom). Bottom panel: dissolved copper distributions across the shelf in November (top), April (middle) and July (bottom).

Copper

Dissolved Cu concentrations are presented in Table 6 and Figure 3.11 and ranged between 1.025 – 2.150 nmol kg^{-1} in November, 1.027 – 2.083 nmol kg^{-1} in April and 0.922 – 2.125 nmol kg^{-1} in July. Similarly to DZn, the lowest DCu concentrations were observed in the SML and differed significantly (ANOVA (F(2, 105) = 35.2, p = < 0.05)) between Autumn and Summer and Spring and Summer seasons, with no significant difference between Autumn and Spring season concentrations (LSD test, Chapter 2). The DCu concentrations observed in the SML were 1.087 ± 0.035 nmol kg^{-1} (n = 36) in November, 1.101 ± 0.032 nmol kg^{-1} (n = 49) in April and 1.012 ± 0.067

nmol kg^{-1} (n = 23) in July. Below the SML, DCu concentrations generally did not differ seasonally and gradually increased with depth to concentrations of 1.713 ± 0.230 pmol kg^{-1} (n = 48). Summer SML DCu concentrations reported here were in agreement with values reported by Kremling and Pohl (1989)) (1.07 ± 0.13 nmol L^{-1}) but lower than concentrations reported by Cotté-Krief et al. (2002) (1.18 ± 0.19 nmol kg^{-1}). Winter SML DCu concentrations agreed with previous measurements in the study region (1.04 ± 0.31 nmol kg^{-1}) (Cotté-Krief et al. 2002) and values in the open ocean (1.04 ± 0.31 nmol kg^{-1}) for the same season (Saager et al. 1997). In case of deep water DCu concentrations, values reported here were higher than in previous reports for the study region (1.56 ± 0.33 nmol kg^{-1}) (Cotté-Krief et al. 2002) but in agreement with open ocean values (1.73 ± 0.4 nmol kg^{-1}) (Saager et al. 1997). On the continental shelf, DCu concentrations were elevated in comparison to the slope region and ranged between 1.035 – 2.395 nmol kg^{-1} in November, 1.078 – 4.433 nmol kg^{-1} in April and 1.418 – 3.993 nmol kg^{-1} in July.

Cobalt and Aluminium

This chapter focuses on the variability of DCo and DAl in the upper waters on the continental slope only, where a significant correlation with macronutrients was observed ($r^2 > 0.74$). The DCo distributions below the SML are discussed in detail in Chapter 4 and DAl distributions below ENACW are discussed in Chapter 5. Concentrations of DCo and DAl in the SML are presented in Table 6 and Figure 3.12 and ranged between 26.6 – 75.6 pmol kg^{-1} and 2.58 and 14.78 nmol kg^{-1} for DCo and DAl, respectively. The DCo and DAl concentrations in the SML varied significantly between seasons, DCo: ANOVA ($F(2, 102) = 150.5$, p = < 0.05) and DAl: ANOVA ($F(2, 105) = 87.4$, p = < 0.05)) with mean concentrations of 55.1 ± 4.5 pmol kg^{-1} (n = 36), 66.5 ± 4.7 pmol kg^{-1} (n = 47), 41.1 ± 8.9 pmol kg^{-1} (n = 22) for DCo and 4.84 ± 0.63 nmol kg^{-1} (n = 34), 6.61 ± 1.29 nmol kg^{-1} (n = 50), 3.02 ± 0.33 nmol kg^{-1} (n = 21) for DAl in November, April and July, respectively.

3.4 Discussion

The PCA revealed distinct groups of DTMs (Figure 3.3): DCd, DZn, DNi, DAl, DCu, DCo in association with macronutrients (phosphate (PO_4^{3-}) and silicic acid (SiO_4^{4-})), and two separate groups of DTMs (DMn and DPb), which can be associated with the global DTMs categorisation described in the Chapter 1. Dissolved Cd, Zn, Ni and Cu are generally classified as nutrient-like metals due to their resemblance of macronutrient profiles with low surface water concentrations that increase with depth, which is also evident in the PCA results. Dissolved Mn and DPb usually exhibit a scavenged-type depth profile with concentration maximum in the upper waters that decrease with depth (Bruland & Lohan 2004), which would explain the anti-correlation of DMn and nutrient-like DTMs and macronutrients. However, DPb did not correlate with any other

variables suggesting distinct factors influencing its distributions in the study region. Dissolved Co has been reported as a hybrid-type element that features nutrient-like behaviour in the upper waters and scavenged-type in deeper waters (Bruland & Lohan 2004). The results of this PCA—alongside global TMs observations—structured this thesis, dividing it into three chapters: nutrient-like TMs (DCd, DZn, DNi, DCu, DAl) and their relationship with macronutrients (Chapter 3), sedimentary derived DTMs (DMn and DCo) (Chapter 4) and the anthropogenic contaminant DPb (Chapter 5).

3.4.1 Continental shelf break

Dissolved Cd, Zn, Ni and Cu exhibited nutrient-like vertical depth profiles during all seasons, with the lowest concentrations observed in surface waters due to biological utilization and enhanced concentrations with depth due to remineralization of sinking biogenic particles (Bruland & Lohan 2004). These observations are in agreement with global ocean observations of nutrient-like metals (Bruland & Lohan 2004). Surface water concentrations differed significantly between seasons (section 3.4.1.1) and strong correlations (Figure 3.13) with major macronutrients (PO_4^{3-}, nitrate and nitrite (NO_x^-) and SiO_4^{4-}) (r^2 = 0.77 – 0.97) were observed. The strongest correlations were observed between PO_4^{3-} and DCd (r^2 = 0.97), DZn (r^2 = 0.91), DNi (r^2 = 0.90), DCo (r^2 = 0.77)

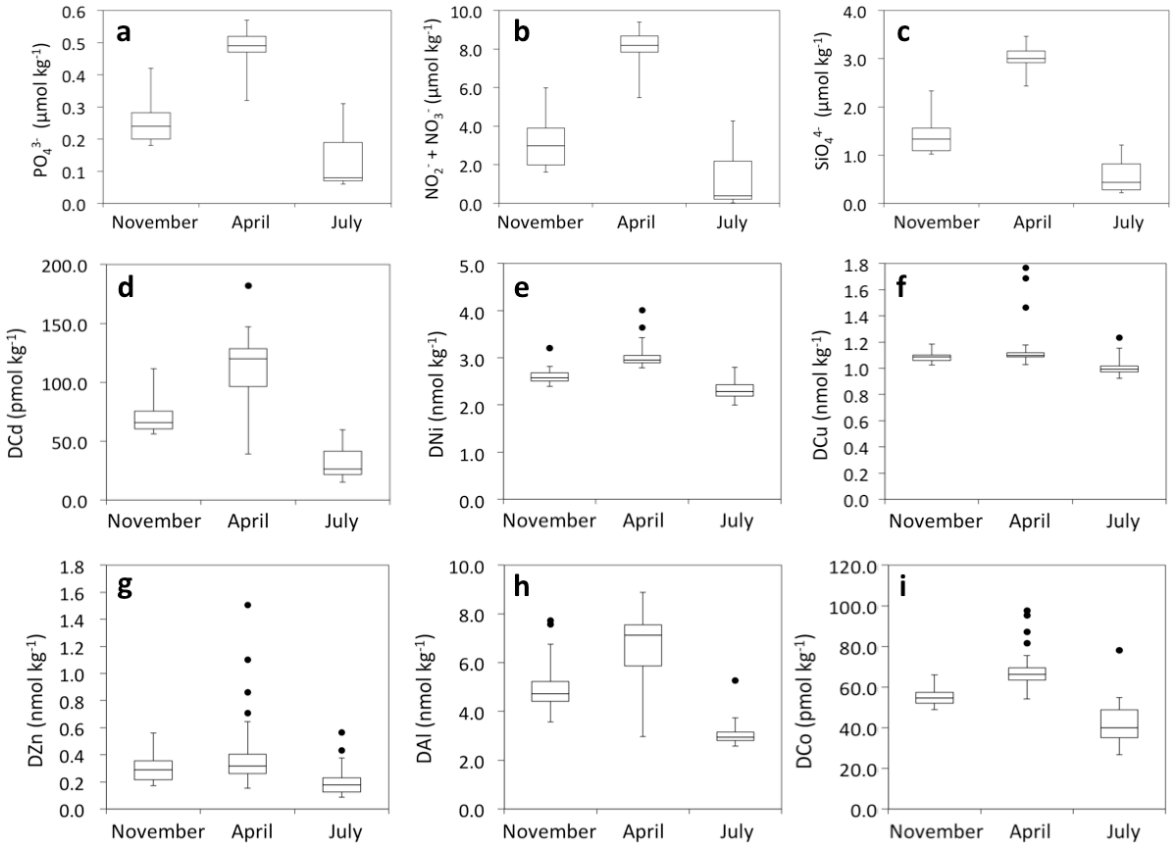


Figure 3.12 Box plots of concentrations of phosphate (a), nitrate and nitrite (b), silicic acid (c), dissolved cadmium (d), nickel (e), copper (f), zinc (g), aluminium (h) and cobalt (i) in November left column of each plot, April middle column and July right column.

and DAl (r^2 = 0.80), and between SiO_4^{4-} and DCu (r^2 = 0.92) and DAl (r^2 = 0.85), and hence this discussion focuses on relationships with these macronutrients. In case of DCo and DAl distributions in deeper waters, the influence of additional biogeochemical processes such as scavenging (DCo) and presence of MOW (DAl) was observed. These processes are further discussed in Chapter 4 and Chapter 5. The following three sections focus on elemental ratios of TMs relative to PO_4^{3-} and SiO_4^{4-}. Section 3.4.1.1 discusses variability of TM concentrations in surface waters and their elemental ratios across three different seasons, whilst sections 3.4.1.2 and 3.4.1.3 focus on full depth profile of TMs and their 'overall' relationships with macronutrients for all seasons.

3.4.1.1 Seasonal variability in surface waters

A significant seasonal signal in concentrations of all metals and macronutrients was observed in off-shelf surface waters between April 2015 and July 2015 due to water column stratification and biological utilization (Figure 3.12). A drawdown of TMs: 80 pmol kg^{-1} (71%) DCd, 0.671 nmol kg^{-1} (23%) DNi, 0.089 nmol kg^{-1} (8%) DCu, 0.165 nmol kg^{-1} (49%) DZn, 3.59 nmol kg^{-1} (54%) DAl and 25.4 pmol kg^{-1} (38%) DCo was observed, with a drawdown of 0.35 μmol kg^{-1} (72%) PO_4^{3-}, 6.68 μmol kg^{-1} (83%) NO_x^- and 2.46 μmol kg^{-1} (81%) SiO_4^{4-} for macronutrients. Drawdown of Cd, Ni and NO_x^- observed between the four months of April to July 2015 in the slope region of the Celtic Sea was higher, and drawdown of Cu was lower than previously reported for the study region between January 1994 and June 1995 (36% NO^{3-}, 41% Cd, 22% Cu, 14% Ni) (Cotté-Krief et al. 2002) and March – June 1987 (56% Cd, 12% Cu, 4% Ni) (Kremling & Pohl 1989). Furthermore, the surface water drawdown reported here, yielded the following 'uptake' ratio as normalised to PO_4^{3-}:

$$(N_{19\pm0.4}Si_{7\pm0.3}P_1)_{1000}Al_{10\pm0.5}Ni_{1.9\pm0.4}Zn_{0.5\pm0.9}Cu_{0.25\pm0.89}Cd_{0.2\pm0.5}Co_{0.07\pm0.49}$$

A significant increase of surface water concentrations of all metals and macronutrients was observed between July and November in the Celtic Sea study region, 37.1 pmol kg^{-1} DCd, 0.303 nmol kg^{-1} DNi, 0.074 nmol kg^{-1} DCu, 0.129 nmol kg^{-1} DZn, 1.83 nmol kg^{-1} DAl and 14.0 pmol kg^{-1} DCo whilst 0.12 μmol kg^{-1} PO_4^{3-}, 1.74 μmol kg^{-1} NO_3^- and 0.82 μmol kg^{-1} SiO_4^{4-} for macronutrients. The surface water build-up reported here, yielded the following 'remineralisation' ratio:

$$(N_{15\pm1.5}Si_{7\pm1.1}P_1)_{1000}Al_{15\pm1}Ni_{2.5\pm1.2}Zn_{1\pm1.32}Cu_{0.6\pm1.4}Cd_{0.3\pm1.1}Co_{0.12\pm1.18}$$

The difference between the 'uptake' ratio and 'remineralisation' ratios, with larger values for all metals in the remineralisation ratio, can be explained by metal inputs from deeper oceanic waters that increased TM:P ratios (Figure 3.13 and Cu:P (r^2 = 0.69, n = 48)):

$$(P_1)_{1000}Al_{18.2}Ni_{1.7}Zn_{2.3}Cu_{0.3}Cd_{0.3}$$

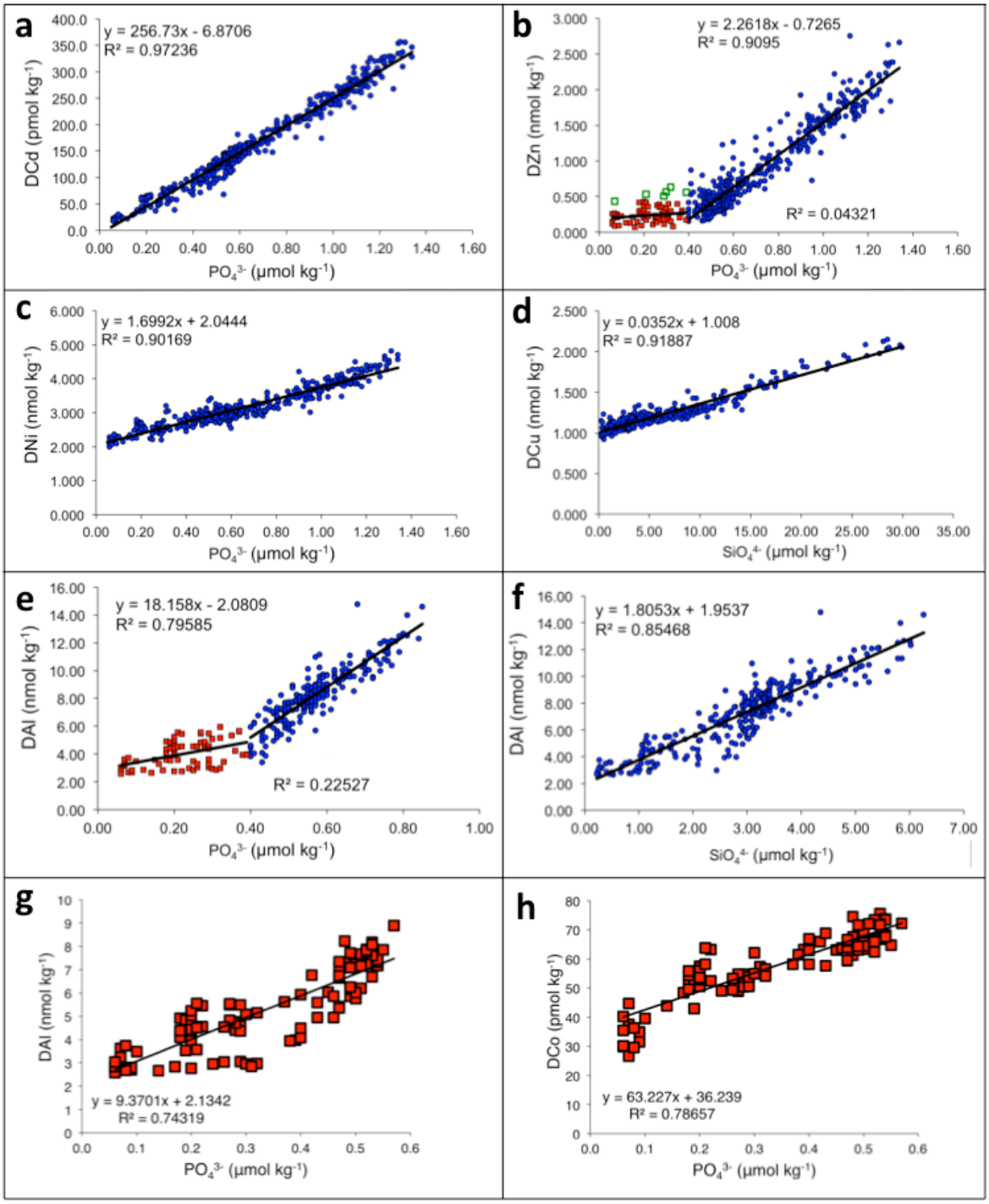


Figure 3.13 Relationships between phosphate and dissolved cadmium (a), zinc (b), nickel (c) and silicate and dissolved copper (d) for full depth profiles during all seasons. Red squares in plot (b) indicate phosphate concentrations < 0.4 µmol kg^{-1} where the linear correlation was not significant, green squares indicate outliers omitted in the linear analysis. Examination of relationships between phosphate and dissolved aluminium (e) and silicic acid and aluminium (f) (waters above Mediterranean Outflow Waters). Dissolved aluminium (g) and dissolved cobalt (h) relationship with phosphate in surface waters during all seasons.

A further increase in concentrations of all metals and macronutrients was observed between November and April, presumably as a result of the resupply of nutrients to surface waters via winter mixing: 42.9 pmol kg^{-1} DCd, 0.368 nmol kg^{-1} DNi, 0.015 nmol kg^{-1} DCu, 0.036 nmol kg^{-1} DZn,

1.77 nmol kg^{-1} DAl and 11.4 pmol kg^{-1} DCo whilst 0.24 μmol kg^{-1} PO_4^{3-}, 4.95 μmol kg^{-1} NO_3^- and 1.64 μmol kg^{-1} SiO_4^{4-} in macronutrients and yielded the following 'remineralization-winter mixing' (from hereafter referred to as 'winter mixing') ratio:

$$(N_{21\pm0.5}Si_{7\pm0.4}P_1)_{1000}Al_{7.4\pm0.9}Ni_{1.5\pm0.6}Zn_{0.2\pm4.32}Cu_{0.06\pm3.25}Cd_{0.2\pm0.7}Co_{0.05\pm0.66}$$

Elemental ratios observed in the Celtic Sea region agreed well with the full depth ratios in the North Atlantic Ocean compiled by Twining and Baines (2013):

$$(P_1)_{1000}Ni_{1.6}Zn_{2.6}Cu_{0.3}Cd_{0.2}Co_{0.06}$$

and with the extended Redfield ratio obtained by Ho et al. (2003), for phytoplankton cultures:

$$(C_{106}N_{16}P_1)_{x1000}Zn_{0.8}Cu_{0.4}Cd_{0.2}Co_{0.2}$$

Nutrient-like TM concentrations are assumed to be influenced by the same biogeochemical processes as macronutrients. However, if this is strictly the case, the elemental 'uptake', 'remineralization' and 'winter mixing' elemental ratios should be uniform. The differences in elemental concentrations between seasons in the Celtic Sea region were significant and the elemental ratios were in excess of error for N, Si and Al but within error for all other elements under consideration. Nevertheless, the potential of metal specific biogeochemical processes relative to PO_4^{3-} over a short time scale (< 4 months) should be considered in future studies. Given that all the nutrient-like TMs, except Al, are not susceptible to scavenging, findings reported here may suggest inter-seasonal differences in TMs remineralisation and/or uptake rates of TMs relative to PO_4^{3-}. Although Fe and manganese (Mn) are crucial bioessential micronutrients, they were not included in the above comparison. A seasonal variability was not observed in DMn distributions in the SML (Chapter 4) and DFe distributions were not considered as part of this thesis. Further interpretation of this dataset in preparation for publication will consider the elemental Fe:P ratio.

A nutrient-like biogeochemical behaviour for DAl was a surprising observation that emerged from the above comparison of elemental ratios. Given that Al has no known biological function in marine organisms and is considered a scavenging-type metal, its correlation with PO_4^{3-} was suggestive of either passive biological uptake or adsorption onto biogenic particles. Further discussion of DAl relationship with macronutrients can be found in section 3.4.1.2

3.4.1.2 DCd, DZn DAl and DCo relationship with PO_4^{3-} in full depth profiles

The strongest positive linear correlation with PO_4^{3-} was observed for DCd (r^2 = 0.97, n = 458) and yielded a Cd:P ratio of 257 μmol mol^{-1} based on a linear regression of dissolved species concentrations across full depth profiles in all seasons. The Cd:P relationship observed in the Celtic Sea can be described by one set of data points without a distinct 'kink'. Full depth profiles

of DCd and PO_4^{3-} were obtained for the GA03 study in the Gulf of Cadiz (Figure 3.14) from the GEOTRACES intermediate product (IDP 2017). The examination of Cd:P correlation in these waters revealed a 'kink' at 0.3 μmol kg^{-1} PO_4^{3-} (Figure 3.15) (stations USGT-10-1-USGT-10-5, IDP 2017). The Cd:P relationship yielded 84 μmol mol^{-1} (r^2 = 0.78, n = 10) Cd:P ratios in waters < 0.3 μmol kg^{-1} PO_4^{3-} and 281 μmol mol^{-1} (r^2 = 0.98, n = 57) in waters above > 0.3 μmol kg^{-1} PO_4^{3-}. The full GA03 dataset from the North Atlantic exhibited Cd:P ratios of 274 μmol mol^{-1} but was limited to waters > 300 m depth (Roshan & Wu 2015). Therefore, the Cd:P ratios in the Celtic Sea agreed well with observations in North Atlantic waters (> 300 m depth) with our study lacking a 'kink' at low PO_4^{3-} concentrations, which is potentially the result of local biological activity in surface waters (Cullen et al. 2003; Cullen 2006; Sunda & Huntsman 1995; Elderfield & Rickaby 2000).

A number of potential biogeochemical processes causing a 'kink' in Cd:P ratios have been suggested: (i) deeper water Cd regeneration relative to PO_4^{3-} (Boyle 1988), (ii) transport of water masses with different Cd:PO_4^{3-} ratios (Xie et al. 2015), (iii) Fe limitation and/or Zn depletion in surface waters (Cullen 2006) leading to enhanced Cd uptake relative to PO_4^{3-} or (iv) Cd substitution for Co/Zn in CA (Sunda & Huntsman 1995; Morel et al. 1994). Considering the consistency of Cd:P ratios in deeper waters for the GA03 and Celtic Sea study regions, the latter two processes (iii and iv) relevant to elemental ratios in surface waters are considered. A significant drawdown of DFe to 0.03 – 0.16 nM (Birchill 2017) and DZn (0.210 ± 0.117 nmol kg^{-1}, n = 20) concentrations was observed in Celtic Sea surface waters in July (Birchill 2017). These potentially phytoplankton growth limiting conditions were supportive of the mechanisms (iii) and consequently formation of a distinct 'kink' in Cd:P relationship, which is in contrast to findings reported here. However, low (micro-nutrient) conditions in the Celtic Sea were observed only in July, and thus were a seasonal, not a persistent feature. It is likely that the short timescale of these conditions was insignificant to affect the overall Cd:P relationship in our study region, in contrast to the permanently oligotrophic surface waters in the North Atlantic gyre (GA03 study region).

Mechanism (iv) suggests a close association of Cd uptake and Co/Zn availability in surface waters and a potential of Cd substitution for Co/Zn in CA (Sunda & Huntsman 1995; Morel et al. 1994; Elderfield & Rickaby 2000). Interestingly, the Zn:P ratio could also be split into two groups of data points separated by a distinct 'kink' at 0.4 μmol kg^{-1} PO_4^{3-}. The 'kink in Zn:P has been observed at 1.5 μmol kg^{-1} PO_4^{3-} globally (Wyatt et al. 2014; Vance et al. 2017). As evident from Figure 3.13, the Zn to P correlation was weak in waters with PO_4^{3-} < 0.4 μmol kg^{-1} (r^2 = 0.04), but for waters PO_4^{3-} > 0.4 μmol kg^{-1} a Zn:P ratio of 2261 μmol mol^{-1} (r^2 = 0.91, n = 378) was observed and in agreement with an estimation of 2161 μmol mol^{-1} for the North Atlantic (Figure 3.15) (stations USGT-10-3 and USGT-10-5, IDP 2017). A Zn:P ratio of 1304 ± 802 μmol mol^{-1} (n = 71) in waters PO_4^{3-} < 0.4 μmol kg^{-1} was determined as the mean Zn:P ratio of all data points, and was

higher than Zn:P estimation in the North Atlantic (440 μmol mol^{-1}, Figure 3.15). Higher Zn:P ratios in the Celtic Sea surface waters were potentially a result of the more nutrient replete conditions throughout the year in comparison to the GA03 study. Although, there was no obvious evidence for off-shelf transport of DZn at a time of sampling (section 3.4.2), and considering elevated DZn concentrations on the shelf (> 3.7 nmol kg^{-1}), the influence of coastal DZn sources on this ratio cannot be ruled out.

A significant linear correlation (r^2 = 0.79, n = 105) of DCo with PO_4^{3-} was observed in surface waters and yielded Co:P ratios of 63 μmol mol^{-1} (Figure 3.13). Below the SML, there was no correlation between DCo and PO_4^{3-} due to scavenging processes (Chapter 4). The Co:P ratio observed in surface waters of the Celtic Sea is in agreement with ratios observed in surface waters of the North Atlantic (64 μmol mol^{-1} (Saito et al. 2017)) and North Atlantic Subtropical Gyre (67 μmol mol^{-1} (Saito et al. 2017)). The observed Co:P ratio of 63 μmol mol^{-1} in the Celtic Sea study region was below the optimal growth requirements of coccolithophore (*E.Huxleyi*) and diatom species (*Thalassiosira oceanica* and *Thalassiosira pseudonana*), but above those for

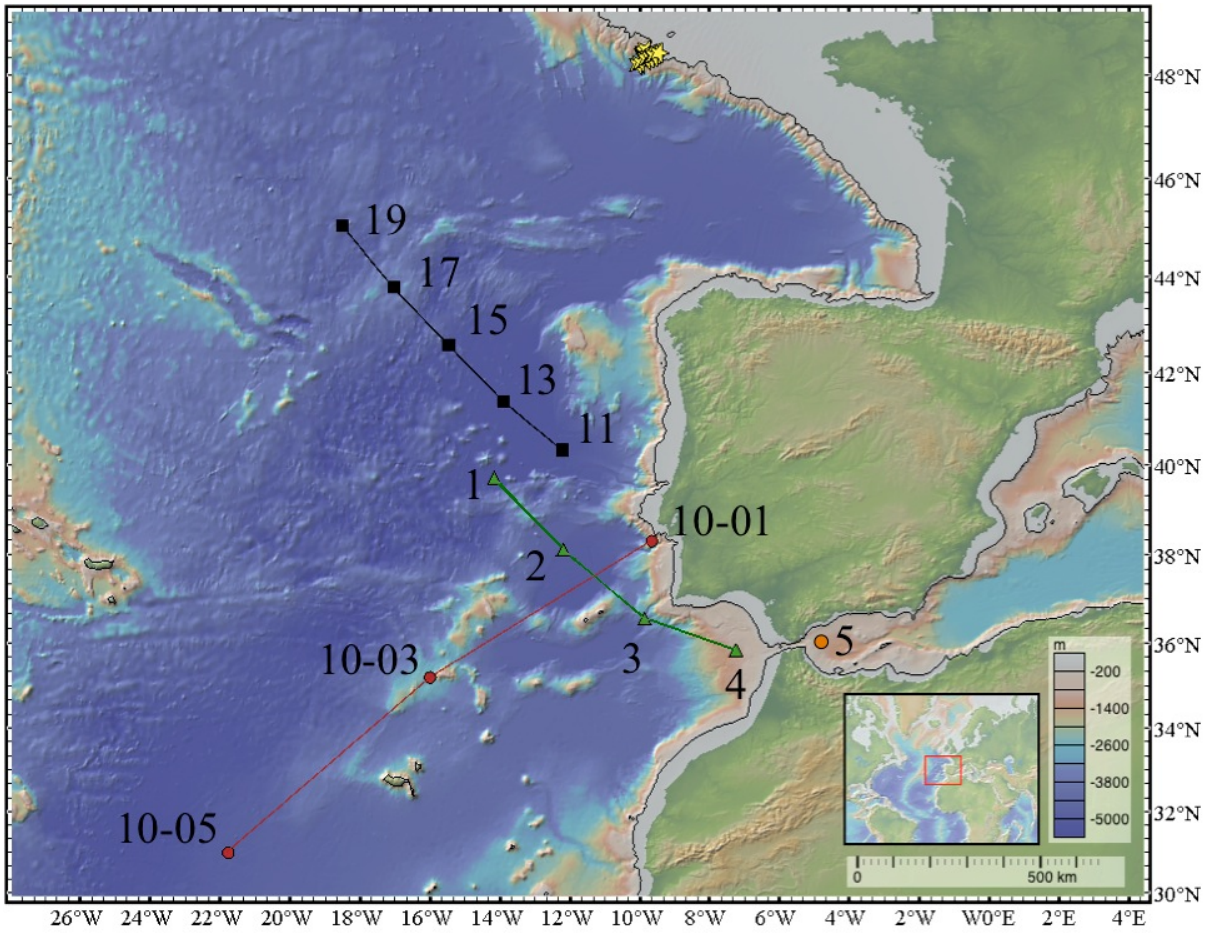


Figure 3.14 Station locations across GEOTRACES sections: GA03 in 2010 (red circles) (Noble et al. 2015), GA04 in 2013 (green triangles), GA01 in 2014 (black squares) and our study region in 2014 (yellow stars). Map generated using GeoMapApp, http://www.geomppapp.org (Ryan et al. 2009). Station 5 in the Alboran Sea (Western Mediterranean Sea) formed part of the GA04 expedition in 2013.

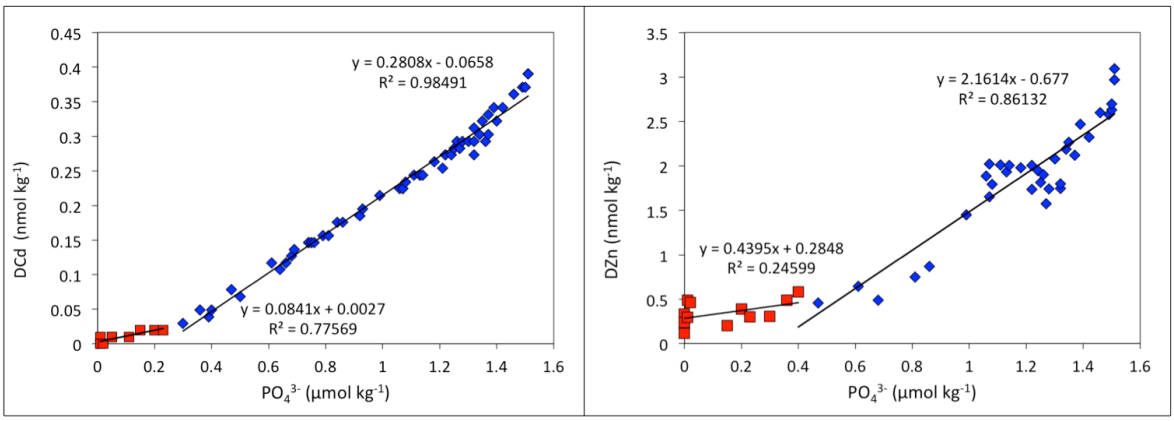


Figure 3.15 Examination of full depth profiles of dissolved cadmium (left) and dissolved zinc (right) along the GA03 GEOTRACES section GA03 section, stations UGT-10-01 – UGT-10-05 (cadmium) and stations UGT-10-03 and UGT-10-05, IDP 2017.

cyanobacteria (*Synechococcus bacillaris*) (Sunda & Huntsman 1995). Therefore, the kink in Zn:P relationship could potentially be a result of Zn-Co cambialism in surface waters where Cd concentrations were not affected.

Surprisingly, the Al:P ratio also exhibited a distinct 'kink' at 0.4 µmol kg^{-1} PO_4^{3-} (Figure 3.13). Similarly to Zn and P, the correlation between Al and P was weak (r^2 = 0.22) in waters < 0.4 µmol kg^{-1} PO_4^{3-}, and we estimated a mean Al:P ratio of 214000 ± 10.7 µmol mol^{-1} (n = 74). In waters > 0.4 µmol kg^{-1} PO_4^{3-} and above the MOW (where a DAl maximum was observed, Chapter 5) the Al:P ratio was 18158 µmol mol^{-1} (r^2 = 0.80, n = 58). The strong correlation of DAl and macronutrients as evident from depth profiles (Figure 3.13) and confirmed by the PCA (Figure 3.3), was an unexpected finding given that aluminium is not thought to be bioessential. The structural association of Al and silica at the stage of biosynthesis has been reported through an examination of diatom opaline frustules (Gehlen et al. 2002). Recently, a correlation and DAl concentrations and silicic acid (r^2 = 0.76) has been observed in the North Atlantic surface waters and connected with diatom abundance (Menzel Barraqueta et al. 2018), further confirming Al association with biogenic particles. A strong correlation (r^2 = 0.85, n = 132) between DAl and SiO_4^{4-} Figure 3.13) was observed in upper waters (SML and ENACW, < 27.30 kg m^{-3} σ_0) in the Celtic Sea study region without a distinct 'kink' suggestive of a close association of DAl with SiO_4^{4-} biogeochemical cycles. Although the Al:P and Zn:P ratios exhibited similar patterns, a strong correlation of DAl with PO_4^{3-} and the apparent 'kink' cannot be explained by the elevated biological uptake of DAl due to low concentrations of other TMs (mechanism iii) or replacement in enzymes (mechanism iv) as suggested for Zn:P. Although passive uptake and/or biogenic particle DAl and DZn scavenging (John & Conway 2014) have been suggested, it is not clear why the PO_4^{3-} relationship with non bioessential DAl mimicked the relationship of the bioessential element Zn. This aspect should be addressed in future studies.

3.4.1.3 Ni and Cu relationship with macronutrients

In the Celtic Sea region, good correlations between DNi and PO_4^{3-} (r^2 = 0.90, n = 458) and between DCu and SiO_4^{4-} (r^2 = 0.92, n = 453) were observed. The correlation of Ni and PO_4^{3-} was suggestive of uptake by phytoplankton in surface waters and deep water remineralization of sinking organic matter but the correlation of DCu with SiO_4^{4-} suggests a more specific association with siliceous diatom frustules. Hard opal frustules remineralize over longer timescales, and hence the SiO_4^{4-} and DCu concentrations enhancement is usually observed in deeper oceanic waters in comparison to shallower remineralisation of sinking soft tissue material with release of PO_4^{3-} and NO_x^-, DCd (Twining et al. 2012). However, Ni has been found within diatom cells, likely as part of urease and superoxide dismutase enzymes or potentially organic material as suggested for Zn (Vance et al. 2017), but also Ni also contributes to opaline frustules (Twining et al. 2012). In contrast to DCo, DCd and DZn, DNi and DCu concentrations did not decrease to sub-nanomolar or picomolar levels and exhibited the smallest drawdown in surface waters in summer (23% DNi, and 8% DCu) suggesting that these metals were potentially in excess of biological requirements. Although both of these micronutrients are bioessential to marine organisms, studies that focus on their biogeochemical cycles are scarce.

3.4.2 Continental shelf system

The residence time of waters in the Celtic Sea is 1 – 2 years (Hydes et al. 2004). Sampling in the Celtic Sea in late autumn (November), spring (April) and summer (July) provided the opportunity to study a seasonal cycle of TMs. Distinctively different biogeochemical behaviours for a range of DTMs (Cu, Co, Ni) were observed in the continental shelf environment in contrast to the shelf break system. For simplicity, the following discussion excludes Site A (unless specifically stated), where strong sediment resuspension events and enhanced turbidity were observed across all seasons, and freshwater inputs were observed in surface waters in April and July. The events were most prominent at Site A and are discussed further in Chapter 4 and Chapter 5, and were not observed to the same extent at any other station in the Celtic Sea. Therefore, stations J02 – J06, CCS and CS2 were selected as representative for the Celtic Sea shelf environment. In general, DTMs on the continental shelf can be divided into two groups according to their correlation with salinity (DCo, DCu and DMn, full depth data) across all the stations, and with PO_4^{3-} (DCd and DZn) across the majority of stations during all seasons. DNi did not show a significant correlation with either salinity (r^2 = 0.24) or macronutrients (r^2 = 0.09, n = 129). Considering that DNi is not susceptible to scavenging, the exact processes influencing DNi distribution on the Celtic Sea continental shelf were unclear. Nevertheless, the relatively high DNi concentrations with little

evidence for biological removal and remineralisation, combined with negligible freshwater inputs, may contribute to the lack of correlations between DNi and salinity or nutrients.

Concentrations of DCu and DCo were elevated on the continental shelf in comparison to concentrations along the off-shelf transects, which is suggestive of continental sources. A strong inverse correlation was observed between salinity and DCu (r^2 = 0.81, n = 129), and DCo (r^2 = 0.78, n = 128) (Figure 3.16) across all seasons, which indicates a fluvial input and physical mixing of low-salinity, metal-enriched waters with saline, low-metal oceanic waters. The strong correlation of DCu with salinity has been previously observed in the study region (Muller et al. 1994).The more coastal stations were in close proximity to the Bristol Channel and River Severn, one of the largest river systems in the UK (Zhao & Marriott 2013). The Severn river has been subject of disposal of commercial and household effluents, with metal refining activities inputs centred around Avonmouth and South Wales (Apte et al. 1990), which form important sources of DTMs. Evidence for sedimentary inputs of DCo was also observed, particularly at Site A where elevated concentrations of these metals towards the seafloor were found. Similar observations were made for DMn, and along with DCo are described in Chapter 4. Therefore, DCo and DCu distributions were mainly controlled by physical mixing of water masses and sedimentary inputs on the continental shelf across all seasons.

Overall, a good correlation between DCd and PO_4^{3-} (r^2 = 0.76, n = 128) was observed on the shelf, in contrast to DZn (r^2 = 0.17, n = 87). However, a closer examination of the relationships with PO_4^{3-} at each station revealed a wide range in linear relationships between Cd and P and Zn and P with various slopes across the shelf in November and April, whilst in July the elemental ratios were more homogenous (Figure 3.17). The autumn season (November) was defined by low irradiance and a weakly stratified water column. A linear correlation of DCd with PO_4^{3-} was observed at stations CS2 and CCS (casts from 11/11/2014 and 29/11/2014) (r^2 = 0.97, n = 29) which yielded a ratio of Cd:P of 213 μmol mol^{-1}. At stations J05 and J06 a linear correlation of DCd

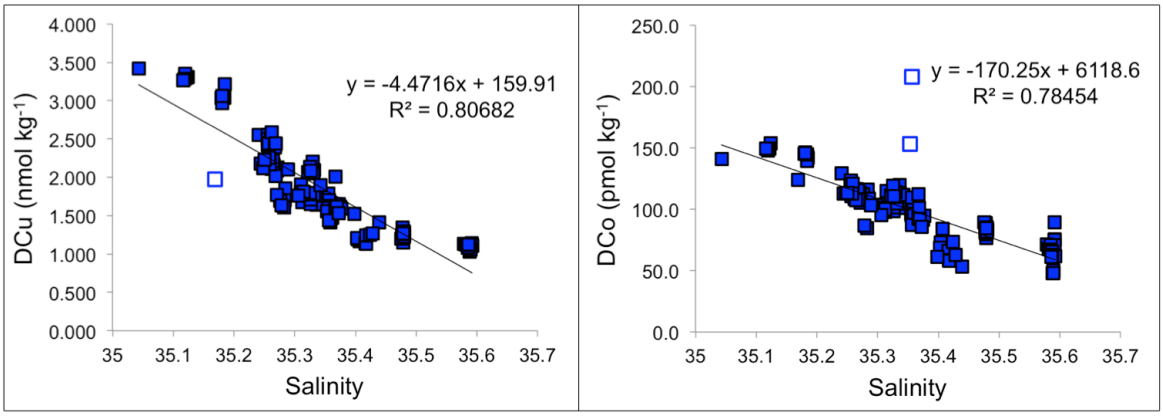


Figure 3.16 Dissolved copper (left) and dissolved cobalt (right) versus salinity for full depth datasets across the shelf during all seasons. Open symbols indicate data points excluded from the linear analysis.

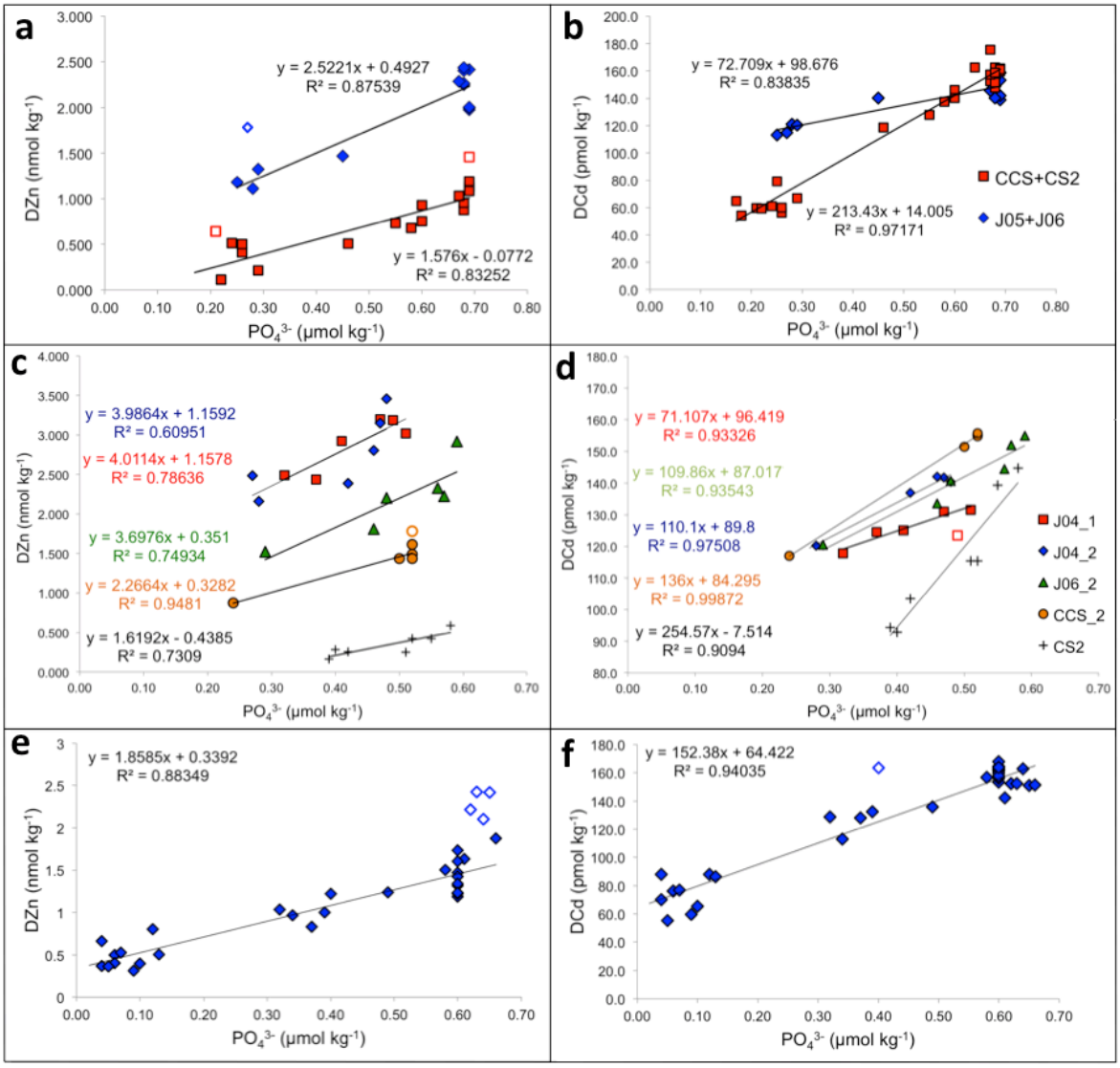


Figure 3.17 Relationship of dissolved Zn (a, c, e) and dissolved Cd (b, d, f) with phosphate in November (DY018) (top), April (DY029) (middle) and July (DY033) (all stations) (bottom) on the continental shelf. Open symbols indicate data points excluded from the linear analysis.

and PO_4^{3-} (r^2 = 0.83, n = 14) resulted in a distinctively lower elemental ratio of 73 µmol mol^{-1}. Contrasting observations were made for the DZn relationship with PO_4^{3-}, with a higher Zn:P ratio of 2522 µmol mol^{-1} at stations J05 and J06 (r^2 = 0.88, n = 13) compared with stations CS2 and CCS (cast 29/11/2014) of 1532 µmol mol^{-1} (r^2 = 0.73, n = 18). The spatial variability of the ratios was more prominent in spring (April), when the water column stratification developed and chlorophyll concentrations were the highest (up to 153 mg m^{-2}) (Poulton et al. 2017) with evidence for a coccolithophore bloom at station J02 (27/04) (Mayers et al. 2018). A linear correlation between DCd, DZn and PO_4^{3-} was not observed at stations J02, J06 and CCS at the beginning of April. At the remaining casts, the slopes of the linear correlations (r^2 = 0.61 – 1.0) between DCd and PO_4^{3-} ranged from as low as 54 µmol mol^{-1} at the most coastal station (J04) to 255 µmol mol^{-1} at the shelf edge CS2 station (Figure 3.17). Opposite trends were observed in the linear relationship between DZn and PO_4^{3-} (r^2 = 0.61 – 0.95) that yielded ratios ranging from 1619 at CS2 to 4011

μmol mol^{-1} at J04 (Figure 3.17). Although, the variability in the ratios for both metals with PO_4^{3-} was relatively large in November and April, the range of Zn/Cd ratios was similar for both seasons and ranged from 35:1 (J05+J06) and 7:1 (CCS+CS2) in November and 74:1 (J04), 34:1 (J06), 16:1 (CCS), 6:1 (CS2) in April (Figure 3.18). In July, a uniform linear relationship was observed between both DCd and DZn and PO_4^{3-} at all stations and yielded ratios of Zn:P 1859 μmol mol^{-1}, Cd:P 152 μmol mol^{-1} and a Zn:Cd ratio of 12:1. In comparison, on the continental slope, Zn/Cd ratio was found to be 5:1 in waters < 0.4 μmol PO_4^{3-} and 9:1 in waters > 0.4 μmol PO_4^{3-}.

The variability in TM:P ratios and the opposite trends for the Cd:P and Zn:P relationships across the shelf may be driven by three not-mutually exclusive processes: (1) different strengths of DZn, DCd and P sources across the shelf and/or (2) distinct water masses propagating across the shelf with different elemental ratios (oceanic vs. coastal) and (3) dynamic shifts in community structure. (1) Distinctively higher DZn concentrations were observed at the most coastal stations and DZn levels gradually decreased away from the coast (Figure 3.10). In general, the DZn concentration gradient was more pronounced than concentration gradients for DCd and PO_4^{3-} (Figure 3.8 and Figure 3.5). The difference in near surface (< 25 m) DCd, DZn and PO_4^{3-} concentrations plotted against the distance from the coast is presented in Figure 3.19. In November, distinctly higher concentrations of DCd and DZn were observed at stations J05 and at J06 in contrast to uniform concentrations at CCS, CS2 and off-shelf transects, whilst no

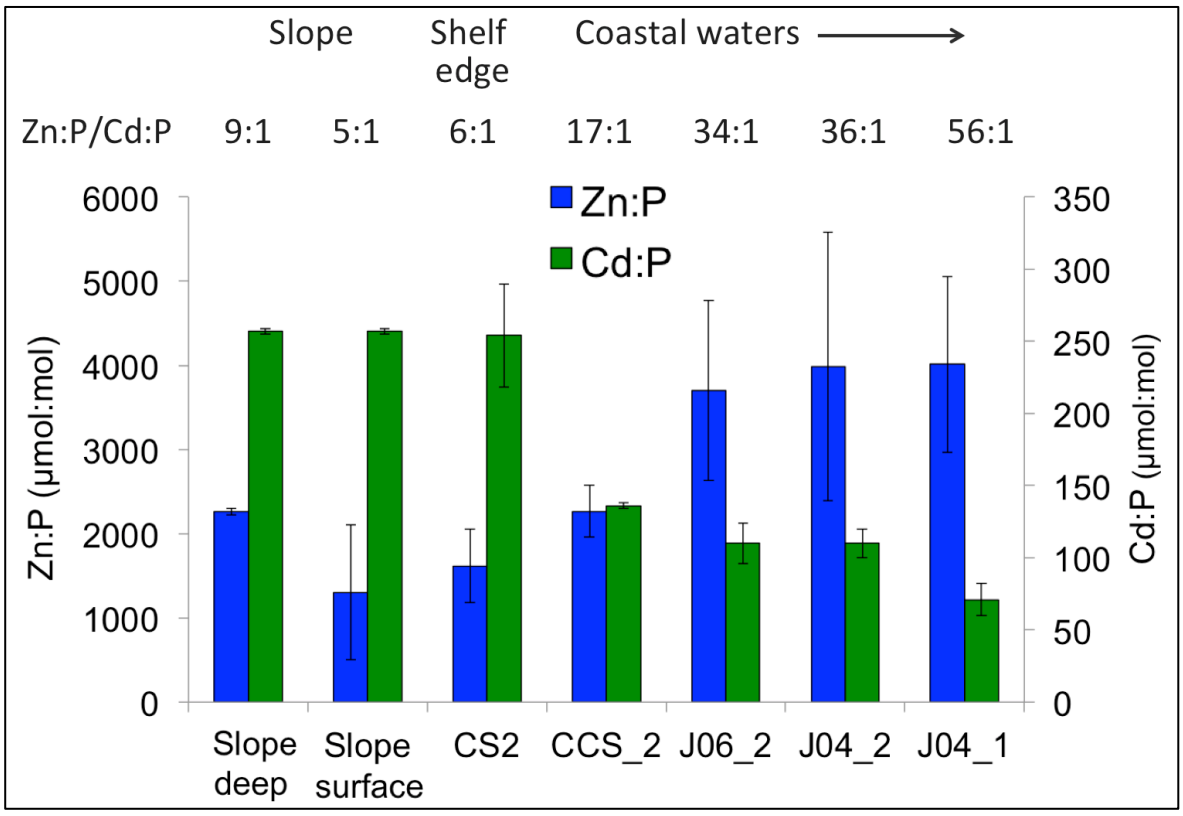


Figure 3.18 Dissolved zinc:phosphate (blue) and dissolved cadmium:phosphate (green) ratios at on-shelf stations (J04 - CCS), shelf edge station (CS2) in April and on the continental slope.

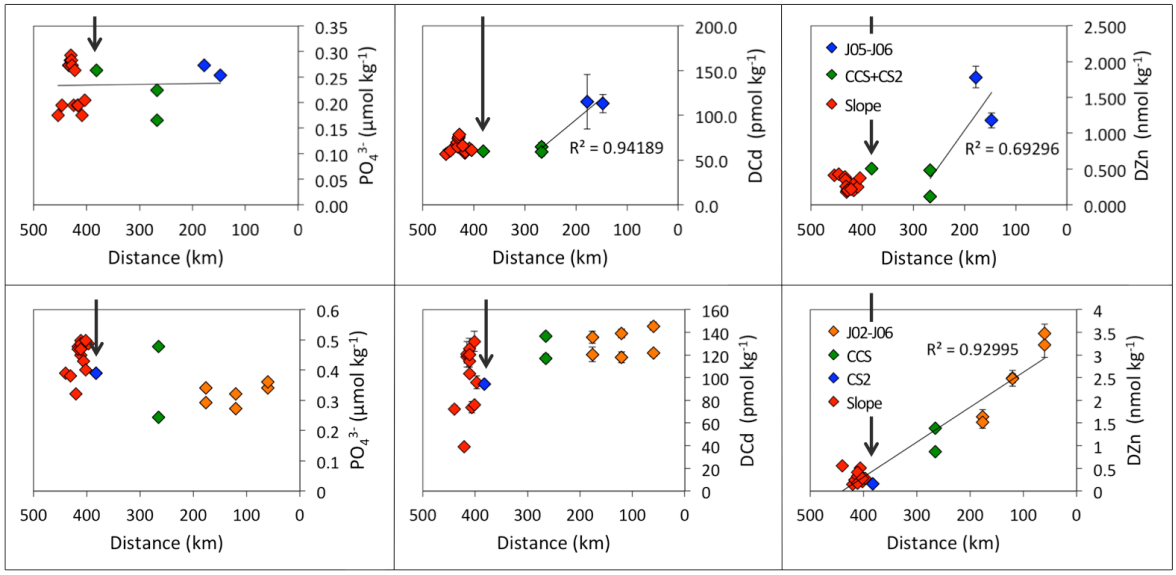


Figure 3.19 Near surface (< 25 m) concentrations of phosphate (left), dissolved cadmium (middle) and dissolved zinc (right) in November (top) and April (bottom) plotted against the section distance from Site A (0 km), across the shelf (J stations and CCS), shelf break (CS2) and off-shelf transects. In the upper panel J05 and J06 stations are indicated in blue, CCS and CS2 stations in green and off-shelf transects stations in red. Bottom panel J02-J06 stations are indicated in orange, CCS in green, CS2 in blue and off-shelf transects stations in red. Black arrow indicates the shelf break at 200 m isobaths.

concentration gradient was observed for PO_4^{3-}. In April, even more distinct differences were observed across the on-shelf stations. A strong DZn concentration gradient between J02 station, CCS and CS2 was observed, whilst this feature was not as prominent for DCd. Interestingly, PO_4^{3-} concentrations increased slightly with distance from the coast (Figure 3.19), which likely was a result of winter water column overturning that supplied higher PO_4^{3-} concentrations to surface waters on the slope or greater PO_4^{3-} utilization on the shelf relative to the slope surface waters. Therefore, the magnitude of the on-shelf DZn sources was greater than DCd, whilst no distinct on-shelf sources of PO_4^{3-} (beside remineralization) were observed. Features observed for the concentration gradients across the shelf stations in November and April exhibited the same patterns as DTM:P elemental ratios (Figure 3.17 and Figure 3.18) described above.

(2) The seasonal variability in salinity gradients across the shelf (Figure 3.4) was indicative of water mass movement across the shelf, with more saline waters observed at CCS in November in comparison to April and July. Almost identical DTM:P ratios were observed in November at CCS, CS2 stations (Zn 1576 µmol mol^{-1}, Cd 213 µmol mol^{-1}) and off-shelf stations (Zn 1304 ± 802 µmol mol^{-1}, Cd 257 µmol mol^{-1}) (Figure 3.17), in contrast to the coastal stations (Zn 2522 µmol mol^{-1}, Cd 72.2 µmol mol^{-1}), which indicates a stronger influence of oceanic waters at CCS and CS2. In April, the gradual characteristics of the salinity gradient across the shelf was also reflected in gradual changes in DTM:P ratios (Figure 3.17 and Figure 3.18). Ratios observed at the shelf break station (CS2) (Zn:P 1619 µmol mol^{-1}, Cd:P 255 µmol mol^{-1}) were almost identical to the 'oceanic' values

and progressively altered towards the coastal J-stations. In July, the coastal system was more uniform across the shelf and was characterised by a stratified water column and surface water drawdown of all elements (section 3.3.3 and 3.3.4) (Birchill et al. 2017; Poulton et al. 2017). Uniform ratios (Zn:P 1859 μmol mol^{-1}, Cd:P 152 μmol mol^{-1}) observed across the on-shelf stations fell between the 'oceanic' and the most 'coastal' values (Zn:P ~ 4000 μmol mol^{-1}, Cd:P < 100 μmol mol^{-1}), reflective of a fully stratified and thus potentially more stable system in comparison to autumn (November) and spring (April). Therefore, the variability in DTM:P ratios could be a result of distinct magnitudes of DCd, DZn and PO_4^{3-} sources imprinted over the coastal zone modification of oceanic signatures across the shelf.

(3) The above explanations focus mainly on chemical (sources) and physical (water mixing) processes. Considering the enhanced primary production in the shelf sea systems, the influence of stoichiometry of biological Zn, Cd and PO_4^{3-} uptake and its relationship to elemental availability and community structure should also be considered. Phosphorus uptake experiments conducted at CCS exhibited seasonal variability in PO_4^{3-} uptake relative to carbon and followed 'non-Redfield' uptake ratios. While a low PO_4^{3-} uptake was observed in autumn and a high PO_4^{3-} uptake was observed in summer, the spring measurements revealed a transition between these two seasons. Phosphorus changes were driven by the plankton community (bacteria vs. phytoplankton) and PO_4^{3-}, light and NO_x^- availability over different seasons (Poulton et al. 2017). These observations could explain seasonal changes in TM:P ratios at CCS but not the gradual changes in TM:P across the shelf over all seasons (Figure 3.17) or the inverse Cd:P and Zn:P ratio pattern on the shelf in April (Figure 3.18). Finkel et al. (2007) showed highly variable Cd:P ratios related to various phytoplankton species, including 50 times higher ratios in coccolithophore (335 μmol mol^{-1}) compared to cyanobacteria (7 μmol mol^{-1}), 40 times higher in dinoflagellates (257 μmol mol^{-1}) and 15 times higher in diatoms (101 μmol mol^{-1}). Therefore the Cd:P ratios observed over all seasons on the Celtic Sea shelf correlated well with Cd:P ratios (42 – 168 μmol mol^{-1}) observed in the diatom taxonomic group. However, the phytoplankton community in our study region was dominated by smaller cells such as nanoeukaryotes (2 – 20 μm) and picoeukaryotes (< 2 μm) (Tarran et al., in prep.). Sunda and Huntsman (1998a) have shown that at enhanced Zn^{2+} (10^{-11} M) and Mn^{2+} ($10^{-6.5}$ M) concentrations in the coastal environment, Cd uptake is strongly suppressed, which leads to lower Cd concentrations in phytoplankton in comparison to the oceanic taxa. Although measurements of Zn^{2+} and Mn^{2+} species were not conducted, as evident from Figure 3.10 and as discussed in Chapter 4, DZn and DMn concentrations gradually decreased towards the shelf break from > 3.5 nmol kg^{-1} (DZn) and > 4 nmol kg^{-1} (DMn) to < 1 nmol kg^{-1}. Therefore, a suppression of free metal (Zn and Mn) concentration of Cd biological uptake could also gradually decrease, along with metal concentrations, towards the shelf break so that changes in the free

Mn or Zn concentration could potentially also influence biological Cd uptake and resultant Cd:P ratios.

According to the extended Redfield ratio, Cd has the lowest biological requirement in marine organisms (Ho et al. 2003). A recent discovery of a Cd-specific CA enzyme provided the first evidence of a direct biological role of Cd (Lane et al. 2005). Considering DCd drawdown of 58.2 pmol L^{-1} at J06 (casts from 27/04 and 28/07) and 63.0 pmol L^{-1} at CCS (casts from 28/04 and 29/07) between April and July with a period of 96 days between sampling, this yields a Cd uptake of 0.63 pmol L^{-1} d^{-1} (J06) and 0.68 pmol L^{-1} d^{-1} (CCS). This is in excellent agreement with Cd uptake radiotracer experimental estimation of Cd uptake in the Celtic Sea, where 0.64 pmol L^{-1} d^{-1} was reported for the spring and summer months (Dixon et al. 2006).

3.5 Summary and conclusions

Sections of DCd, DZn, DCu, and DNi in the Celtic Sea continental slope region demonstrated nutrient-like behaviour of these elements, with strong correlations with macronutrients (r^2 = 0.91 – 0.97). Dissolved Co and Al correlated strongly with macronutrients in the upper waters only (r^2 = 0.74 – 0.80), confirming the biological role of DCo in phytoplankton metabolic functions. Considering that DAl has no known biological function, scavenging of DAl to biogenic particles or passive uptake were likely responsible for the observed behaviour. The strong linear correlation between DCd and PO_4^{3-} surprisingly did not exhibit the 'kink' observed in the other regions of the global ocean. In contrast to the DZn:PO_4^{3-} relationship that displayed a distinct 'kink' at 0.4 μmol kg^{-1}. The DCo concentrations relative to PO_4^{3-} in the SML were potentially below the requirement of some taxa and considering that Co, Zn and Cd can be substituted in carbonic anhydrase in some phytoplankton species, Zn replacement for Co could lead to enhanced Zn uptake relative to PO_4^{3-} and consequently driving the 'kink' in the Zn:P relationship. Interestingly, the Al:P relationship also exhibited a 'kink' at the same PO_4^{3-} concentrations as Zn:P. Whilst a strong Al:P relationship was suggestive of passive uptake and/or adsorption onto biogenic cells, the reason for the apparent 'kink' and potential connection to Zn:P biogeochemical processes were unclear and thus require further studies.

A significant seasonal variation in DTM concentrations in the SML resembled seasonal patterns in macronutrients, with the lowest concentrations observed in summer (July) and highest in spring (April), as a result of biological uptake and winter water column overturning re-supplying nutrients to surface waters. However, the elemental ratios observed in the study region agreed well with full depth ratios in the North Atlantic Ocean (Twining and Baines 2013) and the extended Redfield ratio (Ho et al. 2003) for phytoplankton cultures.

Dissolved TMs exhibited different biogeochemical behaviours in the shelf environment of the Celtic Sea compared to the shelf break system. Strong inverse correlations of DCu and DCo with salinity (r^2 = 0.78 – 0.81) suggested continental sources of these metals with physical mixing of fresher coastal waters with more saline waters across the shelf over all seasons. DCd and DZn generally correlated well with PO_4^{3-}, with however, spatially and temporally variable ratios of DCd:P and DZn:P, as a result of different magnitude of coastal water mass modification between saline oceanic and fresher coastal waters and different magnitudes of DCd, DZn and PO_4^{3-} sources across the shelf. Additionally, the influence of phytoplankton uptake ratios related to bloom development, metal availability and community structure likely played a role in the diverse Cd:P and Zn:P ratios in the shelf system, imprinted by physical mixing processes. The drawdown of DCd between April and July yielded an uptake of 0.63 – 0.68 pmol Cd L^{-1} d^{-1}. These field observations agreed well with results from incubation experiments using radiotracers in the Celtic Sea (Dixon et al. 2006).

Observations from the Celtic Sea stress the importance of seasonal studies in order to gain insights into detailed biogeochemical processes influencing the distributions of TMs in the global ocean. Furthermore, the spatial and temporal variability in elemental ratios of Cd:P and Zn:P observed in coastal waters reflect the dynamic character of shelf systems and thus highlights the necessity of more studies in these productive regions. Additionally, dissolved TMs distributions should be evaluated as combined datasets, and TMs should not be treated as individual entities

Chapter 4 Biogeochemical process controlling manganese and cobalt distributions in European Shelf Seas

The research presented in this chapter is being prepared for publication in *Marine Chemistry*

4.1 Introduction

Cobalt (Co) and manganese (Mn) are crucial micronutrients for marine ecosystems. These metals form part of vital enzymes involved in the cellular processes of marine organisms, such as photosynthesis and respiration (Morel et al. 2003). Cobalt plays an essential role in the functioning of in particular cyanobacteria and diatoms (Sunda & Huntsman 1995). This metal is incorporated in hydrolytic enzymes: carbonic anhydrase and Cobalamin (vitamin B_{12}). Carbonic anhydrase is a catalyst in hydration and dehydration of CO_2 and may be significant in the chemical enhancement of air-sea CO_2 exchange (Raven 1997). Manganese forms a central part of the superoxide dismutase enzyme that protects cells against O_2^- radicals, and acts as an electron acceptor and oxidizes water to O_2 in photosystem II system (Moore et al. 2013; Peers & Price 2004; Sunda 2012). However, in the marine environment these metals can be present at low concentrations and be potentially co-limiting nutrients (Browning et al. 2014; Browning et al. 2017). Recently, addition of various nutrients (nitrate, iron and Co) revealed multi-nutrient co-limitation that stimulated the phytoplankton growth (Browning et al. 2017).

Dissolved Mn (DMn) and Co (DCo) exhibit 'hybrid' nutrient-like and scavenged-type vertical distributions. In surface waters DCo is the scarcest of metallic nutrients with low concentrations of 45 – 85 pmol kg^{-1} in spring and 20 – 40 pmol kg^{-1} in summer, that increase with depth similarly to nutrient-like metals (Saito et al. 2010). Furthermore, a strong correlation of DCo with PO_4^{3-}, has been observed in the Ross Sea (Saito et al. 2010) and the North (Noble et al. 2017), Western (Dulaquais et al. 2014) and South Atlantic basins (Noble et al. 2012). Whilst, DCo exhibit nutrient-like distributions in surface waters, in intermediate and deeper waters DCo concentrations decrease at depth due to particle adsorption (Noble et al. 2012; Noble et al. 2017) or water mass mixing (Dulaquais et al. 2014) demonstrating a scavenged-type behaviour. DMn usually exhibits a contrasting distribution to DCo in upper waters. In surface waters, DMn concentrations are typically elevated (up to 3 nM, (de Jong, van den Berg, et al. 2007)) in comparison to deeper waters due to atmospheric inputs and levels maintained by photoreduction processes that alter redox state of Mn from insoluble Mn (IV) to soluble Mn (II) species and inhibit the activity of Mn-oxidizing bacteria (Sunda et al. 1983; Sunda & Huntsman 1988). Below the euphotic zone, DMn is scavenged due to a high particle affinity and the activity of Mn-oxidizing bacteria that catalyse the oxidation processes (Emerson et al. 1982; Tebo & Emerson 1985), resulting in a decrease in DMn concentration (down to subnanomolar levels, (Le Gall et al. 1999)) with depth that may be elevated towards the seafloor due to benthic inputs. The scavenging of both metals results in relative short residence times (40 – 150 years) in comparison to nutrient-like metals (40 000 – 50 000 years, (Bruland 1980)) and therefore prevents deep water accumulation. However, strong organic ligand complexation is thought to stabilize Co to some degree (Noble et al. 2017). Complexes of Mn (III), an intermediate product in sedimentary redox Mn (II) and Mn (IV)

processes (Madison et al. 2013) with marine siderophores have been reported (Parker et al. 2007) but the influence of organic matter complexation on Mn is still largely unknown.

Dissolved Mn and Co have similar sources and sinks. Natural and anthropogenic atmospheric deposition, riverine discharges and reductive dissolution in sediments and deep water remineralization act as sources of these metals. Biological uptake, particle scavenging, precipitation and Mn-oxidizing bacteria remove these metals from the water column (Bruland & Lohan 2004). Sedimentary inputs of DMn and DCo to the water column have been identified as an important source of these bio-essential micronutrients. (Heggie & Lewis 1984; Stockdale et al. 2010; Bown et al. 2012; Noble et al. 2012). Reduction processes in anoxic sediments solubilize Mn(II) and Co (II) species associated with Mn-oxides (Heggie & Lewis 1984). These soluble species accumulate in pore waters and may be resuspended and/or diffuse to the overlying waters. Continental margins are of particular interest due to their high productivity with oxygen depleted sediments and relatively shallow water-sediment interfaces that may supply these metals to overlying waters. Coastal regions have been reported to supply DMn and DCo to the open ocean in off Benguela-Angola (Noble et al. 2012), Mauritania (Noble et al. 2017), the Californian coast (Biller & Bruland 2013), Ross Sea (Dulaquais et al. 2014) and Bay of Biscay (Laës et al. 2007). However, the exact processes facilitating the transport from shelf seas to offshore ocean regions are poorly constrained.

Strong physical mechanisms such as internal tides, internal waves and slope currents occur along continental slopes, causing sediment resuspension processes resulting in intermediate and bottom depth nepheloid layers (INLs and BNLs, respectively) (McCave et al. 2001), affecting trace element distributions in continental margin regions (Noble et al. 2017; Laës et al. 2007). Yet, very little is known about the role of nepheloid layers in off-shore trace metals transport due to the transient and unpredictable nature of these phenomena. Sediments are the main sources of radium (Ra) short-lived ^{223}Ra (11.4 days) and ^{224}Ra (3.6 days) isotopes (Moore 2000) and thus can be utilized as tracers of recent sedimentary inputs to overlying waters. Radium isotopes are highly soluble in seawater and accumulate in sediments porewaters through continuous radioactive alpha decay of particle reactive thorium (Th). Once transported through sediment water interface, Ra isotopes are dispersed away from the source and their activity gradient decreases through the decay (Burt et al. 2014). However, in addition to remobilisation of trace metals from sediments, scavenging is also expected to occur in the particle rich waters overlying on the shelf break. As a consequence, for efficient transport of DMn and DCo within nepheloid layers to occur, a dynamic exchange of trace metals between particles and water is required (Milne et al. 2017; Achterberg et al. 2018). Additionally, continental slope topography may play a role in sediment resuspension and off-shelf transport of particulate material. Submarine canyons are known hotspots of intense mixing and enhanced sediment flux to the open ocean due to their complex

topography that leads to greater internal wave generation and diapycnal mixing (Gardner 1989; Hotchkiss & Wunsch 1982; Kunze et al. 2002; Carter & Gregg 2002). This study was conducted along a marine spur and canyon (west bank of the Explorer Canyon) on the Celtic Sea continental margin during three separate cruises. The region is characterised by highly complex morphology with over 30 canyons stretching along a 300 km shelf edge (Bourillet et al. 2003) where lateral transport of particulate material within INLs is a common feature (Dickson 1986; Antia et al. 1999; McCave et al. 2001). Therefore, the Celtic Sea serves as an excellent opportunity to examine the influence of seafloor topography, spatial and temporal variability of nepheloid layers and their role on DCo and DMn distributions.

In addition to natural sources, the economic market for Co has expanded tremendously in recent years through the application of Co in for example lithium oxide cathode based batteries (Scrosati & Garche 2010). The environmental impact of inappropriate disposal of Co based batteries and Co alloys along with burning of fossil fuels, mining and smelting (Kim et al. 2006; Banza et al. 2009) will likely increase in future and potentially serve as an anthropogenic source to the marine environment, in particular in coastal regions. Therefore, understanding of the natural cycle of DCo is critical to allow assessment of the potential anthropogenic impacts of increased anthropogenic Co use on the marine environment in future.

The aim of the research reported here was to quantify biogeochemical processes governing the distributions of DMn and DCo in the continental margin and to examine potential role of INLs off-shelf transport of these metals to the open ocean. Work reported here demonstrates first extensive study of DMn and DCo in the North West European Shelf Sea continental margin on small spatial (< 5 km) and temporal (< 4 months) scale.

4.2 Materials and methods

Full details of the study region, sampling and methods are provided in Chapter 2. Briefly, samples for trace metal analysis were collected during three different seasons; November – December 2014 (DY018), April 2015 (DY029), and July – August 2015 (DY033) on the Northeast Atlantic continental margin (Celtic Sea) (Figure 2.1), on board *RRS Discovery.* Two off-shelf transects were conducted along a canyon (T1_C, stations C01 – C07, C15), nearby a spur (T2_S, stations S08 – S09) and one on-shelf transect in the Celtic Sea (stations CS2, CCS, J02 – J06, Site A). Trace metal samples were collected following GEOTRACES protocols (Cutter et al. 2010). Dissolved TMs were filtered using a 0.2 µm pore size cartridge filter (Sartobran 300, Sartorius), preconcentrated using an automated system (SC-4 DX SeaFAST pico; ESI) and analysed by high-resolution inductively coupled plasma-mass spectrometry (HR-ICP-MS; Thermo Fisher Element XR) (Rapp et al. 2017). Evaluation of the accuracy and efficiency of these methods was carried out

using GEOTRACES reference materials with the results showing good agreement (Table 5). Some data points were identified as outliers and were excluded from consideration following the z-score (Chapter 2). Particulate Mn and Co was collected on clean 25 mm Supor® polyethersulfone membrane disc filters (Pall, 0.45 µm) and subjected to a 25% acetic acid-hydroxylamine hydrochloride leach (LpMn, LpCo) (Berger et al. 2008) that represented potentially bioavailable, exchangeable fraction and subsequently an hydrofluoric (HF) acid digestion (PMn, PCo) that represented refractory fraction (Ohnemus et al. 2014). Particulate samples were analysed using ICP-MS (Thermo Fisher X Series 2). Radium (Ra) isotopes ^{223}Ra and ^{224}Ra were extracted from large seawater volumes (60 – 100 L) by adsorption onto Mn acrylic fibers (Sun & Torgersen 1998). Radium activities were analysed at sea by Radium Delayed Coincidence Counting following standard methodology (Annett et al. 2013; Garcia-Solsona et al. 2008; Moore 2008; Moore & Arnold 1996). Radium activities used here ($^{224}Ra_{xs}$ and $^{223}Ra_{xs}$) were in excess of activity supported by the parent isotopes in the water column (Chapter 2). Seawater sampling and handling for macronutrient analysis was carried out according to the International GO-SHIP nutrient manual recommendations (Hydes et al. 2010) and the analysis was carried on board using techniques described in Woodward and Rees (2001). Water mass distribution was quantified using extended Optimum Multiparameter analysis (extOMP) (Hupe & Karstensen 2000; Karstensen & Tomczak 1998; Pollard et al. 2004). Conductivity, temperature and depth (CTD) data was collected and processed on board. Turbidity was measured (Chelsea Technologies Group Aquatrack MKIII fluorometer, wavelength 400nm, bandwidth 80 nm). Salinity was measured (Sea-Bird SBE 4C sensor) and calibrated on-board using in-situ salinity samples analysed with a Guildline Autosal salinometer. Temperature was measured with Sea-Bird SBE 3plus (SBE 3P) temperature sensor. Dissolved oxygen was measured with Sea-Bird SBE 43 oxygen sensor and calibrated against photometric on-board Winkler titration results. Statistical analysis, one way ANOVA and linear regression were performed using StatPlus:mac statistical tool pack. Section plots figures were created with the Ocean Data View (2015) software (Schlitzer 2015) with DIVA gridding settings.

4.3 Results and discussion

4.3.1 Hydrography

Detailed hydrography description can be found in section 3.3.1.

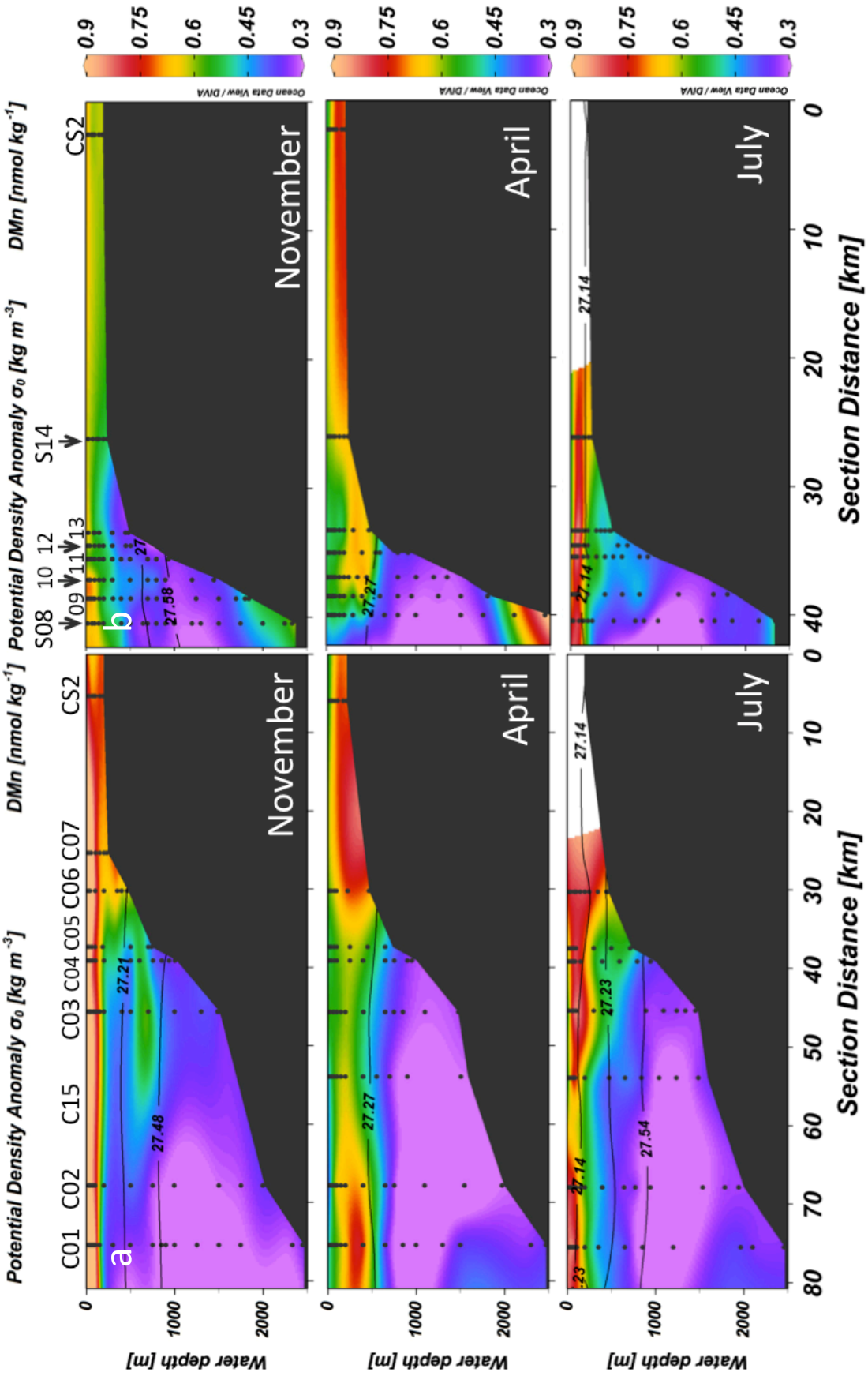


Figure 4.1. Dissolved manganese distribution plots along (a) the canyon transects (T1_C, left), and along (b) the spur transects (T2_S, right), in November (DY018) (top), April (DY029) (middle) and July (DY033) (bottom). Black lines represent the density range of DMn concentration enhancement within identified nepheloid layers.

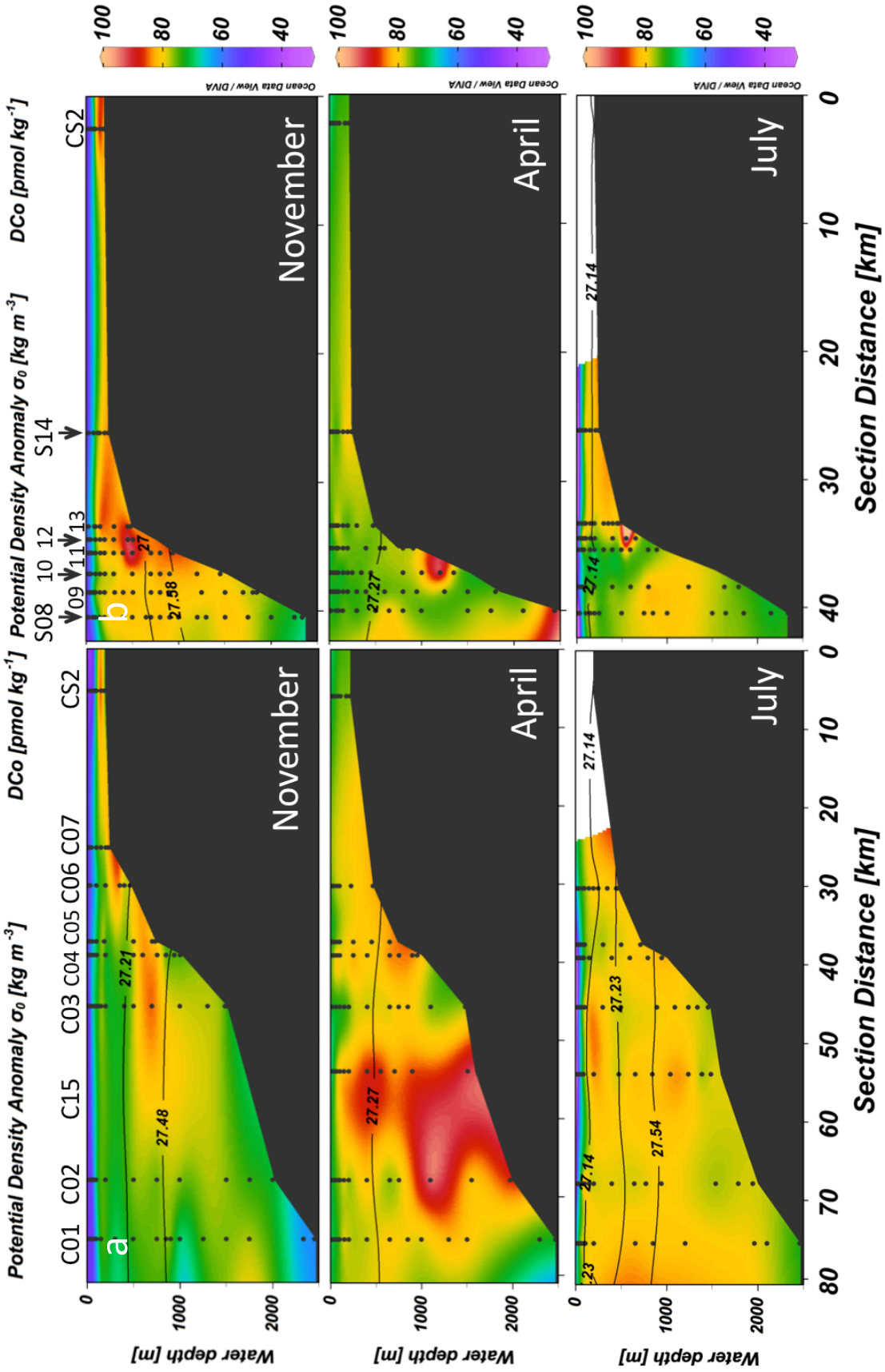


Figure 4.2 Dissolved cobalt distribution plots along (a) the canyon transects (T1_C, left), and along (b) the spur transects (T2_S, right), in November (DY018) (top), April (DY029) (middle) and July (DY033) (bottom). Black lines represent the density range of DMn concentration enhancement within identified nepheloid layers.

4.4 Distributions of DCo and DMn

Dissolved Mn

The concentrations of DMn in the slope region of the Celtic Sea ranged between 0.218 – 1.116 nmol kg^{-1} (Figure 4.1). In general, elevated DMn concentrations were noted in the top 500 m and ranged between 0.312 – 1.116 nmol kg^{-1}. In November, DMn exhibited surface water maxima (0.866 ± 0.174 nmol kg^{-1}, n = 36) that decreased with depth. In contrast, subsurface maxima were observed in April (0.671 ± 0.079 nmol kg^{-1}, n = 32) and July (0.775 ± 0.081 nmol kg^{-1}, n = 51) at <

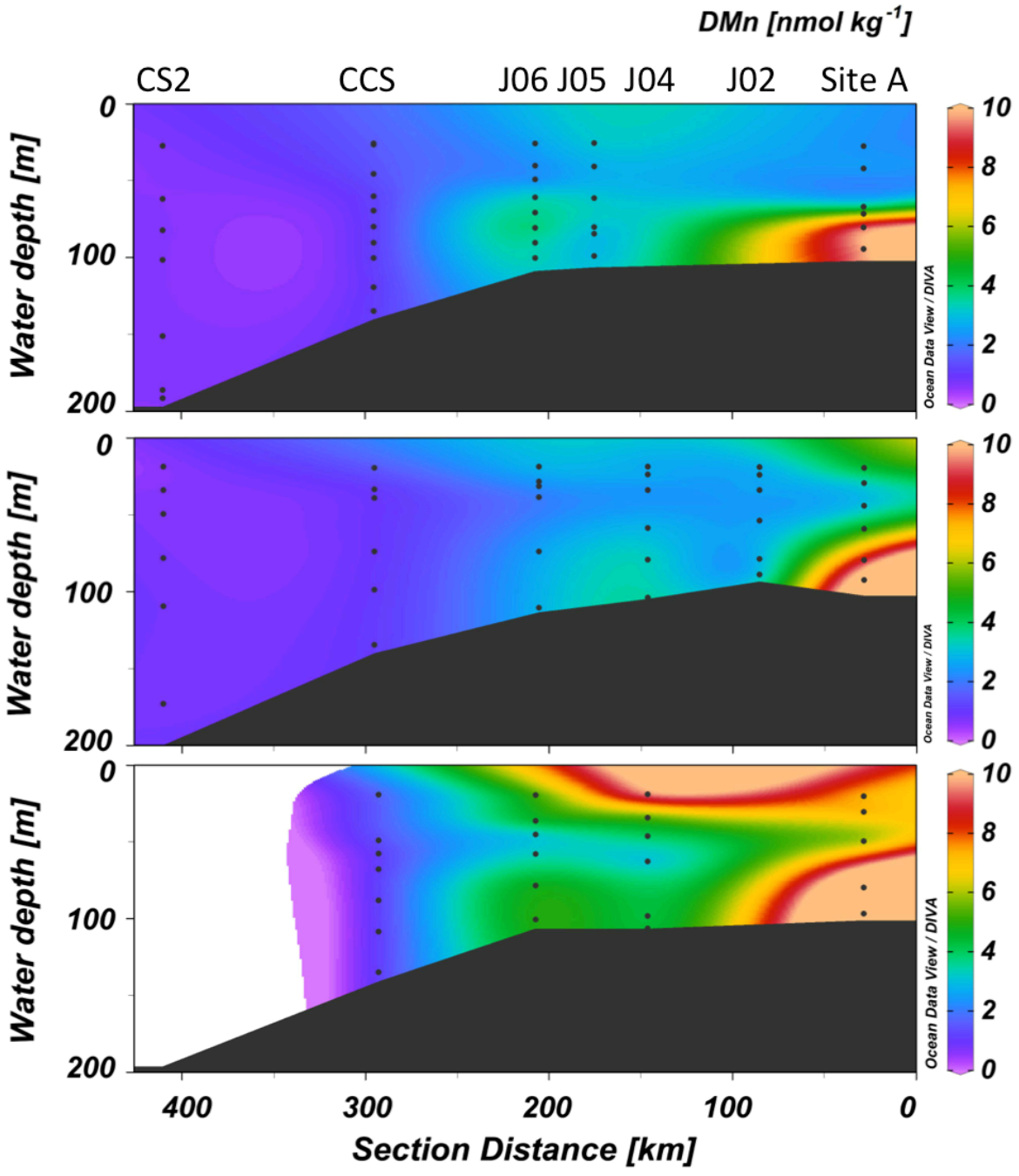


Figure 4.3 Dissolved manganese distribution plots along the on-shelf transect in November (DY018) (top), April (DY029) (middle) and July (DY033) (bottom).

400 m and < 150 m depth respectively. Dissolved Mn minimum (0.350 ± 0.068 nmol kg^{-1}, n = 89) was persistent across all seasons and coincided with salinity maxima at ~ 1000 m depth. In deeper waters, DMn concentrations increased towards the seafloor (up to 0.895 nmol kg^{-1}). These observations are generally consistent with previous observations in the study region (Le Gall et al. 1999), with DMn concentrations being higher than those reported for the East North Atlantic Ocean (0.224 ± 0.125 nmol kg^{-1} , n = 76 (Saager et al. 1997; Hatta et al. 2015)). There was no distinctive seasonal difference in DMn concentrations throughout the water column. Distinctively higher DMn concentrations were observed on the continental shelf (0.600 - 14.49 nmol kg^{-1},

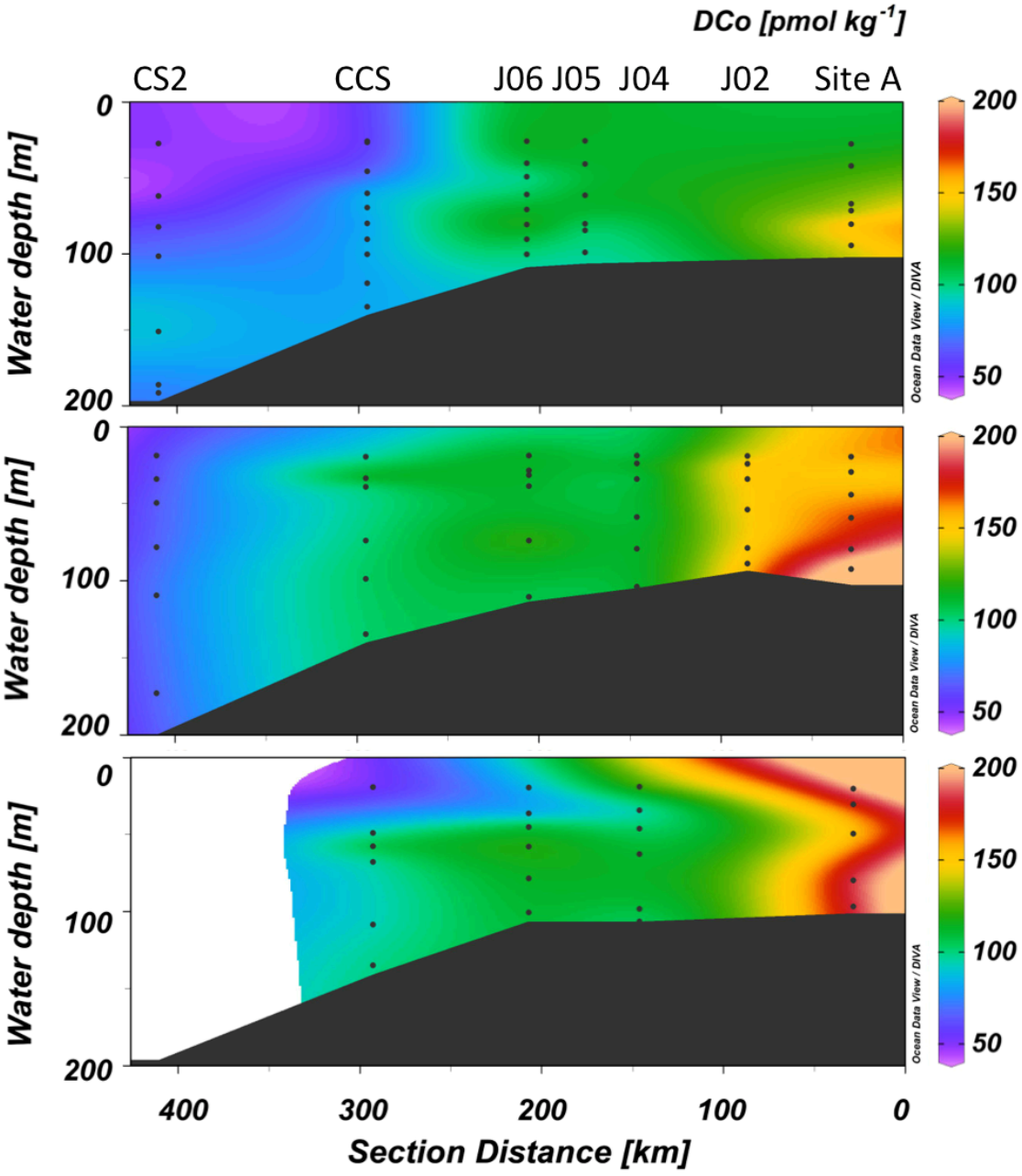


Figure 4.4 Dissolved cobalt distribution plots along the on-shelf transect in November (DY018) (top), April (DY029) (middle) and July (DY033) (bottom).

Figure 4.3) and generally agreed with DMn concentrations of 1 – 10 nmol L^{-1} previously reported in the study region (Muller et al. 1994). The highest DMn concentrations were measured towards the seafloor at Site A in November (9.765 nmol kg^{-1}), April (10.89 nmol kg^{-1}) and July (14.49 nmol kg^{-1}).

Dissolved Co

The concentrations of DCo in the Celtic Sea slope region ranged between 26.6 – 96.8 pmol kg^{-1} (Figure 4.2). In general, the lowest DCo concentrations were measured in the seasonal mixed layer (SML) with differences observed between seasons; 55.1 ± 4.5 pmol kg^{-1} (n = 36), 66.5 ± 4.7 pmol kg^{-1} (n = 47), 41.1 ± 8.9 pmol kg^{-1} (n = 22) in November, April and July respectively. Below the SML, there was no distinctive seasonal difference in DCo concentrations throughout the water column and DCo concentrations increased to 73.7 ± 7.9 pmol kg^{-1} (n = 296) and were fairly uniform until 1500 m depth. Dissolved Co concentrations generally decreased to 71.3 ± 4.7 pmol kg^{-1} (n = 46) below 1500 m along T1_C (canyon) and T2_S (spur) transects. However, in April, DCo concentrations increased towards the seafloor at stations C02 (88.2 pmol kg^{-1}), C15 (94.3 pmol kg^{-1}) and S08 (92.1 pmol kg^{-1}). Dissolved Co concentrations were lower than previously reported values of 100 - 200 pmol L^{-1} (Muller et al. 1994).

Similarly to DMn, higher DCo concentrations were observed on the continental shelf (47.8 pmol kg^{-1} - 211.6 pmol kg^{-1}, Figure 4.4) in agreement with previous findings (100 – 250 pmol L^{-1}, (Muller et al. 1994)) (75 – 143 pmol L^{-1} in surface waters, (Kremling & Hydest 1988)) in the study region. The highest DCo concentrations were observed in bottom waters at Site A in November (153.5 pmol kg^{-1}), April (211.6 pmol kg^{-1}) and July (208.0 pmol kg^{-1}).

4.4.1 Relationship between dissolved cobalt and manganese with phosphate

The relationship between DCo and PO_4^{3-} across all seasons in the study region revealed a shift in biogeochemical processes that dominated the DCo distributions in the water column (Figure 4.5). In contrast, although DMn is a bioessential micronutrient, it did not correlate with PO_4^{3-} due to high surface waters concentrations that decrease with depth. A detailed discussion on seasonal variability of DCo concentrations and the relationship with PO_4^{3-} in the SML can be found in sections 3.4.1.1 and 3.4.1.2 respectively. Briefly, the seasonal variability in DCo concentrations in the SML was similar to that of PO_4^{3-}, NO_3^- and SiO_4^{2-} and other micronutrient (DCd, DZn, DAl, DCu and DNi) (Table 6) (section 3.4.1.1). The strongest positive correlation between DCo and nutrients was noted with PO_4^{3-} ($r = 0.89$, $n = 104$, $p = < 0.05$). This observation is in agreement with other studies (Saito et al. 2010; Noble et al. 2012; Noble et al. 2017) and indicates biological utilization and remineralization as the primary processes influencing DCo in surface waters. The lowest DCo

concentrations were thus observed in summer (41.1 ± 8.9 pmol kg^{-1} (n = 22)((July, post spring bloom) as a result of biological uptake. Highest off shelf surface water DCo concentrations were observed in spring (66.5 ± 4.7 pmol kg^{-1} (n = 47)) (April, pre-spring bloom) as a result of the winter water column overturning that re-supplied nutrients to the surface waters. Below the SML, there was no seasonal variation and the correlation with PO_4^{3-} decreased with depth. Whilst within East North Atlantic Central Water (ENACW) (< 27.30 kg m^{-3} σ_0) the correlation declined (r = 0.64, n = 209, p = < 0.05) in comparison to the SML, within the Mediterranean Outflow Water (MOW) density range (27.30 – 27.75 kg m^{-3} σ_0) there was no correlation (r = -0.25, n = 87, p = < 0.05) and in deep waters (Northeast Atlantic Deep Water (NEADW), > 27.75 kg m^{-3} σ_0) a strong inverse correlation between DCo and PO_4^{3-} was observed (r = -0.72, n = 46, p = < 0.05). This decoupling between DCo and PO_4^{3-} indicates a gradual change in processes influencing DCo distributions through the water column. Whilst PO_4^{3-} concentrations continuously increased with depth due to remineralization of sinking organic matter, uniform DCo concentrations within ENACW and MOW depth ranges were a result of interplay between sources (remineralization) and sinks (scavenging). Progressively more negative relationship with depth was likely a result of scavenging onto sinking particles and/or incorporation onto bacterially formed manganese oxides (Moffett & Ho 1996; Lee & Tebo 1994). However, additional sedimentary sources of DCo were evident in the

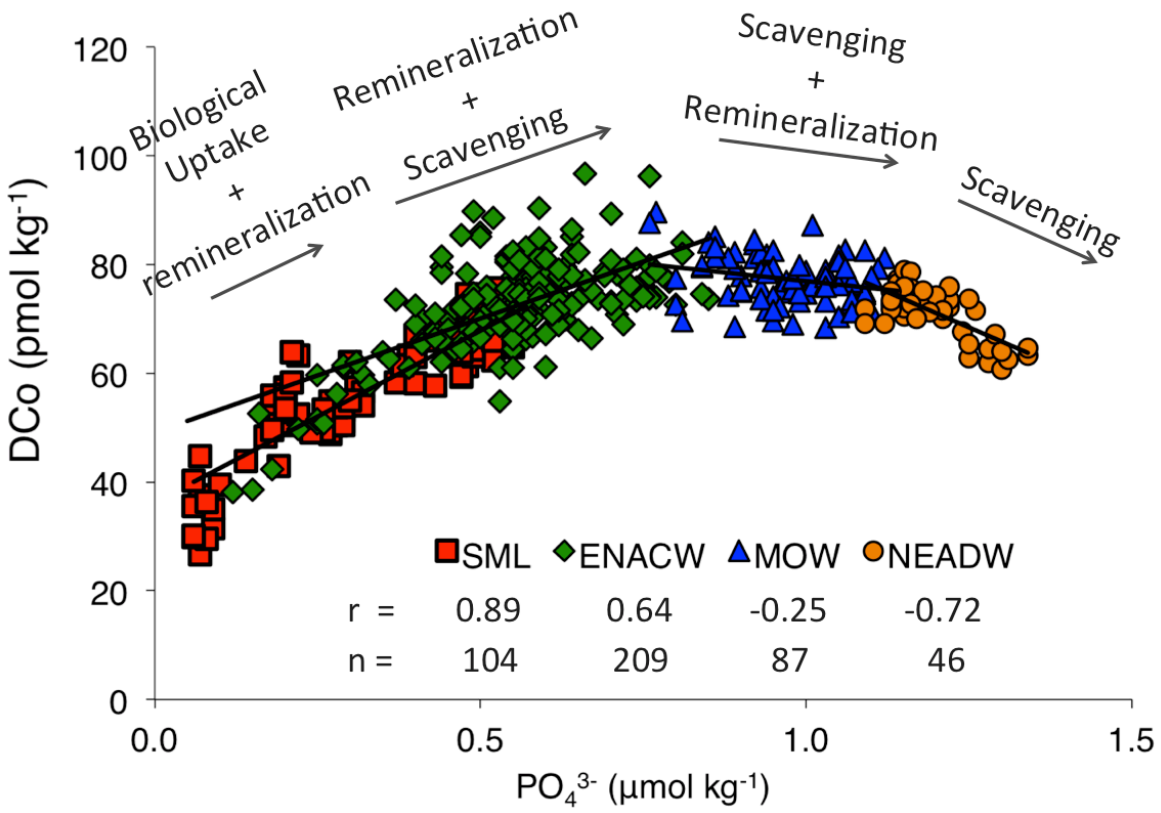


Figure 4.5. Full depth relationship of dissolved cobalt and phosphate in all seasons. Red squares represent seasonal mixed layer (SML), green diamonds represent East North Atlantic Central Waters (ENACW), blue triangles represent Mediterranean Outflow Waters (MOW) and orange circles represent North East Atlantic Deep Waters (NEADW).

distinct nepheloid layers transported off-shore along isopycnals in upper and intermediate waters (section 4.4.4). This source of DCo would contribute to the scatter in the DCo vs. PO_4^{3-} relationship at ENACW and MOW density ranges (Figure 4.5). Therefore, the dominant biogeochemical processes influencing DCo distributions shift from biological uptake in surface waters to remineralization and sedimentary inputs in the mesopelagic waters to scavenging in deep, bathypelagic waters.

4.4.2 DMn spatial variability in surface waters

Dissolved Mn distributions were both temporally and spatially variable in surface waters. However, these changes did not follow seasonal pattern observed for DCo (section3.4.1.1 and 4.4.1), other DTMs (dissolved cadmium, zinc, nickel, copper, aluminium) and macronutrients (section3.4.1.1). Mean DMn concentrations in November (0.866 ± 0.174 nmol kg^{-1}, n = 36) were higher in comparison to April (0.604 ± 0.059 nmol kg^{-1}, n = 52) and July (0.694 ± 0.099 nmol kg^{-1}, n = 23). Elevated DMn concentrations in November along both transects were consistent with previous studies (Saager et al. 1997; Le Gall et al. 1999; de Jong et al. 2007) and likely a result of photoreduction of insoluble Mn (IV) to soluble Mn (II) species and photoinhibition of Mn oxidizing bacteria and/or external sources such as atmospheric input (de Jong et al. 2007; Moffett & Ho 1996). No correlations with macronutrients were observed across seasons, suggesting little influence of biological activity on DMn distributions and DMn concentrations likely exceeded the biological requirement in surface waters in all seasons.

Additionally, a small scale (< 20 km) spatial variability was observed between transects in November, when distinctly higher DMn concentrations were observed along the canyon transect (1.001 ± 0.094 nmol kg^{-1}, n = 20) in comparison to the spur transect (0.696 ± 0.068 nmol kg^{-1}, n = 16). Spatial variability was also observed for Pb with elevated DPb (50.8 ± 3.0 pmol kg^{-1}, n = 20) along the canyon in comparison to the spur transect (DPb 42.5 ± 5.5 pmol kg^{-1} (n = 16) (section 5.3.3). DAl is used as a tracer for atmospheric dust inputs (Measures & Vink 2000), but results did not indicate enhanced surface water concentrations at the time of sampling with also no differences in salinity between transects in November suggesting that atmospheric deposition and transport of lower salinity shelf waters were unlikely the cause of the observed features. However, the SML waters along the canyon transect were 0.8^{o}C warmer in comparison to the spur transect suggestive of different origin of the water masses. Considering that in November the density driven surface water current flows in a poleward direction (Porter et al. 2016; Pingree & Le Cann 1989), the warmer waters observed in November on the canyon transect masses potentially originated south of the study region. This feature was unique for DMn and DPb (Rusiecka et al. 2018). Although the exact source of the surface waters with enhanced DMn (and DPb) measured in November could not be identified, considering their short residence time of 1.9

years for DMn (de Jong et al. 2007) and 5.3 years for DPb, this finding suggests a recent input of both metals to these waters.

4.4.3 DMn minima within MOW

Persistent DMn minima 0.350 ± 0.068 nmol kg^{-1} (n = 89) were observed at a depth range ~ 550 – 1500 m (27.30 – 27.75 σ_0) that coincided with salinity, DAl and DPb maxima associated with MOW (Measures et al. 2015; Noble et al. 2015 and section 5.3.1). The presence of MOW at intermediate depths in the study region was confirmed by the extOMP analysis (Figure 3.2). Saline Mediterranean waters mix with ENACW in the Strait of Gibraltar, and form MOW at intermediate depths. This neutrally buoyant plume spreads across the NE Atlantic at ~ 500 – 1500 m towards the Bay of Biscay and propagates further along the continental slope towards the continental shelf break of the Celtic Sea. The DMn minimum at intermediate depths was consistent with previous reports for the study region (Le Gall et al. 1999) and the Bay of Biscay (Laës et al. 2007). However, in the Celtic Sea study region the mean DMn concentrations were higher than those observed in the Atlantic Ocean at equivalent densities (0.205 ± 0.080 nmol kg^{-1} (n = 31), (de Jong, Boyé, et al. 2007) and the Gulf of Cadiz (GA04 section, 0.211 ± 0.074 nmol kg^{-1} (n = 14, (Rolison 2016)) and the GA03 section, 0.219 ± 0.097 nmol kg^{-1} (n = 11), (Hatta et al. 2015)) but lower than in the Bay of Biscay (0.454 ± 0.144 nmol kg^{-1} (n = 10), (Laës et al. 2007)). Mediterranean Sea surface waters show enhanced DAl (up to 80 nmol kg^{-1}) (Rolison et al. 2015) and DMn (up to 14 nmol kg^{-1}) (Rolison 2016) concentrations as a result of the dissolution of atmospherically deposited Saharan dust, whilst increased DPb generally results from anthropogenic aerosol supplies (Rolison 2016)). Mediterranean Outflow Waters enriched in DAl and DPb were evident in the Gulf of Cadiz at intermediate depths (Measures et al. 2015; Noble et al. 2015) but this feature was not observed for DMn and DFe (Rolison 2016; Hatta et al. 2015). This is likely a result of scavenging processes occurring in the Mediterranean Sea and suggests more efficient scavenging of DMn and DFe in comparison to DPb and DAl.

Variable DMn concentrations within the MOW in the North East Atlantic are indicative of modification of the water masses during transport. Elevated DMn concentrations in the Bay of Biscay in comparison to the Gulf of Cadiz, were associated with resuspended sedimentary inputs during MOW propagation along the continental slopes (Laës et al. 2007; McCave & Hall 2002). DMn concentrations declined between the Bay of Biscay and the Celtic Sea region indicative of further modification of DMn during MOW transit along the continental slopes. Similarly to findings from Bay of Biscay, benthic source and nepheloid layers transporting enhanced concentrations of DMn and DCo were observed in the Celtic Sea study region (see below section 4.4.4).

4.4.4 Benthic source of DMn and DCo

4.4.4.1 Continental shelf sediments

Sedimentary inputs on the continental shelf are exemplified by persistently elevated DMn and DCo concentrations in bottom waters at Site A (Figure 4.8), which coincided with elevated signals in particulate Mn (PMn) (18.87 – 26.0 nmol kg^{-1}), Co (PCo) (304.33 – 456.0 pmol kg^{-1}) and turbidity (Figure 4.8 and Figure 4.6). Similar observations were noted for DFe distributions (Figure 4.8) (Laës et al. 2007; Birchill 2017). A strong positive correlation (r^2 = 0.85, n = 8) between DMn and DFe was observed close to the seafloor (below the thermocline) for all seasons and suggests similar geochemical processes influencing the fate of these metals with reductive dissolution and remobilisation of soluble Mn (II), Mn (III) (Madison et al. 2013) and Fe (II) species from porewaters (Froelich et al. 1979). Indeed, a build-up of Fe (II) species in porewaters was reported at Site A (Klar et al. 2017). Benthic inputs of DMn, DCo and DFe are further supported by increased levels of the short-lived $^{224}Ra_{xs}$ (3.66 days) and $^{223}Ra_{xs}$ (11.4 days) isotopes. Radium-224 and ^{223}Ra are

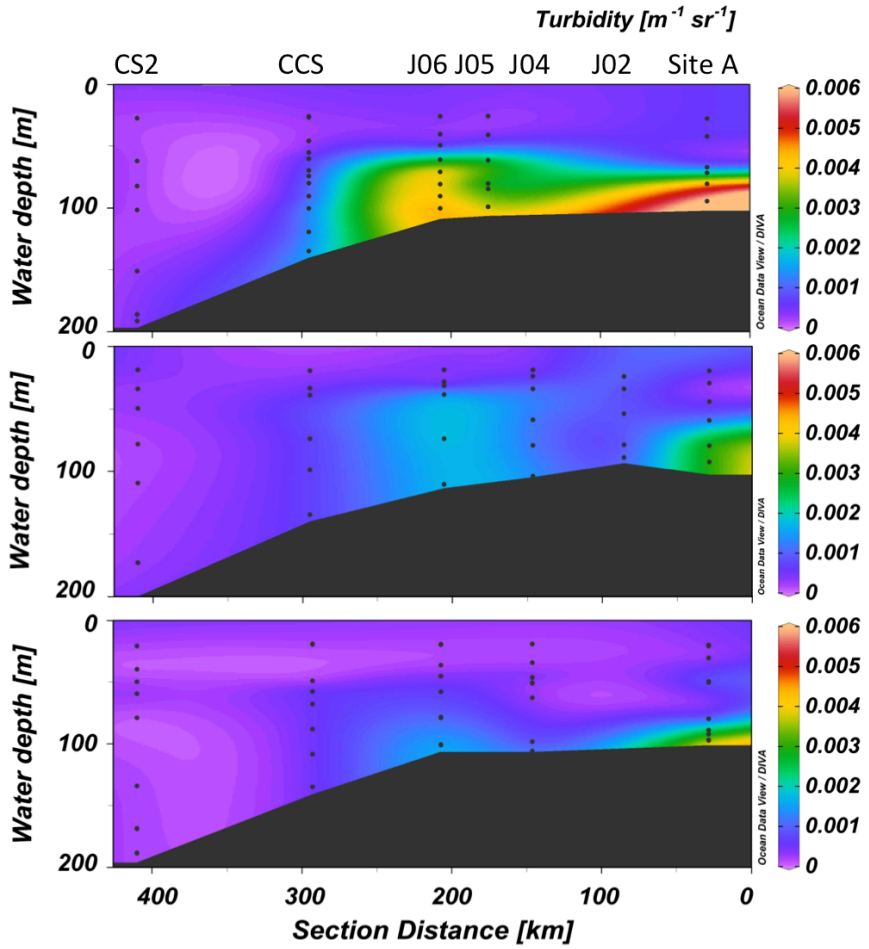


Figure 4.6. Sections of turbidity along the on-shelf transect in November (DY018) (top), April (DY029) (middle) and July (DY033) (bottom).

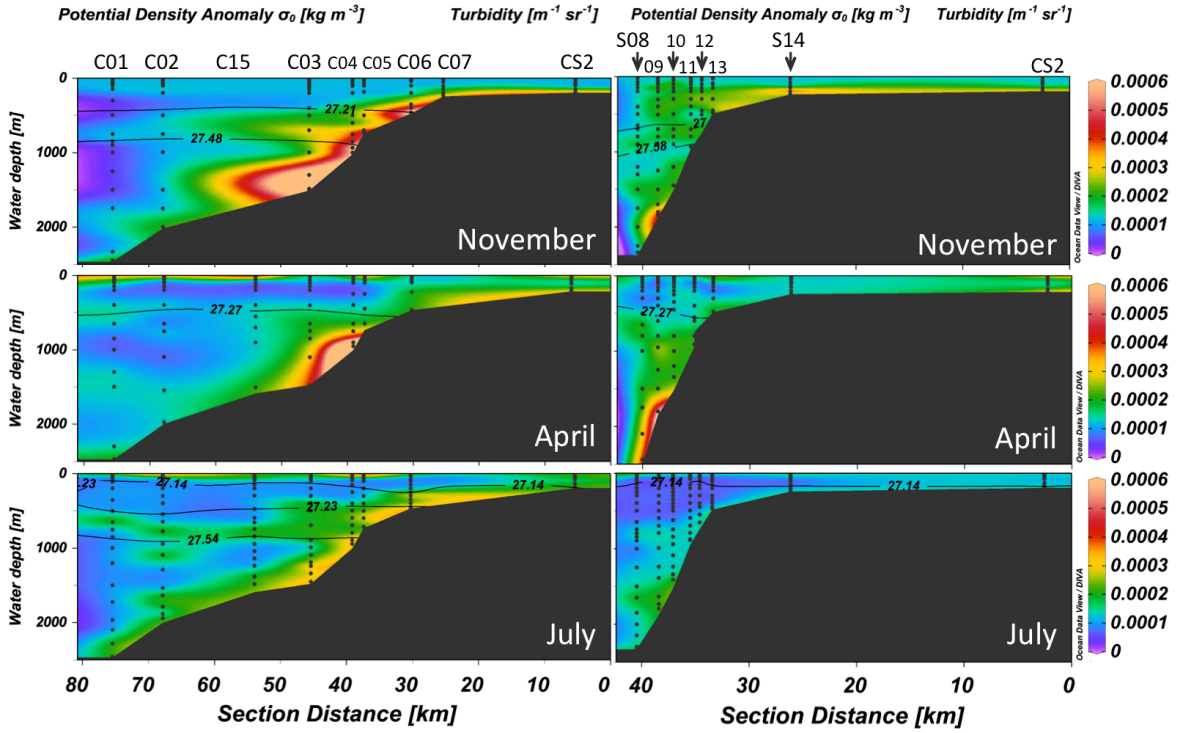


Figure 4.7. Sections of turbidity along the canyon transects (T1_C, left), and along the spur transects (T2_S, right), in November (DY018) (top), April (DY029) (middle) and July (DY033) (bottom). Black lines represent the density range of DMn concentration enhancement.

produced as a result of radioactive decay of particle reactive parent Thorium isotopes (^{227}Th and ^{228}Th) isotopes accumulated in sediments and thus have a primary benthic source. Elevated isotopic signals in the water column are indicative of recent contact of these waters with sediments. Interestingly, a strong positive correlation (r^2 = 1.0, n = 4) of particulate Co (PCo) and Mn (PMn) (Figure 4.8) indicate strong Co association with Mn particulate phases such as Mn-oxihydroxides through incorporation of DCo to Mn particulate phases and deposition in sediments (Moffett & Ho 1996). Although the DCo depth profile generally resembled the depth profiles of DMn and DFe as evident from Figure 4.8, the DCo concentration gradient towards the seafloor was not as prominent as with DMn and DFe and there was no correlation (r^2 = 0.05) between DCo and DMn or DFe. Dissolved Co was likely released from sediments through similar mechanisms as DMn and DFe, but was subsequently influenced by different biogeochemical processes in the water column. Dissolved Co strongly correlated with salinity across the continental shelf (r^2 = 0.78, n = 128) in all seasons (section 3.4.2). Therefore, a fluvial input and physical mixing of low-salinity, metal-enriched waters with saline, low-metal oceanic waters and some sedimentary inputs were the dominant processes controlling distributions of DCo on the continental shelf.

A benthic flux to overlying waters of 8.2 – 9.5 x 10^{-6} moles Mn m^{-2} d^{-1} (n = 3) and 53.8 – 63.0 x 10^{-9} moles Co m^{-2} d^{-1} (n = 3) at Site A in April was determined using Ra_{xs} measurements following the method described in Moore (2000). The vertical sedimentary flux (J_z) was estimated from the

decreasing activity of two short-lived ^{224}Ra and ^{223}Ra isotope and the vertical Mn and Co concentration gradients measured at the same station in April 2015 below the thermocline. The vertical gradient of ln^{224}Ra was described with ln($^{224}Ra_{xs}$) = 0.0621x – 2.2854 (r^2 = 0.83) and ln($^{223}Ra_{xs}$) = 0.0382x – 1.7799 (r^2 = 0.73). The vertical flux of DTM (J_z, mol m^{-2} d^{-1}), was calculated as:

$$J_z = K_h \frac{\partial M}{\partial x}$$

where K_h is the effective vertical eddy diffusion coefficient (m^2 d^{-1}; detailed in Moore 2000 (Moore 2000)) multiplied by the vertical dissolved metal (Mn and Co) concentration gradient $\left(\frac{\partial M}{\partial x}\right)$ (mol m^{-3}). If the exchange is dominated by eddy diffusion, an assumption which can be evaluated by the linearity of ln($^{224}Ra_{xs}$) versus vertical distance, then K_z is constant and the system is under steady state:

$$m = \sqrt{\frac{\lambda}{K_h}} \quad \text{and} \quad \lambda = \frac{\ln(2)}{t_{1/2}}$$

where λ is the decay constant, $t_{1/2}$ is the half-life of ^{224}Ra (3.66 days) and ^{223}Ra (11.4 days) and the slope m. A linear relationship between ln$^{224}Ra_{xs}$ and ln$^{223}Ra_{xs}$ activity with distance assumes an

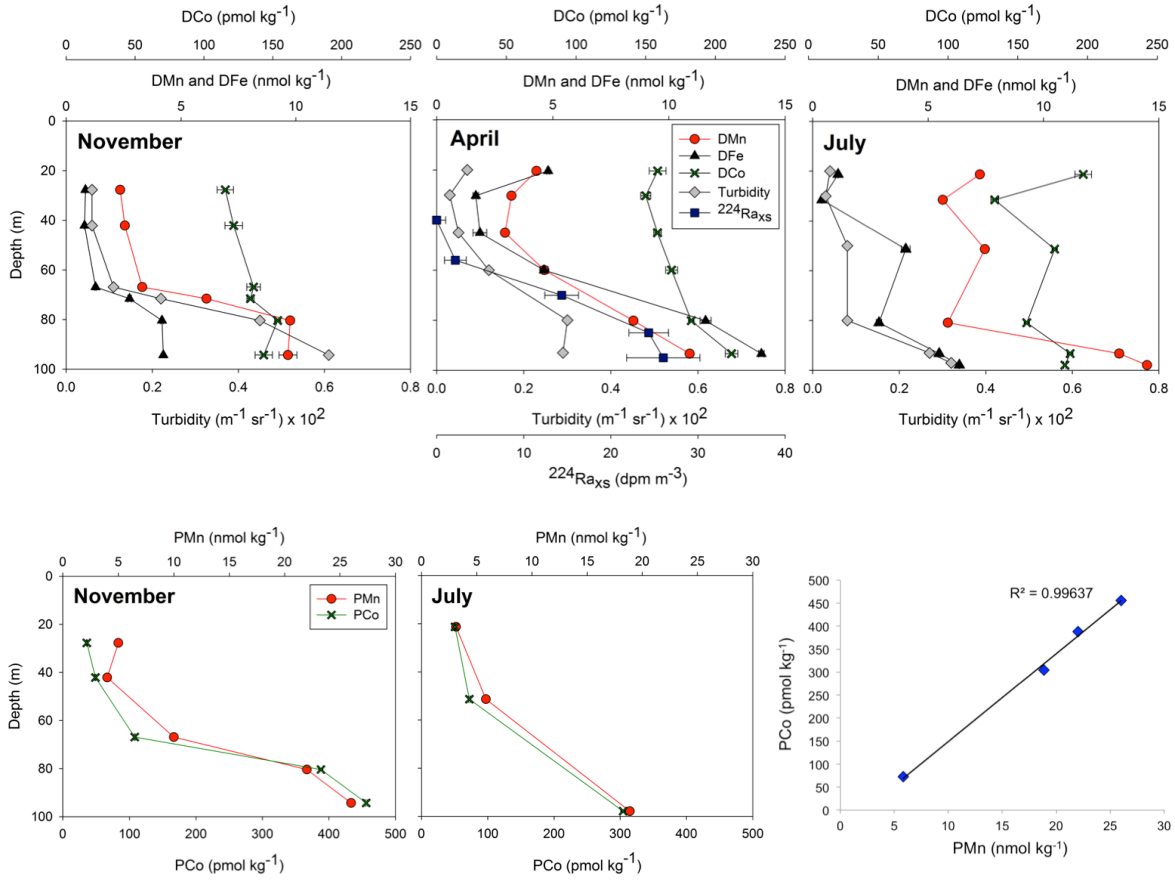


Figure 4.8 Upper panel: dissolved manganese (red circles), iron (blue triangles), cobalt (green crosses), turbidity (grey diamonds) and $^{224}Ra_{xs}$ measurements at Site A in November (left), April (middle) and July (left). Bottom panel: particulate manganese (red circles) and cobalt (green crosses) at Site A in November (left) and July (middle) and relationship of particulate manganese and cobalt below thermocline at Site A in April and July (right).

eddy-diffusive dominated system in steady state. Dissolved Mn benthic fluxes estimated at Site A were in good agreement with the DMn flux estimation (0.1 – 13.3 x 10^{-6} moles Mn m^{-2} d^{-1}) on the Iberian continental margin (van der Zee et al. 2001) and exceeded the atmospheric DMn flux (0.018 – 0.066 x 10^{-6} moles Mn m^{-2} d^{-1}) in the North Atlantic (de Jong et al. 2007).

4.4.4.2 Continental shelf break nepheloid layers

Persistently elevated DMn concentrations (0.339 – 0.895 nmol kg^{-1}) towards the seafloor were observed in deeper waters (> 1500 m, > 27.75 σ_0) along both transects during all seasons (Figure 4.1). The elevated DMn concentrations coincided with an increased signal in $^{224}Ra_{xs}$ (Figure 4.9, Figure 4.10) and turbidity (Figure 4.7) indicating a transfer of DMn from resuspended sediments through nepheloid layers via similar geochemical mechanism as described in section 4.4.4.1, reductive dissolution and remobilisation of soluble Mn (II), Mn (III) and Fe (II) species from porewaters. Persistently higher DMn concentrations were measured along the spur transect (0.441 ± 0.147 nmol kg^{-1} (n = 24)) compared to the canyon transect (0.319 ± 0.033 nmol kg^{-1} (n = 24)) for all seasons. However, the turbidity signal along the canyon transect was higher than along

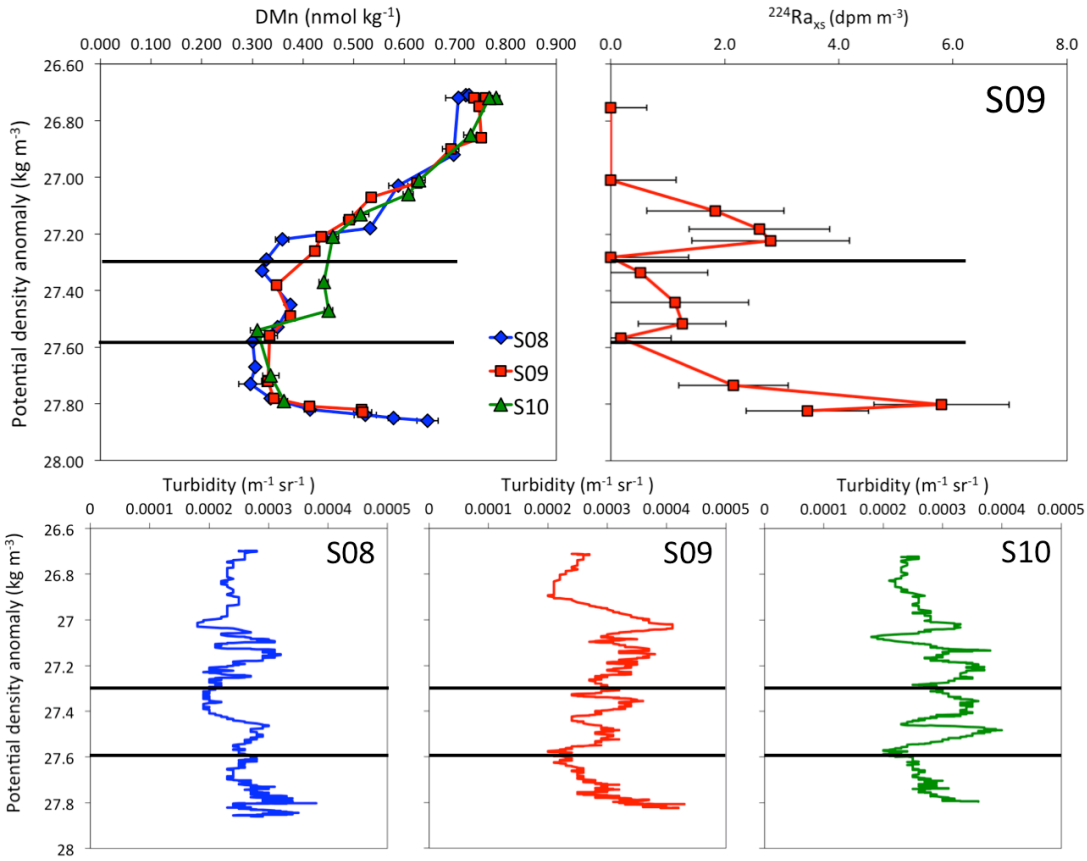


Figure 4.9. Upper panel: depth profiles of DMn (left) and $^{224}Ra_{xs}$ (right) at stations S08 (blue diamonds), S09 (red squares) and S10 (green triangles). Bottom panel: turbidity measurements at stations S08 (left), S09 (middle) and S10 (left) during DY018 (November). Black horizontal lines indicate the density range of elevated concentrations of dissolved manganese and cobalt during DY018 (November).

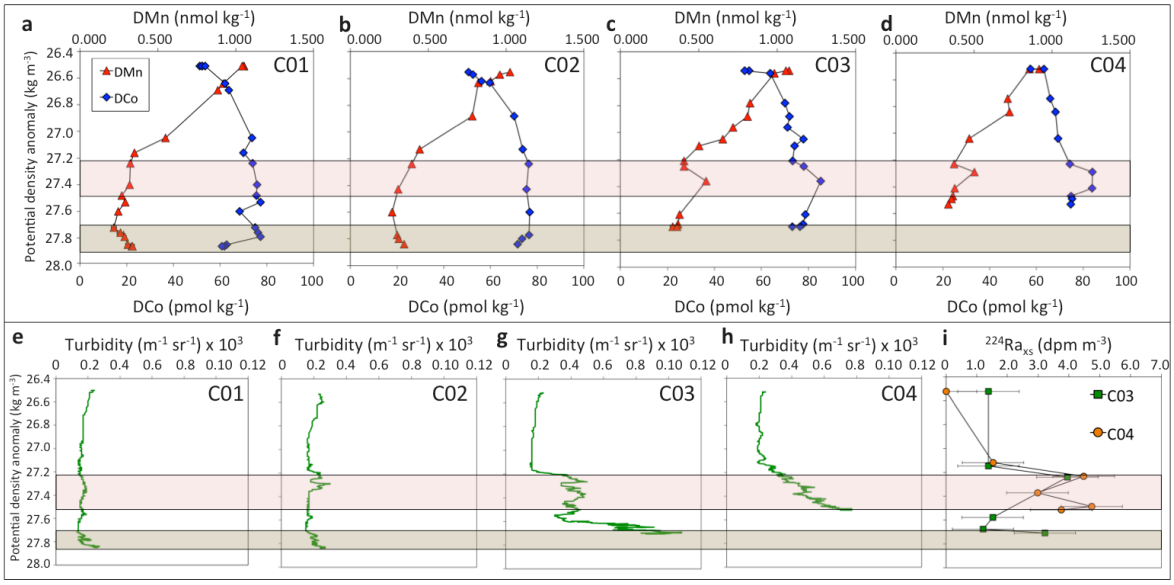


Figure 4.10 Upper panel: vertical depth profiles of dissolved manganese (red triangles) and cobalt (blue diamonds) plotted against potential density anomaly at stations C01 – C04 in November (a-d). Bottom panel: turbidity measurements against potential density anomaly at stations C01 – C04 in November (e-h) and vertical depth profiles $^{224}Ra_{xs}$ measurements at station C03 (green square) and C04 (orange circle) in November. Red horizontal rectangle in both panels indicates the density range of elevated concentrations of dissolved manganese and cobalt. Brown horizontal rectangle indicates elevated concentrations of these metals in bottom waters.

the spur transect (Figure 4.7), which is agreement with the global observations in submarine canyons (Gardner 1989; Hotchkiss & Wunsch 1982; Kunze et al. 2002; Carter & Gregg 2002). This suggests either a non-linear relationship between sediment resuspension and magnitude of DMn sedimentary release or the influence of other factors such as sediment type (Komárek & Zeman 2004), sediment and bottom water oxygen concentrations (Lohan & Bruland 2008) and/or organic matter content in sediments (Slomp et al. 1997) that can also influence the magnitude of DMn sedimentary release. Potentially, considering the potential for DMn scavenging of, the particle rich BNLs may also act as a sink for this metal in the water column.

In addition to the benthic inputs to the deep waters, three distinctive metal rich intermediate nepheloid layers (INLs) that extended away from the continental slope were observed in November and July (Figure 4.1 and Figure 4.2). Resuspended sediments were a persistent feature along the Celtic Sea continental margin as confirmed by elevated signals in turbidity (Figure 4.7), and variable but persistent INLs propagating off-shore along isopycnals that transported DFe and particulate Fe (PFe) have been observed in the study region (Birchill 2017). In November, along the canyon transect, elevated DMn and DCo concentrations of 0.425 ± 0.071 nmol kg^{-1} (n = 7) and 79.1 ± 5.1 pmol kg^{-1} (n = 7) were observed at stations C03 – C04 and decreased off-shore to 0.304 ± 0.030 nmol kg^{-1} (n = 3) and 75.1 ± 1.0 pmol kg^{-1} (n = 3) (C01) along 27.21 – 27.48 kg m^{-3} σ_0 isopycnal (400 – 850 m depth) (Figure 4.1a and Figure 4.10). Similarly to Site A, these elevated DMn and DCo concentrations coincided with increased signals in DFe (Birchill 2017), PMn and

PCo. Particulate Mn decreased from 0.764 ± 0.119 nmol kg^{-1} (n = 5) to 0.217 ± 0.052 nmol kg^{-1} (n = 2), whilst PCo decreased from 31.5 ± 12.7 pmol kg^{-1} (n = 5) to 17.1 ± 3.8 pmol kg^{-1} (n = 2) across C04 – C03 and C01 stations (Figure 4.11). Elevated signals in turbidity and $^{224}Ra_{xs}$ (measurement available for C01, C03 – C04 stations) were also evident (Figure 4.10). Along the spur transect, elevated DMn concentrations of 0.401 ± 0.078 nmol kg^{-1} (n = 3) were observed at station S10 and decreased off-shore to 0.336 ± 0.033 nmol kg^{-1} (n = 4) at station S08 along 27.33 – 27.58 kg m^{-3} σ_0 isopycnal (700 – 1000 m depth) (Figure 4.1b and Figure 4.9). Similarly to the canyon transect, elevated PMn and PCo were observed along the same isopycnals (Figure 4.11). Particulate Mn concentrations decreased from 0.556 nmol kg^{-1} (S10) to 0.352 ± 0.120 nmol kg^{-1} (n = 2) (S08) and PCo concentrations decreased from 26.4 pmol kg^{-1} to 13.3 ± 8.2 pmol kg^{-1} (n = 2) across the respective stations and coincided with elevated signals in turbidity and $^{224}Ra_{xs}$. In contrast to the canyon transect, DCo concentrations were not elevated suggesting lower DCo inputs or scavenging processes removing DCo from the water column. Interestingly, along the spur transect INLs were only observed at the most off-shelf stations. Considering the poleward current direction along slope, this signal could have the same (sedimentary) source but originated south of the sampling stations and was transported northward. An elevated $^{224}Ra_{xs}$ signal was also measured at 400 m at station S09 (Figure 4.9) but this feature was not reflected in the DMn depth profile. Potentially, this elevated DMn signal was masked by the higher DMn concentrations observed in surface waters (see section 4.4.2).

Along the canyon transect in July, elevated DMn concentrations of 0.398 ± 0.028 nmol kg^{-1} (n = 3), 0.342 ± 0.042 nmol kg^{-1} (n = 2), 0.321 ± 0.107 nmol kg^{-1} (n = 2) were observed along 27.23 – 27.54 kg m^{-3} σ_0 isopycnal (500 – 850 m depth) at stations C15, C02 and C01 respectively (Figure 4.1a). Similarly elevated concentrations were observed for DFe with 1.31 – 1.41 nmol L^{-1} DFe at

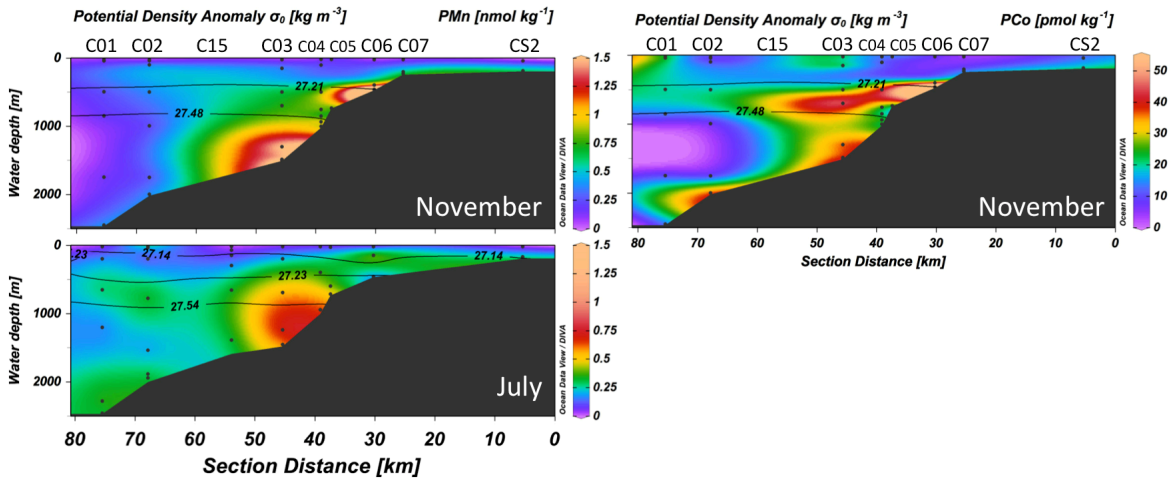


Figure 4.11 Particulate manganese (top left and bottom left) and cobalt (right) distribution plots along the canyon transects (T1_C, left), and along the canyon transect in November (DY018) (top) and July (DY033) (bottom). Black lines represent the density range of DMn concentration enhancement within identified nepheloid layers.

station C15 and decreased to 0.87 – 0.94 nmol L^{-1} at station C01 (Birchill 2017). This observation along with elevated signals in particulate metals, $^{224}Ra_{xs}$ and turbidity confirms a resuspended sedimentary source of DMn and DCo and subsequent lateral off-shelf isopycnal transport.

Elevated DMn concentrations decreased off-shore by 0.065 nmol kg^{-1} over 5 km (spur) and 0.149 nmol kg^{-1} over 30 km (canyon) distance in November and 0.077 nmol kg^{-1} over 20 km in July (canyon). However, DMn concentrations at the most off-shelf stations (C01 and S08) 'exceeded' the NE Atlantic 'background' DMn concentrations. This indicates that potentially the off-shelf transport of DMn had a larger spatial scale than the distance of the transects sampled. Additionally, predominantly poleward direction of the slope current could potentially cause off-shore transport of DTMs in a northerly direction along the slope rather than westward direction, away from the slope. If this is the case, the plumes of dissolved metals would be transported along the continental slopes, and potentially hinder the transport to the open ocean.

4.4.4.3 Subsurface dissolved Mn plumes

DMn maxima were observed in the upper waters at ~ 400 m depth in April and ~ 100 m depth in July along both off-shelf transects (Figure 4.1). DMn maxima propagated off-shore along isopycnals, 27.27 kg m^{-3} σ_0 in April and 27.14 kg m^{-3} σ_0 in July. In April, DMn concentrations decreased off-shore from 0.752 nmol kg^{-1} (S14) to 0.509 nmol kg^{-1} (S08) along the spur transect (~ 15 km) and along the canyon transect (~ 50 km), DMn concentrations decreased off-shore from 0.795 nmol kg^{-1} to 0.524 nmol kg^{-1} between stations C06 and C15 but increased to 0.824 nmol kg^{-1} (C01-C02) further offshore. Considering that stations C01 and C02 were the outermost stations of the canyon transect (Figure 2.1), it was likely that elevated DMn concentrations at these stations originated south of the stations and were transported by the northward slope current. In July, DMn concentrations did not decrease offshore, and remained in the range 0.764 ± 0.087 nmol kg^{-1} (n = 22) and 0.782 ± 0.076 nmol kg^{-1} (n = 29) along the spur and canyon transect respectively.

Similarly to the INLs, elevated $^{224}Ra_{xs}$ signals (data not available for July) were observed at the same depths, which suggests recent contact of these waters with sediments. However, in contrast to INLs, the subsurface maxima did not coincide with increased turbidity or PMn, which suggests a diffusive rather than resuspended sedimentary input of DMn. The DMn distribution in the upper waters could potentially be a result of the elevated biological activity in April (spring) and July (summer) with surface removal and sub-surface regeneration. Though, it was unlikely that the influence of biological activity in pre bloom conditions would considerably affect DMn concentrations and extend to 400 m depth in April but this explanation is more plausible in July when the shoaling of the DMn plume to depths < 100 m and significant drawdown of macro and micro nutrients was observed (3.4.1.1). However, a lack of correlation with macronutrients,

suggests that biological activity was not a major influence on DMn distributions in the upper waters.

4.5 Summary and conclusions

Observations of DMn and DCo distributions in the Celtic Sea region demonstrate a spatially and temporally variable influence of the sedimentary environments of the continental shelf. The elevated DMn and DCo concentrations towards the seafloor on the continental shelf, along with turbidity and $^{224}Ra_{xs}$ measurements confirmed a sedimentary source of these metals to the water column with estimated flux of 8.2 – 9.5 x 10^{-6} moles Mn m^{-2} d^{-1} and 53.8 – 63.0 x 10^{-9} moles Co m^{-2} d^{-1}. Benthic DMn and DCo inputs were also observed on the continental slope in form of BNLs in deeper waters and INLs at intermediate depths that extended away from the slope. Distinctive benthic DMn inputs were also observed in the upper waters in April that also extended off-shore and in contrast to NLs, these observations coincided with elevated signal in $^{224}Ra_{xs}$ but not turbidity, indicative of diffusive rather than resuspended sedimentary DMn source. Additionally, modification of DMn concentrations during MOW transit due to continental slope sedimentary inputs was described through comparison of DMn average concentrations in other studies.

The examination of full depth profile relationship of DCo and PO_4^{3-} on the continental slope revealed a gradual shift in biogeochemical processes influencing DCo distribution. Whilst biological uptake and remineralization were the dominant processes in the upper waters as evident in good linear correlation (r = 0.89 – 0.64), interplay between scavenging, remineralization and sedimentary inputs resulted in a low correlation at intermediate depths and scavenging processes were likely the dominant process in deeper waters and thus responsible for strong inverse correlation (r = -0.72) of DCo and PO_4^{3-}.

Chapter 5 Anthropogenic Signatures of Lead in The Northeast Atlantic

The research presented in this chapter has been published in *Geophysical Research Letters*

Authors: D. Rusiecka[1,2], M. Gledhill[1,2], A. Milne[3], E.P. Achterberg[1,2], A.L. Annett[4], S. Atkinson[3], A. Birchill[3], J. Karstensen[2], M. Lohan[3,1], C. Mariez[5], R. Middag[6], J. M. Rolison[7], T. Tanhua[2], S. Ussher[3], and D. Connelly[8]

[1]Ocean and Earth Sciences, National Oceanography Centre, University of Southampton, Southampton, UK, [2]GEOMAR Helmholtz Centre for Ocean Research Kiel, Germany, [3]School of Geography, Earth and Environmental Sciences, University of Plymouth, Plymouth, UK, [4]School of GeoSciences, University of Edinburgh, Edinburgh, UK, [5]Université de Bretagne Occidentale, France, [6]NIOZ Royal Netherlands Institute for Sea Research, Department of Ocean Systems, Netherlands, [7]Nuclear and Chemical Sciences Division, Lawrence Livermore National Laboratory, Livermore, USA, [8]National Oceanography Centre Southampton, European Way, Southampton, UK

Corresponding authors: Dagmara Rusiecka (drusiecka@gmail.com) and Eric Achterberg (eachterberg@geomar.de)

Key Points:

- Recent sources of Pb were evident despite a 4–fold reduction of Pb in NE Atlantic surface waters since leaded fuel prohibition
- Enhanced Pb was evident in Mediterranean Outflow Waters, transported >2500 km across the NE Atlantic
- Sediments represented an important source of Pb to overlying waters, exceeding the atmospheric flux of Pb

DOI for published article: 10.1002/2017GL076825

The final publication can be found in Appendix B and is available at:

http://onlinelibrary.wiley.com/doi/10.1002/2017GL076825

5.1 Introduction

Lead (Pb) is one of few elements for which the impact of human activity on the marine environment is clearly evident. Anthropogenic perturbation of the natural biogeochemical cycle of Pb in the ocean dates back to ~1850 (Kelly et al. 2009), with coal and leaded fuel combustion serving as major sources of Pb to the atmosphere (Kelly et al. 2009; Wu & Boyle 1997). Anthropogenic Pb is transported in the atmosphere associated with fine aerosol particles that can travel long distances, and are deposited in remote areas resulting in enhanced DPb surface ocean concentrations (Kumar et al. 2014; Véron & Church 1997), reaching >190 pmol kg^{-1} during the peak of the Pb emissions in 1970-80 (Laumond et al. 1984). Anthropogenic Pb has entirely masked signals of naturally sourced Pb (ca. 2.2 pmol kg^{-1} in surface waters (Henderson & Maier-Reimer 2002)). To date, leaded fuel has been virtually phased out (except in 3 countries, as of March 2017, UNEP), and Pb concentrations have decreased significantly from ~170 to <15 pmol kg^{-1} in surface waters (Boyle et al. 2014; Schaule & Patterson 1983), leading to recent evidence for natural Pb signatures re-emerging in the North Atlantic (Bridgestock et al. 2016).

The spatial and temporal variable historic Pb inputs to the marine environment can be used to investigate the reactivity and cycling of this element, and trace long-range ocean circulation patterns (Chen et al. 2016; Fine 2010; Lee et al. 2015). Anthropogenic Pb has been utilised as a tracer of subducted surface waters in the Indian (Lee et al. 2015) and Pacific Oceans (Chien et al. 2017), and ventilated surface waters of the Northwest Atlantic (Boyle et al. 2014). Anthropogenic perturbation of natural Pb concentrations in the ocean has been described as an '*evolving global experiment*' (Boyle et al. 2014) that demonstrates the magnitude of human impact on the environment.

Lead is a particle reactive element in marine waters and is typically removed through scavenging, with the sediments acting as repositories. However, the role of particulate matter and the physico-chemical processes that influence the fate of dissolved Pb (DPb) and facilitate long-range transport are poorly constrained. A slow release of DPb from particles and a rapid isotopic exchange with particulate matter that can influence the fate of particulate Pb (PPb) has recently been reported (Chen, Boyle, et al. 2016). Therefore, in order to gain insights into biogeochemical cycling of Pb in the marine environment, both phases should be considered.

Here the first extensive seasonal study of DPb, PPb and leachable Pb (LpPb) distributions in Northeast Atlantic marginal seas since the phase-out in Europe of leaded fuel use in 1980 – 2011 (European Communities 1978; Economic Commission for Europe 2014) is reported and evaluated. This study provides insights into the dynamic relationship between dissolved and particulate phases and demonstrates the role of benthic Pb release and Pb as a tracer of North Atlantic circulation patterns.

5.2 Study region, materials and methods

Full details of the study region, sampling and methods are provided in Chapter 2. Briefly, samples for trace metal analysis were collected during three different seasons; November – December 2014 (DY018), April 2015 (DY029), and July – August 2015 (DY033) in the Northeast Atlantic continental margin (Celtic Sea) Figure 2.1, on board RRS Discovery. Two off-shelf transects were conducted along a canyon (T1_C, stations C01 – C07, C15), nearby a spur (T2_S, stations S08 – S09) (SI, S1) and one on-shelf transect in the Celtic Sea (stations CS2, CCS, J02 – J06, Site A). Trace metal samples were collected following GEOTRACES protocols (Cutter et al. 2010). Dissolved Pb and Mn (DMn) were filtered using a 0.2 µm cartridge filter (Sartobran 300, Sartorius), preconcentrated using an automated system (SC-4 DX SeaFAST pico; ESI) and analysed by high-resolution inductively coupled plasma-mass spectrometry (HR-ICP-MS; Thermo Fisher Element XR) (Rapp et al. 2017). Dissolved Fe (DFe) (0.2 µm filtered) was analyzed by flow injection with chemiluminescence detection (Hajime. Obata et al. 1993) as detailed in (Birchill et al. 2017). Particulate Pb was collected on clean 25 mm Supor® polyethersulfone membrane disc filters (Pall, 0.45 µm) and subjected to a 25% acetic acid-hydroxylamine hydrochloride leach (LpPb) (Berger et al. 2008) and subsequently an hydrofluoric (HF) acid digestion (PPb) (Ohnemus et al. 2014). Particulate samples were analysed using ICP-MS (Thermo Fisher X Series 2). Dissolved aluminium (DAl) (0.2 µm filtered) was analysed using spectrofluorometry following the method by Hydes and Liss (1976). Evaluation of the accuracy and efficiency of these methods was carried out using Certified Reference Materials with the results showing good agreement (Table 5). Some data points were identified as outliers and were excluded from consideration (Chapter 2). Radium (Ra) isotopes 223Ra and 224Ra were extracted from large seawater volumes (60 – 100 L) by adsorption onto Mn acrylic fibers (Sun & Torgersen 1998). Ra activities were analysed at sea by Radium Delayed Coincidence Counting following standard methodology (Annett et al. 2013; Garcia-Solsona et al. 2008; Moore 2008; Moore & Arnold 1996). Ra activities used here (^{224}Raxs and ^{223}Raxs) are in excess of activity supported by the parent isotopes in the water column (Chapter 2). Water mass distribution was quantified using extended Optimum Multiparameter analysis (extOMP) (Hupe & Karstensen 2000; Karstensen & Tomczak 1998; Pollard et al. 2004). The propagation time of MOW from the Gulf of Cadiz was calculated analogously to (Waugh et al. 2003), using CFC-12 data available in the GLODAPv2 data product (Olsen et al. 2016). Aerosol samples were digested using HF and HNO3 following the method adapted from (Morton et al. 2013), and analysed by the ICP-MS (Thermo Fisher X Series 2). Section plots figures were created with Ocean Data View (2015) software (Schlitzer 2015) with DIVA gridding settings.

5.3 Results and discussion

DPb concentrations in the Celtic Sea region ranged between 29.6 and 122 pmol kg^{-1} (Figure 5.1 a-c and Figure 5.2). Off-shelf distributions showed elevated DPb concentrations (50.8 ± 3.0 pmol kg^{-1} (n = 20)) in the seasonal mixed layer (SML) along the canyon transect in November, and also at stations S08 and S09 along the spur transect. Below the SML, DPb distributions were generally consistent along both transects for all seasons and decreased down to 38 pmol kg^{-1} in the subsurface waters and increased at depths of ~ 550 – 1500 m to 46.6 ± 5.6 pmol kg^{-1} (n = 84). In deeper waters (> 1500 m), DPb concentrations decreased to 37.0 ± 3.2 pmol kg^{-1} (n = 39). On the continental shelf, DPb concentrations were generally higher in comparison to the off-shelf transects and ranged between 36.1 – 122 pmol kg^{-1}. Elevated DPb concentrations were measured in surface waters in April (96.8 pmol kg^{-1}) and July (99.1 pmol kg^{-1}) with somewhat lower levels in November (72.6 pmol kg^{-1}), whereas DPb was persistently elevated in bottom waters (up to 121 pmol kg^{-1}) across all seasons. No correlations between DPb and macronutrients were observed.

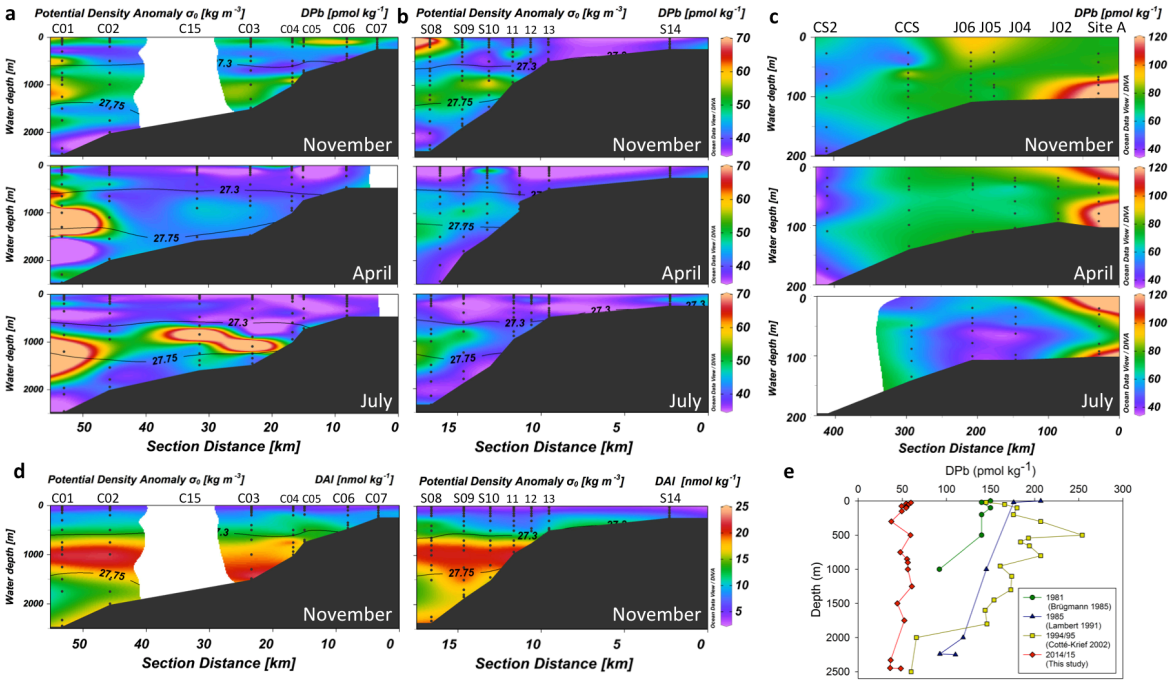


Figure 5.1 Upper panel: dissolved lead distribution plots (a) along the canyon transects (T1_C, left), (b) along the spur transects (T2_S, middle), and (c) and along the on-shelf transect (left) in November (DY018) (top), April (DY029) (middle), and July (DY033) (bottom). Bottom panel: (d) example of dissolved aluminum distribution plots from November (DY018) along the canyon (T1_C) transect (left) and spur (T2_S) transect (right). For the full dissolved aluminum results please see Figure 5.3. Black lines represent Mediterranean Outflow Water density range contour plots. (e) Reduction of DPb concentrations in the Celtic Sea slope region over the last 30 years. Data are from Brügmann et al. (1985, green circles), Lambert et al. (1991, blue triangles), and Cotté-Krief et al. (2002, yellow squares), and this study is represented by the S08 station in April (DY029) by red diamonds.

Table 7 DPb data compilation to date from various European coastal environments. [a] Indicates values extracted from the published figures therefore not representing the exact values reported, [b] indicates measurements by ASV and [c] indicates measurements by GFAAS for the same study.

Region	Year	Level	Pb (pM)	References
North Sea	1981	Surface/water column	22 - 440	(Brügmann et al. 1985)
North Sea	1988	Surface waters	~ 200 - 380[a]	(Muller et al. 1994)
English Channel	1981	Surface/water column	63 - 190	(Brügmann et al. 1985)
English Channel	1988	Surface waters	~ 120 - 290[a]	(Muller et al. 1994)
English Channel	1990	Surface waters	83 - 183	(Helmers & Van der Loeff 1993)
Celtic Sea, shelf	1985	Surface/water column	~ 100 - 250[a]	(Muller et al. 1994)
Celtic Sea, shelf	1988	Surface waters	~ 70 - 200[a]	(Muller et al. 1994)
Celtic Sea, shelf	1994-1995	Surface waters	158 - 431	(Cotté-Krief et al. 2002)
Hebridean Sea, shelf	1993	Surface waters	17 - 55	(Kremling & Streu 2001)
Hebridean Sea, shelf	1996	Surface waters	34 - 68	(Kremling & Streu 2001)
Celtic Sea, slope	1981	Surface/water column	24 - 170	(Brügmann et al. 1985)
Celtic Sea, slope	1984-1985	Surface/water column	~100 - 250[a]	(Muller et al. 1994)
Celtic Sea, slope	1985	Surface/water column	~ 101 - 227[a]	(Lambert et al. 1991)
Celtic Sea, slope	1990	Surface waters	116 - 119	(Helmers & Van der Loeff 1993)
Celtic Sea, slope	1994-1995	Surface/water column	57 - 215	(Cotté-Krief et al. 2002)
Bay of Biscay	1989 - 1990	Surface waters	~100 - 170[a]	(Pohl et al. 2011)
Bay of Biscay, France	2001-2002	Surface/water column	60 - 270	(Waeles et al. 2008)
Bay of Biscay	2005	Surface waters	~ 70[a]	(Pohl et al. 2011)
Cape São, shelf, Portugal	2004	Surface/water column	8 - 74	(Monteiro et al. 2015)
Cape Finisterre, shelf, Spain	2005	Surface/water column	190 - 380	(Prego et al. 2013)
Western Mediterranean Sea	1981	Surface/water column	140 - 845[a,b] 140 - 386[a,c]	(Laumond et al. 1984)

Surface water DPb concentration of 40.2 ± 7.5 pmol kg^{-1} (n = 109) along the shelf break in 2014-2015 showed at least a 4-fold decrease compared to previous reports for the region (Figure 5.1 and Table 7) (Brügmann et al. 1985; Cotté-Krief et al. 2002; Helmers & Van der Loeff 1993; Lambert et al. 1991; Muller et al. 1994), and were generally lower in comparison to other European shelf waters over the last 4 decades (Kremling & Streu 2001; Laumond et al. 1984; Monteiro et al. 2015; Pohl et al. 2011; Prego et al. 2013; Waeles et al. 2008). The diminishing DPb concentrations over the last 2 decades form a success of the phase-out process of leaded fuel. Nevertheless, the observed concentrations in the study region exceeded predicted natural levels of Pb (Henderson & Maier-Reimer 2002) by at least an order of magnitude, indicating that the vast majority of Pb still has an anthropogenic origin. Thus, the elevated DPb concentrations reported in surface waters indicate the presence of recent anthropogenic Pb inputs to Northeast Atlantic waters from sources such as coal burning, smelting or mining (Nriagu & Pacyna 1988; Lee et al. 2014).

5.3.1 Long range Pb transport in MOW

Elevated DPb concentrations of 46.6 ± 5.6 pmol kg^{-1} (n = 84) were a persistent feature in the depth range ~550 – 1500 m (27.30 – 27.75 kg m^{-3} σ_0) in the slope region of the Celtic Sea. The DPb

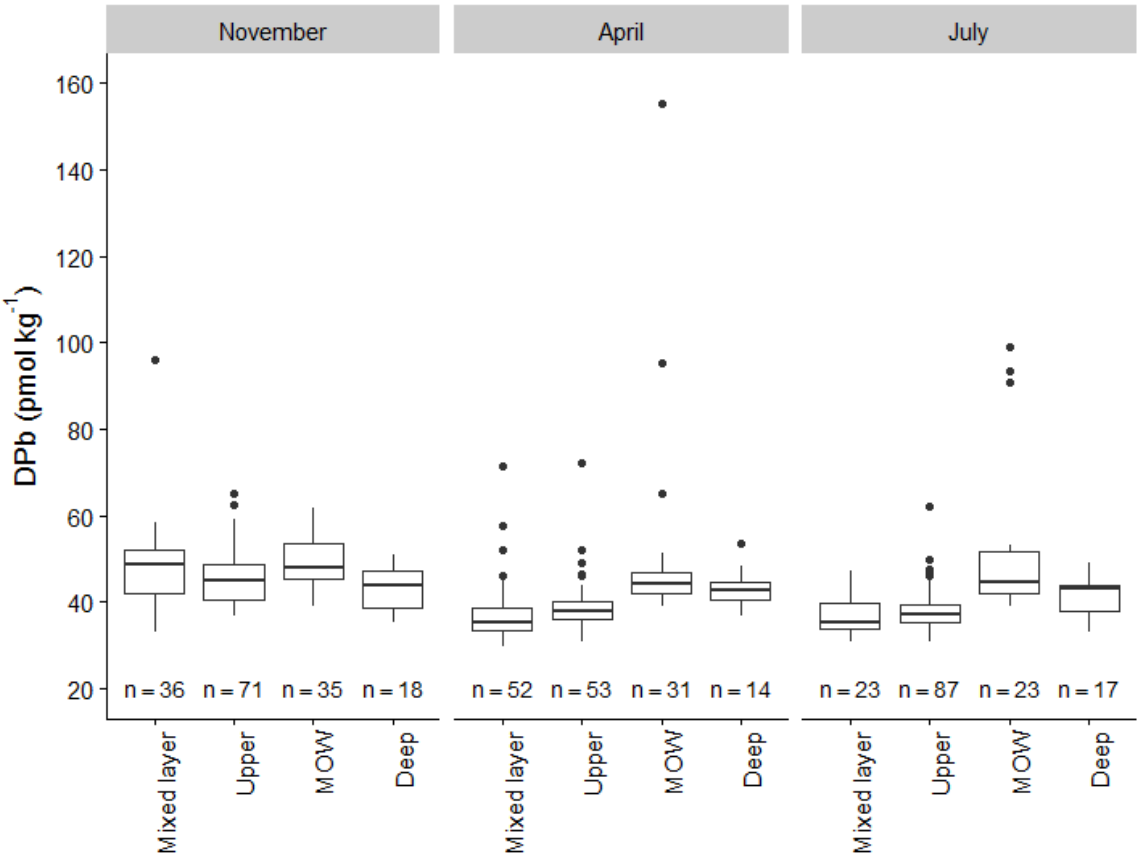


Figure 5.2 Boxplot of DPb concentrations in four distinctive water masses; seasonal mixed layer, upper waters, MOW and deep waters in all three seasons.

maximum coincided with salinity (35.74) (Figure 3.1a) and DAl (17.3 ± 2.6 nmol kg^{-1}, n = 88) maxima (Figure 5.3), signatures of Mediterranean Outflow Water (MOW) (Measures & Edmond 1988; Rolison et al. 2015). Surface waters in the Mediterranean Sea received enhanced atmospheric Pb inputs during the period of leaded fuel use, with maximum surface DPb of >190 pmol kg^{-1} (Laumond et al. 1984). Mediterranean waters also receive enhanced aeolian fluxes of Al from Saharan dust (Rolison et al. 2015). Deep water formation occurs in the Levantine Basin and Gulf of Lions, and the saline deep Mediterranean waters with enhanced DPb (40 - 80 pmol kg^{-1}) (Rolison 2016) and DAl (125 – 170 nmol kg^{-1} (Rolison et al. 2015)) exit the Strait of Gibraltar as bottom waters and mix with ENACW (García-Ibáñez et al. 2015). The MOW spreads across NE Atlantic at a depth ~550 – 1500 m and propagates along the continental slope towards the Celtic Sea shelf break. The mean propagation time of MOW from the Gulf of Cadiz to the Celtic Sea slope region is ~5 years (Figure 5.4). The presence of MOW at intermediate depths in the study region has previously been reported (Cotté-Krief et al. 2002; Lambert et al. 1991) and was confirmed by the extOMP analysis (Figure 3.1b and Figure 3.2). The core of the MOW (up to 55%) was identified at ~1000 m depth with a Gaussian decay (20% at 550 m and 1500 m).

Enhanced DPb concentrations were also observed along GEOTRACES transects in corresponding MOW density layers (27.22 – 27.82 kg m^{-3} σ_0): in the Gulf of Cadiz (49.0 ± 2.6 pmol kg^{-1}, n = 14, GA04 (Rolison 2016)), north (46.1 ± 6.1 pmol kg^{-1}, n = 18, GA01) and south of the Gulf of Cadiz (55.1 ± 5.5 pmol kg^{-1}, n=10, GA03, (Noble et al. 2015)) (Figure 3.14), in agreement with observations reported here. Celtic Sea study region is ~2500 km away from the Strait of Gibraltar,

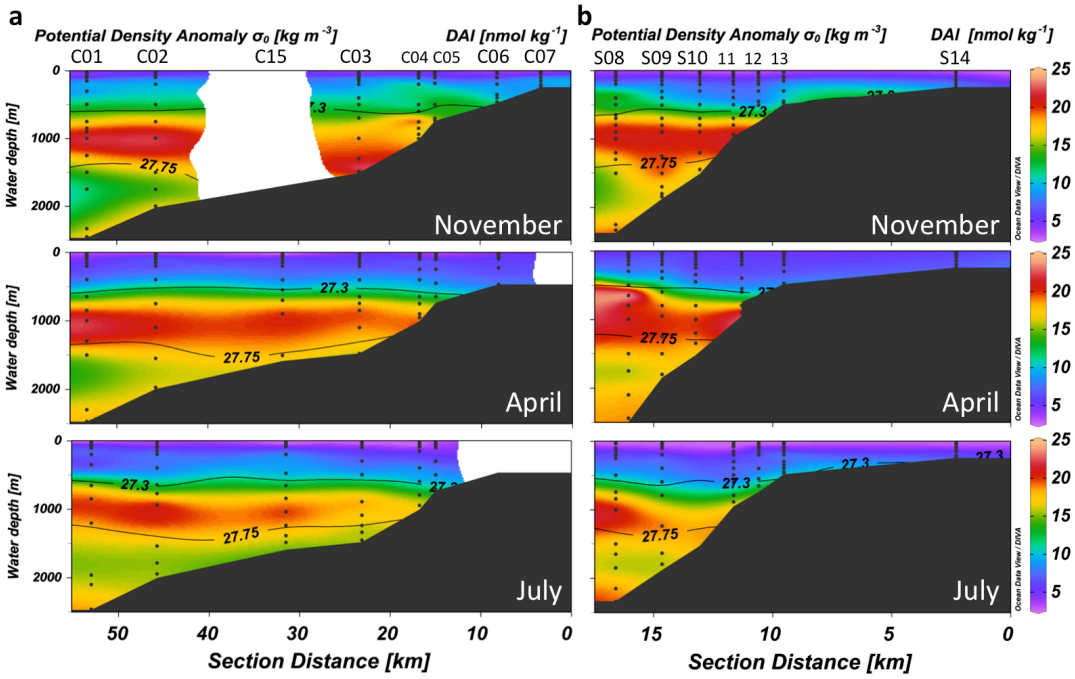


Figure 5.3 Dissolved aluminium distribution plots (a) along the canyon transects (T1_C, left), (b) along the spur transects (T2_S, right) in November (DY018) (top), April (DY029) (middle) and July (DY033) (bottom). Black lines represent MOW density range contour plots.

therefore the concentration of DPb and DAl may be expected to decrease through scavenging and/or dilution processes during transit. Whilst DAl concentrations and salinity correlated well (r^2 = 0.68) and decreased from 27.8 ± 7.2 nmol kg^{-1} and 35.6-36.4 (Gulf of Cadiz) to 17.3 ± 2.6 nmol kg^{-1} and 35.4-35.7, there was no correlation of DPb with salinity and DPb concentrations remained unchanged (Figure 5.5). Suggested are the following processes that maintain elevated DPb signal during MOW transit: i) benthic inputs from the European continental slopes. Shelf break sediments have been suggested as a Pb source in the Philippine Sea (Chien et al. 2017). Local sediment resuspension events in the Bay of Biscay as MOW propagates along the continental slope have also been reported (McCave & Hall 2002). ii) Reversible Pb sorption onto particle surfaces. This mechanism has been suggested to supply DPb to North Pacific deep waters (Wu et al. 2010). Pb isotope exchange between these two phases has been demonstrated (Chen, Boyle, et al. 2016; Sherrell et al. 1992) and the potential of particle reversible sorption has been shown using thorium isotopes (Bacon & Anderson 1982). Potentially, DPb (< 0.2 µm) may be released from particles in the form of small, low specific density inorganic particles (colloids 0.02 – 0.2 µm) with longer residence time. However, PPb dissolution within MOW is also plausible. Results reported here show that the major portion of PPb was in LpPb form (78 ± 10%, n = 205) while overall the majority of the total Pb pool (PPb + DPb) was in the DPb fraction (70 ± 18%, n = 171), thus implying a significant role of particles in DPb distributions.

Partial mixing with other historically Pb polluted waters, such as Northeast Atlantic ventilated surface waters and LSW transported across the North Atlantic (Bridgestock et al. 2018; Zurbrick et

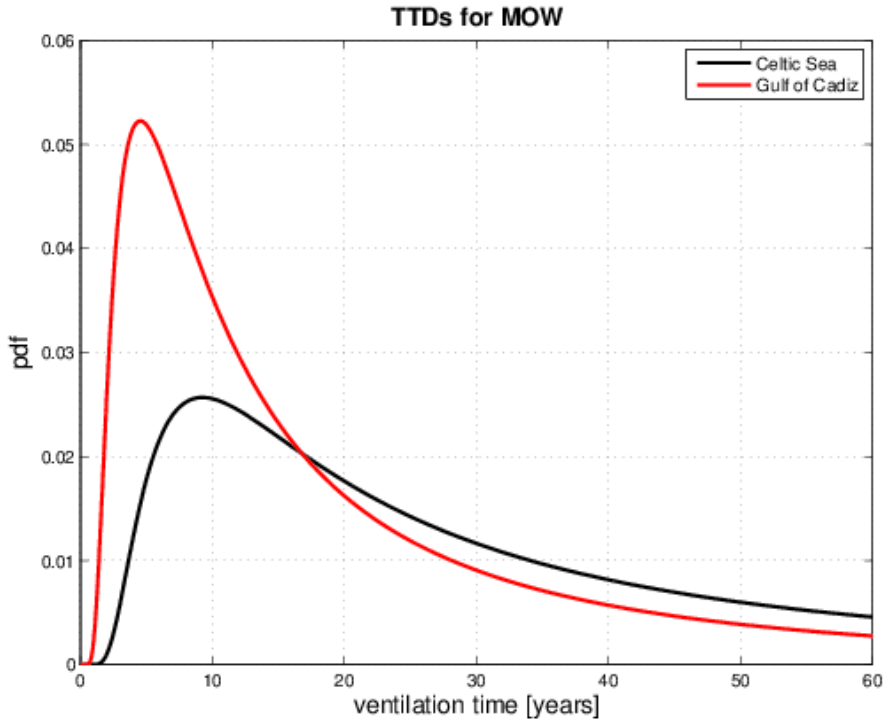


Figure 5.4 Propagation time of MOW from Mediterranean Sea to Gulf of Cadiz (black line) and from Gulf of Cadiz to the Celtic Sea continental shelf break (red line) with y-axis representing probability density function.

al. 2018), has been shown to influence DPb concentrations at intermediate depths and thus also need to be considered. Low-salinity, and high-oxygen LSW underlies the warm, saline MOW (Talley & McCartney 1982). Extended OMP confirmed a layering of the water masses with MOW at a core depth 27.60 kg m^{-3} transiting into the LSW core at 27.79 kg m^{-3} (Figure 3.2) and a potential for vertical mixing of bottom layers of MOW with LSW. Within waters identified as LSW (27.76 – 27.85 kg m^{-3} σ_0), concentrations of DPb (42.9 ± 4.5 pmol kg^{-1} (n = 42)) and DAl (15.8 ± 1.0 nmol kg^{-1} (n = 40)) were somewhat lower, and salinity (34.98 – 35.4) and temperature (from 8.8 ± 1.5 to 5.1 ± 1.0 ^{o} C) were lower in comparison to overlying MOW. These values were higher in comparison to DPb (36.9 ± 7.4 pmol kg^{-1}, n = 60), DAl (13.0 ± 1.2 nmol kg^{-1}, n = 60), salinity (34.94 – 35.2) and temperature (4.3 ± 0.6 ^{o}C) observed within LSW (27.68 – 27.81 kg m^{-3} σ_0) in the NW Atlantic (GA02 section, 2010) (Mawji et al. 2015). Densities of MOW and LSW are similar and a complete differentiation is therefore challenging, preventing us from determining the exact fraction of each water mass. These findings indicate the potential for MOW penetration into deeper waters, altering properties of LSW although the upward vertical mixing cannot be ruled out. Therefore, the DPb maximum in the Celtic Sea region was a result of anthropogenically perturbed MOW masses reaching NE Atlantic continental margins.

5.3.2 Sediment release of particle reactive element

Elevated DPb (65.9 – 121 pmol kg^{-1}) and PPb concentrations (149 – 806 pmol kg^{-1}) were observed in bottom waters at Site A during all seasons, and on the continental slope at C03-C04 stations in November (DPb: 52.5 ± 5.6 pmol kg^{-1}, n = 7, PPb: 29.3 ± 13.9 pmol kg^{-1}, n = 8) (Figure 5.3). Following fluvial or atmospheric inputs to marine waters, Pb is typically scavenged and transferred to the seafloor (Bastami et al. 2015; Marani et al. 1995). Tidal currents, wind driven waves and storm events cause resuspension of sediments (Kalnejais et al. 2007), thereby supplying Pb-enriched porewaters and particles to the water column. This mechanism has been reported for deep ocean (Lee et al. 2015; Noble et al. 2015), coastal (Annibaldi et al. 2009; Chien et al. 2017), estuarine (Rivera-Duarte & Flegal 1994), and riverine systems (Ferrari & Ferrario 1989), and observed in sediment chamber experiments (Kalnejais et al. 2007; Zago et al. 2000).

At Site A, the enhanced DPb and PPb concentrations near the seafloor coincided with persistently elevated turbidity signals (Figure 5.3), indicating particle resuspension and subsequent DPb and PPb remobilization from the sediments to overlying waters. The benthic Pb supply is supported by increased levels of the short-lived isotopes $^{223}Ra_{xs}$ and $^{224}Ra_{xs}$ (half-lives 3.66 and 11.4 days, respectively) near the seafloor (Figure 5.3), indicating recent sedimentary supply. A similar feature was observed on the continental slope along the canyon transect in November where salinity maximum associated with MOW decreased towards the continental shelf break (Figure 3.1a) from 35.74 (C01) to 35.61 (C04) (~1000 m depth) thus DPb

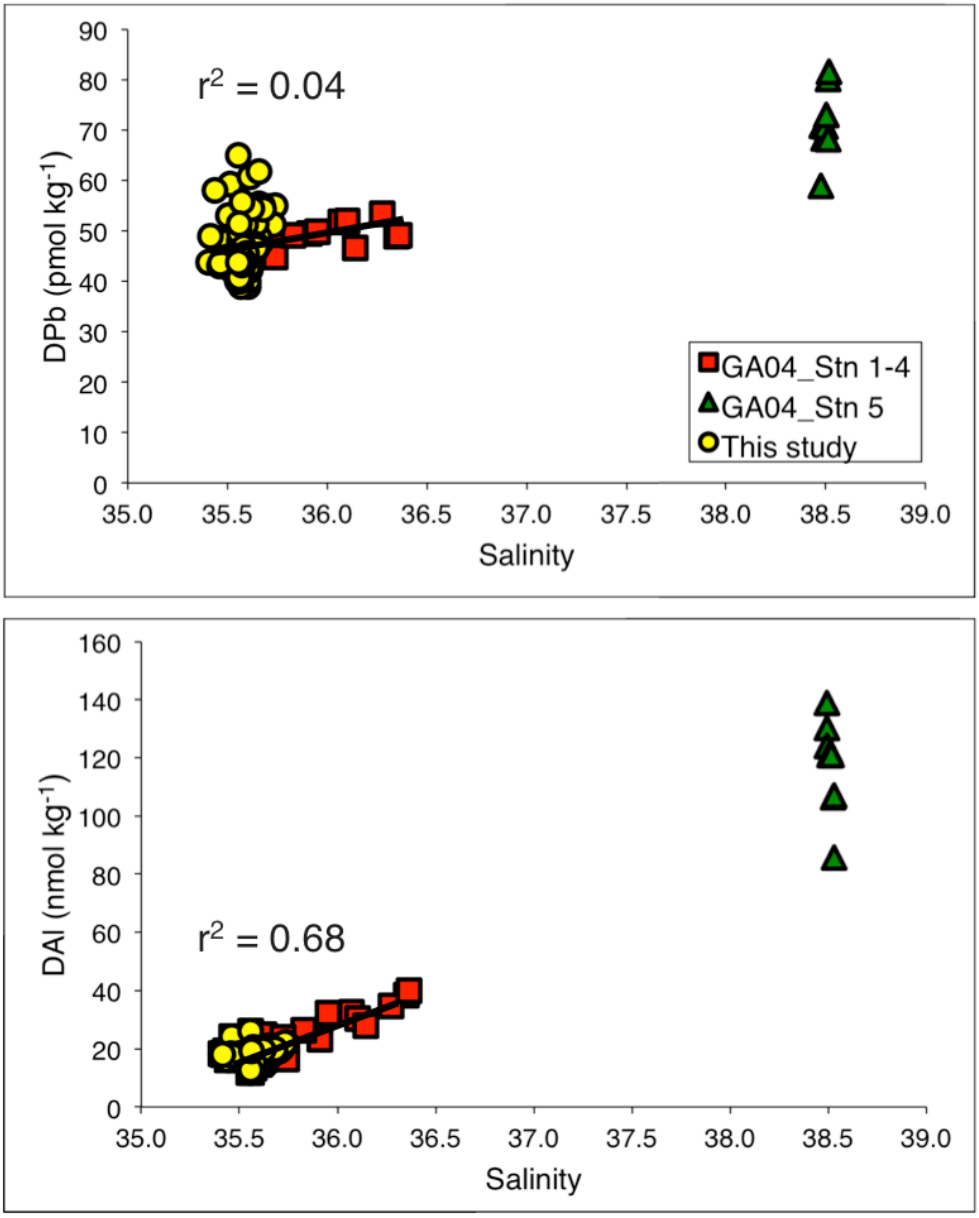


Figure 5.5 DPb (top) and DAl (bottom) concentrations along the salinity gradient across the Strait of Gibraltar, GA04 stations 1 - 4 (red) and this study (yellow). Mediterranean deep water end member concentrations (green) represent GA04 station 5 from the Alboran Sea in close proximity to the Strait of Gibraltar. End member data points were taken below the upper layer inflow of ENACW and above the bottom waters with potential sediment resuspension. Black lines indicate correlations of dissolved metal concentrations and salinity across GA04 stations 1-4 and the Celtic Sea.

concentrations were also expected to decrease. Yet DPb concentrations remained unchanged (Figure 5.1a) and PPb concentrations were elevated, coinciding with increased $^{223}Ra_{xs}$, $^{224}Ra_{xs}$ and turbidity signals (Figure 5.6 and Figure 5.7), indicating a sedimentary Pb source to overlying waters.

Benthic DPb remobilization has been reported by (Noble et al. 2015) and (Chien et al. 2017). To my knowledge, provided here is the first clear evidence of a benthic Pb source supported by

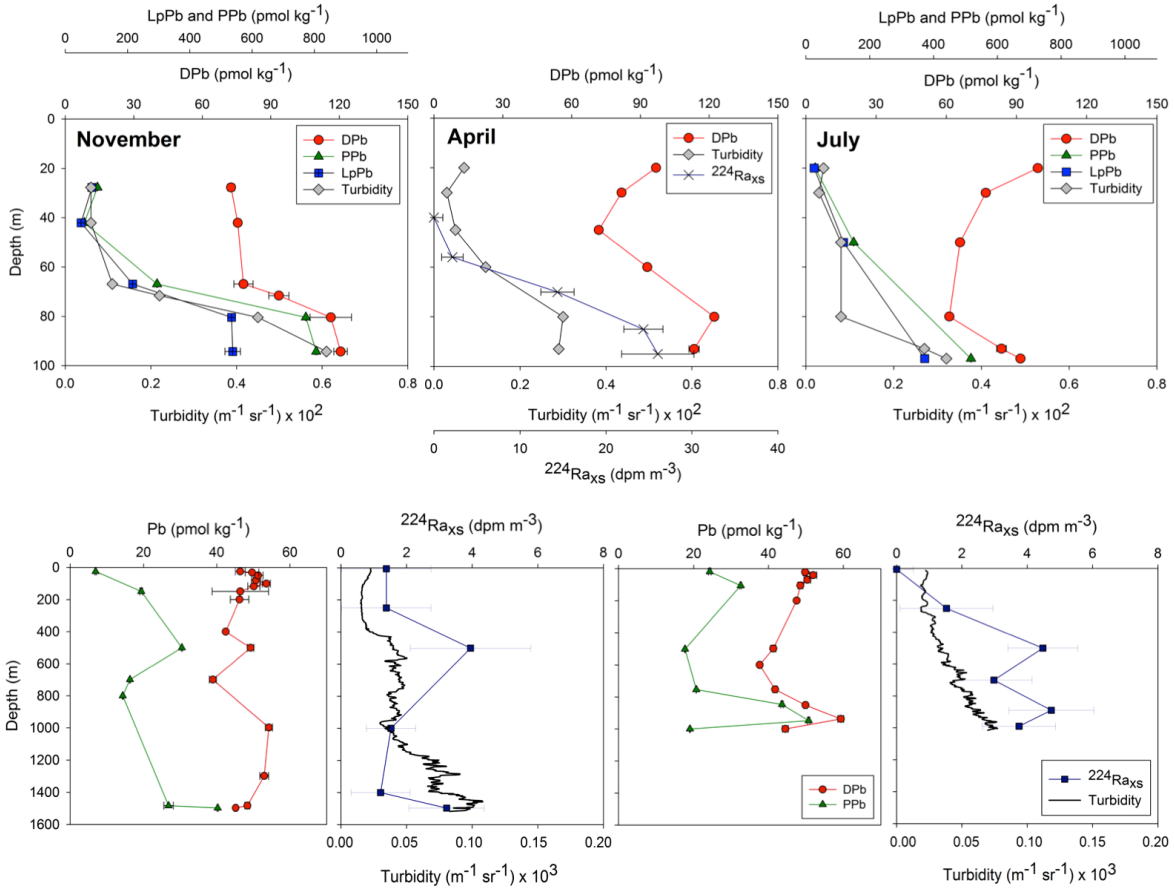


Figure 5.6. Upper panel: depth profiles of DPb (circles), PPb (triangles), LpPb (squares), turbidity (diamonds), and ^{224}Raxs (crosses) at Site A in November (DY018) (left), April (DY029) (middle), and July (DY033) (left). Bottom panel: depth profiles of DPb (circles), PPb (triangles), ^{224}Raxs (squares), and turbidity (black line) at station C03 (left) and C04 (right) in November (DY018).

PPb and Ra field measurements. Furthermore, results reported here showed a strong positive correlation between DPb and PPb (r^2 = 0.97, n = 12), and DPb and LpPb (r^2 = 0.97, n = 12) at Site A and C03/C04 stations (Figure 5.8), indicating a dynamic equilibrium between the phases. Although, little is known about biogeochemical processes facilitating DPb sedimentary release, benthic remobilization could be facilitated through Pb association with Fe/Mn oxi-hydroxide precipitates (Allen et al. 1990; Bastami et al. 2015; Fernex et al. 1992; Kalnejais et al. 2007) with subsequent reductive dissolution of the solid Fe and Mn forms in sediments (Fernex et al. 1992). This mechanism is supported by elevated DFe and DMn concentration towards the seafloor (Figure 5.9) and a build up of Fe(II) in sediments at Site A (Klar et al. 2017), but not at stations C03/C04. Potentially, DPb may be supplied in the form of small colloids deposited onto sediments (Muller 1996; Sen & Khilar 2006), with these Pb-enriched resuspended fine particles having a longer residence time in comparison to bulk sediment particles (Ferrari & Ferrario 1989; Kalnejais et al. 2007).

The vertical sedimentary Pb flux (J_z) of 27 - 41 x 10^{-9} moles Pb m^{-2} d^{-1} (n = 3) to overlying waters at Site A in April was estimated from the decreasing activity of two short-lived ^{224}Ra and ^{223}Ra

isotope (Moore 2000) and horizontal Pb concentration gradient measured at the same station below the thermocline. ^{224}Ra and ^{223}Ra are produced as a result of radioactive decay of parent isotopes accumulated in sediments due to high particle affinity. The vertical gradient of $\ln(^{224}Ra)$ was described with $\ln(^{224}Ra_{xs}) = 0.0621x - 2.2854$ ($r^2 = 0.83$) and $\ln(^{223}Ra_{xs}) = 0.0382x - 1.7799$ ($r^2 = 0.73$). The vertical flux of DPb (J_z, mol m^{-2} d^{-1}), was calculated as:

$$J_z = K_h \frac{\partial Pb}{\partial x}$$

Where K_h is the effective vertical eddy diffusion coefficient (m^2 d^{-1}; detailed in Moore (2000) multiplied by the vertical DPb concentration gradient $\left(\frac{\partial Pb}{\partial x}\right)$ (mol m^{-3}). If the exchange is dominated by eddy diffusion, an assumption which can be evaluated by the linearity of $\ln(^{224}Ra_{xs})$ versus distance, then K_z is constant and the system is under steady state:

$$m = \sqrt{\frac{\lambda}{K_h}} \quad \text{and} \quad \lambda = \frac{\ln(2)}{t_{1/2}}$$

where λ is the decay constant, $t_{1/2}$ is the half-life of ^{224}Ra (3.66 days) and ^{223}Ra (11.6 days) and the slope m.

Assumptions:

A linear relationship between the $\ln^{224}Ra_{xs}$ and $\ln^{223}Ra_{xs}$ activity with distance assumes eddy-diffusive dominated system in a steady state. However, DPb concentrations decreased towards the seafloor and there was curvature in the Ra activity away from the source, which indicate that the system was not in a steady state. Assuming that waters closest to the seafloor are influenced by different processes (eg. tides) consequently violates the assumption of eddy diffusivity in a

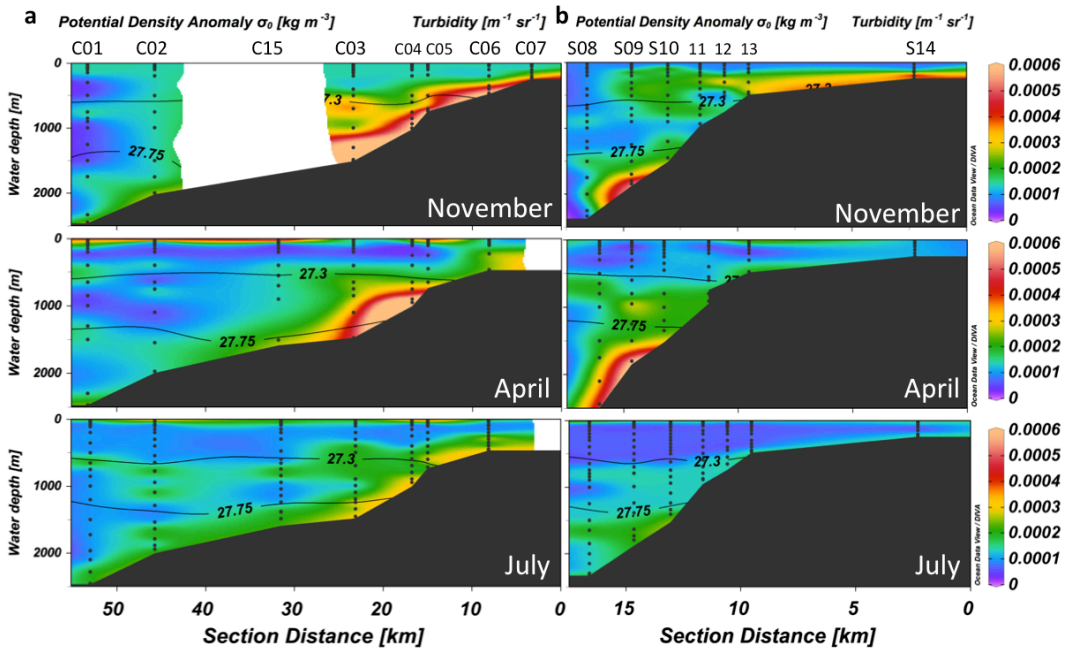


Figure 5.7 Turbidity measurement plots (a) along the canyon transects (T1_C, left), (b) along the spur transects (T2_S, right) in November (DY018) (top), April (DY029) (middle) and July (DY033) (bottom). Black lines represent MOW density range contour plots.

steady state system. Therefore fluxes were recalculated excluding the deepest data point: flux estimates with $^{224}Ra_{xs}$ increased from 34.8 nmol m^{-2} d^{-1} to 41.0 nmol m^{-2} d^{-1} ($ln(^{224}Ra_{xs}) = 0.0833x – 3.6499$ ($r^2 = 0.89$)) and with $^{223}Ra_{xs}$ decreased from 29.5 nmol m^{-2} d^{-1} to 26.9 nmol m^{-2} d^{-1} ($ln(^{223}Ra_{xs}) = 0.0582x – 3.0714$ ($r^2 = 0.91$)). Therefore, reported here is the full ranges of 34.8 – 41.0 nmol Pb m^{-2} d^{-1} and 26.9 – 29.5 nmol Pb m^{-2} d^{-1} with implementation of $^{224}Ra_{xs}$ and $^{223}Ra_{xs}$ respectively. The two short-lived isotopes of Ra are influenced by processes on different timescales (week – month) and therefore, the tidal influence on Ra distributions was likely averaged out above the deepest sample depth. This flux is based on the assumption of a single diffusive sedimentary source of DPb to water column, although other sources such as resuspended particles or influence of strong tides are also plausible. This calculation also does not take into account scavenging processes that likely occur in the water column. Therefore, estimated flux range should be taken with precaution. Nevertheless, to my knowledge, this is the first benthic Pb flux estimate from field observations. Furthermore, this sedimentary Pb flux was up to 2 orders of magnitude higher than the atmospheric flux (0.03 – 12.2 x 10^{-9} moles Pb m^{-2} d^{-1}) observed at nearby Penlee Point Atmospheric Observatory in 2015 (Figure 2.1 (Arimoto et al. 2003)). The benthic DPb flux was likely a result of accumulation in sediments of Pb deposited over time, whilst the recent relatively low atmospheric Pb flux reflects the implementation of strict European air emission regulations. Therefore sediments containing legacy Pb will continue to serve as an important, if not the major source of Pb to overlying waters

5.3.3 Recent Pb sources in the NE Atlantic shelf region

A strong spatial and temporal variability in surface water DPb concentrations were observed over the various transects across the seasons. Elevated surface DPb concentrations (36.1 – 122 pmol kg^{-1}) were observed on the continental shelf during all sampling seasons, with lower levels along off-shelf transects (Figure 5.1c). Elevated DPb concentrations observed in surface waters at Site A in April and July in comparison to November, indicated recent Pb inputs (Figure 5.3). A strong inverse correlation of DPb with salinity r = -0.96 (April, n = 6) and r = -0.94 (July, n = 4) between Site A and CS2 stations suggest a freshwater source of DPb, which could be continental run-off or wet deposition (Figure 5.10). On the continental slope, elevated DPb concentrations in the SML were observed along the canyon (T1_C) transect in November (50.8 ± 3.0 pmol kg^{-1}, n = 20) and at S08 and S09 stations on the spur (T2_S) transect. Lower DPb concentrations were observed during other seasons; 39.6 ± 6.9 pmol kg^{-1} (n = 23, T1_C) and 35.0 ± 4.2 pmol kg^{-1} (n = 30, T2_S) in April and 35.2 ± 3.8 pmol kg^{-1} (n = 9, T1_C) and 37.4 ± 4.9 pmol kg^{-1} (n = 6, T2_S) in July (Figure 5.1a-b). The distinctive changes in DPb over short spatial scale observed between closely spaced stations (<20 km), suggest presence of different water masses with different DPb

input histories over the last months to years. These observations coincided with distinct temperature and DMn concentration differences (Figure 5.11)), that enforce this suggestion.

5.4 Conclusions

Observations reported here demonstrate the widespread impact of anthropogenic Pb emissions on the marine environment. The elevated Pb signal (46.6 ± 5.6 pmol kg^{-1}) in MOW is transported long distances (> 2500 km) at intermediate depths across the Northeast Atlantic following anthropogenic Pb emissions during the past century. Following implementation of stricter environmental regulations in Europe, this oceanic Pb signal will behave similarly to chlorofluorocarbons (CFCs) in that it is predicted to decrease with time. However, considering the residence time of Pb in the deep ocean of ~100 years (Nozaki & Tsunogai 1976), the presence of recent Pb sources (> 90 pmol kg^{-1} in surface waters) and the 're-supply' of Pb to the water column from sediments containing legacy Pb (27 - 41 x 10^{-9} moles Pb m^{-2} d^{-1}), the anthropogenic Pb signal is excepted to remain in the marine environment for decades to come. The role of the particulate

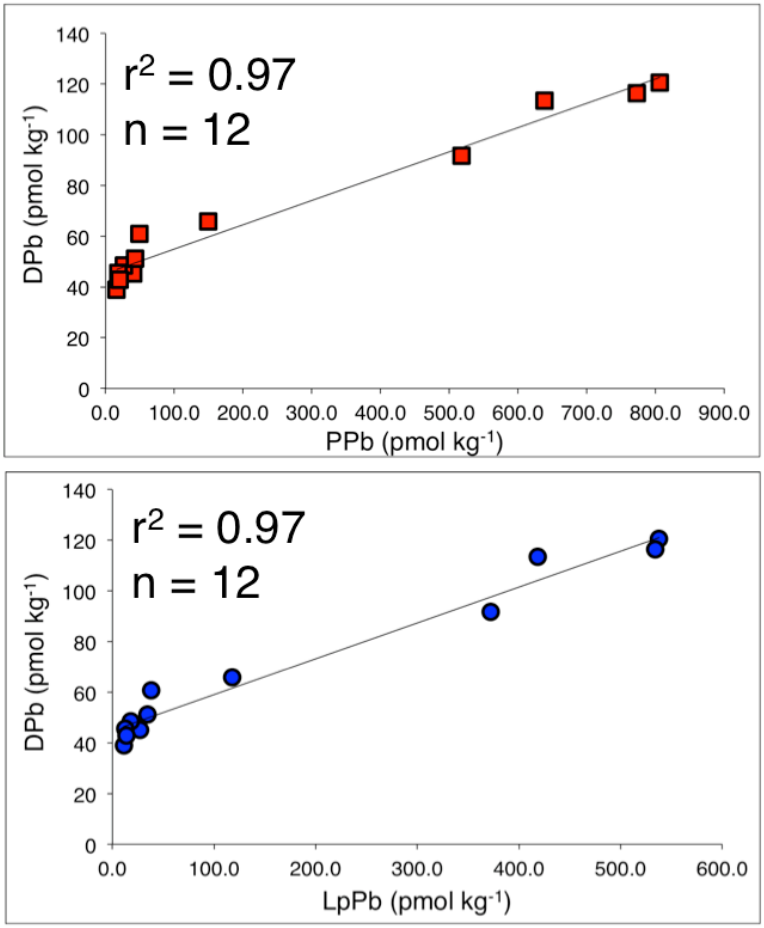


Figure 5.8 Linear correlations between DPb and PPb (top), DPb and LpPb (bottom) at C03:C04 stations in November (> 700 m depth) and Site A in all seasons (below the seasonal thermocline).

phase in buffering Pb concentrations in the water column needs to be considered in the interpretation of oceanic DPb distributions due to a close relationship between the dissolved and particulate phases.

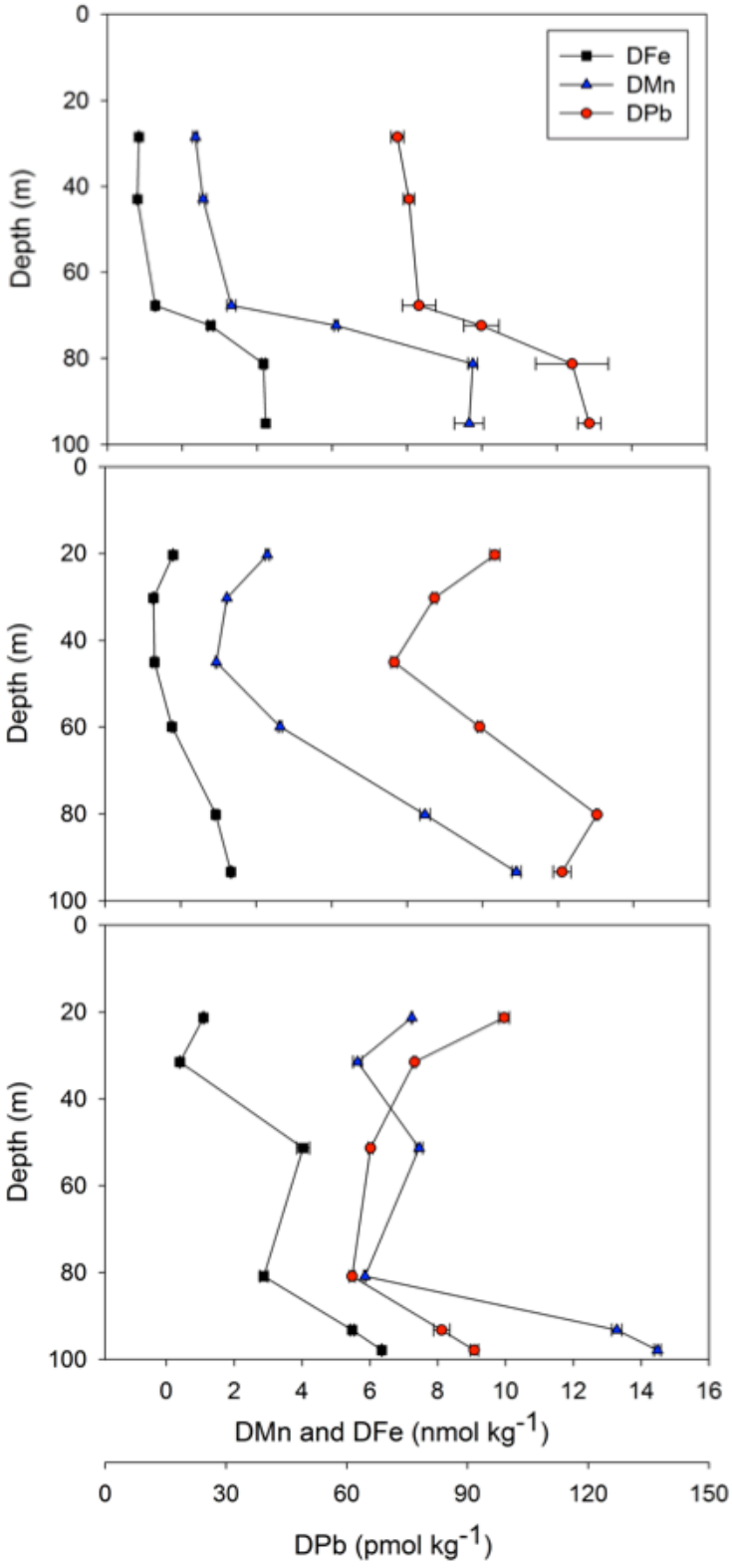


Figure 5.9 Depth profiles of DPb (red circles), DFe (black squares), DMn (blue triangles) at Site A in November (DY018) (top), April (DY029) (middle) and July (DY033) (bottom).

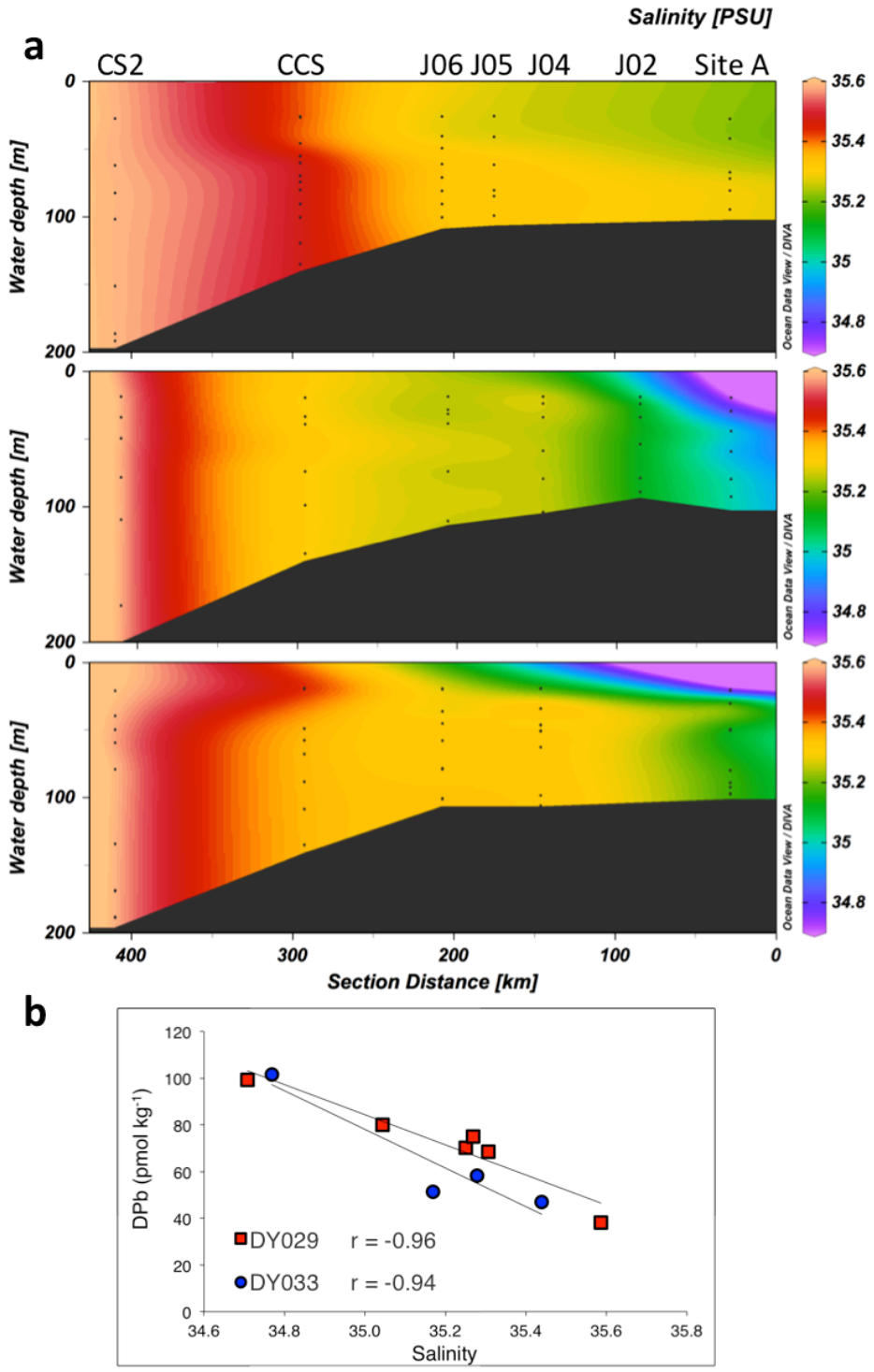


Figure 5.10 (a) The distribution of salinity along the on-shelf transect in November (DY018, top), April (DY029, middle) and July (DY033, bottom). (b) Relationship between DPb and salinity across on-shelf stations at 20 m depth in April (red squares) and July (blue circles).

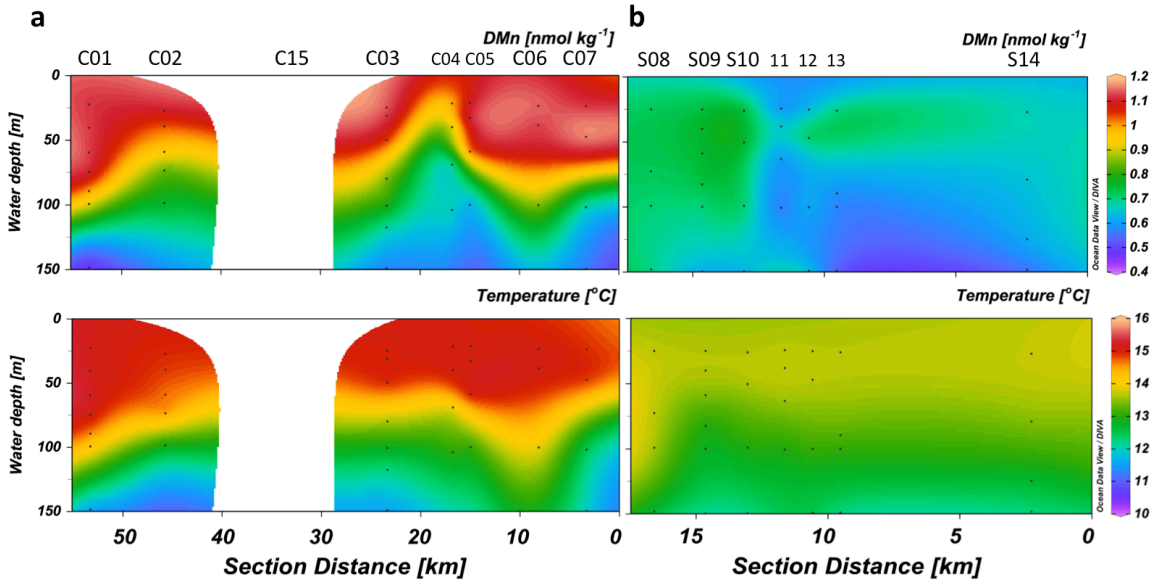


Figure 5.11 DMn concentrations (top) and temperature measurements (bottom) along (a) the canyon transects (T1_C) and (b) along the spur transects (T2_S, right) in November (DY018).

Chapter 6 Conclusions

All marine organisms require trace metals (TMs) for metabolic processes such as uptake and assimilation of inorganic carbon and urea (Morel et al. 2003). The extensive efforts of the international GEOTRACES Programme have improved our understanding of the sources, sinks and biogeochemical cycling of TMs in major oceanic basins, yet process studies in highly productive and dynamic shelf systems still remain scarce. This PhD project contributes to the GEOTRACES Programme as a process study that focused on the seasonal cycling and transport of TMs in the North-West European shelf seas as part of the Shelf Sea Biogeochemistry (SSB) Programme. Considering that shelf sea studies are rare, in particular seasonal investigations, the framework of the SSB Programme is thus unique. Research in this PhD project has not only contributed to our knowledge of the dynamics of several TMs in this region and wider North East Atlantic basin, highlighted the importance of distinct biogeochemical coastal processes but also added to the growing evidence of the impact of stricter environmental regulations on the ocean. This work has been based on three hypotheses described in chapter 1, which are revisited below.

6.1 Hypothesis 1 revisited:

'Off-shelf vertical distributions of DCd, DZn, DNi and DCu in the Celtic Sea strongly correlate with macronutrients over all seasons due to biological uptake and remineralization processes. In shelf waters, DTM distributions de-couple from macronutrients due to multiple TM sources, and modifications in the coastal zone of oceanic and fresh waters.'

Biogeochemical processes of TMs in the dynamic and highly productive shelf seas have the potential to influence open ocean TMs distributions, but comprehensive TM studies in coastal waters are scarce. The international GEOTRACES Programme has provided a large amount of high quality TM data for the major oceanic basins. However, majority of the results to date are generally limited to the open ocean full depth profiles, with a lack of shelf data. Vertical distributions of DCd, DZn, DNi and DCu in off shelf waters of the Celtic Sea exhibited nutrient-like profiles and correlated well with macronutrients and thus confirmed hypothesis 1. Surprisingly, the non bioessential element DAl, also exhibited a nutrient-like depth profile in the upper waters and correlated well with phosphate and silicic acid, suggesting a preferential scavenging onto biogenic particles. A significant seasonal variation of TM concentrations was observed in surface waters, likely a result of biological drawdown and winter mixing processes and yielded diverse 'seasonal' elemental ratios (relative to phosphate). This is the first direct evidence of variable

elemental ratios that yielded a stoichiometry that was in agreement with observations in the North Atlantic and phytoplankton culture studies. Although findings from the Celtic Sea indicate the potential of metal specific biogeochemical processes, this aspect requires further investigation.

On the Celtic Sea continental shelf, the ratios of DCd:P and DZn:P varied spatially and seasonally, which highlighted the distinct and dynamic character of biogeochemical processes with specific DTM sources (benthic and or atmospheric), coastal water mass mixing and biological drawdown that influenced DTM distributions throughout the year.

Findings described in this PhD thesis, along with recent reports of potential phytoplankton growth limitation by DFe in the study region (Birchill et al. 2017) stress the need to better constrain the role of continental shelves in TMs dynamics and their potential exchange with the open ocean for global TMs budgets. In order to expand our knowledge, more emphasis should be placed on comprehensive shelf sea studies, which should include geochemical aspects and also associations with physical and biological studies.

6.2 Hypothesis 2 revisited:

'Shelf sediments supply DMn and DCo to overlying waters. Off-shelf transport of DMn and DCo within nepheloid layers is a persistent feature at the continental margin.'

The supply of DMn and DCo from margin sediments is recognised as an important source to the open ocean (Laës et al. 2007; Noble et al. 2017; van der Zee et al. 2001). The results of repeated shelf break transect sampling revealed elevated concentrations of DMn and DCo within intermediate nepheloid layers (INLs) during all sampling seasons over the Celtic Sea slope. Thus, forming a persistent conduit for DMn and DCo transport to the adjacent North Atlantic Ocean, confirming hypothesis 2. If TMs remobilised from the slope sediments are transported off-shelf within shallow INLs, there is a potential they can be mixed to surface waters through vertical mixing processes eg. winter mixing, internal tides or upwelling and thus serve as an additional TM source to surface waters. Nepheloid layers are formed through strong current interactions with complex, steep topographies of the shelf break and are widely observed in the submarine canyons. Globally there are >9000 submarine canyons along the continental margins comprising of 11.2% (460 km^2) of the total continental slope area (Harris et al. 2014), thus transport of DMn and DCo to the open ocean within INLs is potentially a widespread phenomenon. If the supply of DTMs to surface waters through INLs is plausible, and considering that submarine canyons enhance the formation of INLs, this supply mechanism may be important in micronutrient depleted waters of the Arctic and Southern Oceans where the highest number of submarine

canyons has been reported (Harris et al. 2014). Therefore, potentially elevated sediment transport within INLs may serve as an additional DTMs source to surface waters in these regions.

Beside natural sediment resuspension processes, commercial bottom trawling activities have an important anthropogenic impact on sediment resuspension and its transport (Martín et al. 2014) leading to enhanced NLs (ENLs). Anthropogenically induced NLs convey higher concentrations of suspended particulate matter (SPM) (Wilson 2016) and thus may potentially supply higher concentrations of DTMs relative to natural INLs. Although the distinction between the natural INLs and anthropogenic ENLs is difficult to make, this aspect and its environmental consequences have not been studied and require direct observations. Furthermore, considering some TMs (eg. DAl, DMn, DCo, DPb) that are susceptible to particle scavenging, a higher particle load may also act as a more efficient sink for TMs present suggesting a diverse role of NLs on TMs distributions in seawater. A comprehensive knowledge of TM transport within NLs in continental margins and mechanisms of their transport are critical to further asses the role of NLs on TMs distributions in these regions.

6.3 Hypothesis 3 revisited:

'DPb concentrations in surface waters have decreased since the last reports (1995) due to the phasing out of leaded fuel in Europe (between 1980 and 2011) and implementation of strict environmental regulations'

There has been growing evidence of reductions in Pb surface waters concentrations in the North Atlantic as a consequence of implementation of stricter environmental regulations leading to natural Pb signatures re-emerging in the North Atlantic waters (Bridgestock et al. 2016). The last Pb study in the Celtic Sea was conducted in 1995 that reported DPb concentrations of up to ~ 200 pmol kg^{-1} in surface waters (Cotté-Krief et al. 2002) at the beginning of the phase-out process of leaded fuel in Europe (1980 - 2010). Results presented in this thesis (Chapter 5) indicate at least a 4-fold decrease in DPb concentrations to 40.2 ± 7.5 pmol kg^{-1} (n = 109) in 2014 and 2015 in the Celtic Sea region. This result confirmed hypothesis 3 and further added to the growing evidence of the impact of strict regulations on the environment. Nevertheless, the presence of recent DPb sources to surface waters in the study region was also observed, which was not surprising. Along with a 63% decline in overall atmospheric Pb inputs largely due to the phasing out of leaded fuel, a 130% rise in the commercial and household emissions (2000 – 2015) has been reported within European Union (EU) and Economic European Area (EEA) countries (European Environment Agency 2017). Consequently, DPb concentrations in surface waters and atmospheric Pb emissions have declined over the last three decades in the North Atlantic, yet the evidence of continuous

marine pollution in all major oceanic basins stresses the importance of continuing global efforts to minimize anthropogenic Pb inputs to the environment, in particular in Asia.

Evidence for historic anthropogenic Pb emissions was observed at intermediate depths in the study region. The elevated signal (46.6 ± 5.6 pmol kg^{-1}) was associated with historical pollution of surface waters of the Mediterranean Sea, with subducted deep waters transported long distances (> 2500 km) across the North Atlantic basin at ~1000 m depth. The Mediterranean Sea contains a strong legacy of historical Pb emissions and is still subject to continuous emissions from regions in Europe, Middle East and Africa where environmental regulations are not as strict, in particular in Algeria and in Iraq, where Pb leaded fuel is still in use (as of March 2017, UNEP). Therefore, the Mediterranean Sea will continuously serve as a reservoir of anthropogenic Pb, and consequently as a source of Pb to the Celtic Sea region and entire North East Atlantic basin for decades to come.

Whilst the atmosphere has been recognised as a major input of Pb to the water column, sediments were assumed to be only a sink for Pb (and other contaminants eg. Cu, Zn) due to water column scavenging and subsequent particle sinking. A lack of direct Pb benthic release data has made it hard to assess the validity of this assumption. However, clear benthic DPb signals in the Celtic Sea region were observed. Sedimentary release of DPb was likely a result of continuous Pb supply to the sediments over decades of anthropogenic pollution, with eventual return of the Pb to the water column. Only recently sediments have been proposed as a potential DPb source (Noble et al. 2015; Chien et al. 2017) that in fact formed 49% of Pb inputs to deep Pacific Ocean (Chien et al. 2017) and even exceeded the atmospheric Pb inputs in the Celtic Sea (Chapter 5 and (Rusiecka et al. 2018)). This novel finding raises a few questions concerning Pb cycling in the global ocean and more importantly, its future conditions. Given that anthropogenic Pb contamination dates back to at least the 19th century, why is Pb sedimentary input a recent observation? Potentially, these sediments have reached an 'adsorption saturation point' or only now with declined ambient seawater Pb levels that the concentration gradient is clearly evident. Moreover, given that the global ocean has already received large amount of historical Pb and that Pb inputs will continue to pollute marine environment, the build up of Pb in sediments is expected to increase. Therefore, novel evidence of benthic inputs in the Celtic Sea suggests that modern sediments have turned from a DPb sink to a contemporary DPb source to overlying waters. However, the understanding of the exact processes that facilitate benthic release requires further investigation as benthic fluxes of Pb (and other contaminants eg. Cu and Zn) have been suggested to increase in light of progressive ocean acidification (Martín-Torre et al. 2015; Rodríguez-Romero et al. 2014; Roberts et al. 2013). This finding is particularly important to coastal waters that not only are subject to enhanced anthropogenic pollution but also serve an important role to society in the form of ecosystem services. Anthropogenic Pb inputs to the atmosphere have been reduced through the control of environmental regulations as evident in the 63% reduction in Pb emissions. However, the potential sedimentary Pb release to overlying will be out of our control.

Therefore, it is of critical importance to gain the comprehensive knowledge about the mechanisms of the sedimentary inputs of Pb in order to asses the potential of future benthic inputs to the water column, their magnitude and ecological consequences.

6.4 Future work

Future work related to this PhD project

The studies presented in this PhD thesis combined geochemical measurements of eight different TMs, macronutrients and two short-lived Ra isotopes. Further interpretation of these measurements will be undertaken through connection with physical and biological studies. The interpretations of the seasonally and spatially variable ratios of DCd:P and DZn:P on the continental shelf of the Celtic Sea was based on mainly chemical measurements. Further investigation of potential links of the community structure from Flow Cytometry measurements and microscopic cell counts and physical processes may provide insights into the complex TM-biological relationship in coastal waters.

Intermediate NLs represent a persistent conduit for the supply of DMn and DCo to the ocean interior. However, a key piece of information missing at this point is the rate of the off-shelf DTMs transport. Short-lived Ra isotope measurements can provide estimates of the DTM fluxes and these calculations are currently underway. Additionally, findings in this thesis should be closely linked with the physical data from e.g. Acoustic Doppler Current Profiler (ADCP), gliders and long-term moorings that were collected as part of the SSB Programme. These measurements will supplement the geochemical findings with physical processes occurring in the study region.

Sedimentary inputs of Pb to overlying waters have been reported, which may serve as a contemporary Pb source to marine environment. In order to asses the importance of this source in a future ocean, the exact mechanisms of the benthic release should be further examined and the release and transport of Pb should be investigated using model studies.

In future sample collection in the Celtic Sea continental margin region, waters > 2500 m depth should be included. This approach would enable investigation of Cd:P > 1.3 μmol kg^{-1} PO_4^{3-} relationship (Chapter 3). Additionally sampling plan including waters > 2500 m depth would extend the transect section distance and thus potentially enable the full estimation of the DMn and DCo off-shelf transport.

Future work should also include MoO^+ correction of Cd results in particular at low (< 50 pmol kg^{-1}) concentrations (Chapter 2). The method for corrections of Cd results work was developed at the end of this PhD project and was published in Rapp et al (2017).

Recommendations for the future

Shelf seas contribute to 16% of global oceanic primary production, > 40% of the total annual particulate organic carbon export and serve as an important TM source to the open ocean, yet due to pronounced chronic land based pollution these regions are the most threatened marine ecosystems. Considering expansion of the global population and rapidly growing technological TM requirement of our society, studies in these regions should be of high importance. Given that rivers form an important land-derived source of DTMs to coastal environments, future studies should focus on constraining fluvial DTM fluxes and their fate in proximity to the largest rivers such as eg. Amazon, Congo, Yangtze rivers. Scientific focus should be placed on the biogeochemical cycling of TMs and also anthropogenic pollution assessment and its monitoring. One of the recent GEOTRACES cruise (M121, GA08 section, December 2015) focused on the Congo and Orange rivers in the South Atlantic region, and a forthcoming GEOTRACES process study (M147, GApr11, April – May 2018) will focus on the Amazon estuary and associated fluvial plume. However, to best of my knowledge, there are no plans to study other large rivers such as Yangtze and Yellow rivers in the China Sea or Mississippi river in the Gulf of Mexico. Considering the tremendous industrial growth in Asia, in particular in China, and the Deepwater Horizon accident in the Gulf of Mexico, these coastal regions should receive more scientific focus in future studies.

Shelf sediments have only recently been recognised as an important source of DTMs. In this thesis the sedimentary inputs of TMs to the overlying waters were one of the major controls of bioessential DTM and contaminant distributions. Thus, stronger emphasis should be put on the benthic metal supply from shelf sediments and mechanisms of their potential off-shelf transport to the open ocean. Furthermore, variable elemental stoichiometries of DTMs relative to macronutrients were observed in the continental shelf waters and in off-shelf surface waters over different seasons and highlight the importance of detailed seasonal studies and also the power of multi-elemental dataset for the interpretation of biogeochemical processes. In order to gain insights into specific biogeochemical processes influencing distributions of DTMs in marine environment, DTMs datasets should be treated as whole, not as individual entities as is done in many GEOTRACES publications. Also, a new look at the control of metals other than Fe on productivity and community structure in coastal systems should also receive more scientific attention.

Appendix A Other methods

The responsible researchers that shared their data are acknowledged here and in respective sections.

- Particulate trace metals concentrations: Angie Milne, Plymouth University
- Dissolved Fe concentrations: Antony Birchill, Plymouth University
- Aerosol trace metal concentrations and atmospheric flux calculations: Sov Atkinson, Plymouth University
- Radium isotopes (^{223}Ra, ^{224}Ra) activity: Amber Annett, University of Edinburgh
- Extended Optimum Multiparameter analysis: Johannes Karstensen, GEOMAR
- Mediterranean Water Outflow propagation time: Toste Tanhua, GEOMAR
- Macronutrients concentrations: Malcolm Woodward and Carolyn Harris, Plymouth Marine Laboratory

A.1 Other analytical methods

A.1.1 Dissolved iron

Antony Birchill, Plymouth University

Full method details are available in Birchill et al (2017). Briefly, Dissolved iron (Fe) (0.2 µm filtered), were collected in separate LDPE bottle at the same time as samples other trace metals (TMs) described in this thesis. Dissolved Fe samples were acidified to 0.024 M HCl with high purity HCl (UpA, Romil) under a class 100 flow hood and analysed using flow injection with chemiluminesence detection (Obata et al. 1993), after spiking with hydrogen peroxide. The accuracy of the method was validated with the analysis of SAFe GEOTRACES seawater reference materials. The concentrations of dFe determined was 0.12 ± 0.013 nM (n=4) for SAFe S, 0.96 ± 0.100 nM (n=14) for SAFe D2, 0.15 ± 0.024 nM (n=15) for GEOTRACES Pacific (GSP), 1.51 ± 0.076 nM (n=14) for GEOTRACES Coastal (GSC). These values are in agreement with published values (S=0.10 ± 0.008 nM, D2= 0.96 ± 0.024 nM).

A.1.2 Particulate and leachable trace metals analysis

Angie Milne, Plymouth University

To assess the labile and total metal fraction of the particulate material, filters were processed following a sequential leach-digestion procedure as detailed in (Milne et al. 2017). Filter blanks were processed in the same manner as samples. All acids and bases used were of ultra-pure grade (Romil, UpA) while the H_2O_2 was supplied by Merck (Optima grade). For the labile-metal fraction a leaching protocol similar to that described in (Berger et al. 2008) was adopted and represented potentially bioavailable, easily exchangeable fraction. Filters were leached with 2 mL of 25 % acetic acid and hydroxylamine hydrochloride (0.02 M, Romil) solution and heated in a drying oven for 30 min at 90 °C in LDPE vials. After a 2 h contact time, the filters were removed and placed into clean PFA screw cap digestion vials (Savillex). The leachate solution was then centrifuged at 3500 g for 15 min. Following centrifugation, 1 mL of the leachate was transferred to a separate PFA vial and taken down to dryness, the residue was quantitatively diluted in 2 % HNO_3 for analysis. The remaining leachate solution was disposed after centrifugation. Each vial was rinsed with H_2O_2 and added to the digestion PFA vial containing the relevant sample filter. A three step sequential acid addition modified from (Ohnemus et al. 2014) was employed to fully digest the 25 mm Supor® polyethersulfone (PES) membrane disc filters (Pall, 0.45 µm) and any refractory particulate material. In loosely capped vials, 0.2 mL of H_2SO_4 plus 1.0 mL H_2O_2 were heated at

200 °C until the PES filter dissolved. Secondly, a 4 M mix of HF/HCl/HNO_3 (2 mL) was added and heated overnight at 135 °C in tightly capped vials. Finally, 1 mL of a HNO_3/H_2O_2 mix (50%/15% v/v) was heated at 130 ºC for ~ 1 hr. After each stage the sample was heated to dryness. After the final evaporation stage, the samples were quantitatively diluted in 2 % HNO_3. All particulate samples were analysed using inductively coupled plasma-mass spectrometry (ICP-MS; Thermo Fisher X Series 2). Potential interferences (e.g. $^{40}Ar^{16}O$ on ^{56}Fe) were minimized through the use of a collision/reaction cell utilizing 7% H in He.

A.1.3 Trace metal aerosol sample collection, digestion and analysis

Sov Atkinson, Plymouth University

Sample collection

Prior to sampling, all filter membranes were acid-washed using an adapted method from (Morton et al. 2013). The filter membranes were loaded onto the 47 mm Savillex filter holder (QMX Laboratories, UK), using acid cleaned plastic tweezers, with the operator wearing a clean pair of disposable polythene gloves, in a Class-5 laminar flow hood cabinet where they were left to dry. The filter holder was then assembled and stored in a double sealed bag for transport to the sampling site. At Penlee Point Atmospheric Observatory (PPAO) (Figure 1.1), each filter holder was housed in a separate weather shield (with an opening at the bottom) to prevent precipitation from contaminating dry aerosol deposition. The sample (and the sample shield) was attached to the pump via a 9 m re-enforced PVC braided tubing, 10mm ID and 3mm thickness (Fisher, UK). A gas meter (G4, Havelock, UK) was attached to each sample tubing to record the air flow over the filter for the duration of the sampling period. The pump (GAST Rotary vain, CJS Direct, UK) is turned on for 24 hours for a sampling period, with an average flow rate of 91 L min^{-1}, and this is repeated weekly. After the sampling period, the filter holders and loaded filters were removed and brought back to the lab for processing. In a Class 5 laminar flow cabinet, the loaded filter sample was removed from the filter holder using an acid-washed plastic tweezers, placed in acid-cleaned petri dishes inside sealed bags and stored in the freezer (-20 °C) until analysis.

Sample digestion and analysis

In order to determine the total trace metal concentrations, aerosol samples and blanks were completely digested using concentrated hydrofluoric acid (HF) (28.9 M) (Romil, UPA, Ultra Purity Acid grade) and concentrated HNO_3 (15.8 M) (Romil, UPA, Ultra Purity Acid grade). The procedure was adapted from Morton et al. (2013) and as follows:

Step 1: 0.50 mL of concentrated HNO_3 (Romil, UPA, Ultra Purity Acid grade) was added to a 15 mL Teflon, flat bottom/round interior vial (Savillex) and heated to 140°C overnight. Once cooled,

the vials were uncapped and heated to 140°C until the solution was near dryness and formed a bead.

Step 2: 1 mL of the digestion mixture (5:1 of concentrated HNO_3: concentrated HF (Romil, UPA, Ultra Purity Acid grade)) was added to the digestion vial and heated to 140°C overnight. Once cooled, the vials were uncapped and heated to 140°C until the solution was near dryness and formed a bead.

Step 3: 0.50 mL of concentrated HNO_3 was added to the digestion vial and heated to 130°C overnight. Once cooled, the vials were uncapped and heated to 130°C until the solution was near dryness and formed a bead.

Each aerosol filter sample was used as whole, folded using an acid-washed plastic tweezers and placed into a 15 mL Teflon, flat bottom vial (Savillex). The first step involved an addition of 0.5 mL of concentrated HNO_3 and heating to 140°C on a hotplate overnight. Once cooled, the vial was left uncapped and the acid was heated to 140°C on the hotplate until most of the acid was evaporated and left a bead of solution. The digest was further repeated using 1mL of 5:1 mixture of concentrated HNO_3 and concentrated HF, followed by 0.5 mL of concentrated HNO_3. Once the 3 steps were completed, the digest was made up to 20 mL of 2% v/v solution of HNO_3 (Romil, UPA) and analysed on a ICP-MS (Thermo Fisher).

Atmospheric flux calculations

Penlee Point Atmospheric Observatory (PPAO) sampling site was established by the Plymouth Marine Laboratory in May 2014 for long term observations of ocean-atmosphere interaction and is situated at 50° 19.08’ N, 4° 11.35’ W (Figure 2.1), Plymouth Sound.

Total daily atmospheric fluxes of Pb to the Coastal Plymouth Sounds via dry deposition were estimated by multiplying the concentration of these trace metals in sampled air by a deposition velocity of 0.01 ms^{-1} for particles > 1µm associated with seas salt (Arimoto et al. 2003):

$$\text{Total daily flux} = \frac{\text{Concentration of Pb } (\text{nmolm}^{-3})}{\text{Deposition velocity } (\text{ms}^{-1})} \qquad \text{eg. 11}$$

The PPAO site station was chosen as a result of its close proximity to our sampling site and overlapping sampling time with the Shelf Sea Biogeochemistry Programme expeditions (March 2015).

A.1.4 Radium isotopes sampling and analysis

Amber Annett, University of Edinburgh

Large volume samples for radium (Ra) analysis were collected from the Niskin bottles deployed on a stainless steel CTD frame. Water from multiple bottles closed at the same depth was transferred into acid-washed 20 L collapsible containers, and slowly (<750 mL min^{-1}) passed through a column filled with 20 g of MnO_2-impregnated acrylic fiber. This approach has been shown to quantitatively extract Ra from up to 1000 L of seawater (Moore 2008). Fibers were rinsed with deionised water to remove salts, and partially dried to optimize emanation of the radon daughter (Sun & Torgersen 1998). Samples were counted immediately on-board ship using a Radium Delayed Coincidence Counter [RaDeCC; (Moore 2008), which discriminates between the radon daughters of different short-lived Ra isotopes based on the time between subsequent decay events. Counting was repeated after an interval of ~30 (~90) days to determine the ^{224}Ra (^{223}Ra) activity supported by the parent isotopes ^{228}Th (^{227}Ac) which are also retained on the fiber. Uncertainty calculations follow the methods of Garcia-Solsona et al. (2008), and efficiencies of the RaDeCC systems were calibrated and monitored using standards prepared from actinium-227 and thorium-232 (Annett et al. 2013). Ra activities used here ($^{224}Ra_{xs}$ and $^{223}Ra_{xs}$) are in excess of activity supported by the parent isotopes in the water column.

A.1.5 Extended Optimum Multiparameter (extOMP) analysis

Johannes Karstensen, GEOMAR

Water mass fractions and the amount of remineralized nutrients/respired oxygen (in one single bulk number) were calculated using the extOMP analysis (Karstensen & Tomczak 1998; Hupe & Karstensen 2000). The method was used for all observational data points where multiple parameters were available (temperature, salinity, oxygen, nitrate, phosphate, silicate). In brief, the method is based on a non-negative least square fit of fractions of source water types using all parameters (Table 8) but with linear corrections on parameters that are also impacted by biogeochemical cycling (oxygen, nitrate, phosphate, silicate) based on a defined stoichiometric ratio (Table 8). A weighting is applied to control the impact of a parameter on the solution (Table 8) based on their variability in respective source regions, depending primarily on environmental variability and to a lesser degree also on instrumental/measurement errors.

Source water types identified by OMPext were: Eastern North Atlantic Central Water (ENACW; a water mass that is created by subduction in the North Atlantic subtropical gyre), Subarctic Intermediate Water (SAIW; lightest part of the subpolar Modewater formation process and formed in the eastern subpolar gyre), Mediterranean Outflow Water (MOW; water mass defined

close to the Gulf of Cadiz), Labrador Sea Water (LSW; of western subpolar gyre origin), and Northeast Atlantic Deep Water (NEADW; a water mass that is created by mixing of various sources of subpolar Mode waters and Iceland Scotland Overflow Water). The characteristics of the source water masses were obtained from literature values (García-Ibáñez et al. 2015) except for MOW and NEADW, which were taken from observational data that has been compiled from the GLODAPv2 data set (Olsen et al. 2016). The final configuration used for the results presented here is given in Table 8. It can be considered a weakness of any water mass analysis (incl. extOMP analysis) that fractions in absolute numbers are sensitive to changes in source water definitions. This is because moving points in parameter space will change distances. However, here interest is on the vertical "layering" of the water masses and the selected parameters were robust for the different configurations tested (varying source water definitions, weights, stoichiometry).

Table 8 Configuration of the input for the extOMP analysis. Source water definitions for the respective parameters were taken from (García-Ibáñez et al. 2015) except were noted - ENACW: Eastern North Atlantic Central Water; MOW: Mediterranean Outflow Water (GLODAPv2); SAIW: Subarctic Intermediate Water; LSW: Labrador Sea Water; NEADW: Northeast Atlantic Deep Water (GLODAPv2). Last rows give the parameter weighting and the stoichiometrical ratio.

Source water types	Potential temperature (°C)	Salinity PSS-78	Oxygen µmol kg^{-1}	Phosphate µmol kg^{-1}	Nitrate µmol kg^{-1}	Silicate µmol kg^{-1}
ENACW	16.0	36.20	241	0.10	0.1	0.85
MOW	10.5	36.30	173	1.20	17.5	9.0
SAIW	6.0	34.70	287	0.86	13.0	6.3
LSW	3.0	34.87	287	1.05	16.5	10.0
NEADW	2.1	34.90	240	1.65	22.5	45.0
Parameter weighting	100%	100%	30%	30%	30%	10%
Stoichiometry ratio	0	0	-170	1	16	40

A.1.6 The propagation time of Mediterranean Outflow Water

Toste Tanhua, GEOMAR

The propagation time of MOW from the Gulf of Cadiz was calculated by comparing ages as calculated from CFC-12 data available in the GLODAPv2 data product (Olsen et al. 2016) from these two areas. The data in GLODAPv2 comes from several different cruises during different years. To compensate for the transient signal of CFC-12 the mode-age of the samples was calculated from the CFC-12 data assuming no change in ocean ventilation. For these calculations we use the transit time distribution (TTD) concept (e.g. (Waugh et al. 2003)) using the common assumption of an Inverse Gaussian shape of the TTD where the two moments Γ (mean-age) and Δ

(width) are equal (the ratio of Δ/Γ giving information on the degree of diffusion vs. advection). For the so calculated TTDs we then calculate the "mode-age", i.e. the age of the peak of the TTD. The change in this variable along a flow path of a water mass is a useful approximation of the propagation time of a signal such as the one that we are investigating in this paper.

A.1.7 Macronutrients

Malcolm Woodward and Carolyn Harris, Plymouth Marine Laboratory

Unfiltered seawater samples for nutrients were taken from the same OTE bottles as TM samples, were stored in 'aged' 10% HCl acid washed and deionised water rinsed HDPE bottles. Nutrient bottles were rinsed three times with seawater sample prior to the final filling. Seawater sampling and handling for macronutrient analysis was carried out according to the International GO-SHIP nutrient manual recommendations (Hydes et al. 2010). Nutrient analysis was carried out on board within few hours of sampling using techniques described in Woodward and Rees (2001).

Appendix B Anthropogenic Signature of Lead in the Northeast Atlantic: original manuscript

AGU PUBLICATIONS

Geophysical Research Letters

RESEARCH LETTER
10.1002/2017GL076825

Key Points:
- Recent sources of Pb were evident despite a fourfold reduction of Pb in NE Atlantic surface waters since leaded gasoline prohibition
- Enhanced Pb was evident in Mediterranean Outflow Waters, transported >2,500 km across the NE Atlantic
- Sediments represented an important source of Pb to overlying waters, exceeding the atmospheric flux of Pb

Supporting Information:
- Supporting Information S1

Correspondence to:
D. Rusiecka and E. P. Achterberg,
drusiecka@gmail.com;
eachterberg@geomar.de

Citation:
Rusiecka, D., Gledhill, M., Milne, A., Achterberg, E. P., Annett, A. L., Atkinson, S., et al. (2018). Anthropogenic signatures of lead in the Northeast Atlantic. *Geophysical Research Letters*, *45*. https://doi.org/10.1002/2017GL076825

Received 15 DEC 2017
Accepted 27 FEB 2018
Accepted article online 5 MAR 2018

©2018. The Authors.
This is an open access article under the terms of the Creative Commons Attribution License, which permits use, distribution and reproduction in any medium, provided the original work is properly cited.

Anthropogenic Signatures of Lead in the Northeast Atlantic

D. Rusiecka[1,2], M. Gledhill[1,2], A. Milne[3], E. P. Achterberg[1,2], A. L. Annett[4], S. Atkinson[3], A. Birchill[3], J. Karstensen[2], M. Lohan[1,3], C. Mariez[5], R. Middag[6], J. M. Rolison[7], T. Tanhua[2], S. Ussher[3], and D. Connelly[8]

[1]Ocean and Earth Sciences, National Oceanography Centre, University of Southampton, Southampton, UK, [2]GEOMAR Helmholtz Centre for Ocean Research Kiel, Kiel, Germany, [3]School of Geography, Earth and Environmental Sciences, University of Plymouth, Plymouth, UK, [4]School of Geosciences, University of Edinburgh, Edinburgh, UK, [5]Université de Bretagne Occidentale, Brest, France, [6]Department of Ocean Systems, NIOZ Royal Netherlands Institute for Sea Research, Texel, Netherlands, [7]Nuclear and Chemical Sciences Division, Lawrence Livermore National Laboratory, Livermore, CA, USA, [8]National Oceanography Centre Southampton, European Way, Southampton, UK

Abstract Anthropogenic activities have resulted in enhanced lead (Pb) emissions to the environment over the past century, mainly through the combustion of leaded gasoline. Here we present the first combined dissolved (DPb), labile (LpPb), and particulate (PPb) Pb data set from the Northeast Atlantic (Celtic Sea) since the phasing out of leaded gasoline in Europe. Concentrations of DPb in surface waters have decreased by fourfold over the last four decades. We demonstrate that anthropogenic Pb is transported from the Mediterranean Sea over long distances (>2,500 km). Benthic DPb fluxes exceeded the atmospheric Pb flux in the region, indicating the importance of sediments as a contemporary Pb source. A strong positive correlation between DPb, PPb, and LpPb indicates a dynamic equilibrium between the phases and the potential for particles to "buffer" the DPb pool. This study provides insights into Pb biogeochemical cycling and demonstrates the potential of Pb in constraining ocean circulation patterns.

Plain Language Summary Lead (Pb) is a toxic element to all living organisms and may cause health impacts upon exposure to high levels. Humans have introduced large amounts of Pb into environment over last 150~years mainly through combustion of leaded gasoline and coal. The anthropogenic Pb is transported over long distances in the atmosphere and deposited in remote ocean regions resulting in elevated Pb concentrations. Since the implementation of stricter environmental regulations over last decades, Pb levels in surface waters have declined. In this study we report five times lower Pb concentrations in European surface waters compared with those from the 1980s and also present recent Pb inputs. Once anthropogenic Pb is introduced into the marine environment, it can be used to trace specific water mass transport throughout the global ocean. In this study we use Pb signal to demonstrate transport of Mediterranean Sea surface water over 2,500~km across the Atlantic Ocean. Our results serve as evidence of the positive impact of environmental regulations on Pb inputs and highlight the requirement of continuing efforts in regulating Pb emissions.

1. Introduction

Lead (Pb) is one of few elements for which the impact of human activity on the marine environment is clearly evident. Anthropogenic perturbation of the natural biogeochemical cycle of Pb in the ocean dates back to circa 1850 (Kelly et al., 2009), with coal and leaded gasoline combustion serving as major sources of Pb to the atmosphere (Kelly et al., 2009; Wu & Boyle, 1997). Anthropogenic Pb is transported in the atmosphere in the form of fine aerosol particles that can travel long distances and are deposited in remote areas resulting in enhanced DPb surface ocean concentrations (Kumar et al., 2014; Véron & Church, 1997), reaching >190 pmol kg^{-1} during the peak of the Pb emissions in 1970–1980 (Laumond et al., 1984). Anthropogenic Pb has entirely masked signals of naturally sourced Pb (approximately 2.2 pmol kg^{-1} in surface waters; Henderson & Maier-Reimer, 2002). To date, leaded gasoline has been virtually phased out (except in three countries, as of March 2017, United Nations Environment Programme), and Pb concentrations have decreased significantly from ~170 to <15 pmol kg^{-1} in surface waters (Boyle et al., 2014; Schaule & Patterson, 1983), leading to recent evidence for natural Pb signatures reemerging in the North Atlantic (Bridgestock et al., 2016).

The spatial and temporal variable historic Pb inputs to the marine environment can be used to investigate the reactivity and cycling of this element and trace long-range ocean circulation patterns (Chen,

AGU Geophysical Research Letters 10.1002/2017GL076825

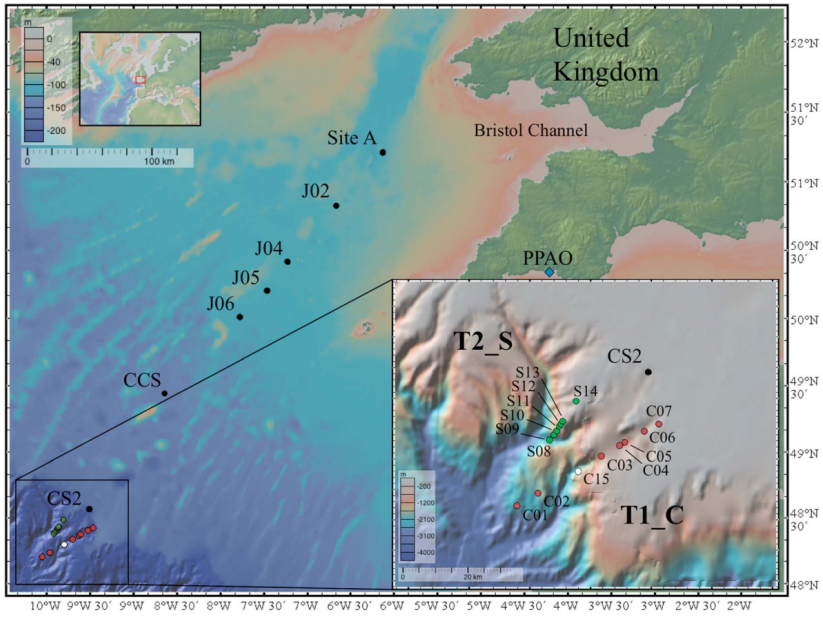


Figure 1. Station locations across canyon T1_C (white and red circles), spur T2_S (green circles) transects, and on-shelf transect (black circle) during three research expeditions in November (DY018), April (DY029), and July (DY033). Blue diamond represents PPAO station. Map was generated using GeoMapApp, http://www.geomapapp.org (Ryan et al., 2009).

Goodkin, et al., 2016; Fine, 2010; Lee et al., 2015). Anthropogenic Pb has been utilized as a tracer of subducted surface waters in the Indian (Lee et al., 2015) and Pacific Oceans (Chien et al. 2017) and ventilated surface waters of the Northwest Atlantic (Boyle et al., 2014). Anthropogenic perturbation of natural Pb concentrations in the ocean has been described as an "evolving global experiment" (Boyle et al., 2014) that demonstrates the magnitude of human impact on the environment.

Lead is a particle reactive element in marine waters and is typically removed through scavenging, with the sediments acting as repositories. However, the role of particulate matter and the physicochemical processes that influence the fate of dissolved Pb (DPb) and facilitate long-range transport are poorly constrained. A slow release of DPb from particles and a rapid isotopic exchange with particulate matter that can influence the fate of particulate Pb (PPb) has recently been reported (Chen, Boyle, et al., 2016). Therefore, in order to gain insights into biogeochemical cycling of Pb in the marine environment, both phases should be considered.

Here we report and evaluate the first extensive seasonal study of DPb, PPb, and leachable Pb (LpPb) distributions in Northeast Atlantic marginal seas since the phaseout in Europe of leaded gasoline use in 1980–2011 (European Communities, 1978; Economic Commission for Europe, 2014). This study provides insights into the dynamic relationship between dissolved and particulate phases and demonstrates the role of benthic Pb release and Pb as a tracer of North Atlantic circulation patterns.

2. Study Region, Materials, and Methods

Full details of the study region, sampling and methods are provided in the supporting information (SI) Text S1. Briefly, samples for trace metal analysis were collected during three different seasons: November–December 2014 (DY018), April 2015 (DY029), and July–August 2015 (DY033) in the Northeast Atlantic continental margin (Celtic Sea) (Figure 1), on board *RRS Discovery*. Two off-shelf transects were conducted along a canyon (T1_C,

AGU Geophysical Research Letters 10.1002/2017GL076825

stations C01–C07 and C15), nearby a spur (T2_S, stations S08–S09) (SI Text S1) and one on-shelf transect in the Celtic Sea (stations CS2, CCS, J02–J06, and Site A). Trace metal samples were collected following GEOTRACES protocols (Cutter et al., 2010). Dissolved Pb and Mn (DMn) were filtered using a 0.2 μm cartridge filter (Sartobran 300, Sartorius), preconcentrated using an automated system (SC-4 DX SeaFAST pico; ESI), and analyzed by high-resolution inductively coupled plasma-mass spectrometry (HR-ICP-MS; Thermo Fisher Element XR) (Rapp et al., 2017). Dissolved Fe (DFe) (0.2 μm filtered) was analyzed by flow injection with chemiluminescence detection (Obata et al., 1993) as detailed in Birchill et al. (2017). Particulate Pb was collected on clean 25 mm Supor® polyethersulfone membrane disc filters (Pall, 0.45 μm) and subjected to a 25% acetic acid-hydroxylamine hydrochloride leach (LpPb) (Berger et al., 2008) and subsequently an acid digestion (PPb) (Ohnemus et al., 2014). Particulate samples were analyzed using ICP-MS (Thermo Fisher X Series 2). Dissolved aluminum (DAl) (0.2 μm filtered) was analyzed using spectrofluorometry following the method by Hydes and Liss (1976). Evaluation of the accuracy and efficiency of these methods was carried out using Certified Reference Materials with the results showing good agreement (SI Table S1). Some data points were identified as outliers and were excluded from consideration (SI Text S2). Radium (Ra) isotopes ^{223}Ra and ^{224}Ra were extracted from large seawater volumes (60–100 L) by adsorption onto Mn acrylic fibers (Sun & Torgersen, 1998). Ra activities were analyzed at sea by Radium Delayed Coincidence Counting following standard methodology (Annett et al., 2013; Garcia-Solsona et al., 2008; Moore, 2008; Moore & Arnold, 1996). Ra activities used here ($^{224}Ra_{xs}$ and $^{223}Ra_{xs}$) are in excess of activity supported by the parent isotopes in the water column (SI Text S1). Water mass distribution was quantified using extended Optimum Multiparameter (extOMP) analysis (Hupe & Karstensen, 2000; Karstensen & Tomczak, 1998; Pollard et al., 2004). The propagation time of Mediterranean Outflow Water (MOW) from the Gulf of Cadiz was calculated analogously to (Waugh et al., 2003), using chlorofluorocarbon-12 data available in the GLODAPv2 data product (Olsen et al., 2016). Aerosol samples were digested using hydrofluoric acid and HNO_3 following the method adapted from Morton et al. (2013) and analyzed by the ICP-MS (Thermo Fisher X Series 2). Section plots figures were created with Ocean Data View (2015) software (Schlitzer, 2015) with Data-Interpolating Variational Analysis gridding settings.

3. Results and Discussion

DPb concentrations in the Celtic Sea region ranged between 29.6 and 122 pmol kg^{-1} (Figures 2a–2c and S1). Off-shelf distributions showed elevated DPb concentrations (50.8 ± 3.0 pmol kg^{-1} (n = 20)) in the seasonal mixed layer (SML) along the canyon transect in November and also at stations S08 and S09 along the spur transect. Below the SML, DPb distributions were generally consistent along both transects for all seasons and decreased down to 38 pmol kg^{-1} in the subsurface waters and increased at depths of ~550–1,500 m to 46.6 ± 5.6 pmol kg^{-1} (n = 84). In deeper waters (>1,500 m), DPb concentrations decreased to 37.0 ± 3.2 pmol kg^{-1} (n = 39). On the continental shelf, DPb concentrations were generally higher in comparison to the off-shelf transects and ranged between 36.1 and 122 pmol kg^{-1}. Elevated DPb concentrations were measured in surface waters in April (96.8 pmol kg^{-1}) and July (99.1 pmol kg^{-1}) with somewhat lower levels in November (72.6 pmol kg^{-1}), whereas DPb was persistently elevated in bottom waters (up to 121 pmol kg^{-1}) across all seasons. No correlations between DPb and macronutrients were observed.

Our surface water DPb concentration of 40.2 ± 7.5 pmol kg^{-1} (n = 109) along the shelf break in 2014–2015 showed at least a fourfold decrease compared to previous reports for the region (Figure 2e and Table S2) (Brügmann et al., 1985; Cotté-Krief et al., 2002; Helmers & Van der Loeff, 1993; Lambert et al., 1991; Muller et al., 1994) and were generally lower in comparison to other European shelf waters over the last 4 decades (Kremling & Streu, 2001; Laumond et al., 1984; Monteiro et al., 2015; Pohl et al., 2011; Prego et al., 2013; Waeles et al., 2008). The diminishing DPb concentrations over the last two decades form a success of the phaseout process of leaded gasoline. Nevertheless, the observed concentrations in our study region exceeded predicted natural levels of Pb (Henderson & Maier-Reimer, 2002) by at least an order of magnitude, indicating that the vast majority of Pb still has an anthropogenic origin. Thus, the elevated DPb concentrations we report in surface waters indicate the presence of recent anthropogenic Pb inputs to Northeast Atlantic waters from sources such as coal burning, smelting, or mining (Lee et al., 2014; Nriagu & Pacyna, 1988).

3.1. Long-Range Pb Transport in MOW

Elevated DPb concentrations of 46.6 ± 5.6 pmol kg^{-1} (n = 84) were a persistent feature in the depth range ~550–1,500 m (27.30–27.75 kg m^{-3} σ_0) in the slope region of the Celtic Sea. The DPb maximum coincided

AGU Geophysical Research Letters 10.1002/2017GL076825

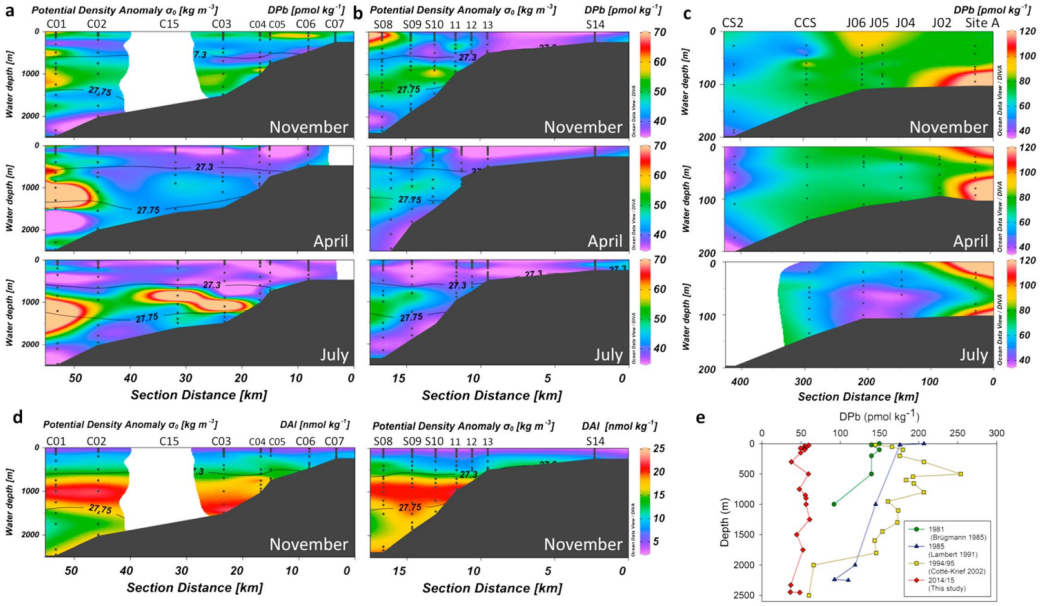


Figure 2. Upper panel: dissolved lead distribution plots (a) along the canyon transects (T1_C, left), (b) along the spur transects (T2_S, middle), and (c) and along the on-shelf transect (left) in November (DY018) (top), April (DY029) (middle), and July (DY033) (bottom). Bottom panel: (d) example of dissolved aluminum distribution plots from November (DY018) along the canyon (T1_C) transect (left) and spur (T2_S) transect (right). For the full dissolved aluminum results please see SI Figure S2. Black lines represent Mediterranean Outflow Water density range contour plots. (e) Reduction of DPb concentrations in the Celtic Sea slope region over the last 30 years. Data are from Brügmann et al. (1985, green circles), Lambert et al. (1991, blue triangles), and Cotté-Krief et al. (2002, yellow squares), and this study is represented by the S08 station in April (DY029) by red diamonds.

with salinity (35.74) (Figure 3a) and DAl (17.3 ± 2.6 nmol kg^{-1}, n = 88) maxima (Figure S2), signatures of MOW (Measures & Edmond, 1988; Rolison et al., 2015). Surface waters in the Mediterranean Sea received enhanced atmospheric Pb inputs during the period of leaded gasoline use, with maximum surface DPb of >190 pmol kg^{-1} (Laumond et al., 1984). Mediterranean waters also receive enhanced eolian fluxes of Al from Saharan dust (Rolison et al., 2015). Deep water formation occurs in the Levantine Basin and Gulf of Lions, and the saline deep Mediterranean waters with enhanced DPb (40–80 pmol kg^{-1}) (Rolison, 2016) and DAl (125–170 nmol kg^{-1} (Rolison et al., 2015)) exit the Strait of Gibraltar as bottom waters and mix with Eastern North Atlantic Central Water (García-Ibáñez et al., 2015). The MOW spreads across NE Atlantic at a depth ~550–1,500 m and propagates along the continental slope toward the Celtic Sea shelf break. The mean propagation time of MOW from the Gulf of Cadiz to the Celtic Sea slope region is ~5 years (Figure S3). The presence of MOW at intermediate depths in the study region has previously been reported (Cotté-Krief et al., 2002; Lambert et al., 1991) and was confirmed by the extOMP analysis (Figures 3b and S4). The core of the MOW (up to 55%) was identified at ~1,000 m depth with a Gaussian decay (20% at 550 m and 1,500 m).

Enhanced DPb concentrations were also observed along GEOTRACES transects in corresponding MOW density layers (27.22–27.82 kg m^{-3} σ_0): in the Gulf of Cadiz (49.0 ± 2.6 pmol kg^{-1}, n = 14, GA04; Rolison, 2016), north (46.1 ± 6.1 pmol kg^{-1}, n = 18, GA01), and south of the Gulf of Cadiz (55.1 ± 5.5 pmol kg^{-1}, n = 10, GA03, Noble et al., 2015) (Figure S5), in agreement with our observations. Our study region is ~2,500 km away from the Strait of Gibraltar; therefore, the concentration of DPb and DAl may be expected to decrease through scavenging and/or dilution processes during transit. While DAl concentrations and salinity correlated well (r^2 = 0.68) and decreased from 27.8 ± 7.2 nmol kg^{-1} and 35.6–36.4 (Gulf of Cadiz)

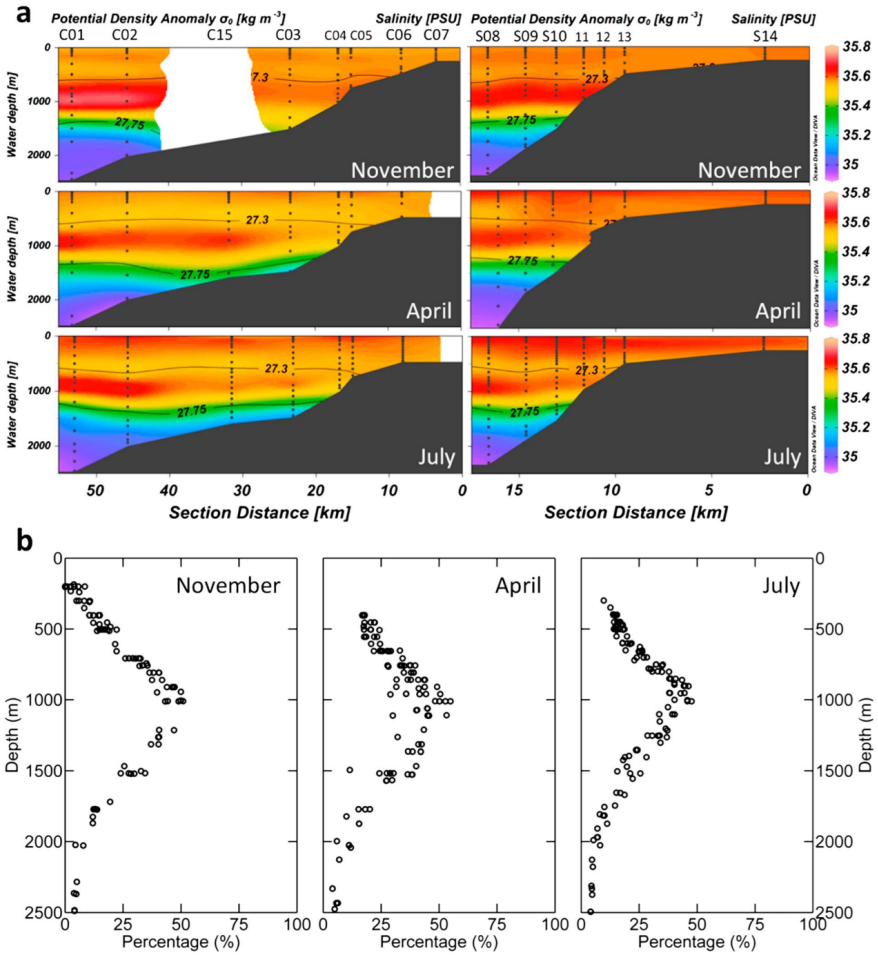


Figure 3. Upper panel (a): salinity distribution plots along the canyon transects (T1_C, left) and along the spur transects (T2_S, right) in November (DY018) (top), April (DY029) (middle), and July (DY033) (bottom). Bottom panel (b): the percentage distribution of Mediterranean Outflow Water along the canyon (T1_C) and spur (T2_S) transects in November (DY018) (left), April (DY029) (middle), and July (DY033) (left). For the full Optimum Multiparameter results see SI Figure S4.

to 17.3 ± 2.6 nmol kg^{-1} and 35.4–35.7, there was no correlation of DPb with salinity and DPb concentrations remained unchanged (Figure S6). We suggest the following processes that maintain elevated DPb signal during MOW transit: (i) benthic inputs from the European continental slopes. Shelf break sediments have been suggested as a Pb source in the Philippine Sea (Chien et al. 2017). Local sediment resuspension events in the Bay of Biscay as MOW propagates along the continental slope have also been reported (McCave & Hall, 2002). (ii) Reversible Pb sorption onto particle surfaces. This mechanism has been suggested to supply DPb to North Pacific deep waters (Wu et al., 2010). Pb isotope exchange between these two phases has been demonstrated (Chen, Goodkin, et al., 2016; Sherrell et al., 1992), and the

potential of particle reversible sorption has been shown using thorium isotopes (Bacon & Anderson, 1982). Potentially, DPb (<0.2 μm) may be released from particles in the form of small, low specific density inorganic particles (colloids 0.02–0.2 μm) with longer residence time. However, PPb dissolution within MOW is also plausible. Our results show that the major portion of PPb was in LpPb form (78 ± 10%, n = 205), while overall the majority of the total Pb pool (PPb + DPb) was in the DPb fraction (70 ± 18%, n = 171), thus implying a significant role of particles in DPb distributions.

Partial mixing with other historically Pb polluted waters, such as Northeast Atlantic ventilated surface waters and Labrador Sea Water (LSW) transported across the North Atlantic (Bridgestock et al., 2018; Zurbrick et al., 2018), has been shown to influence DPb concentrations at intermediate depths and thus also need to be considered. Low-salinity and high-oxygen LSW underlies the warm, saline MOW (Talley & McCartney, 1982). Our extOMP confirmed a layering of the water masses with MOW at a core depth 27.60 kg m^{-3} transiting into the LSW core at 27.79 kg m^{-3} (Figure S4) and a potential for vertical mixing of bottom layers of MOW with LSW. Within waters identified as LSW (27.76–27.85 kg m^{-3} σ_0), concentrations of DPb (42.9 ± 4.5 pmol kg^{-1} (n = 42)), and DAl (15.8 ± 1.0 nmol kg^{-1} (n = 40)) were somewhat lower, and salinity (34.98–35.4) and temperature (from 8.8 ± 1.5 to 5.1 ± 1.0°C) were lower in comparison to overlying MOW. These values were higher in comparison to DPb (36.9 ± 7.4 pmol kg^{-1}, n = 60), DAl (13.0 ± 1.2 nmol kg^{-1}, n = 60), salinity (34.94–35.2), and temperature (4.3 ± 0.6°C) observed within LSW (27.68–27.81 kg m^{-3} σ_0) in the NW Atlantic (GA02 section, 2010) (Mawji et al., 2015). Densities of MOW and LSW are similar, and a complete differentiation is therefore challenging, preventing us from determining the exact fraction of each water mass. Our findings indicate the potential for MOW penetration into deeper waters, altering properties of LSW although the upward vertical mixing cannot be ruled out. We conclude that the DPb maximum in the Celtic Sea region was a result of anthropogenically perturbed MOW masses reaching NE Atlantic continental margins.

3.2. Sediment Release of a Particle Reactive Element

Elevated DPb (65.9–121 pmol kg^{-1}) and PPb concentrations (149–806 pmol kg^{-1}) were observed in bottom waters at Site A during all seasons and on the continental slope at C03–C04 stations in November (DPb: 52.5 ± 5.6 pmol kg^{-1}, n = 7, PPb: 29.3 ± 13.9 pmol kg^{-1}, n = 8) (Figure 4). Following fluvial or atmospheric inputs to marine waters, Pb is typically scavenged and transferred to the seafloor (Bastami et al., 2015; Marani et al., 1995). Tidal currents, wind-driven waves, and storm events cause resuspension of sediments (Kalnejais et al., 2007), thereby supplying Pb-enriched pore waters and particles to the water column. This mechanism has been reported for deep ocean (Lee et al., 2015; Noble et al., 2015), coastal (Annibaldi et al., 2009; Chien et al., 2017; Sañudo-Wilhelmy & Flegal, 1994), estuarine (Rivera-Duarte & Flegal, 1994), and riverine systems (Ferrari & Ferrario, 1989) and observed in sediment chamber experiments (Kalnejais et al., 2007; Zago et al., 2000).

At Site A, the enhanced DPb and PPb concentrations near the seafloor coincided with persistently elevated turbidity signals (Figure 4), indicating particle resuspension and subsequent DPb and PPb remobilization from the sediments to overlying waters. The benthic Pb supply is supported by increased levels of the short-lived isotopes $^{223}Ra_{xs}$ and $^{224}Ra_{xs}$ (half-lives 3.66 and 11.4 days, respectively) near the seafloor (Figure 4), indicating recent sedimentary supply. A similar feature was observed on the continental slope along the canyon transect in November where salinity maximum associated with MOW decreased toward the continental shelf break (Figure 3a) from 35.74 (C01) to 35.61 (C04) (~1,000 m depth); thus, DPb concentrations were also expected to decrease. Yet DPb concentrations remained unchanged (Figure 2a) and PPb concentrations were elevated, coinciding with increased $^{223}Ra_{xs}$, $^{224}Ra_{xs}$ and turbidity signals (Figures 4 and S7), indicating a sedimentary Pb source to overlying waters.

Benthic DPb remobilization has been reported by Noble et al. (2015) and Chien et al. (2017). To our knowledge, we provide the first clear evidence of a benthic Pb source supported by PPb and Ra field measurements. Furthermore, our results showed a strong positive correlation between DPb and PPb (r^2 = 0.97, n = 12), and DPb and LpPb (r^2 = 0.97, n = 12) at Site A and C03/C04 stations (Figure S8), indicating a dynamic equilibrium between the phases. Although little is known about biogeochemical processes facilitating DPb sedimentary release, we suggest that benthic remobilization could be facilitated through Pb association with Fe/Mn oxi-hydroxide precipitates (Allen et al., 1990; Bastami et al., 2015; Fernex et al., 1992; Kalnejais et al., 2007) with subsequent reductive dissolution of the solid Fe and Mn forms in sediments (Fernex et al., 1992). This mechanism is supported by elevated DFe and DMn concentration toward the

AGU Geophysical Research Letters 10.1002/2017GL076825

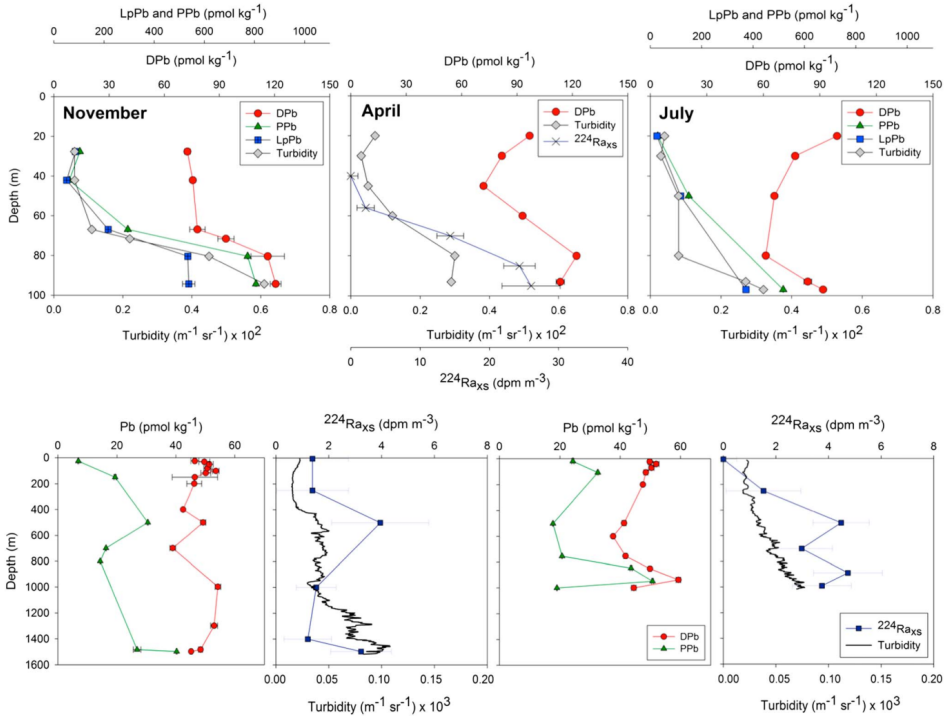


Figure 4. Upper panel: depth profiles of DPb (circles), PPb (triangles), LpPb (squares), turbidity (diamonds), and $^{224}Ra_{xs}$ (crosses) at Site A in November (DY018) (left), April (DY029) (middle), and July (DY033) (left). Bottom panel: depth profiles of DPb (circles), PPb (triangles), $^{224}Ra_{xs}$ (squares), and turbidity (black line) at station C03 (left) and C04 (right) in November (DY018).

seafloor (Figure S9) and a buildup of Fe(II) in sediments at Site A (Klar et al., 2017) but not at stations C03/C04. Potentially, DPb may be supplied in the form of small colloids deposited onto sediments (Muller, 1996; Sen & Khilar, 2006), with these Pb-enriched resuspended fine particles having a longer residence time in comparison to bulk sediment particles (Ferrari & Ferrario, 1989; Kalnejais et al., 2007).

We determined a benthic Pb flux to overlying waters of 27–41 $\times 10^{-9}$ mole Pb m^{-2} d^{-1} ($n = 3$) at Site A in April (SI Text S4) using short-lived Ra isotopes (Moore, 2000). To our knowledge, this is the first benthic Pb flux estimate from field observations. Furthermore, this sedimentary Pb flux was up to 2 orders of magnitude higher than the atmospheric flux (0.03–12.2 $\times 10^{-9}$ mole Pb m^{-2} d^{-1}) observed at nearby Penlee Point Atmospheric Observatory in 2015 (Figures 1 and S5; Arimoto et al., 2003). The benthic DPb flux was likely a result of accumulation in sediments of Pb deposited over time, while the recent relatively low atmospheric Pb flux reflects the implementation of strict European air emission regulations. We therefore stress that sediments containing legacy Pb will continue to serve as an important, if not the major source of Pb to overlying waters.

3.3. Recent Pb Sources in the NE Atlantic Shelf Region

A strong spatial and temporal variability in surface water DPb concentrations were observed over the various transects across the seasons. Elevated surface DPb concentrations (36.1–122 pmol kg^{-1}) were observed on the continental shelf during all sampling seasons, with lower levels along off-shelf transects (Figure 2c). Elevated DPb concentrations observed in surface waters at Site A in April and July in comparison to

November indicated recent Pb inputs (Figure 4). A strong inverse correlation of DPb with salinity $r = -0.96$ (April, $n = 6$) and $r = -0.94$ (July, $n = 4$) between Site A and CS2 stations suggests a freshwater source of DPb, which could be continental runoff or wet deposition (Figure S10). On the continental slope, elevated DPb concentrations in the SML were observed along the canyon (T1_C) transect in November (50.8 ± 3.0 pmol kg^{-1}, $n = 20$) and at S08 and S09 stations on the spur (T2_S) transect. Lower DPb concentrations were observed during other seasons; 39.6 ± 6.9 pmol kg^{-1} ($n = 23$, T1_C) and 35.0 ± 4.2 pmol kg^{-1} ($n = 30$, T2_S) in April and 35.2 ± 3.8 pmol kg^{-1} ($n = 9$, T1_C) and 37.4 ± 4.9 pmol kg^{-1} ($n = 6$, T2_S) in July (Figures 2a and 2b). The distinctive changes in DPb over short spatial scale observed between our closely spaced stations (<20 km) suggest presence of different water masses with different DPb input histories over the last months to years. These observations coincided with distinct temperature and DMn concentration differences (Figure S11), which enforce this suggestion.

4. Conclusions

Our observations demonstrate the widespread impact of anthropogenic Pb emissions on the marine environment. The elevated Pb signal (46.6 ± 5.6 pmol kg^{-1}) in MOW is transported long distances (>2,500 km) at intermediate depths across the Northeast Atlantic following anthropogenic Pb emissions during the past century. Following implementation of stricter environmental regulations in Europe, this oceanic Pb signal will behave similarly to chlorofluorocarbons in that it is predicted to decrease with time. However, considering the residence time of Pb in the deep ocean of ~100 years (Nozaki & Tsunogai, 1976), the presence of recent Pb sources (>90 pmol kg^{-1} in surface waters), and the "resupply" of Pb to the water column from sediments containing legacy Pb (27–41 × 10^{-9} mole Pb m^{-2} d^{-1}), we expect the anthropogenic Pb signal to remain in the marine environment for decades to come. The role of the particulate phase in buffering Pb concentrations in the water column needs to be considered in the interpretation of oceanic DPb distributions due to a close relationship between the dissolved and particulate phases.

Acknowledgments
This project was funded by the UK Natural Environment Research Council (NE/K001973/1 (E. A. and M. G.), NE/K001779/1 (M. L.), NE/K002023/1 (A. A.), and NE/L501840/1 (A. B.)). The authors declare no competing financial interests. The authors thank the captain and crew of *RRS Discovery* for their assistance during research expeditions and Malcolm Woodward and Carolyn Harrys for the macronutrient data. We thank Insa Rapp for the training in the sample analysis and Alex Zavarsky for the help with the Matlab scripts and Cheryl Zurbrick and Ed Boyle for the GA01 section data set and their contribution to IDP 2017. The GA04 cruises were funded by the Netherlands Organization for Scientific Research (882.01.015). Analysis was funded by the University of Otago and the Royal Netherlands Institute for Sea Research. Data have been submitted to BODC.

References

Allen, J. R. L., Rae, J. E., & Zanin, P. E. (1990). Metal speciation (Cu, Zn, Pb) and organic-matter in an oxic salt marsh, Severn Estuary, southwest Britain. *Marine Pollution Bulletin*, *21*(12), 574–580. https://doi.org/10.1016/0025-326X(90)90606-9

Annett, A. L., Henley, S. F., Van Beek, P., Souhaut, M., Ganeshram, R., Venables, H. J., et al. (2013). Use of radium isotopes to estimate mixing rates and trace sediment inputs to surface waters in northern Marguerite Bay, Antarctic Peninsula. *Antarctic Science*, *25*(03), 445–456. https://doi.org/10.1017/S0954102012000892

Annibaldi, A., Truzzi, C., Illuminati, S., & Scarponi, G. (2009). Recent sudden decrease of lead in Adriatic coastal seawater during the years 2000–2004 in parallel with the phasing out of leaded gasoline in Italy. *Marine Chemistry*, *113*(3–4), 238–249. https://doi.org/10.1016/j.marchem.2009.02.005

Arimoto, R., Duce, R. A., Ray, B. J., & Tomza, U. (2003). Dry deposition of trace elements to the western North Atlantic. *Global Biogeochemical Cycles*, *17*(1), 1010. https://doi.org/10.1029/2001GB001406

Bacon, M. P., & Anderson, R. F. (1982). Distribution of thorium isotopes between dissolved and particulate forms in the deep sea. *Journal of Geophysical Research*, *87*(C3), 2045–2056. https://doi.org/10.1029/JC087iC03p02045

Bastami, K. D., Neyestani, M. R., Shemirani, F., Soltani, F., Haghparast, S., & Akbari, A. (2015). Heavy metal pollution assessment in relation to sediment properties in the coastal sediments of the southern Caspian Sea. *Marine Pollution Bulletin*, *92*(1–2), 237–243. https://doi.org/10.1016/j.marpolbul.2014.12.035

Berger, C. J. M., Lippiatt, S. M., Lawrence, M. G., & Bruland, K. W. (2008). Application of a chemical leach technique for estimating labile particulate aluminum, iron, and manganese in the Columbia River plume and coastal waters off Oregon and Washington. *Journal of Geophysical Research*, *113*, C00B01. https://doi.org/10.1029/2007JC004703

Birchill, A. J., Milne, A., Woodward, E. M. S., Harris, C., Annett, A., Rusiecka, D., et al. (2017). Seasonal iron depletion in temperate shelf seas. *Geophysical Research Letters*, *44*, 8987–8996. https://doi.org/10.1002/2017GL073881

Boyle, E., Lee, J., Echegoyen, Y., Noble, A., Moos, S., Carrasco, G., & Zhao, N. (2014). Anthropogenic lead emissions in the ocean: The evolving global experiment. *Oceanography*, *27*(1), 69–75. https://doi.org/10.5670/oceanog.2014.10

Bridgestock, L., van de Flierdt, T., Rehkämper, M., Paul, M., Middag, R., Milne, A., et al. (2016). Return of naturally sourced Pb to Atlantic surface waters. *Nature Communications*, *7*, 12,921. https://doi.org/10.1038/ncomms12921

Bridgestock, L., Rehkämper, M., van de Flierdt, T., Paul, M., Milne, A., Lohan, M. C., & Achterberg, E. P. (2018). The distribution of lead concentrations and isotope compositions in the eastern tropical Atlantic Ocean. *Geochimica et Cosmochimica Acta*, *225*, 36–51. https://doi.org/10.1016/j.gca.2018.01.018

Brügmann, L., Danielsson, L.-G., Magnusson, B., & Westerlund, S. (1985). Lead in the North Sea and the north east Atlantic Ocean. *Marine Chemistry*, *16*(1), 47–60. https://doi.org/10.1016/0304-4203(85)90027-1

Chen, M., Goodkin, N. F., Boyle, E. A., Switzer, A. D., & Bolton, A. (2016). Lead in the western South China Sea: Evidence of atmospheric deposition and upwelling. *Geophysical Research Letters*, *43*, 4490–4499. https://doi.org/10.1002/2016GL068697

Chen, M., Boyle, E. A., Lee, J., Nurhati, I., Zurbrick, C., Switzer, A. D., & Carrasco, G. (2016). Lead isotope exchange between dissolved and fluvial particulate matter: A laboratory study from the Johor River estuary. *Philosophical Transactions of the Royal Society A: Mathematical, Physical and Engineering Sciences*, *374*(2081), 20160054. https://doi.org/10.1098/rsta.2016.0054

Chien, C. T., Ho, T. Y., Sanborn, M. E., Yin, Q. Z., & Paytan, A. (2017). Lead concentrations and isotopic compositions in the Western Philippine Sea. *Marine Chemistry*, *189*, 10–16. https://doi.org/10.1016/j.marchem.2016.12.007

Communities, E. (1978). Council directive 78/611/EEC of 29 June 1978 on the approximation of the laws of the member states concerning the lead content of petrol. *Official Journal of the European Communities*, *21*(6), 196–121. https://doi.org/10.1039/ap9842100196
Cotté-Krief, M.-H., Thomas, A. J., & Martin, J.-M. (2002). Trace metal (Cd, Cu, Ni and Pb) cycling in the upper water column near the shelf edge of the European continental margin (Celtic Sea). *Marine Chemistry*, *79*(1), 1–26. https://doi.org/10.1016/S0304-4203(02)00013-0
Cutter, G., Andersson, P., Codispoti, L., Croot, P., François, R., Lohan, M. C., et al. (2010). Sampling and sample-handling protocols for GEOTRACES cruises, (December).
Economic Commission for Europe (2014). Convention on long-range transboundary air pollution. Geneva, 52nd session, 30 June–3 July 2014.
Fernex, F., Février, G., Bénaïm, J., & Arnoux, A. (1992). Copper, lead and zinc trapping in Mediterranean deep-sea sediments: Probable coprecipitation with Mn and Fe. *Chemical Geology*, *98*(3–4), 293–306. https://doi.org/10.1016/0009-2541(92)90190-G
Ferrari, G. M., & Ferrario, P. (1989). Behavior of Cd, Pb, and Cu in the marine deltaic area of the Po River (North Adriatic Sea). *Water, Air, and Soil Pollution*, *43*(3-4), 323–343. https://doi.org/10.1007/BF00279200
Fine, R. A. (2010). Observations of CFCs and SF6 as ocean tracers. *Annual Review of Marine Science*, *3*(1), 173–195. https://doi.org/10.1146/annurev.marine.010908.163933
García-Ibáñez, M. I., Pardo, P. C., Carracedo, L. I., Mercier, H., Lherminier, P., Ríos, A. F., & Pérez, F. F. (2015). Structure, transports and transformations of the water masses in the Atlantic Subpolar Gyre. *Progress in Oceanography*, *135*, 18–36. https://doi.org/10.1016/j.pocean.2015.03.009
Garcia-Solsona, E., Garcia-Orellana, J., Masqué, P., & Dulaiova, H. (2008). Uncertainties associated with ^{223}Ra and ^{224}Ra measurements in water via a Delayed Coincidence Counter (RaDeCC). *Marine Chemistry*, *109*(3–4), 198–219. https://doi.org/10.1016/j.marchem.2007.11.006
Helmers, E., & Van der Loeff, M. M. R. (1993). Lead and aluminum in Atlantic surface waters (50°N to 50°S) reflecting anthropogenic and natural sources in the Eolian transport. *Journal of Geophysical Research*, *98*(C11), 20,261–20,273. https://doi.org/10.1029/93JC01623
Henderson, G. M., & Maier-Reimer, E. (2002). Advection and removal of ^{210}Pb and stable Pb isotopes in the ocean: A general circulation model study. *Geochimica et Cosmochimica Acta*, *66*(2), 257–272. https://doi.org/10.1016/S0016-7037(01)00779-7
Hupe, A., & Karstensen, J. (2000). Redfield stoichiometry in Arabian Sea subsurface waters. *Global Biogeochemical Cycles*, *14*(1), 357–372. https://doi.org/10.1029/1999GB900077
Hydes, D. J., & Liss, P. S. (1976). Fluorimetric method for the determination of low concentrations of dissolved aluminium in natural waters. *Analyst*, *101*(1209), 922–931. https://doi.org/10.1039/an9760100922
Kalnejais, L. H., Martin, W. R., Signell, R. P., & Bothner, M. H. (2007). Role of sediment resuspension in the remobilization of particulate-phase metals from coastal sediments. *Environmental Science and Technology*, *41*(7), 2282–2288. https://doi.org/10.1021/es061770z
Karstensen, J., & Tomczak, M. (1998). Age determination of mixed water masses using CFC and oxygen data. *Journal of Geophysical Research*, *103*(C9), 18,599–18,609. https://doi.org/10.1029/98JC00889
Kelly, A. E., Reuer, M. K., Goodkin, N. F., & Boyle, E. A. (2009). Lead concentrations and isotopes in corals and water near Bermuda, 1780–2000. *Earth and Planetary Science Letters*, *283*(1–4), 93–100. https://doi.org/10.1016/j.epsl.2009.03.045
Klar, J. K., Homoky, W. B., Statham, P. J., Birchill, A. J., Harris, E. L., Woodward, E. M. S., et al. (2017). Stability of dissolved and soluble Fe(II) in shelf sediment pore waters and release to an oxic water column. *Biogeochemistry*, *135*(1-2), 49–67. https://doi.org/10.1007/s10533-017-0309-x
Kremling, K., & Streu, P. (2001). The behaviour of dissolved Cd, Co, Zn, and Pb in North Atlantic near-surface waters (30°N/60°W–60°N/2°W). *Deep Sea Research, Part I*, *48*(12), 2541–2567. https://doi.org/10.1016/S0967-0637(01)00036-X
Kumar, A., Abouchami, W., Galer, S. J. G., Garrison, V. H., Williams, E., & Andreae, M. O. (2014). A radiogenic isotope tracer study of transatlantic dust transport from Africa to the Caribbean. *Atmospheric Environment*, *82*, 130–143. https://doi.org/10.1016/j.atmosenv.2013.10.021
Lambert, C., Nicolas, E., Veron, A., Buatmenard, P., Klinkhammer, G., Lecorre, P., & Morin, P. (1991). Anthropogenic lead cycle in the northeastern Atlantic. *Oceanologica Acta*, *14*(1), 59–66.
Laumond, F., Copin-Montegut, G., Courau, P., & Nicolas, E. (1984). Cadmium, copper and lead in the western Mediterranean Sea. *Marine Chemistry*, *15*(3), 251–261. https://doi.org/10.1016/0304-4203(84)90021-5
Lee, J. M., Boyle, E. A., Suci Nurhati, I., Pfeiffer, M., Meltzner, A. J., & Suwargadi, B. (2014). Coral-based history of lead and lead isotopes of the surface Indian Ocean since the mid-20th century. *Earth and Planetary Science Letters*, *398*, 37–47. https://doi.org/10.1016/j.epsl.2014.04.030
Lee, J. M., Boyle, E. A., Gamo, T., Obata, H., Norisuye, K., & Echegoyen, Y. (2015). Impact of anthropogenic Pb and ocean circulation on the recent distribution of Pb isotopes in the Indian Ocean. *Geochimica et Cosmochimica Acta*, *170*, 126–144. https://doi.org/10.1016/j.gca.2015.08.013
Marani, D., Macchi, G., & Pagano, M. (1995). Lead precipitation in the presence of sulphate and carbonate: Testing of thermodynamic predictions. *Water Research*, *29*(4), 1085–1092. https://doi.org/10.1016/0043-1354(94)00232-V
Mawji, E., Schlitzer, R., Dodas, E., Abadie, C., Abouchami, W., et al. (2015). The GEOTRACES Intermediate Data Product 2014. *Marine Chemistry*, *177*(Part 1), 1–8. https://doi.org/10.1016/j.marchem.2015.04.005
McCave, I. N., & Hall, I. R. (2002). Turbidity of waters over the Northwest Iberian continental margin. *Progress in Oceanography*, *52*(2–4), 299–313. https://doi.org/10.1016/S0079-6611(02)00012-5
Measures, C. I., & Edmond, J. M. (1988). Aluminium as a tracer of the deep outflow from the Mediterranean. *Journal of Geophysical Research*, *93*(C1), 591–595. https://doi.org/10.1029/JC093iC01p00591
Monteiro, C. E., Cardeira, S., Cravo, A., Bebianno, M. J., Sánchez, R. F., & Relvas, P. (2015). Influence of an upwelling filament on the distribution of labile fraction of dissolved Zn, Cd and Pb off Cape São Vicente, SW Iberia. *Continental Shelf Research*, *94*, 28–41. https://doi.org/10.1016/j.csr.2014.12.004
Moore, W. S. (2000). Determining coastal mixing rates using radium isotopes. *Continental Shelf Research*, *20*(15), 1993–2007. https://doi.org/10.1016/S0278-4343(00)00054-6
Moore, W. S. (2008). Fifteen years experience in measuring ^{224}Ra and ^{223}Ra by delayed-coincidence counting. *Marine Chemistry*, *109*(3–4), 188–197. https://doi.org/10.1016/j.marchem.2007.06.015
Moore, W. S., & Arnold, R. (1996). Measurement of ^{223}Ra and ^{224}Ra in coastal waters using a delayed coincidence counter. *Journal of Geophysical Research*, *101*(C1), 1321–1329. https://doi.org/10.1029/95JC03139
Morton, P. L., Landing, W. M., Hsu, S.-C., Milne, A., Aguilar-Islas, A. M., Baker, A. R., et al. (2013). Methods for the sampling and analysis of marine aerosols: Results from the 2008 GEOTRACES aerosol intercalibration experiment. *Limnology and Oceanography: Methods*, *11*(2), 62–78. https://doi.org/10.4319/lom.2013.11.62
Muller, F. L. L. (1996). Interactions of copper, lead and cadmium with dissolved colloidal and particulate components of estuarine and coastal waters. *Marine Chemistry*, *52*.
Muller, F. L. L., Tappin, A. D., Statham, P. J., Burton, J. D., & Hydes, D. J. (1994). Trace metal fronts in waters of the Celtic Sea. *Oceanologica Acta*, *17*, 383–396.
Noble, A. E., Echegoyen-Sanz, Y., Boyle, E. A., Ohnemus, D. C., Lam, P. J., Kayser, R., et al. (2015). Dynamic variability of dissolved Pb and Pb isotope composition from the U.S. North Atlantic GEOTRACES transect. *Deep-Sea Research Part II: Topical Studies in Oceanography*, *116*, 208–225. https://doi.org/10.1016/j.dsr2.2014.11.011

Nozaki, Y., & Tsunogai, S. (1976). ^{226}Ra, ^{210}Pb and ^{210}Po disequilibria in the western North Pacific. *Earth and Planetary Science Letters*, *32*(2), 313–321. https://doi.org/10.1016/0012-821X(76)90071-6

Nriagu, J. O., & Pacyna, J. M. (1988). Quantitative assessment of worldwide contamination of air, water and soils by trace metals. *Nature*, *333*(6169), 134–139. https://doi.org/10.1038/333134a0

Obata, H., Karatani, H., & Nakayama, E. (1993). Automated determination of iron in seawater by chelating resin concentration and chemiluminescence detection. *Analytical Chemistry*, *65*(11), 1524–1528. https://doi.org/10.1021/ac%2000059a007

Ohnemus, D. C., Auro, M. E., Sherrell, R. M., Lagerström, M., Morton, P. L., Twining, B. S., et al. (2014). Laboratory intercomparison of marine particulate digestions including piranha: A novel chemical method for dissolution of polyethersulfone filters. *Limnology and Oceanography: Methods*, *12*(8), 530–547. https://doi.org/10.4319/lom.2014.12.530

Olsen, A., Key, R. M., van Heuven, S., Lauvset, S. K., Velo, A., Lin, X., et al. (2016). The Global Ocean Data Analysis Project version 2 (GLODAPv2)—An internally consistent data product for the world ocean. *Earth System Science Data*, *8*(2), 297–323. https://doi.org/10.5194/essd-8-297-2016

Pohl, C., Croot, P. L., Hennings, U., Daberkow, T., Budeus, G., & v.d. Loeff, M. R. (2011). Synoptic transects on the distribution of trace elements (Hg, Pb, Cd, Cu, Ni, Zn, Co, Mn, Fe, and Al) in surface waters of the Northern- and Southern East Atlantic. *Journal of Marine Systems*, *84*(1–2), 28–41. https://doi.org/10.1016/j.jmarsys.2010.08.003

Pollard, R. T., Read, J. F., Holliday, N. P., & Leach, H. (2004). Water masses and circulation pathways through the Iceland Basin during Vivaldi 1996. *Journal of Geophysical Research*, *109*, C04004. https://doi.org/10.1029/2003JC002067

Prego, R., Santos-Echeandía, J., Bernárdez, P., Cobelo-García, A., & Varela, M. (2013). Trace metals in the NE Atlantic coastal zone of Finisterre (Iberian peninsula): Terrestrial and marine sources and rates of sedimentation. *Journal of Marine Systems*, *126*, 69–81. https://doi.org/10.1016/j.jmarsys.2012.05.008

Rapp, I., Schlosser, C., Rusiecka, D., Gledhill, M., & Achterberg, E. P. (2017). Automated preconcentration of Fe, Zn, Cu, Ni, Cd, Pb, Co, and Mn in seawater with analysis using high-resolution sector field inductively-coupled plasma mass spectrometry. *Analytica Chimica Acta*, *976*, 1–13. https://doi.org/10.1016/j.aca.2017.05.008

Rivera-Duarte, I., & Flegal, A. R. (1994). Benthic lead fluxes in San Francisco Bay, California, USA. *Geochimica et Cosmochimica Acta*, *58*(15), 3307–3313. https://doi.org/10.1016/0016-7037(94)90059-0

Rolison, J. M. (2016). *The biogeochemistry of trace metals and their isotopes in the Mediterranean and Black Seas* (Doctoral dissertation thesis). University of Otago.

Rolison, J. M., Middag, R., Stirling, C. H., Rijkenberg, M. J. A., & de Baar, H. J. W. (2015). Zonal distribution of dissolved aluminium in the Mediterranean Sea. *Marine Chemistry*, *177*, 87–100. https://doi.org/10.1016/j.marchem.2015.05.001

Ryan, W. B. F., Carbotte, S. M., Coplan, J. O., O'Hara, S., Melkonian, A., Arko, R., et al. (2009). Global multi-resolution topography synthesis. *Geochemistry, Geophysics, Geosystems*, *10*, Q03014. https://doi.org/10.1029/2008GC002332

Sañudo-Wilhelmy, S. A., & Flegal, A. R. (1994). Temporal variations in lead concentrations and isotopic composition in the Southern California Bight. *Geochimica et Cosmochimica Acta*, *58*(15), 3315–3320. https://doi.org/10.1016/0016-7037(94)90060-4

Schaule, B. K., & Patterson, C. C. (1983). In C. S. Wong, et al. (Eds.), *Perturbations of the natural lead depth profile in the Sargasso Sea by industrial lead BT trace metals in sea water* (pp. 487–503). Boston, MA: Springer US. https://doi.org/10.1007/978-1-4757-6864-0_29

Schlitzer, R. (2015). Ocean Data View. Retrieved from http://odv.awi.de. http://odv.awi.de

Sen, T. K., & Khilar, K. C. (2006). Review on subsurface colloids and colloid-associated contaminant transport in saturated porous media. *Advances in Colloid and Interface Science*, *119*(2–3), 71–96. https://doi.org/10.1016/j.cis.2005.09.001

Sherrell, R. M., Boyle, E. A., & Hamelin, B. (1992). Isotopic equilibration between dissolved and suspended particulate lead in the Atlantic Ocean: Evidence from ^{210}Pb and stable Pb isotopes. *Journal of Geophysical Research*, *97*(C7), 11,257–11,268. https://doi.org/10.1029/92JC00759

Sun, Y., & Torgersen, T. (1998). The effects of water content and Mn-fiber surface conditions on measurement by emanation. *Marine Chemistry*, *62*(3-4), 299–306. https://doi.org/10.1016/S0304-4203(98)00019-X

Talley, L. D., & McCartney, M. S. (1982). Distribution and circulation of Labrador Sea Water. *Journal of Physical Oceanography*, *12*(11), 1189–1205. https://doi.org/10.1175/1520-0485(1982)012%3C1189:DACOLS%3E2.0.CO;2

Véron, A. J., & Church, T. M. (1997). Use of stable lead isotopes and trace metals to characterize air mass sources into the eastern North Atlantic. *Journal of Geophysical Research*, *102*(D23), 28,049–28,058. https://doi.org/10.1029/97JD01527

Waeles, M., Riso, R. D., Maguer, J. F., Guillaud, J. F., & Le Corre, P. (2008). On the distribution of dissolved lead in the Loire estuary and the North Biscay continental shelf, France. *Journal of Marine Systems*, *72*(1–4), 358–365. https://doi.org/10.1016/j.jmarsys.2007.01.012

Waugh, D. W., Hall, T. M., & Haine, T. W. N. (2003). Relationships among tracer ages. *Journal of Geophysical Research*, *108*(C5), 3138. https://doi.org/10.1029/2002JC001325

Wu, J. F., & Boyle, E. A. (1997). Lead in the western North Atlantic Ocean: Completed response to leaded gasoline phaseout. *Geochimica et Cosmochimica Acta*, *61*(15), 3279–3283. https://doi.org/10.1016/s0016-7037(97)89711-6

Wu, J., Rember, R., Jin, M., Boyle, E. A., & Flegal, A. R. (2010). Isotopic evidence for the source of lead in the North Pacific abyssal water. *Geochimica et Cosmochimica Acta*, *74*(16), 4629–4638. https://doi.org/10.1016/j.gca.2010.05.017

Zago, C., Capodaglio, G., Ceradini, S., Ciceri, G., Abelmoschi, L., Soggia, F., et al. (2000). Benthic fluxes of cadmium, lead, copper and nitrogen species in the northern Adriatic Sea in front of the river Po outflow, Italy. *Science of the Total Environment*, *246*(2–3), 121–137. https://doi.org/10.1016/S0048-9697(99)00421-0

Zurbrick, C. M., Boyle, E. A., Kayser, R., Reuer, M. K., Wu, J., Planquette, H., et al. (2018). Dissolved Pb and Pb isotopes in the North Atlantic from the GEOVIDE transect (GEOTRACES GA-01) and their decadal evolution. *Biogeosciences Discussions*, 1–34. https://doi.org/10.5194/bg-2018-29

References

Abraham, M.R. & Susan, T.B., 2017. Water contamination with heavy metals and trace elements from Kilembe copper mine and tailing sites in Western Uganda; implications for domestic water quality. *Chemosphere*, 169, pp.281–287.

Achterberg, E.P. et al., 2001. Determination of iron in seawater. *Analytica Chimica Acta*, 442(1), pp.1–14.

Achterberg, E.P. et al., 2018. Iron Biogeochemistry in the High Latitude North Atlantic Ocean. *Scientific Reports*, 8(1), p.1283.

Achterberg, E.P. et al., 2013. Natural iron fertilization by the Eyjafjallajökull volcanic eruption. *Geophysical Research Letters*, 40(5), pp.921–926.

Achterberg, E.P., Colombo, C. & van den Berg, C.M.G., 1999. The distribution of dissolved Cu, Zn, Ni, Co and Cr in English coastal surface waters. *Continental Shelf Research*, 19(4), pp.537–558.

Allen, J.R.L., Rae, J.E. & Zanin, P.E., 1990. Metal Speciation (Cu,Zn,Pb) and Organic-Matter in an Oxic Salt- Marsh, Severn Estuary, Southwest Britain. *Marine Pollution Bulletin*, 21(12), pp.574–580.

Anderson, R. et al., 2014. GEOTRACES: Changing the Way We Explore Ocean Chemistry. *Oceanography*, 27(1), pp.50–61.

Annett, A.L. et al., 2013. Use of radium isotopes to estimate mixing rates and trace sediment inputs to surface waters in northern Marguerite Bay, Antarctic Peninsula. *Antarctic Science*, 25(3), pp.445–456.

Annibaldi, A. et al., 2009. Recent sudden decrease of lead in Adriatic coastal seawater during the years 2000-2004 in parallel with the phasing out of leaded gasoline in Italy. *Marine Chemistry*, 113(3–4), pp.238–249.

Antia, A.N., von Bodungen, B. & Peinert, R., 1999. Particle flux across the mid-European continental margin. *Deep Sea Research Part I: Oceanographic Research Papers*, 46(12), pp.1999–2024.

Apte, S.C. et al., 1990. Trace metals in the Severn estuary: a reappraisal. *Marine Pollution Bulletin*, 21(8), pp.393–396.

Arimoto, R. et al., 2003. Dry deposition of trace elements to the western North Atlantic. *Global Biogeochemical Cycles*, 17(1), p.n/a-n/a.

Atkinson, C.A., Jolley, D.F. & Simpson, S.L., 2007. Effect of overlying water pH, dissolved oxygen, salinity and sediment disturbances on metal release and sequestration from metal contaminated marine sediments. *Chemosphere*, 69(9), pp.1428–1437.

Bacon, M.P. & Anderson, R.F., 1982. Distribution of thorium isotopes between dissolved and particulate forms in the deep sea. *Journal of Geophysical Research: Oceans*, 87(C3), pp.2045–2056.

Bacon, M.P., Spencer, D.W. & Brewer, P.G., 1976. 210Pb/226Ra and 210Po/210Pb diequilibria in seawater and suspended particulate matter. *Earth and Planetary Science Letters*, 32, pp.277–296.

Baker, A.R. et al., 2013. Estimation of atmospheric nutrient inputs to the Atlantic Ocean from 50°N to 50°S based on large-scale field sampling: Iron and other dust-associated elements. *Global Biogeochemical Cycles*, 27(3), pp.755–767.

Banza, C.L.N. et al., 2009. High human exposure to cobalt and other metals in Katanga, a mining area of the Democratic Republic of Congo. *Environmental Research*, 109(6), pp.745–752.

Bastami, K.D. et al., 2015. Heavy metal pollution assessment in relation to sediment properties in the coastal sediments of the southern Caspian Sea. *Marine Pollution Bulletin*, 92(1–2), pp.237–243.

Beaulieu, S.E., Baker, E.T. & German, C.R., 2015. Where are the undiscovered hydrothermal vents on oceanic spreading ridges? *Deep Sea Research Part II: Topical Studies in Oceanography*, 121, pp.202–212.

Bellanco, M.J. & Sánchez-Leal, R.F., 2016. Spatial distribution and intra-annual variability of water masses on the Eastern Gulf of Cadiz seabed. *Continental Shelf Research*, 128, pp.26–35.

Berelson, W. et al., 2003. A time series of benthic flux measurements from Monterey Bay, CA. *Continental Shelf Research*, 23(5), pp.457–481.

Berger, C.J.M. et al., 2008. Application of a chemical leach technique for estimating labile particulate aluminum, iron, and manganese in the Columbia River plume and coastal waters off Oregon and Washington. *Journal of Geophysical Research*, 113, p.C00B01.

Biller, D. V. & Bruland, K.W., 2013a. Sources and distributions of Mn, Fe, Co, Ni, Cu, Zn, and Cd relative to macronutrients along the central California coast during the spring and summer upwelling season. *Marine Chemistry*, 155, pp.50–70.

Biller, D. V. & Bruland, K.W., 2013b. Sources and distributions of Mn, Fe, Co, Ni, Cu, Zn,

and Cd relative to macronutrients along the central California coast during the spring and summer upwelling season. *Marine Chemistry*, 155, pp.50–70.

Birchill, A., 2017. *The seasonal cycling and physico-chemical speciation of iron in the Celtic and Hebridean shelf seas*. (Doctoral dissertation thesis). University of Plymouth.

Birchill, A.J. et al., 2017. Seasonal iron depletion in temperate shelf seas. *Geophysical Research Letters*, 44(17), pp.8987–8996.

Bollhöfer, A. & Rosman, K.J.R., 2001. Isotopic source signatures for atmospheric lead: The Northern Hemisphere. *Geochimica et Cosmochimica Acta*, 65(11), pp.1727–1740.

Bourillet, J.-F. et al., 2003. The "Fleuve Manche": the submarine sedimentary features from the outer shelf to the deep-sea fans. *Journal of Quaternary Science*, 18(3–4), pp.261–282.

Bown, J. et al., 2012. Imprint of a dissolved cobalt basaltic source on the Kerguelen Plateau. *Biogeosciences*, 9(12), pp.5279–5290.

Boyd, P.W. & Ellwood, M.J., 2010a. The biogeochemical cycle of iron in the ocean. *Nature Geoscience*, 3(10), pp.675–682.

de Boyer Montégut, C. et al., 2004. Mixed layer depth over the global ocean: An examination of profile data and a profile-based climatology. *Journal of Geophysical Research: Oceans*, 109(C12), p.n/a-n/a.

Boyle, E. et al., 2014. Anthropogenic Lead Emissions in the Ocean: The Evolving Global Experiment. *Oceanography*, 27(1), pp.69–75.

Boyle, E.A., 1988. Cadmium: Chemical tracer of deepwater paleoceanography. *Paleoceanography*, 3(4), pp.471–489.

Boyle, E.A., Edmond, J.M. & Sholkovitz, E.R., 1977. The mechanism of iron removal in estuaries. *Geochimica et Cosmochimica Acta*, 41(9), pp.1313–1324.

Boyle, E.A., Sclater, F. & Edmond, J.M., 1976. On the marine geochemistry of cadmium. *Nature*, 263, p.42.

Brand, L.E., Sunda, W.G. & Guillard, R.R.L., 1986. Reduction of marine phytoplankton reproduction rates by copper and cadmium. *Journal of Experimental Marine Biology and Ecology*, 96(3), pp.225–250.

Bridgestock, L. et al., 2016. Return of naturally sourced Pb to Atlantic surface waters. *Nature Communications*, 7, p.12921.

Bridgestock, L. et al., 2018. The distribution of lead concentrations and isotope compositions in the eastern Tropical Atlantic Ocean. *Geochimica et Cosmochimica*

Acta, 225, pp.36–51.

Browning, T.J. et al., 2017. Nutrient co-limitation at the boundary of an oceanic gyre. *Nature*, 551(7679), pp.242–246.

Browning, T.J. et al., 2014. Strong responses of Southern Ocean phytoplankton communities to volcanic ash. *Geophysical Research Letters*, 41(8), pp.2851–2857.

Brügmann, L. et al., 1985. Lead in the North Sea and the north east Atlantic Ocean. *Marine Chemistry*, 16(1), pp.47–60.

Bruland, K.W., 1992. Complexation of cadmium by natural organic ligands in the central North Pacific. *Limnology and Oceanography*, 37(5), pp.1008–1017.

Bruland, K.W., 1989. Complexation of zinc by natural organic ligands in the central North Pacific. *Limnology and Oceanography*, 34(2), pp.269–285.

Bruland, K.W., 1980. Oceanographic distributions of cadmium, zinc, nickel, and copper in the North Pacific. *Earth and Planetary Science Letters*, 47(2), pp.176–198.

Bruland, K.W., Knauer, G.A. & Martin, J.H., 1978. Cadmium in northeast Pacific waters. *Limnology and Oceanography*, 23(4), pp.618–625.

Bruland, K.W. & Lohan, M.C., 2004. Controls of trace metals in seawater. *The oceans and marine geochemistry*, 6, pp.23–47.

Buck, K.N. & Bruland, K.W., 2005. Copper speciation in San Francisco Bay: A novel approach using multiple analytical windows. *Marine Chemistry*, 96(1–2), pp.185–198.

Burt, W.J. et al., 2014. Radium isotopes as a tracer of sediment-water column exchange in the North Sea. *Global Biogeochemical Cycles*, pp.786–804.

Carter, G.S. & Gregg, M.C., 2002. Intense, Variable Mixing near the Head of Monterey Submarine Canyon. *Journal of Physical Oceanography*, 32(11), pp.3145–3165.

Charette, M.A. et al., 2016. Coastal ocean and shelf-sea biogeochemical cycling of trace elements and isotopes: lessons learned from GEOTRACES. *Philosophical Transactions of the Royal Society A: Mathematical, Physical and Engineering Sciences*, 374(2081), p.20160076.

Chen, M., Goodkin, N.F., et al., 2016. Lead in the western South China Sea: Evidence of atmospheric deposition and upwelling. *Geophys.Res.Lett.*, pp.4490–4499.

Chen, M., Boyle, E.A., et al., 2016. Lead isotope exchange between dissolved and fluvial particulate matter: a laboratory study from the Johor River estuary. *Philosophical Transactions of the Royal Society A: Mathematical, Physical and Engineering Sciences*, 374(2081), p.20160054.

Chien, C. Te et al., 2017. Lead concentrations and isotopic compositions in the Western Philippine Sea. *Marine Chemistry*, 189, pp.10–16.

Coale, K.H. & Bruland, K.W., 1988. Copper complexation in the Northeast Pacific. *Limnology and Oceanography*, 33(5), pp.1084–1101.

Cotté-Krief, M.-H., Thomas, A.J. & Martin, J.-M., 2002. Trace metal (Cd, Cu, Ni and Pb) cycling in the upper water column near the shelf edge of the European continental margin (Celtic Sea). *Marine Chemistry*, 79(1), pp.1–26.

Cullen, J.T. et al., 2003. Effect of iron limitation on the cadmium to phosphorus ratio of natural phytoplankton assemblages from the Southern Ocean. *Limnology and Oceanography*, 48(3), pp.1079–1087.

Cullen, J.T., 2006. On the nonlinear relationship between dissolved cadmium and phosphate in the modern global ocean: Could chronic iron limitation of phytoplankton growth cause the kink? *Limnology and Oceanography*, 51(3), pp.1369–1380.

Cutter, G. et al., 2010. Sampling and Sample-handling Protocols for GEOTRACES Cruises. , (December).

Von Damm, K.L. et al., 1985. Chemistry of submarine hydrothermal solutions at 21 °N, East Pacific Rise. *Geochimica et Cosmochimica Acta*, 49(11), pp.2197–2220.

Danielsson, L., Magnusson, B. & Westerlund, S., 1985. Cadmium, copper, iron, nickel and zinc in the north-east Atlantic Ocean. *Marine Chemistry*, 17(1), pp.23–41.

Delgado, J. et al., 2011. Speciation and ecological risk of toxic elements in estuarine sediments affected by multiple anthropogenic contributions (Guadiana saltmarshes, SW Iberian Peninsula): I. Surficial sediments. *Science of The Total Environment*, 409(19), pp.3666–3679.

Dickson, R.R., 1986. Nepheloid layers on the continental slope west of Porcupine Bank. *Deep Sea Research Part B. Oceanographic Literature Review*, 33(12), p.1012.

Dixon, J.L. et al., 2006. Cadmium uptake by marine micro-organisms in the English Channel and Celtic Sea. *Aquatic microbial ecology*, 44(1), pp.31–43.

Dulaquais, G. et al., 2014. Physical and remineralization processes govern the cobalt distribution in the deep western Atlantic Ocean. *Biogeosciences*, 11(6), pp.1561–1580.

Echegoyen, Y. et al., 2014. Recent distribution of lead in the Indian Ocean reflects the impact of regional emissions. , 111(43), pp.15328–15331.

Eckel, W.P., Rabinowitz, M.B. & Foster, G.D., 2002. Investigation of unrecognized former secondary lead smelting sites: confirmation by historical sources and elemental ratios in soil. *Environmental Pollution*, 117(2), pp.273–279.

Economic Commission for Europe, 2014. *Convention on Long-range Transboundary Air Pollution*, Geneva, 52nd session, 30 June–3 July 2014.

Edmond, J.M. et al., 1979. Ridge crest hydrothermal activity and the balances of the major and minor elements in the ocean: The Galapagos data. *Earth and Planetary Science Letters*, 46(1), pp.1–18.

Elderfield, H. & Rickaby, R.E.M., 2000. Oceanic Cd / P ratio and nutrient utilization in the glacial Southern Ocean. *Nature*, 405(May).

Ellwood, M.J. & Van den Berg, C.M.G., 2000. Zinc speciation in the Northeastern Atlantic Ocean. *Marine Chemistry*, 68(4), pp.295–306.

Elrod, V. et al., 2004. The flux of iron from continental shelf sediments: A missing source for global budgets. *Geophysical Research Letters*, 31(12), p.L12307.

Emerson, S. et al., 1982. Environmental oxidation rate of manganese(II): bacterial catalysis. *Geochimica et Cosmochimica Acta*, 46(6), pp.1073–1079.

European Communities, 1978. Council Directive 78/611/EEC of 29 June 1978 on the approximation of the laws of the Member States concerning the lead content of petrol. *Official Journal of the European Communities*, L 197, pp.19–21.

European Environment Agency, 2017. *Air quality in Europe — 2017 report*,

Falkowski, P.G., 2000. Rationalizing elemental ratios in unicellular algae. *Journal of Phycology*, 36(1), pp.3–6.

Fernex, F. et al., 1992. Copper, lead and zinc trapping in Mediterranean deep-sea sediments: probable coprecipitation with Mn and Fe. *Chemical Geology*, 98(3–4), pp.293–306.

Ferrari, G.M. & Ferrario, P., 1989. Behavior of Cd, Pb, and Cu in the marine deltaic area of the Po River (North Adriatic Sea). *Water, Air, and Soil Pollution*, 43(3), pp.323–343.

Fine, R.A., 2010. Observations of CFCs and SF6 as Ocean Tracers. *Annual Review of Marine Science*, 3(1), pp.173–195.

Finkel, Z. V et al., 2007. Phylogenetic diversity in cadmium : phosphorus ratio regulation by marine phytoplankton. *Limnology and Oceanography*, 52(3), pp.1131–1138.

Froelich, P.N. et al., 1979. Early oxidation of organic matter in pelagic sediments of the eastern equatorial Atlantic: suboxic diagenesis. *Geochimica et Cosmochimica Acta*,

43(7), pp.1075–1090.

Gaillardet, J., Viers, J. & Dupré, B., 2003. Trace Elements in River Waters. In *Surface and Groundwater Weathering and Soils*. Amsterdam: Elsevier, pp. 225–272.

Le Gall, A.C. et al., 1999. Processes influencing distributions and concentrations of Cd, Cu, Mn and Ni at the North West European shelf break. *Marine Chemistry*, 68(1–2), pp.97–115.

Gallon, C. et al., 2011. Asian Industrial Lead Inputs to the North Pacific Evidenced by Lead Concentrations and Isotopic Compositions in Surface Waters and Aerosols. *Environmental Science & Technology*, 45(23), pp.9874–9882.

García-Ibáñez, M.I. et al., 2015. Structure, transports and transformations of the water masses in the Atlantic Subpolar Gyre. *Progress in Oceanography*, 135, pp.18–36.

Garcia-Ordiales, E. et al., 2017. Trace metal pollution in freshwater sediments of the world's largest mercury mining district: sources, spatial distribution, and environmental implications. *Journal of Soils and Sediments*, 17(7), pp.1893–1904.

Garcia-Solsona, E. et al., 2008. Uncertainties associated with 223Ra and 224Ra measurements in water via a Delayed Coincidence Counter (RaDeCC). *Marine Chemistry*, 109(3–4), pp.198–219.

Gardner, W.D. et al., 2017. Benthic storms, nepheloid layers, and linkage with upper ocean dynamics in the western North Atlantic. *Marine Geology*, 385, pp.304–327.

Gardner, W.D., 1989. Periodic resuspension in Baltimore canyon by focusing of internal waves. *Journal of Geophysical Research: Oceans*, 94(C12), pp.18185–18194.

Gehlen, M. et al., 2002. Unraveling the atomic structure of biogenic silica: evidence of the structural association of Al and Si in diatom frustules. *Geochimica et Cosmochimica Acta*, 66(9), pp.1601–1609.

German, C.R., Campbell, A.C. & Edmond, J.M., 1991. Hydrothermal scavenging at the Mid-Atlantic Ridge: Modification of trace element dissolved fluxes. *Earth and Planetary Science Letters*, 107(1), pp.101–114.

Gledhill, M. et al., 1997. The toxicity of copper (II) species to marine with particular reference to macroalgae. *Journal of Phycology*, 33(1), pp.2–11.

Gledhill, M. & van den Berg, C.M.G., 1994. Determination of complexation of iron(III) with natural organic complexing ligands in seawater using cathodic stripping voltammetry. *Marine Chemistry*, 47(1), pp.41–54.

Gustafsson, Ö. et al., 2000. Colloid dynamics and transport of major elements through a

boreal river — brackish bay mixing zone. *Marine Chemistry*, 71(1), pp.1–21.

Halpern, B.S. et al., 2008. A Global Map of Human Impact on Marine Ecosystems. *Science*, 319(5865), p.948 LP-952.

Harris, P.T. et al., 2014. Geomorphology of the oceans. *Marine Geology*, 352, pp.4–24.

Hatta, M. et al., 2015. Deep-Sea Research II An overview of dissolved Fe and Mn distributions during the 2010 – 2011 U . S . GEOTRACES north Atlantic cruises : GEOTRACES GA03. *Deep-Sea Research Part II*, 116, pp.117–129.

Heggie, D. & Lewis, T., 1984. Cobalt in pore waters of marine sediments. *Nature*, 311, p.453.

Helmers, E. & Van der Loeff, M.M.R., 1993. Lead and aluminum in Atlantic surface waters (50 degree N to 50 degree S) reflecting anthropogenic and natural sources in the eolian transport. *Journal of Geophysical Research*, 98(C11), pp.20261–20273.

Henderson, G.M. & Maier-Reimer, E., 2002. Advection and removal of 210Pb and stable Pb isotopes in the ocean: A general circulation model study. *Geochim. Cosmochim. Acta*, 66(2), pp.257–272.

Ho, T.-Y. et al., 2003. The elemental composition of some marine phytoplankton. *Journal of Phycology*, 39(6), pp.1145–1159.

Homoky, W.B. et al., 2013. Distinct iron isotopic signatures and supply from marine sediment dissolution. *Nature Communications*, 4, pp.1–10.

Homoky, W.B. et al., 2011. Iron and manganese diagenesis in deep sea volcanogenic sediments and the origins of pore water colloids. *Geochimica et Cosmochimica Acta*, 75(17), pp.5032–5048.

Homoky, W.B. et al., 2016. *Quantifying trace element and isotope fluxes at the ocean–sediment boundary: a review*,

Hong, Y.S., Kinney, K.A. & Reible, D.D., 2011. Effects of cyclic changes in pH and salinity on metals release from sediments. *Environmental Toxicology and Chemistry*, 30(8), pp.1775–1784.

Hotchkiss, F.S. & Wunsch, C., 1982. Internal waves in Hudson Canyon with possible geological implications. *Deep Sea Research Part A. Oceanographic Research Papers*, 29(4), pp.415–442.

Howard, A.G., 2005. *Aquatic Environmental Chemistry* 3rd ed., New York: Oxford Chemistry Primers.

Hupe, A. & Karstensen, J., 2000. Redfield stoichiometry in Arabian Sea subsurface waters.

Global Biogeochemical Cycles, 14(1), pp.357–372.

Hutchins, D.A. & Bruland, K.W., 1994. Grazer-mediated regeneration and assimilation of Fe, Zn and Mn from planktonic prey. *Marine Ecology Progress Series*, 110(2–3), pp.259–270.

Huthnance, J.M., 1984. Slope Currents and "JEBAR." *Journal of Physical Oceanography*, 14(4), pp.795–810.

Hydes, D.J. et al., 2010. Determination of dissolved nutrients (N, P, Si) in seawater with high precision and inter-comparability using gas-segmented continuous flow analysers. *In The GO-SHIP Repeat Hydrography Manual : A Collection of Expert Reports and guidelines.*, IOCCP No 1(OCPO Publication Series No. 134, version 1), pp.1–87.

Hydes, D.J. et al., 2004. External and internal control of winter concentrations of nutrients (N, P and Si) in north-west European shelf seas. *Estuarine, Coastal and Shelf Science*, 59(1), pp.151–161.

Hydes, D.J. & Liss, P.S., 1976. Fluorimetric method for the determination of low concentrations of dissolved aluminium in natural waters. *Analyst*, 101(922), pp.922–931.

Jabłońska-Czapla, M. et al., 2016. Impact of the Pb and Zn ore mining industry on the pollution of the Biała Przemsza River, Poland. *Environmental Monitoring and Assessment*, 188(5), p.262.

Jacquot, J.E. & Moffett, J.W., 2015. Copper distribution and speciation across the International GEOTRACES Section GA03. *Deep Sea Research Part II: Topical Studies in Oceanography*, 116, pp.187–207.

Jickells, T.D., 2005. Global Iron Connections Between Desert Dust, Ocean Biogeochemistry, and Climate. *Science*, 308(5718), pp.67–71.

Jickells, T.D., Baker, A.R. & Chance, R., 2016. Atmospheric transport of trace elements and nutrients to the oceans Subject Areas :

John, S.G. & Conway, T.M., 2014. A role for scavenging in the marine biogeochemical cycling of zinc and zinc isotopes. *Earth and Planetary Science Letters*, 394, pp.159–167.

Johnson, K.S. et al., 1992. Manganese Flux from Continental Margin Sediments in a Transect Through the Oxygen Minimum. *Science*, 257(5074), pp.1242–1245.

de Jong, J.T.M., van den Berg, C.M.G., et al., 2007. Inputs of iron, manganese and

aluminium to surface waters of the Northeast Atlantic Ocean and the European continental shelf. *Marine Chemistry*, 107(2), pp.120–142.

de Jong, J.T.M., Boyé, M., et al., 2007. Inputs of iron, manganese and aluminium to surface waters of the Northeast Atlantic Ocean and the European continental shelf. *Marine Chemistry*, 107(2), pp.120–142.

Kagaya, S. et al., 2009. A solid phase extraction using a chelate resin immobilizing carboxymethylated pentaethylenehexamine for separation and preconcentration of trace elements in water samples. *Talanta*, 79(2), pp.146–152.

Kalnejais, L.H. et al., 2007. Role of sediment resuspension in the remobilization of particulate-phase metals from coastal sediments. *Environmental Science and Technology*, 41(7), pp.2282–2288.

Karstensen, J. & Tomczak, M., 1998. Age determination of mixed water masses using CFC and oxygen data. *Journal of Geophysical Research: Oceans*, 103(C9), pp.18599–18609.

Kelly, A.E. et al., 2009. Lead concentrations and isotopes in corals and water near Bermuda , 1780 – 2000. *Earth and Planetary Science Letters*, 283(1–4), pp.93–100.

Kim, J.H., Gibb, H.J. & Howe, P.D., 2006. *Cobalt and inorganic cobalt compounds. Concise International Chemical Assessment Document 69 of the World Health Organization*,

Klar, J.K. et al., 2017. Stability of dissolved and soluble Fe(II) in shelf sediment pore waters and release to an oxic water column. *Biogeochemistry*.

Komárek, M. & Zeman, J., 2004. Dynamics of Cu, Zn, Cd, and Hg release from sediments at surface conditions. *Bulletin of Geosciences*, 79(2), pp.99–106.

Kremling, K. & Hydest, D., 1988. Summer distribution of dissolved Al , Cd , Co , Cu , Mn and Ni in surface waters around the British Isles. *Continental Shelf Research*, 8(l), pp.89–105.

Kremling, K. & Pohl, C., 1989. Studies on the Spatial and Seasonal Variability of Dissolved Cadmium , Copper and Nickel in North-. , 27, pp.43–60.

Kremling, K. & Streu, P., 2001. The behaviour of dissolved Cd, Co, Zn, and Pb in North Atlantic near-surface waters (30° N/60° W - 60° N/2° W). *Deep Sea Res. I*, 48, pp.2541–2567.

Kumar, A. et al., 2014. A radiogenic isotope tracer study of transatlantic dust transport from Africa to the Caribbean. *Atmospheric Environment*, 82, pp.130–143.

Kunze, E. et al., 2002. Internal Waves in Monterey Submarine Canyon. *Journal of Physical*

Oceanography, 32(6), pp.1890–1913.

L'vov, B. V, 1969. The potentialities of the graphite crucible method in atomic absorption spectroscopy. *Spectrochimica Acta Part B: Atomic Spectroscopy*, 24(1), pp.53–70.

Laës, A. et al., 2007. Sources and transport of dissolved iron and manganese along the continental margin of the Bay of Biscay. *Biogeosciences*, 4(2), pp.181–194.

Lagerström, M.E. et al., 2013. Automated on-line flow-injection ICP-MS determination of trace metals (Mn, Fe, Co, Ni, Cu and Zn) in open ocean seawater: Application to the GEOTRACES program. *Marine Chemistry*, 155, pp.71–80.

Lam, P.J., Ohnemus, D.C. & Auro, M.E., 2015. Size-fractionated major particle composition and concentrations from the US GEOTRACES North Atlantic Zonal Transect. *Deep-Sea Research Part II: Topical Studies in Oceanography*, 116, pp.303–320.

Lambert, C. et al., 1991. Anthropogenic Lead Cycle in the Northeastern Atlantic. *Oceanologica Acta*, 14(1), pp.59–66.

Landing, W.M. & Bruland, K.W., 1987. The contrasting biogeochemistry of iron and manganese in the Pacific Ocean. *Geochimica et Cosmochimica Acta*, 51(1), pp.29–43.

Landry, M. et al., 2000. Biological response to iron fertilization in the eastern equatorial Pacific (IronEx II). III. Dynamics of phytoplankton growth and microzooplankton grazing. *Marine Ecology Progress Series*, 201, pp.57–72.

Lane, T.W. et al., 2005. A cadmium enzyme from a marine diatom. *Nature*, 435, p.42.

Laumond, F. et al., 1984. Cadmium, copper and lead in the western Mediterranean Sea. *Marine Chemistry*, 15(3), pp.251–261.

Lee, J.M. et al., 2014. Coral-based history of lead and lead isotopes of the surface Indian Ocean since the mid-20th century. *Earth and Planetary Science Letters*, 398, pp.37–47.

Lee, J.M. et al., 2015. Impact of anthropogenic Pb and ocean circulation on the recent distribution of Pb isotopes in the Indian Ocean. *Geochimica et Cosmochimica Acta*, 170, pp.126–144.

Lee, Y. & Tebo, B.M., 1994. Cobalt(II) Oxidation by the Marine Manganese(II)-Oxidizing Bacillus sp. Strain SG-1. *Applied and Environmental Microbiology*, 60(8), pp.2949–2957.

Liu, X. & Millero, F.J., 2002. The solubility of iron in seawater. *Marine Chemistry*, 77(1), pp.43–54.

Lohan, M.C. & Bruland, K.W., 2008. Elevated Fe(II) and Dissolved Fe in Hypoxic Shelf

Waters off Oregon and Washington: An Enhanced Source of Iron to Coastal Upwelling Regimes. *Environmental Science & Technology*, 42(17), pp.6462–6468.

Longerich, H.P., 2012. Inductively Coupled Plasma-Mass Spectrometry (ICP-MS): a Personal Odyssey III. *Journal of Analytical Atomic Spectrometry*, 27(8), pp.1181–1184.

Luo, C. et al., 2008. Combustion iron distribution and deposition. *Global Biogeochemical Cycles*, 22(1), p.n/a-n/a.

Madison, A.S. et al., 2013. Abundant Porewater Mn(III) Is a Major Component of the Sedimentary Redox System. *Science*, 341(6148), p.875 LP-878.

Marani, D., Macchi, G. & Pagano, M., 1995. Lead precipitation in the presence of sulphate and carbonate: Testing of thermodynamic predictions. *Water Research*, 29(4), pp.1085–1092.

Martín-Torre, M.C. et al., 2015. Generalised mathematical model to estimate Zn, Pb, Cd, Ni, Cu, Cr and As release from contaminated estuarine sediment using pH-static leaching tests. *Chemical Engineering Science*, 138, pp.780–790.

Martín, J. et al., 2014. Trawling-induced daily sediment resuspension in the flank of a Mediterranean submarine canyon. *Deep Sea Research Part II: Topical Studies in Oceanography*, 104, pp.174–183.

Martin, J.H. & Fitzwater, S.E., 1988. Iron deficiency limits phytoplankton growth in the north-east Pacific subarctic. *Nature*, 331, pp.341–343.

Martin, J.H., Gordon, R.M. & Fitzwater, S.E., 1990. Iron in Antarctic waters. *Nature*, 345, p.156.

Mason, R.P., 2013. Metal(loid)s in the Atmosphere and their Inputs to Surface Waters. In *Trace Metals in Aquatic Systems*. John Wiley & Sons, Ltd, pp. 167–218.

Mawji, E. et al., 2015. The GEOTRACES Intermediate Data Product 2014. *Marine Chemistry*, 177(Part 1), pp.1–8.

Mayer, L.M., 1982. Retention of riverine iron in estuaries. *Geochimica et Cosmochimica Acta*, 46(6), pp.1003–1009.

Mayers, K.M.J. et al., 2018. Growth and mortality of coccolithophores during spring in a temperate Shelf Sea (Celtic Sea, April 2015). *Progress in Oceanography*.

McCartney, M., 1992. Recirculating components to the deep boundary current of the northeern North Atlantic. *Progress in Oceanography*, 29, pp.283–383.

McCave, I.N. et al., 2001. Distribution, composition and flux of particulate material over

the European margin at 47°–50°N. *Deep Sea Research Part II: Topical Studies in Oceanography*, 48(14), pp.3107–3139.

McCave, I.N. & Hall, I.R., 2002. Turbidity of waters over the Northwest Iberian continental margin. *Progress in Oceanography*, 52(2–4), pp.299–313.

McLaren, J.W., Beauchemin, D. & Berman, S.S., 1987. Application of Isotope Dilution Inductively Coupled Plasma Mass Spectrometry to the Analysis of Marine Sediments. *Anal. Chem. J . Chromatogr*, 5932(57), pp.610–613.

McManus, J. et al., 2012. Benthic manganese fluxes along the Oregon-California continental shelf and slope. *Continental Shelf Research*, 43, pp.71–85.

Measures, C. et al., 2015. Dissolved Al in the zonal N Atlantic section of the US GEOTRACES 2010/2011 cruises and the importance of hydrothermal inputs. *Deep-Sea Research Part II: Topical Studies in Oceanography*, 116, pp.176–186.

Measures, C.I. et al., 2008. High-resolution Al and Fe data from the Atlantic Ocean CLIVAR-CO2 Repeat Hydrography A16N transect: Extensive linkages between atmospheric dust and upper ocean geochemistry. *Global Biogeochemical Cycles*, 22(1), p.n/a-n/a.

Measures, C.I. & Edmond, J.M., 1988. Aluminium as a tracer of the deep outflow from the Mediterranean. *Journal of Geophysical Research: Oceans*, 93(C1), pp.591–595.

Measures, C.I. & Vink, S., 2000. On the use of dissolved aluminum in surface waters to estimate dust deposition to the ocean. *Global Biogeochemical Cycles*, 14(1), pp.317–327.

Menard, H.W. & Smith, S.M., 1966. Hypsometry of ocean basin provinces. *Journal of Geophysical Research*, 71(18), pp.4305–4325.

Menzel Barraqueta, J.-L. et al., 2018. Aluminium in the North Atlantic Ocean and the Labrador Sea (GEOTRACES GA01 section): roles of continental inputs and biogenic particle removal. *Biogeosciences Discuss.*, 2018, pp.1–28.

Metz, S. & Trefry, J.H., 1993. Field and laboratory studies of metal uptake and release by hydrothermal precipitates. *Journal of Geophysical Research: Solid Earth*, 98(B6), pp.9661–9666.

Middag, R. et al., 2015. Dissolved aluminium in the ocean conveyor of the West Atlantic Ocean: Effects of the biological cycle, scavenging, sediment resuspension and hydrography. *Marine Chemistry*, 177, pp.69–86.

Milne, A. et al., 2010b. Determination of Mn, Fe, Co, Ni, Cu, Zn, Cd and Pb in seawater

using high resolution magnetic sector inductively coupled mass spectrometry (HR-ICP-MS). *Analytica chimica acta*, 665(2), pp.200–7.

Milne, A. et al., 2017. Particulate phases are key in controlling dissolved iron concentrations in the (sub)tropical North Atlantic. *Geophysical Research Letters*, 44(5), pp.2377–2387.

Moffett, J.W. & Ho, J., 1996. Oxidation of cobalt and manganese in seawater via a common microbially catalyzed pathway. *Geochimica et Cosmochimica Acta*, 60(18), pp.3415–3424.

Monteiro, C.E. et al., 2015. Influence of an upwelling filament on the distribution of labile fraction of dissolved Zn, Cd and Pb off Cape São Vicente, SW Iberia. *Continental Shelf Research*, 94, pp.28–41.

Moore, C.M., Mills, M.M., Arrigo, K.R., Berman-Frank, I., Bopp, L., Boyd, P.W., Galbraith, E.D., Geider, R.J., Guieu, C., Jaccard, S.L., Jickells, T.D., Roche, J.L., et al., 2013. Processes and patterns of oceanic nutrient limitation. *Nature Geoscience*, 6(9), pp.701–710.

Moore, W.S., 2000. Determining coastal mixing rates using radium isotopes. *Continental Shelf Research*, 20(15), pp.1993–2007.

Moore, W.S., 2008. Fifteen years experience in measuring 224Ra and 223Ra by delayed-coincidence counting. *Marine Chemistry*, 109(3–4), pp.188–197.

Moore, W.S. & Arnold, R., 1996. Measurement of 223Ra and 224Ra in coastal waters using a delayed coincidence counter. *Journal of Geophysical Research: Oceans*, 101(C1), pp.1321–1329.

More, A.F. et al., 2017. Next-generation ice core technology reveals true minimum natural levels of lead (Pb) in the atmosphere: Insights from the Black Death. *GeoHealth*, 1(4), pp.211–219.

Morel, F.M.M. et al., 1994. Zinc and carbon co-limitation of marine phytoplankton. *Nature*, 369, p.740.

Morel, F.M.M., Milligan, A.J. & Saito, M.A., 2003. Marine Bioinorganic Chemistry : The Role of Trace Metals in the Oceanic Cycles of Major Nutrients. *Treatise on Geochemistry*, 6, pp.113–143.

Morris, A.W., 1984. The chemistry of the Severn Estuary and the Bristol Channel. *Marine Pollution Bulletin*, 15(2), pp.57–61.

Morton, P.L. et al., 2013. Methods for the sampling and analysis of marine aerosols:

results from the 2008 GEOTRACES aerosol intercalibration experiment. *Limnology and Oceanography: Methods*, 11(2), pp.62–78.

Muller-Karger, F.E. et al., 2005. The importance of continental margins in the global carbon cycle. *Geophysical Research Letters*, 32(1), p.n/a-n/a.

Muller, F.L.L., 1996. Interactions of copper, lead and cadmium with dissolved colloidal and particulate compoenents of estuarine and coastla waters. *Marine Chemistry*, 52, pp.245–268.

Muller, F.L.L. et al., 1994. Trace metal fronts in waters of the Celtic Sea. *Oceanologica Acta*, 17, pp.383–396.

Nédélec, F., Statham, P.J. & Mowlem, M., 2007. Processes influencing dissolved iron distributions below the surface at the Atlantic Ocean-Celtic Sea shelf edge. *Marine Chemistry*, 106, pp.365–379.

Nimmo, M., van den Berg, C.M.G. & Brown, J., 1989. The chemical speciation of dissolved nickel, copper, vanadium and iron in Liverpool Bay, Irish Sea. *Estuarine, Coastal and Shelf Science*, 29(1), pp.57–74.

Nimmo, M. & Chester, R., 1993. The chemical speciation of dissolved nickel and cobalt in Mediterranean rainwaters. *Science of The Total Environment*, 135(1), pp.153–160.

Noble, A.E. et al., 2012. Basin-scale inputs of cobalt, iron, and manganese from the Benguela-Angola front to the South Atlantic Ocean. *Limnology and Oceanography*, 57(4), pp.989–1010.

Noble, A.E. et al., 2017. Coastal sources, sinks and strong organic complexation of dissolved cobalt within the US North Atlantic GEOTRACES transect GA03. *Biogeosciences*, 14(11), pp.2715–2739.

Noble, A.E. et al., 2015. Dynamic variability of dissolved Pb and Pb isotope composition from the U.S. North Atlantic GEOTRACES transect. *Deep-Sea Research Part II: Topical Studies in Oceanography*, 116, pp.208–225.

Nozaki, Y., Thomson, J. & Turekian, K.K., 1976. The distribution of 210Pb and 210Po in the surface waters of the Pacific Ocean. *Earth and Planetary Science Letters*, 32(2), pp.304–312.

Nozaki, Y. & Tsunogai, S., 1976. 226Ra, 210Pb and 210Po disequilibria in the Western North Pacific. *Earth and Planetary Science Letters*, 32(2), pp.313–321.

Nriagu, J.O. & Pacyna, J.M., 1988. Quantitative assessment of worldwide contamination of air, water and soils by trace metals. *Nature*, 333, p.134.

Obata, H., Karatani, H. & Nakayama, E., 1993. Automated Determination of Iron in Seawater by Chelating Resin Concentration and Chemiluminescence Detection. *Analytical Chemistry*, 65(12), pp.1524–1528.

Ohnemus, D.C. et al., 2014. Laboratory intercomparison of marine particulate digestions including Piranha: a novel chemical method for dissolution of polyethersulfone filters. *Limnology and Oceanography: Methods*, 12(8), pp.530–547.

Olgun, N. et al., 2011. Surface ocean iron fertilization: The role of airborne volcanic ash from subduction zone and hot spot volcanoes and related iron fluxes into the Pacific Ocean. *Global Biogeochemical Cycles*, 25(4), p.n/a-n/a.

Olsen, A. et al., 2016. The Global Ocean Data Analysis Project version 2 (GLODAPv2) – an internally consistent data product for the world ocean. *Earth System Science Data*, 8(2), pp.297–323.

Orians, K.J. & Bruland, K.W., 1986. The biogeochemistry of aluminum in the Pacific Ocean. *Earth and Planetary Science Letters*, 78(4), pp.397–410.

Parker, D.L. et al., 2007. Inter-relationships of MnO2 precipitation, siderophore–Mn(III) complex formation, siderophore degradation, and iron limitation in Mn(II)-oxidizing bacterial cultures. *Geochimica et Cosmochimica Acta*, 71(23), pp.5672–5683.

Patey, M.D. et al., 2015. Aerosol time-series measurements over the tropical Northeast Atlantic Ocean: Dust sources, elemental composition and mineralogy. *Marine Chemistry*, 174, pp.103–119.

Peers, G. & Price, N.M., 2004. A role for manganese in superoxide dismutases and growth of iron-deficient diatoms. *Limnology and Oceanography*, 49(5), pp.1774–1783.

Pingree, R.D. & Le Cann, B., 1989. Celtic and Armorican slope and shelf residual currents. *Progress in Oceanography*, 23(4), pp.303–338.

Pohl, C. et al., 2011. Synoptic transects on the distribution of trace elements (Hg, Pb, Cd, Cu, Ni, Zn, Co, Mn, Fe, and Al) in surface waters of the Northern- and Southern East Atlantic. *Journal of Marine Systems*, 84(1–2), pp.28–41.

Pollard, R.T. et al., 2004. Water masses and circulation pathways through the Iceland Basin during Vivaldi 1996. *Journal of Geophysical Research: Oceans*, 109(C4), p.n/a-n/a.

Porter, M. et al., 2016. Glider observations of enhanced deep water upwelling at a shelf break canyon: A mechanism for cross-slope carbon and nutrient exchange. *Journal of Geophysical Research: Oceans*, 121(10), pp.7575–7588.

Poulton, A.J. et al., 2017. Seasonal phosphorus and carbon dynamics in a temperate shelf sea (Celtic Sea). *Progress in Oceanography*.

Powell, C.F. et al., 2015. Estimation of the Atmospheric Flux of Nutrients and Trace Metals to the Eastern Tropical North Atlantic Ocean. *Journal of the Atmospheric Sciences*, 72(10), pp.4029–4045.

Prego, R. et al., 2013. Trace metals in the NE Atlantic coastal zone of Finisterre (Iberian Peninsula): Terrestrial and marine sources and rates of sedimentation. *Journal of Marine Systems*, 126, pp.69–81.

Price, N.M. & Morel, F.M.M., 1990. Cadmium and cobalt substitution for zinc in a marine diatom. *Nature*, 344, p.658.

Prohaska, T. et al., 2015. *Sector Field Mass Spectrometry for Elemental and Isotopic Analysis*, The Royal Society of Chemistry.

Rapp, I. et al., 2017. Automated preconcentration of Fe, Zn, Cu, Ni, Cd, Pb, Co, and Mn in seawater with analysis using high-resolution sector field inductively-coupled plasma mass spectrometry. *Analytica Chimica Acta*, 976, pp.1–13.

Raven, J.A., 1997. Inorganic Carbon Acquisition by Marine Autotrophs. In J. A. B. T.-A. in B. R. Callow, ed. *Classic Papers*. Academic Press, pp. 85–209.

Rijkenberg, M.J.A. et al., 2014. The distribution of dissolved iron in the West Atlantic Ocean. *PLoS ONE*, 9(6), pp.1–14.

Ring, G. et al., 2016. Trace metal determination as it relates to metallosis of orthopaedic implants: Evolution and current status. *Clinical Biochemistry*, 49(7), pp.617–635.

Rivera-Duarte, I. & Flegal, A.R., 1994. Benthic lead fluxes in San Francisco Bay, California, USA. *Geochimica et Cosmochimica Acta*, 58(15), pp.3307–3313.

Roberts, D.A. et al., 2013. Ocean acidification increases the toxicity of contaminated sediments. *Global Change Biology*, 19(2), pp.340–351.

Rodríguez-Romero, A. et al., 2014. Simulation of CO2 leakages during injection and storage in sub-seabed geological formations: Metal mobilization and biota effects. *Environment International*, 68, pp.105–117.

Rolison, J.M., 2016. *The biogeochemistry of trace metals and their isotopes in the Mediterranean and Black Seas*. (Doctoral dissertation thesis). University of Otago.

Rolison, J.M. et al., 2015. Zonal distribution of dissolved aluminium in the Mediterranean Sea. *Marine Chemistry*, 177, pp.1–14.

Roshan, S. & Wu, J., 2015. Cadmium regeneration within the North Atlantic. *Global*

Biogeochemical Cycles, 29(12), pp.2082–2094.

Roshan, S., Wu, J. & DeVries, T., 2017. Controls on the Cadmium-Phosphate Relationship in the Tropical South Pacific. *Global Biogeochemical Cycles*, 31(10), pp.1516–1527.

Rue, E.L. & Bruland, K.W., 1995. Complexation of iron(III) by natural organic ligands in the Central North Pacific as determined by a new competitive ligand equilibration/adsorptive cathodic stripping voltammetric method. *Marine Chemistry*, 50(1), pp.117–138.

Rusiecka, D. et al., 2018. Anthropogenic Signatures of Lead in the Northeast Atlantic. *Geophysical Research Letters*, 45(6), pp.2734–2743.

Ryan, W.B.F. et al., 2009. Global Multi-Resolution Topography synthesis. *Geochemistry, Geophysics, Geosystems*, 10(3), p.n/a-n/a.

Saager, P.M. et al., 1997. Hydrography and local sources of dissolved trace metals Mn, Ni, Cu, and Cd in the northeast Atlantic Ocean. *Marine Chemistry*, 57(3–4), pp.195–216.

Saager, P.M., De Baar, H.J.W. & Howland, R.J., 1992. Cd, Zn, Ni and Cu in the Indian Ocean. *Deep Sea Research Part A. Oceanographic Research Papers*, 39(1), pp.9–35.

Saito, M.A. et al., 2010. A seasonal study of dissolved cobalt in the Ross Sea, Antarctica: Micronutrient behavior, absence of scavenging, and relationships with Zn, Cd, and P. *Biogeosciences*, 7(12), pp.4059–4082.

Saito, M.A. et al., 2017. The acceleration of dissolved cobalt's ecological stoichiometry due to biological uptake, remineralization, and scavenging in the Atlantic Ocean. *Biogeosciences*, 14(20), pp.4637–4662.

Saito, M.A. & Moffett, J.W., 2001. Complexation of cobalt by natural organic ligands in the Sargasso Sea as determined by a new high-sensitivity electrochemical cobalt speciation method suitable for open ocean work. *Marine Chemistry*, 75(1), pp.49–68.

Saito, M.A., Rocap, G. & Moffett, J.W., 2005. Production of cobalt binding ligands in a Synechococcus feature at the Costa Rica upwelling dome. *Limnology and Oceanography*, 50(1), pp.279–290.

Sander, S.G. & Koschinsky, A., 2011. Metal flux from hydrothermal vents increased by organic complexation. *Nature Geoscience*, 4, p.145.

Sanial, V. et al., 2017. Radium-228 as a tracer of dissolved trace element inputs from the Peruvian continental margin. *Marine Chemistry*.

Sañudo-Wilhelmy, S. a. & Flegal, A.R., 1994. Temporal variations in lead concentrations and isotopic composition in the Southern California Bight. *Geochimica et*

Cosmochimica Acta, 58(15), pp.3315–3320.

Schaule, B.K. & Patterson, C.C., 1983. Perturbations of the Natural Lead Depth Profile in the Sargasso Sea by Industrial Lead BT - Trace Metals in Sea Water. In C. S. Wong et al., eds. Boston, MA: Springer US, pp. 487–503.

Schlitzer, R., 2015. Ocean Data View, http://odv.awi.de.

Scholz, F. et al., 2011. Early diagenesis of redox-sensitive trace metals in the Peru upwelling area – response to ENSO-related oxygen fluctuations in the water column. *Geochimica et Cosmochimica Acta*, 75(22), pp.7257–7276.

Scrosati, B. & Garche, J., 2010. Lithium batteries: Status, prospects and future. *Journal of Power Sources*, 195(9), pp.2419–2430.

Sen, T.K. & Khilar, K.C., 2006. Review on subsurface colloids and colloid-associated contaminant transport in saturated porous media. *Advances in Colloid and Interface Science*, 119(2–3), pp.71–96.

Sherrell, R.M., Boyle, E.A. & Hamelin, B., 1992. Isotopic Equilibration Between Dissolved and Suspended Particulate Lead in the Atlantic Ocean: Evidence From 210 Pb and Stable Pb Isotopes. *Journal of Geophysical Research*, 97(C7), pp.11257–11268.

Simpson, J.H. & Sharples, J., 2012. *Introduction to the Physical and Biological Oceanography of Shelf Seas*, Cambridge: Cambridge University Press.

Slomp, C.P. et al., 1997. Iron and manganese cycling in different sedimentary environments on the North Sea continental margin. *Continental Shelf Research*, 17(9), pp.1083–1117.

Stockdale, A. et al., 2010. The Association of Cobalt with Iron and Manganese (Oxyhydr)oxides in Marine Sediment. *Aquatic Geochemistry*, 16(4), pp.575–585.

Stoker, M.S., Evans, D. & Cramp, A., 1998. Geological Processes on Continental Margins: Sedimentation, Mass-wasting and stability. In London: The Geological Society London, p. 344.

Sun, Y. & Torgersen, T., 1998. The effects of water content and Mn-fiber surface conditions on measurement by emanation. *Marine Chemistry*, 62, pp.299–306.

Sunda, W.G., 2012. Feedback Interactions between Trace Metal Nutrients and Phytoplankton in the Ocean. *Frontiers in Microbiology*, 3(June), p.204.

Sunda, W.G. & Huntsman, S.A., 1995. Cobalt and zinc interreplacements in marine phytoplanktion: Biological and geochemical aspects. *Limnology and Oceanography*, 40(8), pp.1404–1417.

Sunda, W.G. & Huntsman, S.A., 1998a. Control of Cd Concentrations in a Coastal Diatom by Interactions among Free Ionic Cd, Zn, and Mn in Seawater. *Environmental Science & Technology*, 32(19), pp.2961–2968.

Sunda, W.G. & Huntsman, S.A., 1988. Effect of sunlight on redox cycles of manganese in the southwestern Sargasso Sea. *Deep Sea Research Part A. Oceanographic Research Papers*, 35(8), pp.1297–1317.

Sunda, W.G. & Huntsman, S.A., 1998b. Interactive effects of external manganese, the toxic metals copper and zinc, and light in controlling cellular manganese and growth in a coastal diatom. *Limnology and Oceanography*, 43(7), pp.1467–1475.

Sunda, W.G., Huntsman, S.A. & Harvey, G.R., 1983. Photoreduction of manganese oxides in seawater and its geochemical and biological implications. *Nature*, 301(5897), pp.234–236.

Sunda, W.G., Tester, P.A. & Huntsman, S.A., 1987. Effects of cupric and zinc ion activities on the survival and reproduction of marine copepods. *Marine Biology*, 94(2), pp.203–210.

Sundby, B. & Silverberg, N., 1985. Manganese fluxes in the benthic boundary layer1. *Limnology and Oceanography*, 30(2), pp.372–381.

Talley, L.D. & McCartney, M.S., 1982. Distribution and Circulation of Labrador Sea Water. *Journal of Physical Oceanography*, 12(11), pp.1189–1205.

Taylor, S.R., 1964. Abundance of chemical elements in the continental crust: a new table. *Geochimica et Cosmochimica Acta*, 28(8), pp.1273–1285.

Tebo, B.M. & Emerson, S., 1985. Effect of Oxygen Tension, Mn(II) Concentration, and Temperature on the Microbially Catalyzed Mn(II) Oxidation Rate in a Marine Fjord. *Applied and Environmental Microbiology*, 50(5), pp.1268–1273.

Thi Dieu Vu, H. & Sohrin, Y., 2013. Diverse stoichiometry of dissolved trace metals in the Indian Ocean. *Scientific Reports*, 3, pp.1–5.

Thuróczy, C.E., Boye, M. & Losno, R., 2010. Dissolution of cobalt and zinc from natural and anthropogenic dusts in seawater. *Biogeosciences*, 7(6), pp.1927–1936.

Tian, Z. et al., 2008. Atmospheric Fe deposition modes at Bermuda and the adjacent Sargasso Sea. *Geochemistry, Geophysics, Geosystems*, 9(8), p.n/a-n/a.

Tsuda, A. et al., 2003. A Mesoscale Iron Enrichment in the Western Subarctic Pacific Induces a Large Centric Diatom Bloom. *Science*, 300(5621), p.958 LP-961.

Twining, B.S. et al., 2012. Role of diatoms in nickel biogeochemistry in the ocean. *Global*

Biogeochemical Cycles, 26(4), p.n/a-n/a.

Twining, B.S. & Baines, S.B., 2013. The Trace Metal Composition of Marine Phytoplankton. *Annual Review of Marine Science*, 5(1), pp.191–215.

Vance, D. et al., 2017. Silicon and zinc biogeochemical cycles coupled through the Southern Ocean. *Nature Geoscience*, 10(3), pp.202–206.

Véron, A.J. & Church, T.M., 1997. Use of stable lead isotopes and trace metals to characterize air mass sources into the eastern North Atlantic. *Journal of Geophysical Research*, 102(D23), p.28049.

Visbeck, M., 2018. Ocean science research is key for a sustainable future. *Nature Communications*, 9(1), p.690.

Vlasenko, V. & Stashchuk, N., 2015. Internal tides near the Celtic Sea shelf break: A new look at a well known problem. *Deep-Sea Research Part I: Oceanographic Research Papers*, 103, pp.24–36.

De Vleeschouwer, F. et al., 2007. Atmospheric lead and heavy metal pollution records from a Belgian peat bog spanning the last two millenia: Human impact on a regional to global scale. *Science of The Total Environment*, 377(2), pp.282–295.

Waeles, M. et al., 2008. On the distribution of dissolved lead in the Loire estuary and the North Biscay continental shelf, France. *Journal of Marine Systems*, 72(1–4), pp.358–365.

Warnken, K.W. et al., 2001. Sediment-water exchange of Mn, Fe, Ni and Zn in Galveston Bay, Texas. *Marine Chemistry*, 73(3), pp.215–231.

Waugh, D.W., Hall, T.M. & Haine, T.W.N., 2003. Relationships among tracer ages. *Journal of Geophysical Research: Oceans*, 108(C5), p.n/a-n/a.

WHO, 1995. *Inorganic lead*, Geneva, World Health Organization, International Programme on Chemical Safety (Environmental Health Criteria 165).

Wilson, A.M., 2016. *Lateral transport of suspended particulate matter in nepheloid layers along the Irish continental margin - a case study of the Whittard Canyon, North-East Atlantic Ocean*. (Doctoral dissertation thesis). National University of Ireland, Galway.

Woodward, E.M.S. & Rees, A.P., 2001. Nutrient distributions in an anticyclonic eddy in the northeast Atlantic Ocean, with reference to nanomolar ammonium concentrations. *Deep Sea Research Part II: Topical Studies in Oceanography*, 48(4), pp.775–793.

Wu, J. et al., 2010. Isotopic evidence for the source of lead in the North Pacific abyssal water. *Geochimica et Cosmochimica Acta*, 74(16), pp.4629–4638.

Wu, J. & Boyle, E.A., 1997. Low Blank Preconcentration Technique for the Determination of Lead, Copper, and Cadmium in Small-Volume Seawater Samples by Isotope Dilution ICPMS. *Analytical Chemistry*, 69(13), pp.2464–2470.

Wu, J. & Roshan, S., 2015. Cadmium in the North Atlantic: Implication for global cadmium-phosphorus relationship. *Deep-Sea Research Part II: Topical Studies in Oceanography*, 116, pp.226–239.

Wu, J.F. & Boyle, E.A., 1997. Lead in the western North Atlantic Ocean: Completed response to leaded gasoline phaseout. *Geochimica Et Cosmochimica Acta*, 61(15), pp.3279–3283.

Wyatt, N.J. et al., 2014. Biogeochemical cycling of dissolved zinc along the GEOTRACES South Atlantic transect GA10 at 40°S. *Global Biogeochemical Cycles*, 28(1), pp.44–56.

Xie, R.C. et al., 2015. The cadmium–phosphate relationship in the western South Atlantic — The importance of mode and intermediate waters on the global systematics. *Marine Chemistry*, 177, pp.110–123.

Yeats, P.A., 1998. An isopycnal analysis of cadmium distributions in the Atlantic Ocean. *Marine Chemistry*, 61(1), pp.15–23.

Zago, C. et al., 2000. Benthic fluxes of cadmium, lead, copper and nitrogen species in the northern Adriatic Sea in front of the River Po outflow, Italy. *Science of the Total Environment*, 246(2–3), pp.121–137.

van der Zee, C., van Raaphorst, W. & Epping, E., 2001. Absorbed Mn2+ and Mn redox cycling in Iberian continental margin sediments (northeast Atlantic Ocean). *Journal of Marine Research*, 59(1), pp.133–166.

Zhao, Y. & Marriott, S.B., 2013. Dispersion and Remobilisation of Heavy Metals in the River Severn System, UK. *Procedia Environmental Sciences*, 18, pp.167–173.

Zierenberg, R.A., Adams, M.W.W. & Arp, A.J., 2000. Life in extreme environments: Hydrothermal vents. *Proceedings of the National Academy of Sciences*, 97(24), p.12961 LP-12962.

Zurbrick, C.M. et al., 2018. Dissolved Pb and Pb isotopes in the North Atlantic from the GEOVIDE transect (GEOTRACES GA-01) and their decadal evolution. *Biogeosciences Discussions*, pp.1–34.